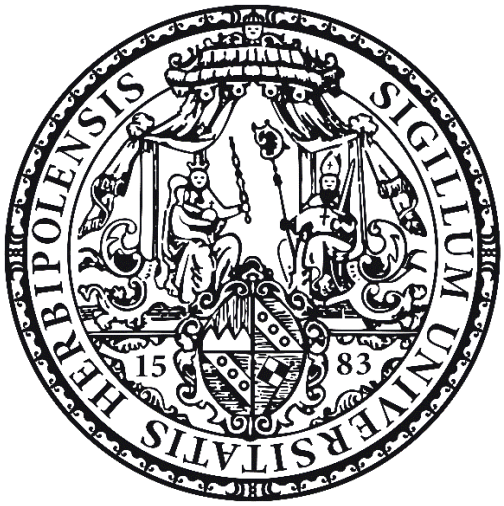

Chemical and physical nature of the barrier against active ingredient penetration into leaves: effects of adjuvants on the cuticular diffusion barrier

Chemische und physikalische Beschaffenheit der Barriere gegenüber Wirkstoffen: Adjuvantieneffekte auf die kutikuläre Diffusionsbarriere

Doctoral thesis for a doctoral degree
at the Graduate School of Life Sciences,
Julius-Maximilians-Universität Würzburg,
Section Integrative Biology

submitted by

Simona Staiger

from

Bietigheim-Bissingen

Würzburg 2019

Submitted on: ……..……..

Office stamp

Members of the *Promotionskomitee*:

Chairperson: Prof. Dr. Thomas Müller

Primary Supervisor: Prof. Dr. Markus Riederer

Supervisor (Second): Prof. Dr. Dr. Lorenz Meinel

Supervisor (Third): Dr. Christian Popp

Supervisor (Fourth): Dr. Katja Arand

Date of Public Defence: ……..……

Date of Receipt of Certificates: ……..

Table of contents

Summary

Agrochemicals like systemic active ingredients (AI) need to penetrate the outermost barrier of the plant, known as the plant cuticle, to reach its right target site. Therefore, adjuvants are added to provide precise and efficient biodelivery by *i.a.* modifying the cuticular barrier and increasing the AI diffusion. This modification process is depicted as plasticization of the cuticular wax which mainly consists of very long-chain aliphatic (VLCA) and cyclic compounds. Plasticization of cuticular waxes is pictured as an increase of amorphous domains and/or a decrease of crystalline fractions, but comprehensive, experimental proof is lacking to date. Hence, the objective of this thesis was to i) elucidate the permeation barrier of the plant cuticle to AIs in terms of the different wax fractions and ii) holistically investigate the modification of this barrier using selected oil and surface active adjuvants, an aliphatic leaf wax and an artificial model wax. Therefore, the oil adjuvant methyl oleate (MeO) and other oil derivatives like methyl linolenate (MeLin), methyl stearate (MeSt) and oleic acid (OA) were selected. Three monodisperse, non-ionic alcohol ethoxylates with increasing ethylene oxide monomer (EO) number (C10E2, C10E5, C10E8) were chosen as representatives of the group of surface active agents (surfactants). Both adjuvant classes are commonly used as formulation aids for agrochemicals which are known for its penetration enhancing effect. The aliphatic leaf wax of *Schefflera elegantissima* was selected, as well as a model wax comprising the four most abundant cuticular wax compounds of this species. Permeation, transpiration and penetration studies were conducted using enzymatically isolated cuticles of *Prunus laurocerasus* and *Garcinia xanthochymus*.

Cuticular permeability to the three organic solutes theobromine, caffeine and azoxystrobin differing in lipophilicity was measured using a steady-state two-chamber system separated by the isolated leaf cuticles of the evergreen species *P. laurocerasus* and *G. xanthochymus.* Treating the isolated cuticles with methanol selectively removed the cyclic fraction, and membrane permeability to the organic compounds was not altered. In contrast, fully dewaxing the membranes using chloroform resulted in a statistically significant increase in permeance for all compounds and species, except caffeine with cuticles of *G. xanthochymus* due to a matrix-specific influence on the semi-hydrophilic compound. Crystalline regions may reduce the accessibility to the lipophilic pathway across the waxes and also block hydrophilic domains in the cuticle.

Knowing that the aliphatic wax fraction builds the cuticular diffusion barrier, the influence of the adjuvants on the phase behaviour of an aliphatic cuticular wax as well as the influence on the cuticular penetration of AIs were investigated. Differential scanning calorimetry (DSC) and Fourier-transform infrared spectroscopy (FTIR) were selected to investigate the phase behaviour and thus possible plasticization of pure *Schefflera elegantissima* leaf wax, its artificial model wax comprising the four most abundant compounds (*n*-nonacosane, *n*-hentriacontane, 1-triacontanol and 1-dotriacontanol) and wax adjuvant mixtures. DSC thermograms showed a shift of the melting ranges to lower temperatures and decreased absolute values of the total enthalpy of transition (EOT) for all adjuvant leaf wax blends at 50 % (*w/w*) adjuvant proportion. The highest decrease was found for C10E2 followed by MeO > OA and C10E8 > MeLin > MeSt. The aliphatic crystallinity determined by FTIR yielded declined values for the leaf and the artificial wax with 50 % MeO. All other adjuvant leaf wax blends did not show a significant decrease of crystallinity. As it is assumed that the cuticular wax is formed by crystalline domains which consist of aliphatic hydrocarbon chains and an amorphous fraction comprising aliphatic chain ends and functional groups, the plasticizers are depicted as wax disruptors influencing amorphization and/or crystallization. The adjuvants can increase crystalline domains using the aliphatic tail whereas their more hydrophilic head is embedded in the amorphous wax fraction. DSC and FTIR showed similar trends using the leaf wax and the model wax in combination with the adjuvants.

In general, cuticular transpiration increased after adding the pure adjuvants to the surface of isolated cuticles or leaf envelopes. As waxes build the cuticular permeation barrier not only to AIs but also to water, the adjuvant wax interaction might affect the cuticular barrier properties leading to increased transpiration. Direct evidence for increased AI penetration with the adjuvants was given using isolated cuticles of *P. laurocerasus* in combination with the non-steady-state setup simulation of foliar penetration (SOFP) and caffeine at relative humidity levels (RH) of 30, 50 and 80 %. The increase in caffeine penetration was much more pronounced using C10E5 and C10E8 than MeO but always independent of RH. Only C10E2 exhibited an increased penetration enhancing effect positively related to RH. The role of the molecular structure of adjuvants in terms of humectant and plasticizer properties are discussed.

Hence, the current work shows for the first time that the cuticular permeation barrier is associated with the VLCAs rather than the cyclic fraction and that adjuvants structurally influence this barrier resulting in penetration enhancing effects. Additionally, this work demonstrates that an artificial model wax is feasible to mimic the wax adjuvant interaction in conformity with a leaf wax, making it feasible for *in-vitro* experiments on a larger scale (*e.g.* screenings). This provides valuable knowledge about the cuticular barrier modification to enhance AI penetration which is a crucial factor concerning the optimization of AI formulations in agrochemistry.

Zusammenfassung

Um ihren optimalen Wirkort in der Pflanze zu erreichen, müssen Agrochemikalien wie systemische Wirkstoffe zunächst die Kutikula überwinden, die die äußerste Barriere der Pflanze darstellt. Es werden sogenannte Adjuvantien verwendet, die unter anderem die kutikuläre Barriere modifizieren, um eine präzise und effiziente Bereitstellung des Wirkstoffs wie auch eine erhöhte Wirkstoffdiffusion zu ermöglichen. Diese Modifikation wird als Weichmachereffekt der Adjuvantien im kutikulären Wachs verstanden. Die Wachse umfassen hauptsächlich langkettige Aliphaten (VLCA) und zyklische, organische Komponenten. Da die Wachse aus kristallinen, für Wirkstoffe unzugänglichen und amorphen, zugänglichen Bereichen bestehen, wird angenommen, dass der Weichmacherprozess eine Zunahme der amorphen Phase und/oder eine Abnahme der kristallinen Phase hervorruft. Allerdings sind umfassende, experimentelle Beweise bisher nicht verfügbar. Daher lag der Schwerpunkt dieser Arbeit auf i) der Aufklärung, wie die verschiedenen Wachsfraktionen zur kutikulären Permeationsbarriere gegenüber Wirkstoffen beitragen und ii) der ganzheitlichen Untersuchung der kutikulären Penetrationsbarriere hinsichtlich eines aliphatischen Pflanzen- und Modelwachses und des Einflusses ausgewählter Öl- und Tensid-Adjuvantien. Hierfür wurden die Öle Methyloleat (MeO), Methyllinolenat (MeLin), Methylstearat (MeSt) und Ölsäure (OA) und drei monodisperse, nicht-ionische Alkoholethoxylate (C10E2, C10E5, C10E8) mit zunehmender Ethylenoxidmonomerzahl (EO) verwendet. Beide Gruppen sind gängige Hilfsstoffe der Formulierung von Agrochemikalien, die für die Aufnahmebeschleunigung des Wirkstoffs bekannt sind. Das aliphatische Blattwachs von *Schefflera elegantissima* wurde verwendet wie auch ein Modelwachs, dass die vier Hauptkomponenten dieses kutikulären Blattwachses enthielt. Permeabilitäts-, Transpirations- und Penetrationsstudien wurden unter Verwendung enzymatisch isolierter Kutikeln von *Prunus laurocerasus* und *Garcinia xanthochymus* durchgeführt.

Die kutikuläre Permeabilität gegenüber drei organischen Stoffen unterschiedlicher Lipophilie (Theobromin, Coffein und Azoxystrobin) wurde an isolierten Blattkutikeln der immergrünen Spezies *Prunus laurocerasus* und *Garcinia xanthochymus* mittels des Zweikammersystems im steady-state Zustand gemessen. Die zyklische Wachsfraktion konnte mit Hilfe von Methanol aus den isolierten Membranen extrahiert werden und die Membranen wiesen keine Veränderung in der Permeabilität gegenüber den drei

Wirkstoffen auf. Im Gegensatz dazu konnte ein signifikanter Anstieg der Permeabilität für alle Substanzen und Spezies beobachtet werden, nachdem die Membranen vollkommen mittels Chloroform entwachst wurden. Einzig und allein für Coffein und Membranen von *G. xanthochymus* konnte keine Veränderung des Leitwerts festgestellt werden, was auf einen Matrix-spezifischen Einfluss auf semi-hydrophile Substanzen zurückzuführen ist. Hydrophile Bereiche in der Kutikula können durch kristalline, aliphatische Wachse blockiert werden und sind somit unzugänglich für hydrophile Substanzen.

Auf Basis dieses neu gewonnenen Wissens der kutikulären Diffusionsbarriere wurde der Einfluss der Adjuvantien auf das Phasenverhalten eines aliphatischen Wachses wie auch ihr Einfluss auf die kutikuläre Wirkstoffpenetration untersucht. Dynamische Differenzkalorimetrie (DSC) und Fourier-Transform-Infrarotspektroskopie (FTIR) wurden verwendet, um das Phasenverhalten des Blattwachses von *Schefflera elegantissima*, ihres artifiziellen Modelwachses, das die vier Hauptkomponenten *n*-Nonacosan, *n*-Hentriacontan, 1-Triacontanol und 1-Dotriacontanol enthielt, und mögliche Weichmachereffekte durch Adjuvantien zu untersuchen. Mittels DSC konnten Schmelzbereiche, die zu niedrigeren Temperaturen verschobenen waren, und verringerte Beträge der Übergangsenthalpien (EOT) für alle Blattwachs-Adjuvantien-Mischungen bei 50 % Adjuvans-Zugabe (*w/w*) festgestellt werden. Die stärkste Abnahme wurde für C10E2 gefunden, gefolgt von MeO > OA und C10E8 > MeLin > MeSt. Die mittels FTIR bestimmte aliphatische Kristallinität war bei einem MeO-Anteil von 50 % signifikant gegenüber dem puren Blattwachs vermindert. Alle anderen Adjuvantien zeigten keine signifikanten Veränderungen der Kristallinität im Vergleich zum nativen Blattwachs. Es wird angenommen, dass das kutikuläre Wachs aus kristallinen und amorphen Bereichen aufgebaut ist: erstere umfassen aliphatische Kohlenwasserstoffketten, letztere ihre Kettenenden und funktionellen Gruppen. Die Weichmacheradjuvantien können auf diese Bereiche mit einer Erhöhung der amorphen und/oder Erniedrigung der kristallinen Fraktion einwirken. Sie können mit ihrer aliphatischen Kette in die kristallinen Bereiche eindringen und diese erhöhen, wohingegen sich ihr hydrophilerer Kopf in der amorphen Phase verteilen kann. DSC und FTIR zeigten ähnliche Trends für das Pflanzen- und das Modelwachs in Kombination mit den Adjuvantien.

Im Allgemeinen wiesen die isolierten Kutikeln und Blattumschläge von *P. laurocerasus* und *G. xanthochymus* erhöhte Leitwerte in Verbindung mit den Adjuvantien auf. Da die

Wachse nicht nur die Permeationsbarriere für Wirkstoffe, sondern auch für Wasser darstellen, wird angenommen, dass die Wachs-Adjuvans-Interaktion verantwortlich für die erhöhte Transpiration ist. Erhöhte Wirkstoffpenetration durch Adjuvantien wurde mittels des non-steady-state Versuchs der Simulation der Blattpenetration (SOFP) an isolierten, kutikulären Membranen von *P. laurocerasus* unter Verwendung von Koffein bei relativen Luftfeuchten (RH) von 30, 50 und 80 % nachgewiesen. Die Zunahme der Flussrate unter Verwendung von C10E5 und C10E8 war deutlich höher als für C10E2, jedoch unabhängig von der RH. Nur für C10E2 konnte eine Abhängigkeit des Effekts von der Luftfeuchte festgestellt werden. Die Rolle der molekularen Struktur der Adjuvantien in Bezug auf „Humectant"- und Weichmachereigenschaften wird diskutiert.

Die vorliegende Arbeit zeigt zum ersten Mal, dass die kutikuläre Permeationsbarriere mit den VLCAs und nicht mit der zyklischen Fraktion assoziiert ist und dass Adjuvantien wie Öle und Tenside diese Barriere strukturell beeinflussen können, was zu einer erhöhten Penetration führt. Außerdem veranschaulicht diese Arbeit, dass ein artifizielles Modelwachs die Wachs-Adjuvans-Interaktion eines Blattwachses imitieren kann und es gut geeignet für *in-vitro* Experimente ist, die in größerem Maßstab durchgeführt werden (z.B. Screenings). Das liefert bedeutsames Wissen über die kutikuläre Barriere und ihre Modifikation zur Erhöhung der Wirkstoffpenetration, die wichtige Faktoren in Bezug auf die optimierte Wirkstoffformulierung in der Agrarchemie darstellen.

.

Abbreviations

AFM	atomic force microscopy
AI	active ingredient
BIDE	simultaneous bilateral desorption
CA	contact angle
CF	chloroform
CM	cuticular membrane
cmc	critical micelle concentration
C6E3	triethylene glycol monohexyl ether
C8C1.6	2 -ethyl hexyl glycoside
C10E2	diethylene glycol monodecyl ether
C10E5	pentaethylene glycol monodecyl ether
C10EO7	heptaethylene glycol mono iso-decyl ether
C10E8	octaethylene glycol monodecyl ether
C24	*n*-tetradecane
C24-1-ol	1-tetradecanol
C28	*n*-octadecane
C28-1-ol	1-octadecanol
C29	*n*-nonacosane
C30-1-ol	1-triacontanol
C32-1-ol	1-dotricontanol
C33	*n*-tritriacontane
DSC	differential scanning calorimetry
EO	ethylene oxide monomer
EOT	enthalpy of transition
ESI	electrospray ionization
ESR	electron-spin resonance spectroscopy
FTIR	Fourier-transform infrared spectroscopy
GC-FID	gas chromatography flame ionization detection
GC-MS	gas chromatography mass spectrometry
GRAS	generally recognized as safe compounds
^{2}H-NMR	Deuterium nuclear magnetic resonance spectroscopy

h-ATR	horizontal attenuated total reflectance
HLB	hydrophilic-lipophilic-balance
IR	infrared
LTA	localized thermal analysis
M	methanol treated cuticular membrane
MeLin	methyl linolenate
MeO	methyl oleate
MeOH	methanol
MeSt	methyl stearate
MX	chloroform treated membrane/matrix
OA	oleic acid
QCM-D	Quartz Crystal Microbalance with Dissipation
RH	relative humidity
Span® 65	sorbitan tristearate
SEM	scanning electron microscopy
SOFP/SOFU	simulation of foliar penetration/uptake
UDOS	unilateral desorption from the outer surface
UHPLC-MS	ultra-high performance liquid chromatography mass spectrometry
VLCA	very long-chain aliphatic compounds
XRD	X-ray diffraction spectroscopy

1 Introduction

1.1 The plant cuticle

1.1.1 Function and structure

The cuticle is the outermost surface of the plant that covers all aerial organs of higher land-living plants (Martin and Juniper, 1970). As green algae induced the invasion of land, the cuticle was built to prevent themselves from water loss (Graham, 1993). Forming the cuticle was a key-innovation to enable the live of plants in dehydrating habitats (Edwards, 1993). The plant cuticle was not only build to prevent desiccation but also to provide protection against UV radiation (Krauss *et al.*, 1997). Additionally, the cuticle minimizes the adhesion of pollen, dust and other particles (Barthlott and Neinhuis, 1997), provides mechanical stability (Wiedemann and Neinhuis, 1998; Matas *et al.*, 2004), acts as an interface for biotic interactions (Blakeman, 1993; Eigenbrode and Jetter, 2002) and prevents organ fusion (Smirnova *et al.*, 2013). It consists of a thin continuous layer built of cutin, polysaccharides and solvent-soluble lipids (Jeffree, 1996). Due to its microscopic structure, the cuticle can be divided into two parts: the cuticular layer and the cuticle proper (Figure 1). The first mainly contains cutin with embedded polysaccharides and is attached to epidermal cells by a pectinaceous layer (Yeats and Rose, 2013). The cuticle proper consists of a high proportion of waxes which are situated intracuticularly (Jeffree, 1996). The pectin-rich layer, which connects cutin and the epidermal cells, is continuous with the middle lamella. By enzymatic hydrolysis, the cuticle can be isolated for further investigations (Orgell, 1955). This procedure is a rough method as it involves enzymatic isolation up to several months. Nevertheless, it was reported that permeances of different solutes using isolated cuticles, leaves and reconstituted waxes did not differ (Kirsch *et al.*, 1997). Epicuticular wax films are situated above the cuticle proper (Jeffree, 1996) and can be covered by epicuticular wax granules or crystals of various shapes which determine surface properties like hydrophobicity (Jeffree, 1986). Cuticular thickness differs widely among species ranging from 30 nm (*Arabidopsis thaliana*, leaf) to 30 µm (*Malus domestica*, fruit) (Schreiber and Schönherr, 2009). Attempts to correlate cuticular thickness to permeability to water and organic solutes were unsuccessful, as the pathway can be longer than expected by the thickness of the barrier (Schreiber and Riederer, 1996; Baur *et al.*, 1999a; Riederer and Schreiber, 2001; Jetter and Riederer, 2016).

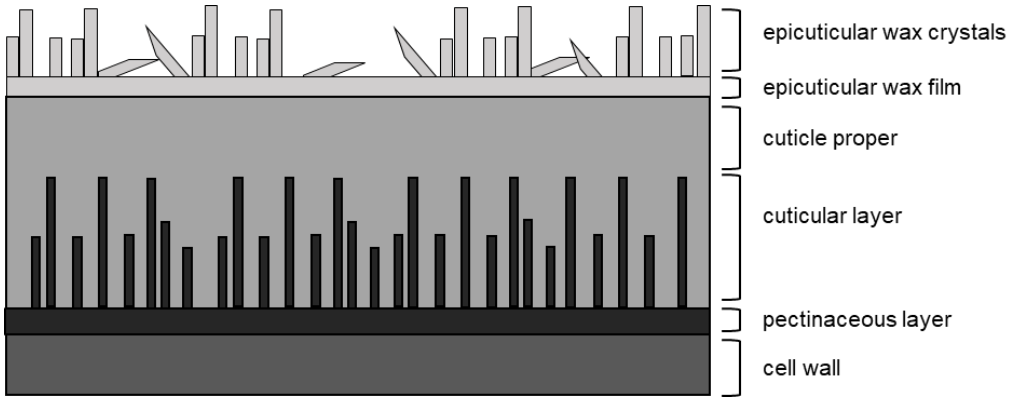

Figure 1 Structure of a plant cuticle after Buchholz (2006) and Yeats and Rose (2013)

Compounds of cuticular waxes show a high variability among different species, environment and ontogeny (Jeffree, 1986; Jetter *et al.*, 2006). These compounds mainly consist of primary *n*-alcohols, *n*-aldehydes, fatty acids and *n*-alkanes with chain-lengths between 20 to 40 carbons. Alkyl esters (C38 to C70) can also be present. Altogether, these compound classes can be summarized as very long-chain aliphatic compounds (VLCA). Depending on the species, cyclic compounds like triterpenoids *e.g.* oleanolic acid, ursolic acid or β-amyrin (Figure 2, I-III), aromatic compounds like ferulic acid or *p*-coumaric acid (Figure 3, IV, V), tocopherols and sterols (Figure 4, VI, VII) may also be present.

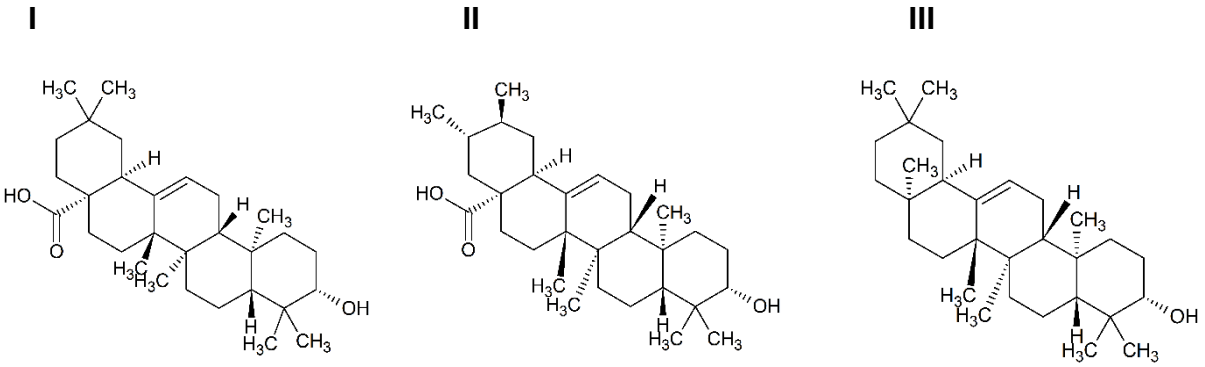

Figure 2 Chemical structures of oleanolic acid (I), ursolic acid (II) and β-amyrin (III)

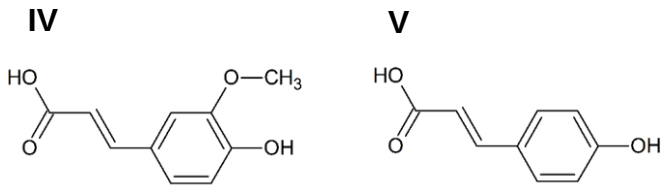

Figure 3 Chemical structures of ferulic acid (IV) and *p*-coumaric acid, in most cases bound to cutin as ester (V)

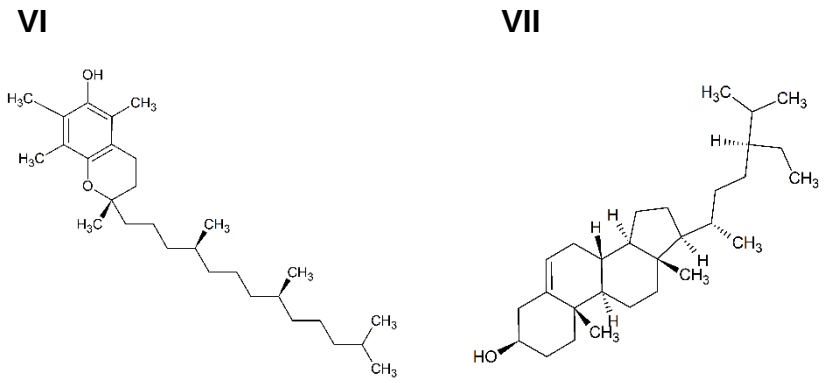

Figure 4 Chemical structures of α-tocopherol (VI) and β-sitosterol (VII)

Zeisler and Schreiber (2016) found that removal of epicuticular wax did not alter the cuticular water permeance for *P. laurocerasus*. Therefore, they assumed that epicuticular wax did not constitute the transpiration barrier. In contrast, Vogg *et al.* (2004) observed that water permeance of tomato fruit cuticles (*Solanum lycopersicum*) showed a 2-fold increase after removal of epicuticular waxes using gum arabicum. Another study in 2016 reported that intracuticular waxes primarily constituted the transpiration barrier, but that epicuticular waxes might also have an species-depending influence on it (Jetter and Riederer, 2016). In contrast to that, a previous study by Zeisler-Diehl *et al.* (2018) showed that in addition to *P. laurocerasus* (Zeisler and Schreiber, 2016) also several other species did not show a significant difference of the water permeance after removing the epicuticular wax fraction. Due to the differing results of several authors, the function and impact of epicuticular waxes concerning the transpiration barrier is still a matter of debate.

1.1.2 The hydrophilic and lipophilic pathway

The main function of the cuticle is to protect plants from desiccation. In general, it is believed that water transpiration through stomata is the major factor accounting for water loss (Martin and Juniper, 1970). However, transpiration due to diffusion across the cuticular membrane occurs to a significant degree. Not only water, but also organic solutes like non-ionic and ionic agrochemicals can permeate through the cuticle after the application process (Riederer and Schreiber, 1995). As shown in Figure 5, permeation pathways of organic solutes and water can be distinguished between the hydrophilic (Franke, 1967; Schreiber, 2005; Schönherr, 2006) and lipophilic pathway (Schönherr and Baur, 1994; Buchholz, 2006).

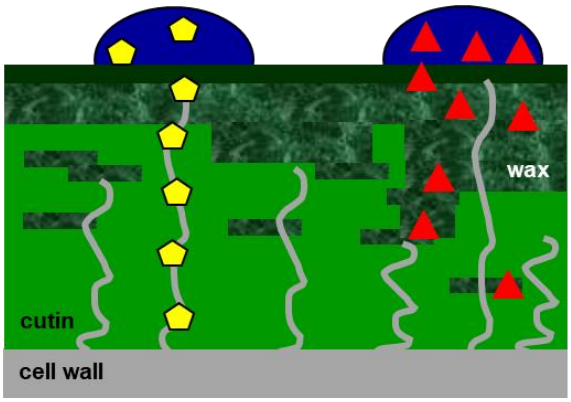

Figure 5 Model of the hydrophilic and lipophilic pathway across the plant cuticle (yellow - hydrophilic active ingredient, red triangles - lipophilic active ingredient) consisting of swollen polar domains like polysaccharide strands (grey) and wax domains (dark green)

Small, hydrophilic non-ionic and also ionic substances can permeate across the hydrophilic pathway (Schönherr and Schreiber, 2004; Popp *et al.*, 2005; Arand *et al.*, 2010; Remus-Emsermann *et al.*, 2011). It is assumed that this pathway, amongst others, consists of polysaccharide strands reaching from the cell wall through the cuticle to the physiological outer surface (Domínguez and Heredia, 1999; Popp *et al.*, 2005). Hydration of the cuticle is assumed to result in formation of water clusters within the cuticle, termed as “dynamic aqueous continuum” (Fernández *et al.*, 2017). These domains are permeable to hydrophilic active ingredients (AI), whereas they are inaccessible for lipophilic compounds. It is well known that waxes constitute the major permeation barrier to water and lipophilic organic solutes (Schönherr, 1976; Riederer and Schönherr, 1985; Kerler and Schönherr, 1988b). As shown in Figure 6, lipophilic AIs are assumed to permeate through lipophilic wax domains consisting of crystalline and amorphous fractions (Riederer and Schreiber, 1995; Buchholz, 2006). The crystalline fraction comprises very long aliphatic chains forming a regular,

orthorhombic lattice at room temperature, while their chain ends and functional groups constitute the amorphous domain (Riederer and Schneider, 1990; Reynhardt and Riederer, 1991). This is known as the ‘brick and mortar model’ assuming that the brick are the crystalline domains whereas the mortar represents the amorphous phase. Lipophilic compounds can only permeate through amorphous parts, while the crystalline fraction is inaccessible. Due to crystalline domains, the pathway becomes tortuous and the actual length of the pathway can be longer than expected by cuticular thickness (Baur *et al.*, 1999a).

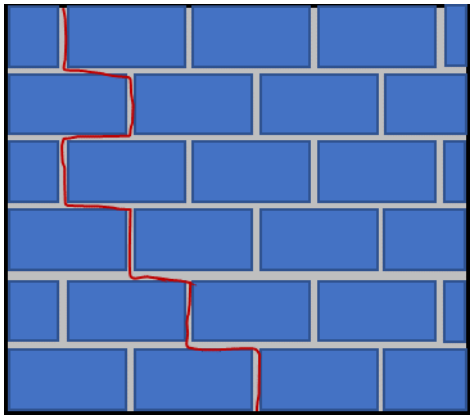

Figure 6 Model of the lipophilic pathway according to Riederer and Schreiber (1995). The red line represents a possible permeation pathway of a lipophilic solute while the blue rectangles represent crystalline domains. The amorphous part is indicated by grey areas.

1.2 Adjuvants and their mode of action

Pest organisms have a wide range of mechanisms to attack the plant (Stoytcheva, 2011). These mechanisms can range from sucking insects to fungi penetrating the plant tissue. As the farmer is the end consumer of the pesticide product, high biodelivery plays a pivotal role in agriculture. Therefore, agrochemicals like AIs need to reach the right target site when applied to plants. Depending on the mode of action of the AI and the pest that needs to be treated, the AI is supposed to either stay at the surface of the plant or be systemically distributed within the plant (Stoytcheva, 2011). Precise pest targeting and effective biodelivery is crucial, as drift into the environment would lead to environmental pollution and ecotoxicological consequences. Therefore, AIs are applied as formulations. These formulations are complex mixtures containing so called 'formulants' which can influence the foliar penetration process, the spray and application process (Falk, 1994). Holland gave an extensive overview of the most important definitions related to pesticides (Holland, 1996). According to his glossary, a formulant is defined as any other material in a pesticide formulation than the AI, whereas adjuvants are "formulant[s] designed to enhance the activity or other properties of a pesticide mixture". The American Society for Testing and Materials (1999) defined an adjuvant as "a material added to a tank mix to aid or modify the action of an agrochemical, or the physical characteristics of the mixture". Unfortunately, there is no standard system to classify adjuvants. Nevertheless, several authors tried to classify adjuvants in terms of terminology, classification, and chemistry (Kirkwood, 1993; Hazen, 2000).

The mode of action of adjuvants can vary widely. As shown in Figure 7, not only droplet drying (IV), retention (II) and spreading (III) processes can be influenced, but also solute mobility in the cuticle can be enhanced leading to an improved AI biodelivery (Schönherr, 1993a, 1993b; Burghardt *et al.*, 2006; Asmus *et al.*, 2016).

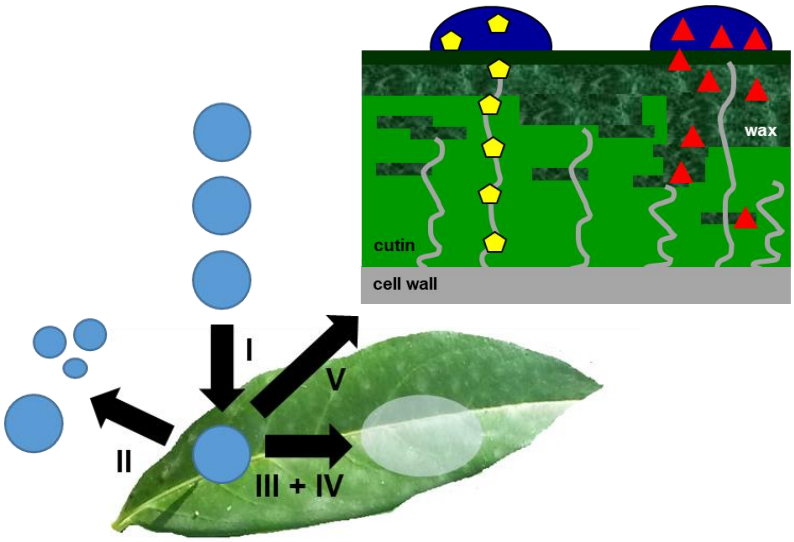

Figure 7 The fate of a droplet after spraying (I) on to a leaf surface showing retention or bouncing/shattering (II), spreading (III) and droplet drying (IV) and penetration into the plant tissue (V).

As the droplet containing the AI and adjuvants is sprayed onto the leaf surface (Figure 7, I), several processes can occur. The droplet can undergo bouncing, shattering or retention on the surface which is mainly influenced by the dynamic surface tension during the first 100 ms (Wirth *et al.*, 1991). Addition of adjuvants like surface active agents (surfactants) can reduce the surface tension, leading to a higher retention on the leaf. As the droplet is retained by the leaf surface, spreading can occur (Forster *et al.*, 2012). If the droplet doesn't shatter, this process is followed by recoiling of the droplet due to surface tension. During the spreading and recoiling phase the droplet loses energy. Bouncing off the leaf surface can emerge when the energy loss is small leaving enough energy for the bouncing process. Larger energy losses will lead to adherence. High surface activity is a prerequisite for an adjuvant to act properly as a spreader reducing the contact angle below 90°C (Wenzel, 1936; Holloway *et al.*, 1994). After a certain amount of time, the droplet starts to dry. This process is mainly influenced by humidity and temperature which affect hydration of the cuticle and deposit formation (Kudsk *et al.*, 1990; Ramsey *et al.*, 2006). Hygroscopic adjuvants, so called humectants, are used to store water within the droplet by absorbing moisture of the surrounding atmosphere (Price, 1982; Asmus *et al.*, 2016b). Maintaining the moisture keeps the AI in solution, consequently leading to a higher biodelivery.

Some adjuvants improve foliar penetration by increasing the mobility of the AI and are known as accelerators (Schönherr, 1993b). Several studies observed this effect using so called plasticizer surfactants like alcohol ethoxylates and oil adjuvants (Schönherr,

1993a; Santier and Chamel, 1996; Schönherr and Baur, 1996; Baur *et al.*, 1997b; Burghardt *et al.*, 2006).

1.2.1 Plasticizer adjuvants

Plasticizers are known from polymer technology and increase flexibility, workability and extensibility of the polymer (Graham, 1973). To plasticize a material, the plasticizer needs to be incorporated in the material and may influence viscosity, the temperature of a second-order transition or the elastic modulus (Daniels, 2009). In plant science, accelerator adjuvants that affect waxes structurally are named plasticizers, but the exact mode of action on the waxy barrier has not been entirely identified to date (Schönherr, 1993a; Schreiber *et al.*, 1997). The plasticizer effect of surfactants, *e.g.* alcohol ethoxylates, has been extensively studied using different techniques reporting increased penetration or permeability after addition of surfactants (Riederer and Schönherr, 1985; Riederer *et al.*, 1995; Baur *et al.*, 1996b; Schreiber *et al.*, 1996; Baur *et al.*, 1997b; Burghardt *et al.*, 1998; Shi *et al.*, 2005; Perkins *et al.*, 2005; Burghardt *et al.*, 2006; Grant *et al.*, 2008; Gutenberger *et al.*, 2013; Fagerström *et al.*, 2014; Zhang *et al.*, 2016).

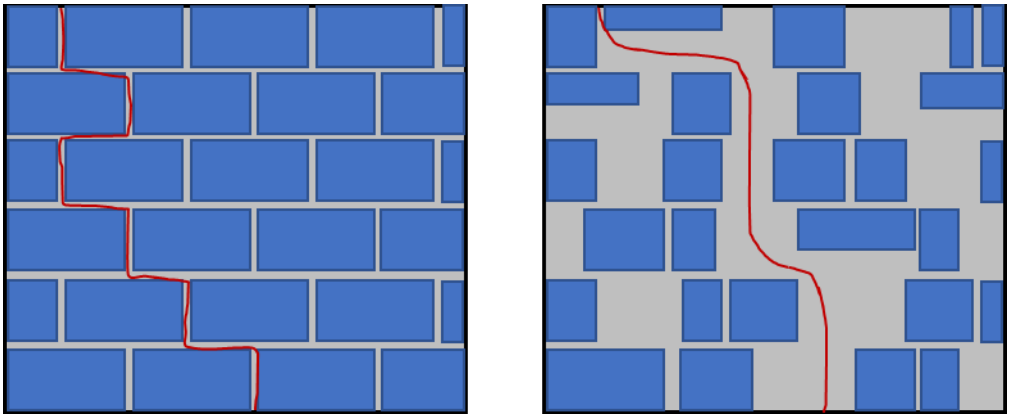

Figure 8 The diffusion pathway of a lipophilic AI (red line) across the lipophilic pathway without (left) and after application of an adjuvant (right). The red line represents a possible permeation pathway of a lipophilic solute while the blue rectangles represent crystalline domains. The amorphous part is indicated by grey areas.

Two possible modes of action of accelerator adjuvants have been proposed as i) the increase of the amorphous wax fraction and/or ii) the decrease of the crystalline wax fraction, both resulting in a decrease of tortuosity of the pathway (Buchholz, 2006; Fagerström *et al.*, 2014; Zhang *et al.*, 2016). A decrease of tortuosity results in a shorter diffusion pathway and therefore enhanced diffusion of the AI (Figure 8). Early investigations of plasticizer adjuvants were done by Schreiber *et al.* (1996) and

Schreiber *et al.* (1997) using electron spin resonance spectroscopy (ESR) and ^{2}H-nuclear magnetic resonance spectroscopy (^{2}H-NMR). ESR revealed an unspecific plasticizing effect of monodisperse alcohol ethoxylates on reconstituted barley wax, describing similar effects for temperature and the addition of adjuvant. This was the first study to show that increased proportion of adjuvants and increasing the temperature resulted in similar effects of the physicochemical behaviour. Using ^{2}H-NMR, amorphous and crystalline domains were found in barley leaf wax when combined with two deuterated aliphatic compounds (fatty acid and alkane). The addition of the alcohol ethoxylate triethylene glycol monohexyl ether (C6E3) reduced the order of the fatty acid label, but not the alkane label. It was assumed that the alkane is situated in the crystalline phase, whereas the fatty acid is located in the amorphous domain. Fagerström *et al.* (2014) hypothesized that surfactants not only affect amorphous parts of the wax but also absorb in crevices between crystalline domains. The authors used differential scanning calorimetry (DSC) and Quartz Crystal Microbalance with Dissipation (QCM-D) to quantify the softening effect of a model wax and observed a stronger fluidizing effect for the surfactant heptaethylene glycol mono iso-decyl ether (C10EO7) than for 2-ethyl hexyl glycoside (C8C1.6). A plasticizing effect on cuticular wax was also seen for reconstituted wax of *Prunus laurocerasus* leaves in combination with the alcohol ethoxylate Synperonic A7 using DSC and localised thermal analysis (LTA) (Perkins *et al.*, 2005). Reconstituted wax of *Beta vulgaris* L. showed plasticization after adding an ethoxylated non-ionic surfactant using atomic force spectroscopy (AFM) (Grant *et al.*, 2008). In addition to the previously listed techniques, which focused on the physicochemical properties of the wax adjuvant mixture, several permeation studies and the effect of plasticizer adjuvants on the permeation process exist showing the direct evidence of enhanced AI permeation (Riederer *et al.*, 1995; Burghardt *et al.*, 1998; Shi *et al.*, 2005; Burghardt *et al.*, 2006). It was reported that the accelerator needs to penetrate the cuticle and remain in the limiting barrier until most of the solutes have penetrated to achieve good uptake effects (Shi *et al.*, 2005). As was described earlier, the plasticizing effect is depicted as an interaction of the adjuvant with the cuticular wax affecting the crystallinity and/or the amorphousness, but comprehensive determination of these parameters have been lacking to date. Only one study about the plasticization of carnauba wax with generally recognized as safe compounds (GRAS) has been published (Zhang *et al.*, 2016), but data on crystallinity of other plant cuticular wax in combination with other adjuvants

does not exist. Zhang *et al.* (2016) used various polysorbates and sorbitan tristearate (Span® 65) in combination with carnauba wax and studied mechanical properties, crystallinity, crystallite size, surface roughness and melting points. While plasticization was observed with polysorbates, Span® 65 did not show this effect. It was stated that polysorbates could increase amorphous zones to a higher extent than Span® 65 due to their ethoxyl groups and molecular structure. In general, Zhang *et al.* (2016) proposed a model in close relation to the 'brick and mortar model', suggesting that the lipophilic part of the GRAS are embedded in the crystalline zone of the wax, while the hydrophilic head is situated in the amorphous phase. Therefore, amorphization and crystallization can occur simultaneously.

1.2.2 Oils and oil derivatives

Before synthetic AIs were discovered, oils, *e.g.* mineral and seed oils, had been commonly used as insecticides, herbicides, fungicides and defoliants (Rohrbaugh, 1941; Laville, 1963; Gauvrit and Cabanne, 1993). With the invention of synthetic AIs, oils disappeared as pesticides, but have still been used as diluents, solvents or especially adjuvants. Paraffinic oils were widely used, but concerns about biodegradability and ecotoxicological consequences were raised (Knowles, 1998). The discovery of vegetable oils provided a solution by offering sustainability according to their good biodegradability. Several oil adjuvant classes are used in agriculture: crop oil concentrates, vegetable seed oils and esterified seed oils (Miller and Westra, 1998). Crop oil concentrates are a mixture of paraffinic oil and surfactants, whereas vegetable seed oils are made of soybean or cottonseed oil blended with surfactants. They are generally cheaper than esterified seed oils, *e.g.* methylated or ethylated seed oils, which comprise an alkyl ester of a vegetable seed oil (soybean, corn, canola, sunflower) mixed with a surfactant. As esterification is a chemical modification, these adjuvants can be grouped into the adjuvant class of oil derivatives. These oil derivatives accelerate the uptake of AIs by influencing spreading, recrystallization, the physical properties of the wax and thus the permeation process of the AI (Nalewaja *et al.*, 1986; Mcwhorter and Barrentine, 1988; Wanamarta *et al.*, 1989; Manthey and Nalewaja, J. D., Szelezniak, E. F., 1989; Schott *et al.*, 1991; Mcwhorter *et al.*, 1993; Webster *et al.*, 2018).

As several studies showed, emulsified oils act as spreaders used purely or in combination with surfactants (Mcwhorter and Barrentine, 1988; Schott *et al.*, 1991;

Mcwhorter *et al.*, 1993). It was reported, that spreading depended on the leaf surface morphology and the emulsifier used, as it has surface active properties itself. Attempts to correlate the spreading area and the droplet deposit area respectively with the herbicide penetration were unsuccessful (Price, 1982; Wanamarta *et al.*, 1989).

After AI application, recrystallization of the AI is an important process, as the physical state of the AI on the leaf surface influences the uptake process (Hess and Falk, 1990). As water and solvents evaporate from the leaf surface, the AI often recrystallizes being less absorbable by the leaf surface in a solid crystalline state than in a liquid one. Therefore, the oil adjuvant can prevent recrystallization of the AI on the leaf surface and keeping it in a more liquid phase (Hess and Falk, 1990). Oil adjuvants are not only used in agrochemistry to enhance AI biodelivery but also in the field of grape drying to improve drying rates (Bolin and Stafford, 1980; Saravacos *et al.*, 1988; Doymaz and Pala, 2002). Thereby, dipping of the berries into a solution of oleic acid alkyl esters and potassium carbonate is done to accelerate the drying process. Ethyl oleate and methyl oleate (MeO) are the two most commonly used oil derivatives. It is assumed that these oil derivatives can act in two ways to increase the transpiration rate by i) partly dissolving cuticular waxes which constitute the permeation barrier and ii) permeating into the wax layer and interacting with the wax compounds. As reported by Holloway *et al.* (1994) and Gauvrit and Cabanne (1993), oil derivatives have a low ability to solve wax compounds. Thus, the interaction of oil derivatives with cuticular wax and influencing the wax structure appears to be more reasonable. This could be depicted as a change in physical properties of the wax, *e.g.* an increase in wax fluidity (Gauvrit and Cabanne, 1993). As a previous study by Räsch *et al.* (2018) showed *in vivo*, also minimal leaf conductance of *Brassica oleracea* (kohlrabi) can be increased after using methylated rape seed oil. The authors proposed an interaction of the penetration enhancer with the waxes like plasticization leading to an increased water transpiration. Not only plant desiccation can be influenced by oils but also the permeation of AIs from the outside into the inner plant tissue. This has been extensively studied by several authors (Manthey and Nalewaja, J. D., Szelezniak, E. F., 1989; Gauvrit and Dufour, 1990; Urvoy and Gauvrit, 1991; Schott *et al.*, 1991; Urvoy *et al.*, 1992; Zhang *et al.*, 2013; Brabham *et al.*, 2019). All authors detected an increase of penetration rates of a lipophilic AI after addition of oil adjuvants, but did not comprehensively explain the mechanism behind this increased penetration. Hazen (2000) suggested that chemically modified seed oils like methylated seed oil primarily act as wax softeners

or wax disruptors, but direct evidence has been lacking so far. One study about wax-oil adjuvant interaction using tristearin and *Ficus macrophylla* leaf wax in combination with MeO and several other oil adjuvants found a decrease of the enthalpy of transition using DSC, but the authors did not discuss the effect of plasticization (Webster *et al.*, 2018). A study by Santier and Chamel (1996) proposed that the oils have a similar effect on wax fluidity as nonylphenol surfactants with low ethylene oxide content, as they can interact with the cuticle and therefore increase the mobility of the AI (Coret and Chamel, 1994).

1.2.3 Alcohol ethoxylates

Fatty alcohol polyglycol ethers (alcohol ethoxylates) are commonly used adjuvants in agrochemistry (Kirkwood, 1993). They belong to the class of non-ionic surfactants and possess amphiphilic properties comprising a hydrophilic and lipophilic component. The lipophilic part consists of the aliphatic fatty alcohol chain (tail) whereas the hydrophilic compartment is formed by the polyethylene glycol group, the so called head (Figure 9) (Semenov *et al.*, 2015).

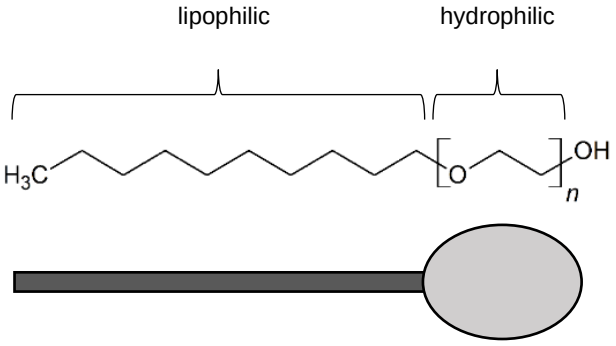

Figure 9 Example of an alcohol ethoxylate showing the lipophilic and hydrophilic part

If the surfactant is dissolved in water, a solution of individual monomers is formed, and the surface tension is lowered. This is an important physical property of surfactants leading to a wide application as detergents, wetters, antifoamers and emulsifiers (van Os, 1997). Higher concentrations of the surfactant lead to further lowering of the surface tension and saturating of the surface until the point of critical micelle concentration (cmc) is reached. The cmc is the concentration of surfactant in solution above which micelles form and the surface tension does not decrease any more or with a lower slope (Nič *et al.*, 2009). Another parameter to describe surfactant properties is the hydrophilic-lipophilic balance (HLB) (Hess and Foy, 2000). According

to Griffin (1954), the HLB can be calculated using the molar mass of the lipophilic part of the non-ionic surfactant (M_{lipophil}) and its total molar mass (M_{total}, Equation 1).

$$HLB = 20\left(1 - \frac{M_{\mathrm{lipophil}}}{M_{\mathrm{total}}}\right) \qquad \text{Equation 1}$$

Hydrophilic surfactants have HLB values above 11, whereas lipophilic ones show values below 8 (Hess and Foy, 2000). Intermediate surfactants possess values between 8 and 11. It was reported that altering the number of ethylene oxide monomers (EO) of an alcohol ethoxylate with constant aliphatic tail correlates positively with the HLB value (Stock *et al.*, 1993; Asmus, 2016).

Surfactants like non-ionic alcohol ethoxylates may act as wetters, spreaders, antifoamers, humectants or accelerator adjuvants (Kirkwood, 1993; Ramsey *et al.*, 2005). Due to their physicochemical properties, surfactants influence the surface tension of a spray droplet and the contact angle between a sessile droplet and the plant surface, as well as spray drift, adhesion, spreading, wetting and the wax microstructure (Wirth *et al.*, 1991; Zhang *et al.*, 2017; Pambou *et al.*, 2018). Wetting and spreading behaviour on difficult-to-wet species can be improved using surfactants, but correlating the efficiency of the AI uptake and the actual AI deposit area was unsuccessful (Stock and Holloway, 1993). It was reported that species possessing epicuticular wax crystals like winter wheat, quackgrass and pea retained much less spray solution than smooth surfaces (Ruiter *et al.*, 1990). Addition of a non-ionic surfactant (polyoxyethylene nonyl phenol) lead to an increased retention. Enhanced spreading of a droplet consisting of an aqueous solution of different herbicides and secondary alcohol ethoxylate surfactants on plant leaves having microcrystalline or amorphous wax structures were reported by Manthey *et al.* (1996). Here, spreading was higher on leaves having microcrystalline epicuticular wax. As was shown by Wirth *et al.* (1991), retention of the spray droplet was related to dynamic surface tension. Both parameters are concentration dependent above the cmc. The cmc is not only a crucial parameter to describe surfactant properties in terms of surface activity, but also as far as sorption behaviour into cuticular wax and cutin is concerned (Riederer *et al.*, 1995; Burghardt *et al.*, 1998). It was shown that above the cmc of the surfactant in the surrounding solution of the specimen (cutin matrix or wax disc), no more surfactant is sorbed to it and the maximum amount is reached. Hence, the cmc determines the

amount of sorbed surfactant into the cuticular matrix and wax. Correlating the alcohol ethoxylate effect on permeation of AIs to the maximum sorbed amount in the wax/matrix, yielded a linear curve, revealing an intrinsic activity for all alcohol ethoxylates used.

The octanol/water partition coefficient (K_{OW}) as a proxy for water solubility of the AI and the HLB of the surfactant can be used to predict the effect on permeation of the AI across the cuticle. It was shown that low water solubility (log $K_{OW} > 1$) of the AI and low HLB values of the surfactant resulted in the ideal enhancement (Nalewaja *et al.*, 1996; Ruiter *et al.*, 1996). Surfactants can improve the solubility of the AI in water and maintaining the AI in solution after application on the leaf surface (Hess and Foy, 2000).

Several studies proposed humectant effects for alcohol ethoxylates, as they are able to retain moist after AI application (Stevens and Bukovac, 1987b, 1987a; Gaskin and Holloway, 1992; Baur, 1999). Surfactants with a high number (≥10) of ethylene oxide monomers (EO) absorb water from the atmosphere due to their hygroscopic properties keeping the AI in a liquid/gel-like state after droplet application (Cook *et al.*, 1977; Stock and Holloway, 1993; Asmus, 2016). Furhtermore, a recent study by Arand *et al.* (2018) showed that also surfactants with EO numbers starting at 6 possess humectant properties.

Enhanced penetration of an AI using alcohol ethoxylates was reported, describing the surfactant effect as a plasticization of cuticular wax (Schönherr, 1993a; Schönherr and Baur, 1996; Baur *et al.*, 1997b; Burghardt *et al.*, 2006). Stock and Holloway (1993) found that the uptake of lipophilic AIs is higher with alcohol ethoxylate having EOs of 5 to 6 whereas hydrophilic compounds are effected the most with EOs of 10 to 20. It is assumed that surfactants with a low EO value enhance lipophilic AI permeation by affecting the physicochemical properties of the cuticle (Coret and Chamel, 1994; Coret and Chamel, 1995). Trying to identify the plastization process of surfactants, DSC and nonylphenol ethoxylates were used resulting in a decreased melting enthalpy and melting point with surfactants of low EO-content. In contrast, EO values above 9 did not alter these parameters. As far as alcohol ethoxylates are concerned, one study by Perkins *et al.* (2005) studied the plasticizing effect of two polydisperse surfactants with C13/C15 alkyl chains having an EO average of 7 and 20 mol. In contrast to the low EO surfactant, DSC revealed no decrease of the melting enthalpy for the surfactant with higher EO values and therefore no plasticizing effect.

1.3 Basic models and methodologies used within this thesis

1.3.1 Cuticular permeability

As an extracellular membrane of the plant, the cuticle is permeable to solutes, *e.g*. AIs, nutrients and environmental pollutants (Schreiber and Schönherr, 2009). Cuticular permeability varies widely across different species, while reasons to explain this phenomenon have still been lacking (Kirsch *et al.*, 1997). As depicted in Figure 10, the process of cuticular permeation can be divided into three processes: sorption into the cuticle, diffusion across the membrane and desorption into the apoplast (Bukovac and Petracek, 1993; Kirkwood, 1999).

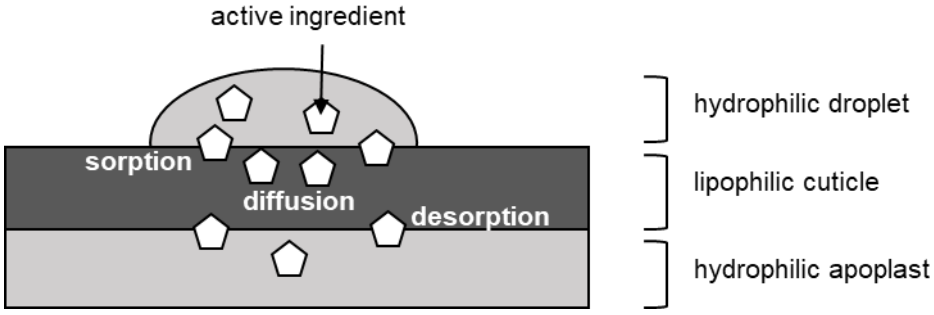

Figure 10: The process of cuticular permeation modified after Buchholz (2006)

Sorption into the membrane

As the solute first encounters the cuticle, it is absorbed into the membrane before permeating across it. The cuticle/water partition coefficient (K_{CW}) can be used to describe cuticular sorption capacity. It is the quotient of the concentration of a solute within the cuticle c_{cuticle} and the concentration of the solute in a solution at equilibrium state c_{water} (Kerler and Schönherr, 1988a) (Equation 2).

$$K_{\mathrm{CW}} = \frac{c_{\mathrm{cuticle}}}{c_{\mathrm{water}}} \qquad \text{Equation 2}$$

Several investigators determined K_{CW} for various solutes (Riederer and Schönherr, 1985; Kerler and Schönherr, 1988b, 1988a; Schreiber and Schönherr, 1992; Baur *et al.*, 1996; Kirsch *et al.*, 1997; Burghardt *et al.*, 1998). A linear relation between K_{CW} and the octanol/water partition coefficient (K_{OW}) of lipophilic compounds was reported (Schönherr and Riederer, 1989).

Mass transfer across the membrane

Diffusion of solutes in cuticles is a physical process, as there are no transporters or carriers available (Schönherr and Riederer, 1989). According to Cussler (2009), diffusion is a movement of the solute from a higher to a lower concentration until equilibrium state. Therefore, diffusion of molecules across the cuticle can be described by Fick's first law and the diffusion flux J_{Fick}:

$$J_{\mathrm{Fick}} = -D\frac{\partial c}{\partial x} \qquad \text{Equation 3.}$$

D describes the diffusion coefficient while c is the concentration and x the path length. Plotting the amount (amt) of a compound that permeated through the membrane as a function of time (t), the flux (J) can be calculated by using the slope (Equation 4).

$$J = \frac{\Delta \mathrm{amt}}{\Delta t} \qquad \text{Equation 4}$$

Using the concentration difference (Δc), between donor and receiver compartment representing the driving force, J and the membrane area (A), permeance (P) of a solute can be calculated by Equation 5 (Kerler *et al.*, 1984).

$$P = \frac{J}{A \cdot \Delta c} \qquad \text{Equation 5}$$

Kerler and Schönherr (1988b) found a linear correlation between log permeance and log K_{CW} for lipophilic compounds. Same was reported by Popp *et al.* (2005) for lipophilic compounds as well as for hydrophilic ones showing that AIs take different pathways depending on the lipophilicity of the AI.

Steady-state condition with a constant driving force is a prerequisite for the determination of the permeance. Hereby, the concentration difference Δc between two compartments (receiver and donor) which are separated by the cuticular membrane stays nearly constant over time. The double chamber system described by Schreiber *et al.* (1995) can be used for steady-state experiments. Two stainless-steel chambers are used mounting the isolated cuticular membrane between the compartments facing the morphological outer surface towards the receiver (Figure 11). The donor is filled with aqueous solution of the AI, while the receiver is filled with water or phospholipid suspension (Schreiber and Schönherr, 2009). At different time-intervals, aliquots are removed from the receiver and quantified. The reader is referred to 2.2 for a detailed description of the experimental setup.

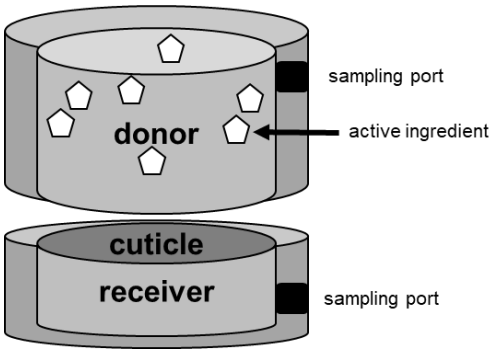

Figure 11 Double chamber system used for determination of the permeance in steady-state condition

It is well known, that cuticular waxes build the barrier to organic solutes and water (Schönherr, 1976; Riederer and Schönherr, 1985; Kerler and Schönherr, 1988a; Popp *et al.*, 2005). The effect of wax extraction after removing the waxes can be calculated by using the permeance with the matrix (P_{MX}) and the isolated cuticular membrane (P_{CM}) (Equation 6).

$$Effect = \frac{P_{MX}}{P_{CM}} \qquad \text{Equation 6}$$

1.3.2 Simulation of foliar penetration

Simulation of foliar penetration or uptake (SOFP/SOFU) is a common method to study the penetration behaviour of AIs across the plant cuticle and the effect of penetration enhancing adjuvants (Schönherr and Baur, 1994; Schreiber and Schönherr, 2009). The abbreviation SOFP is the more correct one as the penetration process of an AI across the plant cuticle is a physical process and does not include active participations of the membrane, *e.g.* transport proteins. Therefore, the term 'simulation of foliar penetration' (SOFP) will be further used. For SOFP experiments isolated cuticular membranes from the adaxial hypostomatous side of leaves or fruits were used (Schreiber and Schönherr, 2009). A small droplet containing the AI and the adjuvant is applied to the morphological outer surface of the membrane acting as donor for the penetration experiment. The AI, as well as the adjuvant diffuse across the membrane and into the aqueous receiver. As the droplet is applied, water evaporates leaving an AI-surfactant deposit on the waxy surface. The actual concentration and driving force of the AI penetrating the cuticle changes during the experiment and hence, the driving force is unknown (Baur *et al.*, 1997b). As described previously (1.3.1), the penetration process of the AI can be divided into three main steps (Bukovac and Petracek, 1993; Kirkwood, 1999):

i) the sorption into the membrane
ii) the diffusion of the AI within the membrane
iii) the desorption from the membrane into the receiver or apoplast.

The sorption of the AI into the membrane (i) is affected by several factors during the spray and retention process, *e.g.* relative humidity (RH), temperature, adjuvants etc. These factors change during the application process and can hardly be investigated selectively. As shown in Figure 12, the penetration process can be influenced by physicochemical properties of the AI, environmental conditions and cuticular properties (Buchholz, 2006). For instance, a high log K_{OW} would mean high partitioning into the cuticle due to lipophilicity of the cuticle. In contrast to that, a low water solubility in combination with a high log K_{OW} would lead to a low concentration of the AI (c_1) in the applied solution. Hence, the low c_1 would lead to a low sorption into the wax which derives from the wax/water partition coefficient (K_{wax}). Additives like emulsifiers can influence the solubility of the AI and therefore lead to a higher penetration into the

cuticle due to increased AI concentrations (Baur *et al.*, 1997c). Environmental factors like the pH, temperature or RH can affect the penetration in different ways, as well as cuticular properties like differences amongst plant species and therefore wax composition. To achieve effective penetration, it is important that the amount of AI in the droplet c_1 is optimized as well as the partitioning into the plant wax (K_{wax}) (Buchholz, 2006).

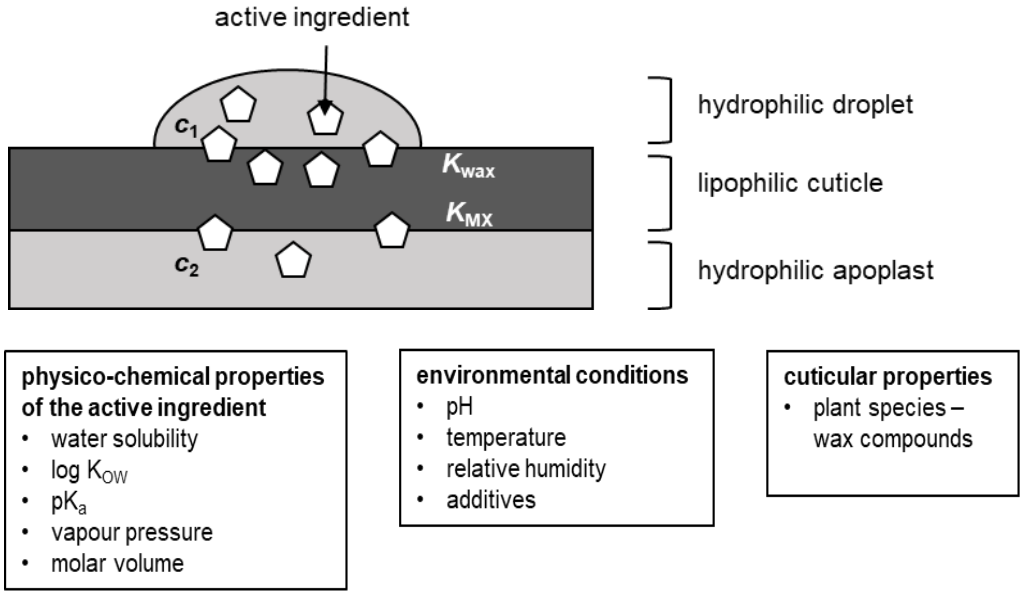

Figure 12 The process of cuticular penetration of a lipophilic active ingredient and the factors influencing the penetration process modified after Buchholz (2006). c_1 - concentration of the AI in the droplet, c_2 - concentration of the AI in the apoplast, K_{wax} - water/wax partition coefficient, K_{MX} - water/matrix partition coefficient

After diffusion across the membrane, the partitioning from the matrix (K_{MX}) into the hydrophilic apoplast and the access to the symplast becomes the determining factor for distribution into underlying tissue.

As mentioned above, the actual concentration and driving force of the AI penetrating the cuticle is unknown due to droplet evaporation after the application process (Baur *et al.*, 1997b). Therefore, the flux (J) as the slope of the plotted amount (amt) *versus* the time (t) can be used to compare the penetration of the AI under different conditions, *e.g.* with adjuvants (Equation 4).

1.3.3 Infrared spectroscopy

Infrared (IR) spectroscopy is an analytical method on the base of molecular vibrations (Günzler and Gremlich, 2012) in the range of IR radiation (0.78 - 1000 µm). This method has been widely used to broaden the knowledge of functional groups within the cuticle and their structural role (Chamel and Marecha, 1992; Ramirez *et al.*, 1992; Luque *et al.*, 1994; Merk *et al.*, 1997; Casado and Heredia, 1999; Villena *et al.*, 2000; Benitez *et al.*, 2004; Heredia-Guerrero *et al.*, 2012; Heredia-Guerrero *et al.*, 2014; Heredia-Guerrero *et al.*, 2016). As cuticular waxes comprise long-chain aliphatic molecules, the polymethylene section can undergo several different vibrational modes (Figure 13). Measuring plant cuticular wax using IR in the wavenumber range of 670 to 4000 cm^{-1}, a spectra with three main groups of absorption bands can be detected (Ramirez *et al.*, 1992; Chamel and Marecha, 1992; Merk *et al.*, 1997). Signals of adaxial cuticular wax of *P. laurocerasus* show asymmetric stretching bonds (ν_{as}) between 2923 - 2916 cm^{-1}, while a symmetric stretching (ν_s) bond is visible in the range of 2853 - 2849 cm^{-1} (Figure 14 I). Scissoring (δ_{sciss}) and rocking (δ_{rock}) doublets appear at 1473-1470 cm^{-1} and 730-719 cm^{-1}, respectively.

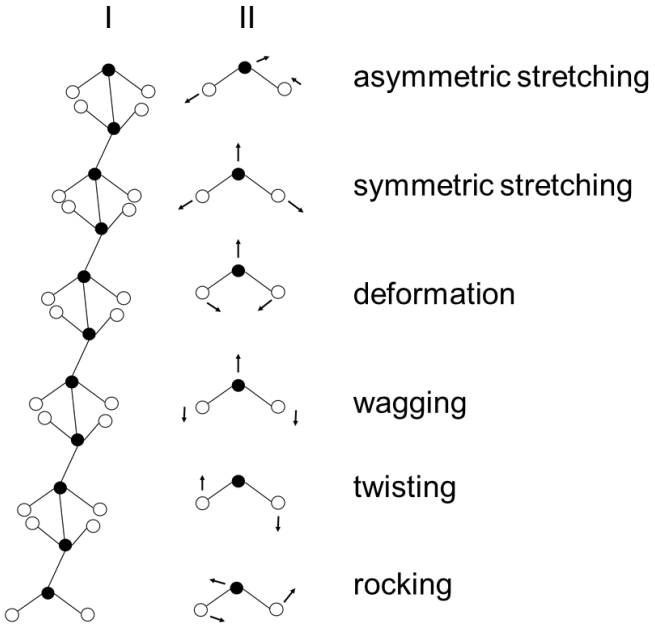

Figure 13 Section of a CH_2- chain (I) with different vibration modes (II) of the methylene group modified according to Fischmeister (1975)

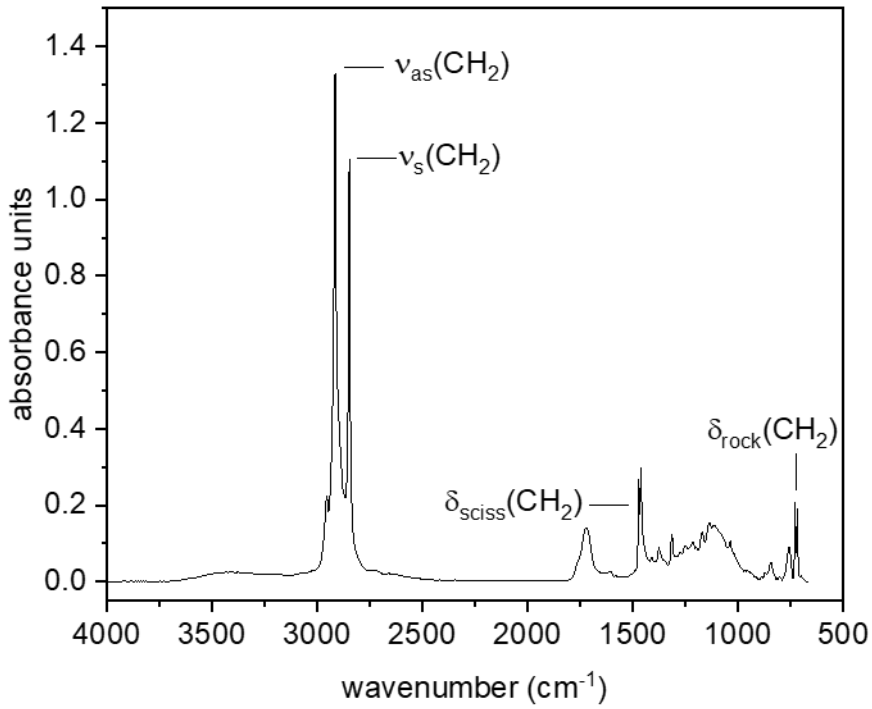

Figure 14 Plant cuticular wax of *Prunus laurocerasus* measured at 20°C using horizontal attenuated total reflectance Fourier-transform infrared spectroscopy showing the asymmetric ($\boldsymbol{\nu_{as}}$) and symmetric ($\boldsymbol{\nu_{s}}$) stretching, scissoring ($\boldsymbol{\delta_{sciss}}$) and rocking ($\boldsymbol{\delta_{rock}}$) mode of the methylene (CH_2) groups.

At room temperature, VLCAs in cuticular waxes are packed in an orthorhombic lattice (Riederer and Schneider, 1990; Reynhardt and Riederer, 1991). The methylene chains are in an all-trans conformation as depicted in Figure 15 I and can transition into a hexagonal state (Basson and Reynhardt, 1991; Reynhardt and Riederer, 1994). The hexagonal state is also known as the rotator-state. In this state, the chains are still in an all-trans conformation, but can rotate around their longitudinal axis (Reynhardt, 1985, 1997). The melting process can lead to a phase transition from all-trans to trans-gauche conformation (Figure 15 II) and so called “kinks” (Hastie and Roberts, 1994).

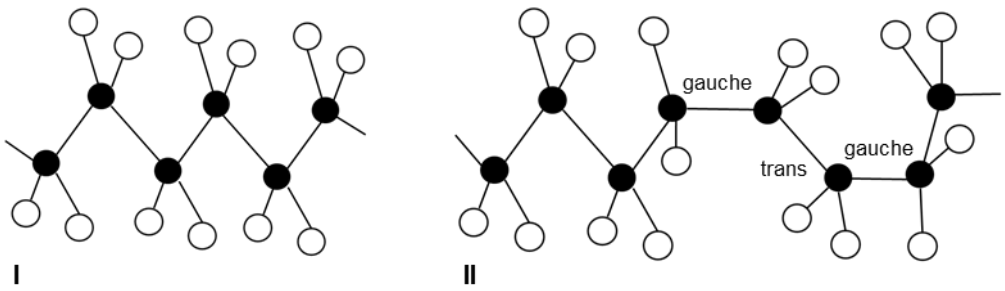

Figure 15 All-trans conformation of a polymethylene section (I) and gauche-trans conformation (II) according to Chapman and Goni (1986) and Hastie and Roberts (1994)

IR is a good method for the determination of the phase transition from orthorhombic to the molten state of plant cuticular waxes (Merk *et al.*, 1997; Merk, 1998). Thereby, the

shift of the asymmetric and symmetric stretching signals with increased temperature can be used to identify the melting range (5 % to 95% wavenumber change) and the midpoint of melting (inflection point). Aliphatic crystallinity can be calculated by using the rocking doublets of the methylene chains at 720 and 730 cm^{-1} (Zerbi *et al.*, 1989). Doublets associated with scissoring between 1470 and 1473 cm^{-1} are not feasible, as other vibrations of compounds within plant cuticular wax interfere with overlapping signals (Merk *et al.*, 1997). In samples containing amorphous and crystalline fractions, the signal at 720 cm^{-1} (I_a) can be assigned to the absorbance of the methylene units in the amorphous fraction whereas the crystalline fraction is equally represented by the doublets at 720 and 730 cm^{-1} (I_b). Therefore, we can assume that the intensity of the bond I_b is the sum of the amorphous (I_b^{am}) and the crystalline intensity (I_b^{cryst}) of signal b:

$$I_b = I_b^{cryst} + I_b^{am} \qquad \text{Equation 7}$$

For pure orthorhombic *n*-alkanes, Zerbi *et al.* (1989) reported a ratio of I_a to I_b^{cryst} of 1.233, due to a setting angle of 42° between planes of the transplanar C-C chain skeletons (Equation 8).

$$\frac{I_a}{I_b^{cryst}} = 1.233 \qquad \text{Equation 8}$$

Suitably normalization leads to the percentage of the amorphous (x_{am}) and crystalline (x_{cryst}) fraction:

$$x_{am}(\%) = 100\frac{I_b^{am}}{(I_a + I_b)} \qquad \text{Equation 9}$$

$$x_{cryst}(\%) = 100 - x_{am}$$
$$= 100 - 100\left[\frac{I_b - \frac{I_a}{1.233}}{I_a + I_b}\right] \qquad \text{Equation 10}$$

1.3.4 Differential scanning calorimetry

Differential scanning calorimetry (DSC) is a technique to measure the phase behaviour (melting, transitions etc.) of chemical compounds and determine parameters like heat capacity, enthalpy and transition temperatures (Höhne *et al.*, 2013). According to Höhne *et al.* (2013), DSC is "the measurement of the difference in heat flow rate to the sample and to a reference sample" as both samples get tempered. Endothermic transitions, *e.g.* melting, dehydrations, reduction reactions, and exothermic transitions, *e.g.* crystallization, oxidation, processes can be observed (Chiavaro, 2014). In general, but depending on the instrument used, endothermic events are plotted up while exothermic ones are plotted down. DSC is a valid method to observe phase transitions

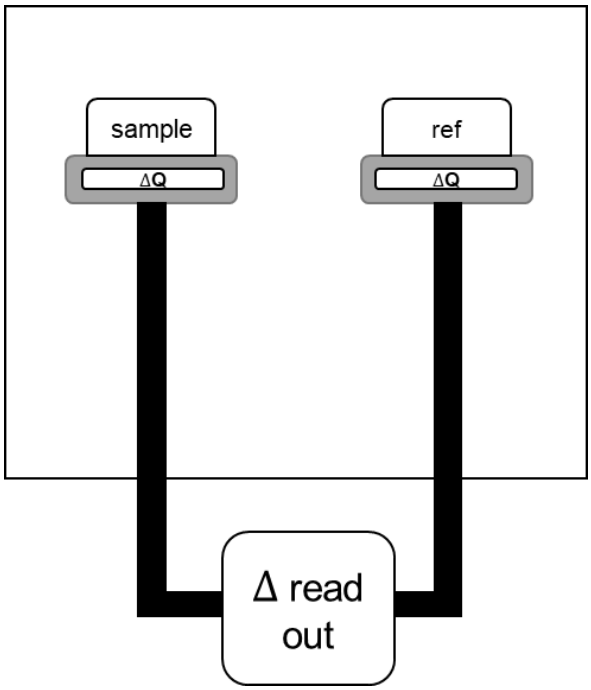

Figure 16 Concept of differential scanning calorimetry using a sample and reference sample (ref). Both crucibles are heated up (ΔQ) and the difference in heat flow is measured as read out.

in cuticular waxes and isolated cuticular membranes as has been reported by Luque and Heredia (1997) and several other authors (Eckl and Gruler, 1980; Aggarwal, 2001; Fagerström *et al.*, 2013b). DSC is also used to study the effects of adjuvants like alcohol ethoxylates and oil adjuvants on the wax melting behaviour (Reynhardt and Riederer, 1994; Coret and Chamel, 1994; Perkins *et al.*, 2005; Fagerström *et al.*, 2014; Webster *et al.*, 2018). Here, the addition of oil adjuvants, *e.g.* MeO, as well as some alcohol ethoxylates decreased the start (onset) and end (offset) of melting and the enthalpy of transition (EOT). Therefore, the authors assumed a plasticizing effect of the plant cuticular wax after adding the adjuvants.

It has been reported that the heating of cuticular wax results in a first phase transition from the orthorhombic lattice to the hexagonal phase (also known as rotator phase), following a melting process (Reynhardt and Riederer, 1994). These phase transitions can also overlap, making it difficult to determine the start and ending temperatures, as the orthorhombic structure can undergo the hexagonal phase transition just below the wax is fully molten (Reynhardt, 1986).

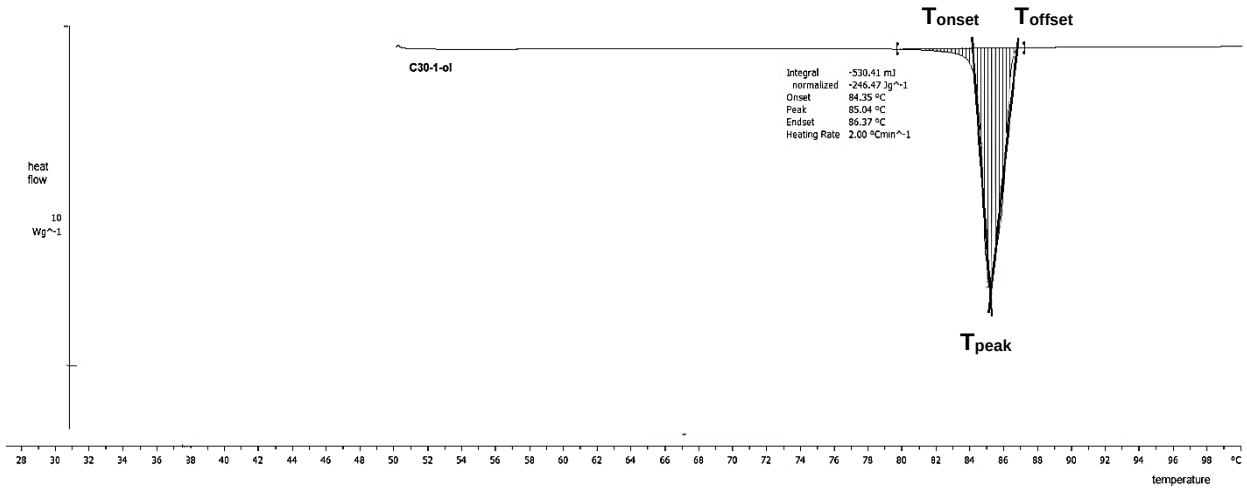

Figure 17 Determination of the onset (T_{onset}), offset (T_{offset}) and peak (T_{peak}) temperature

For DSC measurements, the solid wax samples are weighted into aluminium crucibles and are heated up together with a blank reference crucible (Figure 16). The difference in heat flow between the sample and the reference crucible is measured. Thermograms (heat flow *vs.* temperature) are observed for heating and cooling cycles. Integration of the peaks provides the EOT. Determination of the onset and offset temperatures are depicted in Figure 17. Tangents of the peak are applied to the extrapolated baseline and intersection temperatures are calculated delivering onset and offset temperatures.

1.3.5 Cuticular transpiration

The major function of the plant cuticle is to protect the plant from desiccation (Riederer and Schreiber, 2001). Water loss through stomata is of great relevance, but transpiration across the plant cuticle is also important, especially after stomata closure (Martin and Juniper, 1970). Similar to AI permeation, the transpiration across the cuticle is a diffusion process without any active transporters (Schönherr and Riederer, 1989). Water can take the lipophilic and to some extent also the hydrophilic pathway as it is a small, uncharged and polar molecule (Schreiber, 2005). Its diffusion is limited by crystalline wax domains similar to lipophilic AIs. Cuticular water permeability is highly correlated with cuticular permeability to lipophilic AIs (Niederl *et al.*, 1998; Schreiber, 2002) and also affected using penetration enhancers (Riederer and Schönherr, 1990; Räsch *et al.*, 2018). Furthermore, similar effects of wax extraction (Riederer and Schreiber, 2001) and temperature (Schreiber, 2001) have been found for water and lipophilic AIs.

Cuticular transpiration can be determined gravimetrically using isolated cuticles (Schreiber and Schönherr, 2009). Therefore, a cuticle is mounted on a cell of stainless steel, the physiological outer side facing the atmosphere. The cell is filled with water and placed in a box with silica gel to adjust a constant relative humidity (nearly zero) and driving force of transpiration (Burghardt and Riederer, 2003). The weight of the cells is measured over time. Cuticular transpiration can also be obtained by using leaf envelopes sealing the stomatous abaxial side of the leaf to prevent stomatal water loss (Schuster, 2016; Schuster *et al.*, 2017). Leaf envelopes are also placed in a box with silica gel and weight over time.

The transpiration rate (J) can be calculated from the difference of the fresh weight (leaf) or from the difference of the cell-weight between start and actual time (ΔW) over time (Δt) per area (A):

$$J = \frac{\Delta W}{\Delta t\ A} \qquad \text{Equation 11}$$

Permeance (P) is determined dividing the transpiration rate (J) by the product of the water vapor saturation concentration ${c^*}_{\mathrm{WV}}$ and the difference between water activity of the air (a_{air}) and in the cell or leaf ($a_{\mathrm{cuticle/leaf}}$):

$$P = \frac{J}{c^*_{\mathrm{WV}} \cdot (a_{\mathrm{cuticle/leaf}} - a_{air})}$$ Equation 12

Water vapor saturation concentration c^*_{WV} can be taken from literature (Nobel, 2009) and amounted to 23.07 g m^{-3} at 25°C. Water activity of the air a_{air} over silica is nearly zero (Slavík and Jarvis, 1974) while the water activity in the cell or leaf $a_{\mathrm{cuticle/leaf}}$ is assumed to be unity (Burghardt and Riederer, 2003).

1.3.6 Contact angle measurement

When a droplet is applied to a solid surface, *e.g.* the plant cuticle, the droplet can wet the surface which can be measured using the contact angle (CA) (Koch *et al.*, 2008). CAs from 0° to 10° represent superhydrophilic surfaces, angles between 10° and 90° indicate hydrophilic ones, being easy to wet (Koch *et al.*, 2008). Hydrophobic surfaces

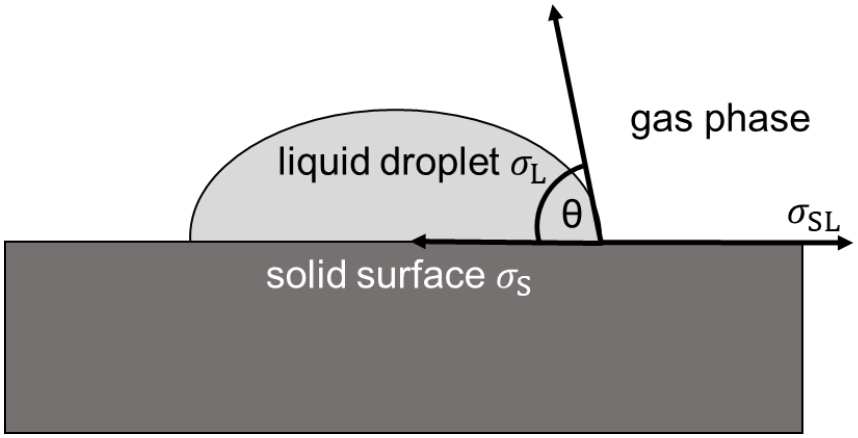

Figure 18 Scheme of a droplet applied on a solid surface for determination of the contact angle ($\boldsymbol{\theta}$) using the surface energy of the soli-liquid interface ($\boldsymbol{\sigma_{SL}}$), the surface energy of the solid ($\boldsymbol{\sigma_S}$) and surface tension of the liquid tangential to droplet the surface ($\boldsymbol{\sigma_L}$)

are indicated by contact angles between 90° and 150° whereas superhydrophobic ones show contact angles above 150°. The CA is dependent on the surface tension of the applied solution, the ambient vapour and the solid surface. The surface structure determines the behaviour of a liquid applied onto a solid surface. Young's equation (Equation 14) can be used to describe the CA and describes a static equilibrium state (Figure 18). Subtracting the surface energy of the solid-liquid interface (σ_{SL}) from the surface energy of the solid (σ_S) and dividing the difference by the surface tension of the liquid tangential to the droplet surface (σ_L) yields the $cos\ \theta_C$ (Equation 13).

$$cos\ \theta_C = \frac{\sigma_S - \sigma_{SL}}{\sigma_L} \qquad \text{Equation 14}$$

In agrochemistry, surfactants are added to a formulation to increase *i.a.* the wetting of the leaf surface (Hazen, 2000). Therefore, the so called 'wetter' is applied to decrease the surface energy of the liquid which is applied onto the leaf surface. The contact angle decreases, allowing the droplet to flatten on the surface and being less spherical than a droplet without surfactant. The droplet can spread under specific conditions and cover a larger area on the leaf surface than applied without the adjuvant.

1.4 Motivation and objectives of this work

As the uptake process of the AI into the plant is directly related to bioefficacy, formulations including adjuvants are used to optimize this process. Spraying of the formulation onto the plant provokes an interaction with the plant cuticle as outermost surface of the plant. This process can be uncoupled into three main interactions:

1) interaction of the AI with the plant cuticle/plant cuticular waxes
2) interaction of the adjuvant with the plant cuticle/plant cuticular waxes
3) interaction of the AI with the adjuvant on the plant cuticle.

The interaction of the AI with the plant cuticle (process 1) has been extensively studied by several authors using a wide range of species, AIs and organic model compounds (Riederer and Schönherr, 1984; Kerler and Schönherr, 1988b; Schreiber *et al.*, 1995; Stammitti *et al.*, 1995; Baur *et al.*, 1996b; Kirsch *et al.*, 1997; Niederl *et al.*, 1998; Popp *et al.*, 2005; Remus-Emsermann *et al.*, 2011). The waxes have been termed as the major permeation barrier to lipophilic solutes, but it is still unclear how exactly the barrier is built in terms of wax composition (Riederer and Schönherr, 1985; Kerler and Schönherr, 1988b). The interaction of the adjuvant with the plant cuticle/cuticular waxes (process 2) was also characterized by several authors (Gauvrit and Dufour, 1990; Abbott *et al.*, 1990; Wirth *et al.*, 1991; Perkins *et al.*, 2005; Grant *et al.*, 2008; Ryckaert *et al.*, 2008; Lavieille *et al.*, 2009; Xu *et al.*, 2011; W.A. Forster *et al.*, 2012; Fagerström *et al.*, 2014; Chiu *et al.*, 2016). Plasticization or softening of the plant cuticular wax after application of adjuvants like alcohol ethoxylates have been discussed as an explanation of enhanced permeation of AIs. However, no direct evidence for the proposed softening effect exists as *e.g.* investigations of wax crystallinity. Previous studies determined melting temperatures and melting enthalpies using DSC (Coret and Chamel, 1994; Perkins *et al.*, 2005; Zhang *et al.*, 2016; Webster *et al.*, 2018), also hyperfine splittings using ESR (Schreiber *et al.*, 1996) and second moments of ^{2}H-NMR spectra (Schreiber *et al.*, 1997), but direct proof of decreased crystallinity has been only found in the study by Zhang *et al.* (2016) using XRD. Enhanced permeation of the AI across the cuticle is provoked due to the interaction of the AI and the adjuvant both applied onto the plant cuticle (process 3). Penetration of the AI increased after application of adjuvants, due to the interaction of both compounds within the cuticle (Schönherr, 1993b, 1993a; Riederer *et al.*, 1995; Baur *et*

al., 1997b; Burghardt *et al.*, 1998; Petracek *et al.*, 1998; Baur *et al.*, 1999b; Shi *et al.*, 2005; Fagerström *et al.*, 2013a).

This thesis dealt with the three interactions described above and had two main objectives:

i) elucidate the permeation barrier of the plant cuticle to AIs in terms of the different wax fractions and

ii) holistically investigate the modification of this barrier using selected oil and surface active adjuvants, an aliphatic leaf wax and an artificial model wax to get a better understanding of the mode of action of the adjuvants.

The actual uptake barrier within the cuticular wax that limits AI permeation should be elucidated (chapter 1) building the base for further investigations on adjuvant-cuticle (chapter 2) and AI-adjuvant interaction (chapter 3). Chapter 2 mainly focused on the phase behaviour and cuticular wax crystallinity while the interaction between AI and adjuvant was studied simulating foliar penetration. Two adjuvant classes were selected: oil adjuvants and non-ionic alcohol ethoxylates (C10E2, C10E5 and C10E8). The adjuvants were used for chapter 2 and 3 while azoxystrobin, theobromine and caffeine served as organic solutes to elucidate the permeation barrier in chapter 1.

1.5 List of chemicals

Table 1 List of chemicals used in chapter 1 to 3

compound	purity (%)	chemical Name	CAS	molecular weight (g mol^{-1})	log K_{OW}[a]	HLB[c]	company
azoxystrobin	97.0	methyl (E)-2-[2-[6-(2-cyanophenoxy)pyrimidin-4-yl]oxyphenyl]-3-methoxyprop-2-enoate	131860-33-8	403.394	2.5	N.D.[a]	Syngenta Crop Protection AG (Münchwilen, Switzerland)
caffeine	> 98	1,3,7-trimethylpurine-2,6-dione	58-08-2	194.194	-0.07	N.D.[a]	Sigma-Aldrich Chemie GmbH (Steinheim, Germany)
theobromine	> 98	3,7-dimethylpurine-2,6-dione	83-67-0	180.167	-0.78	N.D.[a]	Sigma-Aldrich Chemie GmbH (Steinheim, Germany)
methy oleate	99.0	methyl (Z)-octadec-9-enoate	112-62-9	296.495	7.45	N.D.[a]	Sigma-Aldrich Chemie GmbH (Steinheim, Germany)
methyl linolenate	99.0	methyl (9Z,12Z,15Z)-octadeca-9,12,15-trienoate	7361-80-0	292.463	6.92	N.D.[a]	Sigma-Aldrich Chemie GmbH (Steinheim, Germany)
methyl stearate	99.0	methyl octadecanoate	112-61-8	298.511	8.35	N.D.[a]	Sigma-Aldrich Chemie GmbH (Steinheim, Germany)
oleic acid	99.0	(Z)-octadec-9-enoic acid	112-80-1	282.468	7.64	N.D.[a]	Sigma-Aldrich Chemie GmbH (Steinheim, Germany)
C10E2	> 98	diethylene glycol monodecyl ether	3055-93-4	274.445	4.22	10	Sigma-Aldrich Chemie GmbH (Steinheim, Germany)
C10E5	> 98	pentaethylene glycol monodecyl ether	23244-49-7	378.55	2.42	13	Sigma-Aldrich Chemie GmbH (Steinheim, Germany)

C10E8	> 98	octaethylene glycol monodecyl ether	24233-81-6	510.709	1.59	15	Sigma-Aldrich Chemie GmbH (Steinheim, Germany)
chloroform	> 98	trichloromethane	67-66-3	119.369	1.97	N.D.[a]	Carl Roth GmbH + Co. KG (Karlsruhe, Germany)
methanol	> 98	methyl alcohol	67-56-1	32.042	-0.77	N.D.[a]	Carl Roth GmbH + Co. KG (Karlsruhe, Germany)
n-tetracosane	99.0	*n*-tetracosane	646-31-1	338.664	12.13	N.D.[a]	Sigma-Aldrich Chemie GmbH (Steinheim, Germany)
n-hentriacontane	99.0	*n*-hentriacontane	630-04-6	436.853	15.57	N.D.[a]	Sigma-Aldrich Chemie GmbH (Steinheim, Germany)
n-nonacosane	99.0	*n*-nonacosane	630-03-5	408.799	14.6	N.D.[a]	Sigma-Aldrich Chemie GmbH (Steinheim, Germany)
1-triacontanol	> 98.0	1-triacontanol	593-50-0	438.825	N.D.[b]	N.D.[a]	Sigma-Aldrich Chemie GmbH (Steinheim, Germany)
1-dotriacontanol	90.0	1-dotriacontanol	6624-79-9	466.879	N.D.[b]	N.D.[a]	INDOFINE Chemical Company, Inc. (Hillsborough, USA)
cellulase	N.D.[a]	N.D.[a]	N.D.[a]	N.D.[a]	N.D.[b]	N.D.[a]	NCBE, University of Reading, (Reading, United Kingdom)
Pectinase Trenolin Super DF	N.D.[a]	N.D.[a]	N.D.[a]	N.D.[a]	N.D.[b]	N.D.[a]	ERBSLÖH AG (Geisenheim, Germany)
citric acid monohydrate	> 97.0	2-hydroxypropane-1,2,3-tricarboxylic acid;hydrate	5949-29-1	210.138	N.D.[b]	N.D.[a]	AppliChem GmbH (Darmstadt, Germany)
sodium azide	N.D.[a]	sodium azide	26628-22-8	65.01	N.D.[b]	N.D.[a]	Sigma-Aldrich Chemie GmbH (Steinheim, Germany)
BSTFA - *N,O*-Bis-(trimethylsilyl) trifluoroacetamide		trimethylsilyl 2,2,2-trifluoro-N-trimethylsilylethanimidate	25561-30-2	257.403	N.D.[b]	N.D.[a]	Macherey-Nagel GmbH & Co. KG, (Düren, Germany)
water LC-MS grade	99.9	water	7732-18-5	18.015	-1.3	N.D.[a]	Biosolve BV

							(Valkenswaard, The Netherlands)
acetonitrile LC-MS grade	99.9	acetonitrile	75-05-8	41.053	N.D.[b]	N.D.[a]	Biosolve BV (Valkenswaard, The Netherlands)
formic acid	99.9	formic acid	64-18-6	46.025	-0.54	N.D.[a]	Biosolve BV (Valkenswaard, The Netherlands)
methanol LC-MS grade	99.9	methyl alcohol	67-56-1	32.042	-0.77	N.D.[a]	Biosolve BV (Valkenswaard, The Netherlands)
pyridine	99.9	pyridine	110-86-1	79.102	N.D.[b]	N.D.[a]	Carl Roth GmbH + Co. KG (Karlsruhe, Germany)

[a] Values taken from the EPI Suite™ v4.11 (United States Environmental Protection Agency, Washington, DC, USA)

[b] N.D. – not declared

[c] calculated according to Griffin (1954)

2 Chapter 1: Aliphatic or cyclic compounds: what is the permeation barrier of the plant cuticle to organic solutes?

This chapter is based on the following publication.

Staiger S, Seufert P, Arand K, Burghardt M, Popp C, Riederer M. (2019). The permeation barrier of plant cuticles: uptake of active ingredients is limited by very long-chain aliphatic rather than cyclic wax compounds. *Pest Management Science* (doi: 10.1002/ps.5589)

Statement of individual author contributions and of legal second publication rights

	Publication (complete reference): **Staiger S, Seufert P, Arand K, Burghardt M, Popp C, Riederer M.** (2019). The permeation barrier of plant cuticles: uptake of active ingredients is limited by very long-chain aliphatic rather than cyclic wax compounds. *Pest Management Science* (doi: 10.1002/ps.5589)

Participated in	**Author Initials,** Responsibility decreasing from left to right					
Study Design	K.A.	S.S.	P.S.	M.R.	C.P.	M.B.
Methods Development	S.S.	P.S.	K.A.	M.R.	C.P.	M.B.
Data Collection	S.S.	P.S.	K.A.	M.R	C.P.	M.B.
Data Analysis and Interpretation	S.S.	P.S.	K.A.	M.R	M.B.	C.P.
Manuscript Writing	S.S.	P.S.	K.A.	M.B.	C.P.	M.R.
Writing of Introduction	S.S	P.S.	K.A.	M.B.	C.P.	M.R.
Writing of Materials & Methods	S.S	P.S.	K.A.	M.B.	C.P.	M.R.
Writing of Discussion	S.S	P.S.	K.A.	M.B.	C.P.	M.R.
Writing of First Draft	S.S	P.S.	K.A.	M.B.	C.P.	M.R.

Explanations:

Tables and figures except Figure 20, Table 4, Figure 25 and Figure 26 are also illustrated in the publication, but without data for caffeine. Infrared data was not included in the publication. The co-first author Pascal Seufert will not use the published results in his doctoral thesis.

The doctoral researcher confirms that she has obtained permission from both the publishers and the co-authors for legal second publication.

The doctoral researcher and the primary supervisor confirm the correctness of the above mentioned assessment.

Simona Staiger		Würzburg	
Doctoral Researcher's Name	Date	Place	Signature
Markus Riederer		Würzburg	
Primary Supervisor's Name	Date	Place	Signature

2.1 Introduction

2.1.1 *Prunus laurocerasus* and *Garcinia xanthochymus* as model plants

To measure cuticular permeability, isolation of the cuticular membrane was a prerequisite. It is well known that enzymatic isolation does not affect cuticular permeability in comparison to intact membranes on the leaf (Kirsch *et al.*, 1997), but it is limited to a small amount of species. It was reported that enzymatic isolation is only feasible when a continuous pectinaceous layer is present (Buchholz, 2006). In former studies, scientists primarily used isolated cuticles of *Citrus aurantium (Kerler and Schönherr, 1988b; Bauer and Schönherr, 1992; Baur et al., 1996a; Baur et al., 1997a), Prunus laurocerasus* (Schreiber *et al.*, 1995; Stammitti *et al.*, 1995; Kirsch *et al.*, 1997; Baur *et al.*, 1997a; Gutenberger *et al.*, 2013; Arand *et al.*, 2018) and *Hedera helix* (Baur *et al.*, 1997a; Popp *et al.*, 2005; Arand *et al.*, 2010) for transport experiments. These experiments require intact isolated cuticles with no stomatal pores. Therefore, only the stomata-free adaxial cuticular membrane of the leaf can be used. In agricultural industry, crops like *Poaceae* are of great interest as they are an important sector in farming. However, these species are not feasible for cuticular isolation, as they have stomata on both sides of the leaf (Orgell, 1955; Oosterhuis and Walker, 1987). To study the influence of aliphatic and cyclic wax compounds on the permeation barrier properties of the cuticle, the two model plants *Prunus laurocerasus* (cherry laurel) and *Garcina xanthochymus* (Mysore Gamboge) were used. Both species match the criteria of having a non-stomatal adaxial leaf surface, and enzymatic isolation was feasible. *P. laurocerasus* was chosen as a species with a high proportion of cyclic compounds within cuticular wax. *G. xanthochymus* was selected due to its high proportion of VLCAs and low content of cyclic content. Both species are evergreen species. *P. laurocerasus* is native in temperate Asia and Southeastern Europe while *G. xanthochymus* is native in temperate Asia and also tropical Asia (USDA, 2019).

2.1.2 Azoxystrobin, caffeine and theobromine as model compounds

This work was focused on three organic solutes (Figure 19) differing in lipophilicity: azoxystrobin (log $K_{O/W}$ 2.5, Turner, 2018), caffeine (log K_{OW} -0.07; Hansch *et al.*, 1995) and theobromine (log K_{OW} -0.78; Hansch *et al.*, 1995).

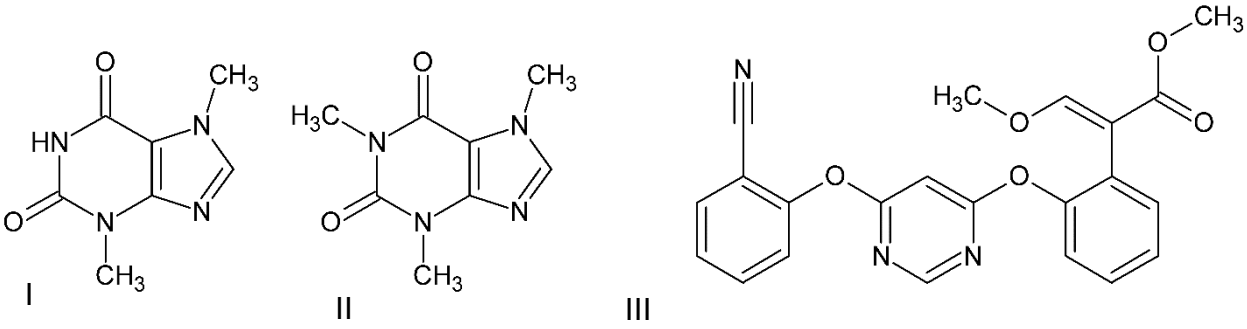

Figure 19 Chemical structure of theobromine (I), caffeine (II) and azoxystrobin (III)

Theobromine (Figure 19 I) belongs to the class of methylxanthines, representing hydrophilic AIs (Fredholm, 2010). It is the prevalent purine alkaloid in seeds of *Theobroma cacao* (cocoa). Its detection by UHPLC-MS is feasible, as well as its non-toxicity.

Caffeine (Figure 19 II) is a semi-hydrophilic compound also belonging to the class of methylxanthines (Fredholm, 2010). It is mostly extracted from the plant *Coffea arabica* (coffee) and was selected as model compound representing semi-hydrophilic AIs. It can be easily detected by UHPLC-MS and has a water solubility of 20 g L^{-1} (Sigma-Aldrich, 2019b). It is non-toxic and therefore a convenient model compound for permeation studies.

Azoxystrobin (Figure 19 III) was chosen as a model compound for lipophilic AIs. It is a broad-spectrum, systemic fungicide which is commonly used in agriculture (Mastovska, 2019). Azoxystrobin belongs to the class of methoxyacrylates which are derived from the strobilurins (Stenersen, 2004). This class inhibits the electron transfer from cytochrome b to cytochrome c_1 in the mitochondrial membrane of the fungi. Azoxystrobin has a low water solubility of 6 mg L^{-1} (Mastovska, 2019). It is used against powdery mildews in cereals and grapes, but also against downy mildew and late blight and early blight in potatoes (Paranjape *et al.*, 2014)

2.1.3 Objectives and research questions

After applying formulations on the field, the AI is exposed to the cuticle. Systemic AIs, which need to be distributed within the whole plant, need to permeate across the cuticle and into the subjacent plant tissue (Robertson *et al.*, 1971). Only then can AIs reach the right target site and act properly against pests. Looking at the uptake process, diffusion across the cuticle is an important step. Therefore, it is of great importance to understand cuticular permeation properties in detail. It is well-known that cuticular waxes build the major permeation barrier of the cuticle to organic solutes (Riederer and Schönherr, 1985; Kerler and Schönherr, 1988b) and to water (Schönherr, 1976). Vogg *et al.* (2004) assumed that VLCA waxes constitute the major barrier to water, whereas triterpenoids are of minor importance. Studies concerning the influence of different wax fractions on the cuticular permeability have only focused on transpiration while studies on organic solutes have been lacking so far. Consequently, the objective of this work was to study the influence of VLCAs and triterpenoids on the cuticular permeation barrier to organic solutes. A study was designed to observe the interaction of the AI with the plant cuticle with a special focus on the wax fractions. The constitution of the cuticular barrier to organic solutes with two evergreen species and different VLCA/triterpenoid proportions was investigated. Therefore, a method to selectively extract the cyclic wax fractions of isolated cuticles was developed using methanol and chloroform. The morphologies of the membranes before and after solvent extraction were examined using scanning electron microscopy (SEM). Transport experiments to determine permeation of three organic solutes differing in lipophilicity were conducted using the solvent extracted and native cuticles. Aliphatic crystallinity of the cuticular wax was determined by Fourier-transform infrared spectroscopy (FTIR).

2.2 Materials and Methods

2.2.1 Chemicals

Isolation of cuticular membranes was done using cellulose, pectinase, citric acid monohydrate and sodium azide (Table 1). Chloroform and methanol were selected for extraction of cuticular membranes. *N*-tetracosane (C24) was used as internal standard for wax analysis. Derivatization was done using *N,O*-Bis-(trimethylsilyl) trifluoroacetamide (BSTFA). Permeation experiments were conducted using the lipophilic fungicide azoxystrobin (log K_{OW} 2.5) and the alkaloids caffeine (log K_{OW} -0.07) and theobromine (log K_{OW} -0.78, Table 1). Caffeine was chosen as a model compound representing semi-hydrophilic AIs while theobromine was selected to represent hydrophilic ones. Permeation experiments were conducted using high-purity water (Millipore Milli-Q Gradient Water Purification System, Burlington, USA).

2.2.2 Preparation of leaf cuticular membranes

Leaves of *Prunus laurocerasus cv.* Herbergii (laurel cherry) and *Garcinia xanthochymus* (Mysore Gamboge) were harvested at the Botanical Garden of the University of Würzburg, Germany. Cuticular membranes (CM) were isolated enzymatically according to the method of Schönherr and Riederer (1986), using the adaxial and non-stomatous side of the leaf. Discs were punched out of fully expanded leaves by a cork borer and put in a solution of 1 % (*v/v*) cellulase, 1 % (*v/v*) pectinase, 1 mM sodium azide and 20 mM citric buffer. After isolation, CM were stored in demineralized water at room temperature until further use.

Dewaxed cuticles (MX) were prepared by extracting CM with 5 mL of chloroform for 30 min. Extraction of CM with methanol (5 mL) for 20 h was done to receive membranes without triterpenoids referred to as M. Successful extraction of triterpenoids using methanol was checked by treating M subsequently with chloroform. After extraction, the membranes were stored in demineralized water until further use. To study the extraction behaviour of a *P. laurocerasus* leaf with methanol in comparison to an isolated cuticle, the adaxial side of the leaf was treated with methanol for 30 s. The wax extracts were evaporated under a flow of nitrogen and stored at room temperature.

2.2.3 Cuticular wax analysis *via* GC-FID and GC-MS

C24 was dissolved in chloroform and added to the wax extracts as an internal standard. The solvent was evaporated under a flow of nitrogen. Derivatization with 10 µL pyridine and 10 µL BSTFA was done at 70 C for 30 min (Pierce Reacti-Therm heating module, Pierce chemical, Dallas, USA). Afterwards, the mixture was dissolved in chloroform and used for gas chromatography.

Identification of wax compounds was done using gas chromatography mass spectrometry (GC-MS; 6890N, GC System; Agilent Technologies, Santa Clara, USA) with Helium as a carrier gas. A mass spectrometric detector (m/z 50-750, MSD 5977A, Agilent Technologies) was used. On-column injection at 50 C with a capillary column (30 m x 0.32 mm, DB-1, 0.1 µm film: J&W Scientific, Agilent Technologies) was applied. Temperature of the column was held at 50°C for 2 min after injection. The temperature was raised to 200°C with a heating rate of 40 C min^{-1} and held at 200 C for 2 min. Subsequently, the temperature was increased to 320°C (heating rate: 3 ° C min^{-1}) and held for 30 min Identification was done using Wiley 10th/NIST 2014 mass spectral library (W10N14; John Wiley & Sons, Hoboken, New Jersey), reference specimen or spectra interpretation. Quantification of wax compounds was done using GC flame ionization detection (GC-FID, 6850N, GC System; Agilent Technologies). Same gas chromatographic conditions as before were used to separate compounds except that hydrogen gas was selected as the carrier gas.

2.2.4 Determination of the permeance of theobromine, caffeine and azoxystrobin *via* transport chambers and UHPLC-MS

Two half-cells made of stainless steel with sampling port were used for permeation experiments. Membranes were mounted between donor and receiver compartment that the physiological outer side of the membranes were orientated towards the donor compartment. The interface between membrane and cell was sealed with Teflon paste (Roth, Karlsruhe, Germany). Cells were sealed with adhesive tape (Beiersdorf, Hamburg, Germany).

One mL of an aqueous solution of caffeine (2000 µg mL^{-1}) was applied to the donor compartment. The receiver compartment was filled with one mL of high-purity water. Subsequently, the sampling ports were sealed with adhesive tape (Beiersdorf). To provide constant circulation, the chambers were placed on a Rotamax 120 (Heidolph Instruments, Schwabach, Germany) with a rotational speed of 50 rpm. Temperature was held at 25 ± 0.1°C using a Peltier-cooled incubator IPP110 (Memmert, Schwabach, Germany). At different time intervals (2 to 24 h), 30 µL aliquots were withdrawn from the receiver compartment and replaced by 30 µL purified water. Aliquots were analyzed by ultra-high performance liquid chromatography coupled with mass spectrometry (UHPLC-MS, ACQUITY H-Class system with QDa detector, Waters, Eschborn, Germany).

Same experiment was done using an aqueous solution of theobromine (100 µg L^{-1}) in the donor compartment. Due to low water solubility of axozystrobin, the following procedure was carried out: A reservoir of azoxystrobin was obtained by pipetting 100 µL of a solution of azoxystrobin in acetonitrile (10000 µg mL^{-1}) into the donor cell. Nitrogen gas was used to evaporate the solvent. This procedure was done to obtain a constantly saturated azoxystrobin solution in the donor compartment. The concentration of azoxystrobin in the donor solution was assumed to be steady, as new azoxystrobin could dissolve into the donor from solid azoxystrobin after permeating across the membrane into the receiver compartment. The membrane was mounted between donor and receiver cell as described before. Cells were sealed with adhesive tape (Beiersdorf) and one mL of high-purity water was applied to donor and receiver compartment. Permeances of theobromine, caffeine and azoxystrobin were determined for CM, M and MX using Equation 5. The concentration in the receiver was nearly zero, while concentration in the donor was determined by UHPLC-MS before removing aliquots from the receiver. For azoxystrobin, Δc was calculated by using the

concentration difference of the saturated donor compartment to the receiver compartment. Therefore, three separate donor cells with saturated azoxystrobin solution were prepared, as described previously. A 100 µL aliquot was removed from the upper solution of the donor compartment, filtrated and diluted. Concentration was determined by UHPLC-MS.

UHPLC-MS analysis

An UHPLC-MS (Waters) was used to identify and quantify organic solutes. A sample volume of 2 µL was injected on a Luna Omega C18 Polar column (particle size 1.6 µm, 50 mm x 2.1 mm, Phenomenex, Aschaffenburg, Germany). Column temperature was set at 35 C while the autosampler (Acquity Flow Through Needle, Waters) was held at 25°C. Initial UHPLC gradient proportion was 97 % formic acid (0.1 %, *v*/*v*) and 3 % acetonitrile with a flow rate of 0.5 mL min^{-1}. After 1.2 min, the amount of formic acid was reduced linearly to 10 % while the proportion of acetonitrile was increased to 90 %. This was held until 1.5 min and initial gradient was reached after 2.2 min. Column was equilibrated with initial gradient until 2.8 min. Prefilter (KrudKatcher ULTRA HPLC In-Line filter 0.5µm depth filter x 0.004in ID, Phenomenex) and precolumn (Security Guard ULTRA Cartridges, UHPLC fully porous C18 and SecurityGuard ULTRA Holder, Phenomenex) were applied.

Electrospray ionization (ESI) was applied using a QDa detector (Waters) in positive mode. Ions with mass of 404 (azoxystrobin), 181 (theobromine) and 195 (caffeine) were detected in Single Ion Recording mode. Sampling frequency was held at 15 Hz. ESI probe temperature was adjusted to 600°C. Capillary voltage was set to 0.8 kV. Cone voltage was held at 20 V. Calibration in the range of 0.001 to 1.0 µg mL^{-1} was done using standard solutions of azoxystrobin, theobromine and caffeine in purified water. Coefficients of determination were greater than 0.997.

2.2.5 Infrared spectroscopy

A Fourier-transform infrared spectrometer (FTIR, Bruker Tensor 27 with BIO-ATR II® unit, Bruker, Ettlingen, Germany) was used for spectra recording in horizontal attenuated total reflection mode (h-ATR). The BIO-ATR II® unit comprised a silicon/ZnSe crystal covered by a stainless-steel envelope. Wax solution of extracted cuticular wax (2.2.2) in chloroform (dry weight of ca. 200 µg) was deposited on the crystal. The crystal was heated up to 90°C to ensure that chloroform was fully evaporated. For FTIR measurement, the crystal was cooled down to 20°C. The infrared spectra were recorded in wavenumber range of 4000 to 670 cm^{-1} at 20°C. Temperature was adjusted by connecting the envelope to water circuit of a thermostat (Thermo Scientific Haake DC30-K20, Karlsruhe, Germany). The BIO-ATR II® unit was purged with dry CO_2-free air (K-MT-LAB 3, Parker Hannifin, Kaarst, Germany). Resolution was set to 2 cm^{-1} with an acquisition time of 120 scans. OPUS 7 software (Bruker) was used to analyse spectra and to control the spectrometer and thermostat. Baseline adjustment was done before smoothing the spectrum. For determination of crystallinity according to Equation 11, spectra were recorded for three samples (n = 3) and OriginPro 2019 (OriginLab, Northampton, USA) was used for Gaussian deconvolution of the two rocking bands at 720 and 730 cm^{-1} to determine maximum intensities.

2.2.6 Scanning electron microscopy

Morphological investigation of the upper side of CM, M and MX was done using scanning electron microscopy (SEM, JEOL JSM-7500F, JEOL GmbH, Freising, Germany). The instrument was equipped with a field emission gun, LEI and SEI detectors. Small pieces of air-dried membranes (ca. 1 mm^2) were placed on aluminum stubs using double-sided adhesive tape. The stubs were sputter-coated with 10 nm to 15 nm gold-palladium (150 s, 25 mA, partial argon pressure 0.05 mbar, SCD005 sputter coater, Bal-Tec, Pfäffikon, Switzerland). Acceleration voltage was set at 5 kV and working distance at 10 mm.

2.2.7 Statistics

Statistical analysis was done using RStudio 2016 (RStudio, Boston, MR, USA) and OriginPro 2019 (OriginLab). Outliers were removed according to the method of the interquartile range. Permeance data did not show normality according to Shapiro-Wilk test ($p < 0.1$). Lognormal transformation of the permeance did not result in normality. Therefore, non-parametric statistical analysis was used to examine the permeance data without transformation. Kruskal-Wallis ANOVA with post-hoc Dunn's test ($p < 0.05$) was selected to detect significant differences between CM, M and MX of one compound and species. Due to non-normality, median values (25^{th} and 75^{th} percentile) instead of mean values (standard deviation) were used in this study and for calculation of the effect of wax extraction. Normality and variance homogeneity (Levene's test, $p < 0.1$) was given for wax data. T-test ($p < 0.05$) was conducted to detect statistically significant difference between pure chloroform extract and combined methanol and chloroform extract. Aliphatic crystallinity according to Zerbi *et al.* (1989) showed normality (Shapiro-Wilk test $p < 0.1$) and variance homogeneity (Levene's test, $p < 0.1$). Therefore, a two-sided t-test ($p < 0.05$) was selected to observe significant differences between the aliphatic crystallinity of *P. laurocerasus* and *G. xanthochymus*.

2.3 Results

2.3.1 Wax extraction

Adaxial cuticular wax of *G. xanthochymus* mainly consisted of VLCAs (97 % of total wax, Table 2, Figure 20). Chain lengths of VLCAs ranged between C29 and C36. *N*-Alkanes were the major fraction of VLCAs (77 % of VLCAs), followed by 23 % of alcohols. Tritriacontane and hentriacontane were the major compounds found in alkanes. The primary alcohols in the wax of *G. xanthochymus* were mainly composed of 1- tetratriacontanol (10 %). Cyclic compounds were a minor fraction found in wax of *G. xanthochymus*. They amounted 3 % of the total wax and consisted of sterols, tocopherols and triterpenoids. VLCAs yielded 6.00 ± 0.03 µg cm^{-2}.

Table 2 Composition of the cuticular waxes of *Garcinia xanthochymus* and *Prunus laurocerasus* determined by combined selective extracts of methanol and chloroform[a,b]

compound classes	*Garcinia xanthochymus*	*Prunus laurocerasus*
fatty acids	N.D.[b]	0.17 ± 0.10
primary alcohols	1.39 ± 0.01	1.33 ± 0.41
n-alkanes	4.60 ± 0.04	4.99 ± 0.17
alkyl esters	N.D. [b]	0.97 ± 0.003
methyl ester	N.D. [b]	0.02 ± 0.003
sterols	0.04 ± 0.002	N.D. [b]
tocopherols	0.04 ± 0.02	0.011 ± 0.011
triterpenoids	0.08 ± 0.003	53.26 ± 3.21
not identified	0.77 ± 0.05	4.11 ± 1.01
total	6.15 ± 0.05	60.76 ± 2.74

[a] Data is given as means ± standard deviations (µg cm^{-2}; n = 4).

[b] N.D - not detected

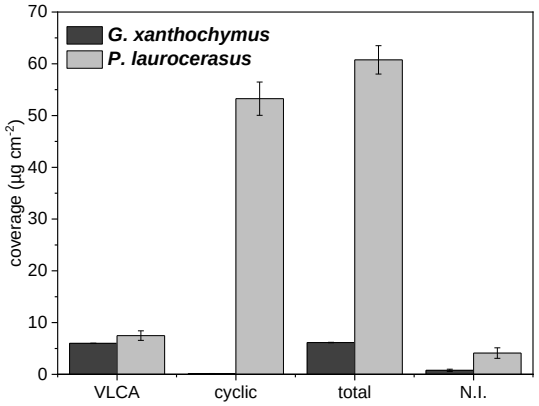

Figure 20 Very long-chain aliphatic (VLCA) and cyclic wax coverage of adaxial leaf cuticles of *Garcinia xanthochymus* and *Prunus laurocerasus* grouped by very long-chain aliphatic compounds (VLCA), cyclic compounds (cyclic), total wax amount (total) and not identifiable compounds (N.I.). Error bars represent standard deviation (n = 4).

Triterpenoids built the major fraction of adaxial cuticular wax of *P. laurocerasus* (Table 2, Figure 20). Ursolic acid as the major triterpenoid amounted to 75 % of the total wax. VLCAs yielded 12 % of the total wax with compounds ranging from C_{20} to C_{50}. *N*-Alkanes comprised 67 % of VLCAs, mainly consisting of nonacosane and hentriacontane.

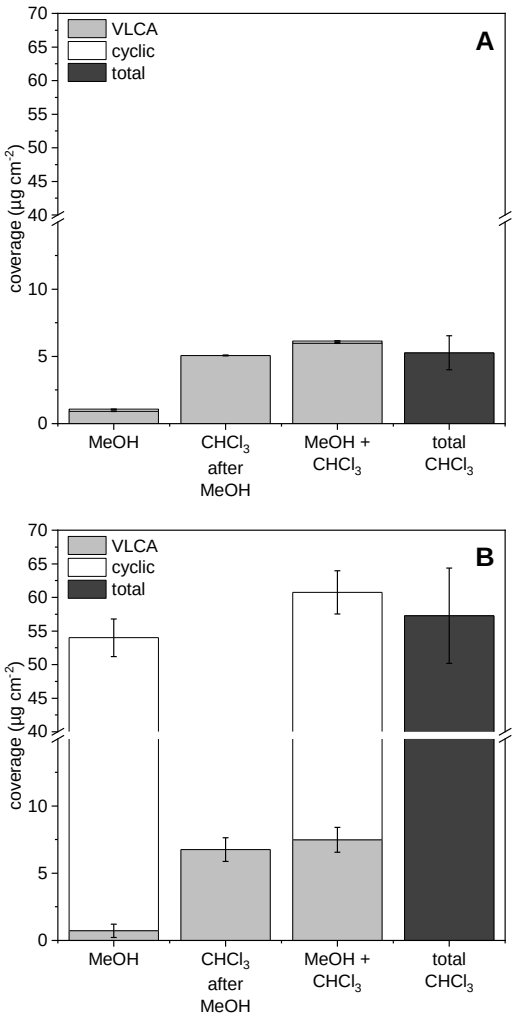

Figure 21 Wax fractions of methanol (MeOH), subsequent chloroform extract ($CHCl_3$ after MeOH), combined wax fractions (MeOH + $CHCl_3$), and total wax amount of mere chloroform extract ($CHCl_3$) of adaxial leaf cuticles of *Garcinia xanthochymus* (A) and *Prunus laurocerasus* (B) grouped by very long-chain aliphatic compounds (VLCA), cyclic compounds (cyclic) and total wax amount (total)**.** Error bars represent standard deviation (*n* = 4). T- test was done to detect possible significant differences between MeOH + $CHCl_3$ and total $CHCl_3$.

Only 4 % of total wax was composed of primary alcohols, alkyl esters and fatty acids. Total adaxial cuticular wax coverage of *G. xanthochymus* amounted to 6.2 ± 0.05 µg cm^{-2}. It was tenfold lower than the total adaxial cuticular wax coverage of *P. laurocerasus* (60.76 ± 2.74 µg cm^{-2}, Figure 21).

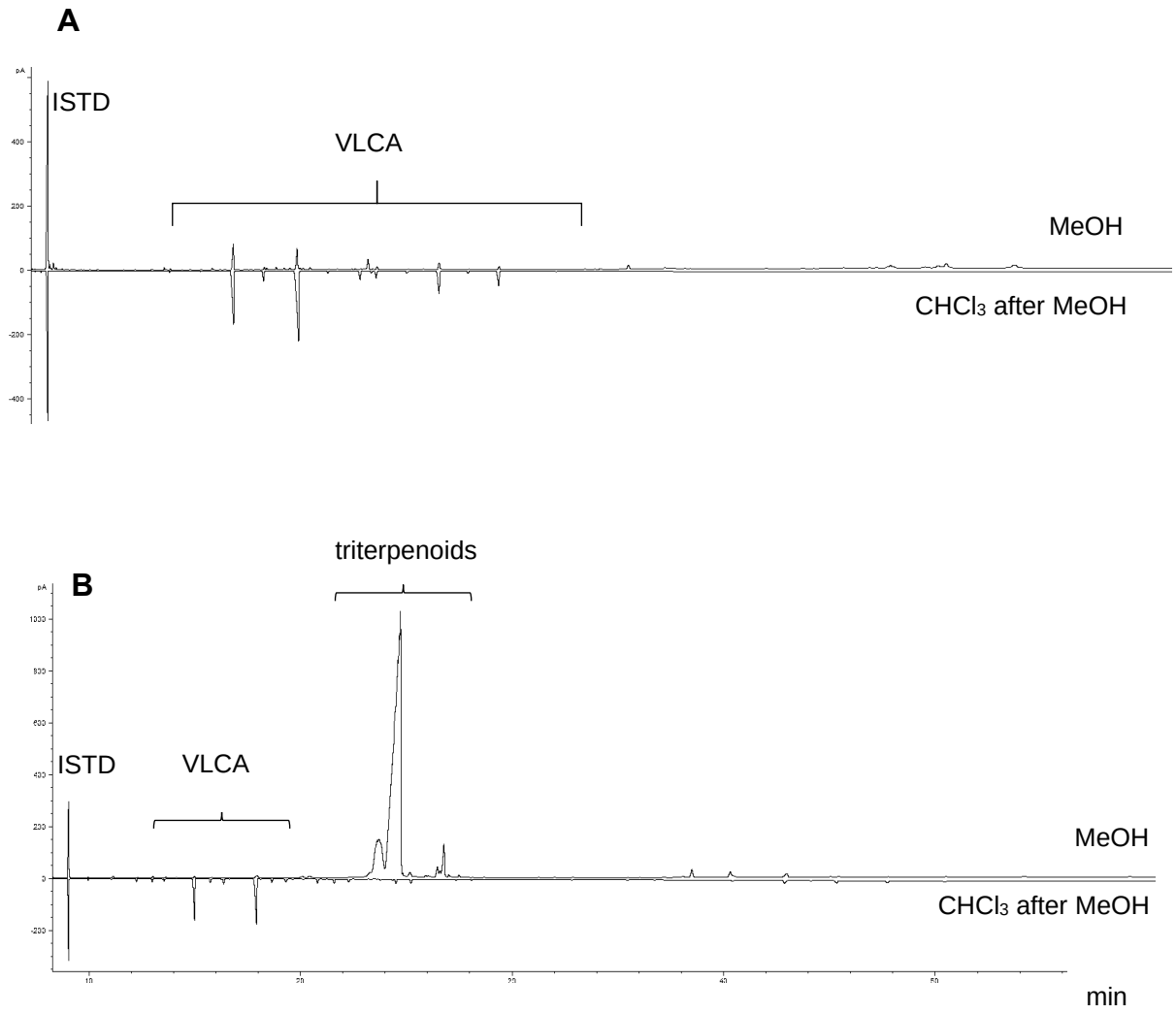

Figure 22 GC-FID chromatograms of the methanol extract (MeOH) and the subsequent chloroform extract ($CHCl_3$ after MeOH) of isolated membranes of *Garcinia xanthochymus* (A) and *Prunus laurocerasus* (B) showing differences in intensities of very long-chain aliphatic compounds (VLCA) and triterpenoids (ISTD = internal standard).

Methanol extraction of cuticles of *G. xanthochymus* resulted in the quantitative extraction of cyclic compounds (Figure 21, Figure 22). The subsequent chloroform extract consisted exclusively of VLCAs. 15 % of VLCAs were extracted using methanol, comprising hentriacontane, tritriacontane and 1-dotriacontanol. Extracting waxes using methanol followed by chloroform resulted in similar total wax coverages, as found in wax extracts using chloroform solely. No significant differences in total wax coverage between these two extraction methods were found (t-test, $p = 0.05$). Looking at the selective extraction of CM of *P. laurocerasus*, the same was observed as described above for *G. xanthochymus*: Methanol extracted the cyclic compounds quantitatively (Figure 21, Figure 22). 10 % of VLCAs were extracted using methanol. These VLCAs mainly consisted of heptacosane, 1-tetracosanol and 1-hexacosanol.

The rest of the VLCAs were found in the subsequent chloroform extract. Treating the adaxial sides of intact leaves of *P. laurocerasus* with methanol for 30 s did not remove any triterpenoids in contrast to the quantitative removal when extracting isolated cuticles with methanol (Figure 23).

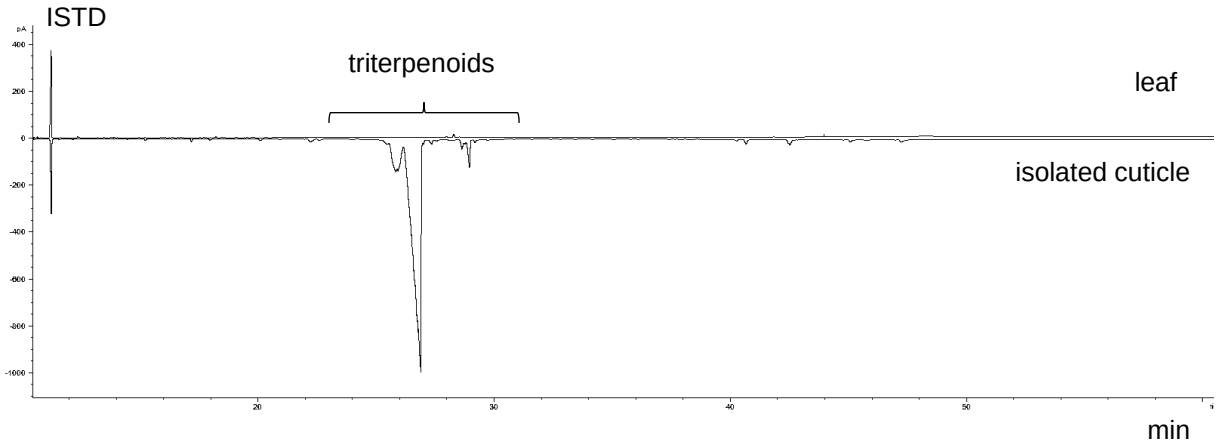

Figure 23 GC-FID chromatograms of methanol extracts of an isolated cuticle and the adaxial side of an intact leaf of *Prunus laurocerasus* (ISTD = internal standard).

2.3.2 Permeances

Permeances of theobromine, caffeine and azoxystrobin measured for the two species *G. xanthochymus* and *P. laurocerasus* with CM, M and MX ranged from 0.2×10^{-11} m s^{-1} to 1.5×10^{-9} m s^{-1} (Table 3). Lowest permeance was observed for caffeine with CM of *P. laurocerasus*. Highest permeance was determined for azoxystrobin with MX of *G. xanthochymus*. Statistical parameters can be found in Appendix 1 - Appendix 3.

Table 3 Permeances *P* of theobromine, caffeine and azoxystrobin with isolated cuticular membranes (CM), methanol extracted membranes (M) and chloroform extracted membranes (MX) of *Prunus laurocerasus* and *Garcinia xanthochymus*[c]

species	membrane	$P_{theobromine} \times 10^{11}$ (m s^{-1})	$P_{caffeine} \times 10^{11}$ (m s^{-1})	$P_{azoxystrobin} \times 10^{11}$ (m s^{-1})
Prunus laurocerasus	CM	0.8 (0.3 - 2.3)	0.2 (0.1 - 1.2)	3.4 (0.7 - 9.6)
	M	0.6 (0.4 - 1.0)	0.7 (0.5 - 1.7)	8.4 (6.5 - 21.6)
	MX	15.4 (12.2 - 18.8)	45.6 (44.8 - 64.6)	123.6 (87.8 - 162.0)
Garcinia xanthochymus	CM	13.9 (1.1 - 32.0)	11.9 (1.1 - 25.8)	14.9 (10.5 - 34.5)
	M	7.9 (1.6 - 25.3)	4.3 (1.6 - 29.8)	15.4 (9.6 - 18.4)
	MX	153.0 (21.6 - 258.3)	5.8 (21.6 - 16.5)	52.3 (38.3 - 131.6)

[c] Data is given as median values (25th percentile – 75th percentile). Sample size was between 9 and 28.

With CM of *G. xanthochymus*, permeances for the three compounds did not differ significantly (Figure 24). They ranged from 4.3×10^{-11} m s^{-1} (caffeine) to 5.2×10^{-10} m s^{-1} (azoxystrobin). Contrastingly, the permeance showed a statistically significant difference (Kruskal-Wallis ANOVA with post-hoc Dunn's test, $p < 0.05$) between theobromine - azoxystrobin and caffeine - azoystrobin with CM of *P. laurocerasus*. (Table 3). Permeance with CM and M of *P. laurocerasus* did not show a statistically significant difference for each compound (Figure 24). Permeance with CM and MX differed significantly. The same trend was seen with membranes of *G. xanthochymus* (Figure 24) except for caffeine. Here, comparison of the permeance with CM, M and MX resulted in no statistically significant difference.

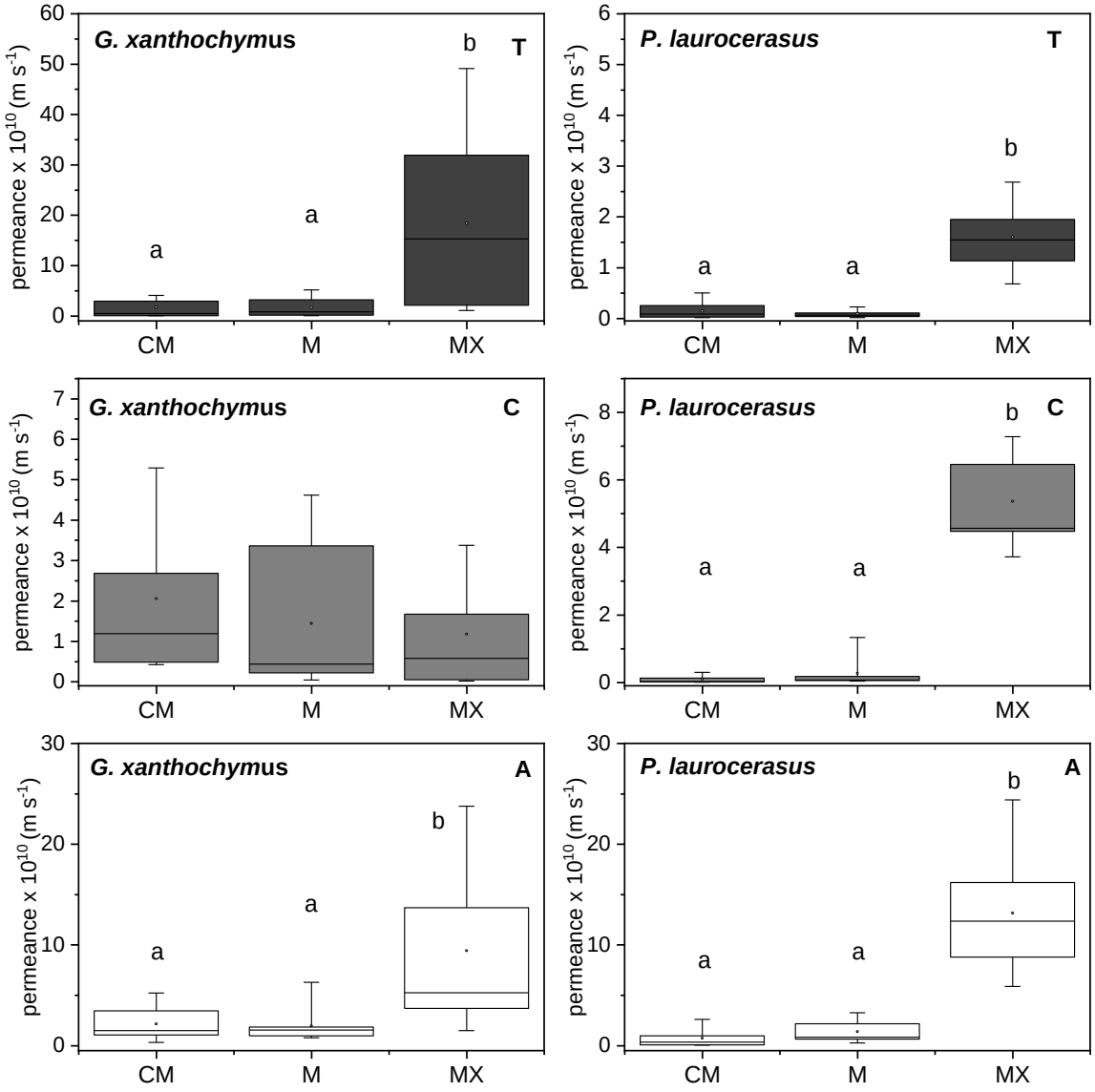

Figure 24 Box plots of permeances of theobromine (T), caffeine (C) and azoxystrobin (A) with isolated cuticular membranes (CM), methanol treated membranes (M) and chloroform treated membranes (MX) of *Garcinia xanthochymus* and *Prunus laurocerasus*. Boxes represent 25th and 75th percentile. Horizontal lines within the boxes represent the median. Whiskers indicate the 10th and 90th percentile. Different letters above the box indicate significant difference (Kruskal-Wallis-Anova with Dunn's test, $p < 0.05$, $9 < \bar{n} < 28$).

Table 4 Effect of wax extraction (P_{MX} P_{CM}^{-1}) on the permeance of theobromine, caffeine and azoxystrobin with cuticular membranes of *Prunus laurocerasus* and *Garcinia xanthochymus*[d]

species	theobromine	caffeine	azoxystrobin
Prunus laurocerasus	19	194	37
Garcinia xanthochymus	11	0.5	4

[d] Data is given as quotients of median values.

The effect of wax extraction (P_{MX} P_{CM}^{-1}) between permeance with MX and permeance with CM of theobromine, caffeine and azoxystrobin is shown in Table 4. For all compounds, *P. laurocerasus* showed higher effects of wax extraction than *G. xanthochymus*. Caffeine showed the highest effect with *P. laurocerasus*, while there was no effect with membranes of *G. xanthochymus*. The use of azoxystrobin resulted in a higher effect than theobromine for *P. laurocerasus*, while *G. xanthochymus* showed a reversed trend.

2.3.3 Aliphatic crystallinity

Aliphatic crystallinity according to Zerbi *et al.* (1989) yielded 88.0 - 88.6 % (whole data range) for G*. xanthochymus* and 78.5 - 83.3% for *P. laurocerasus.*

2.3.4 SEM

CM of *G. xanthochymus* showed grooves probably deriving from epidermal cells of the leaf (Figure 25). Wax fibrils could be observed on the edges of these grooves. The morphology of M was similar to CM, except that the wax showed a lamellar look surrounding the epidermal cell imprints. No surface wax could be observed for MX.

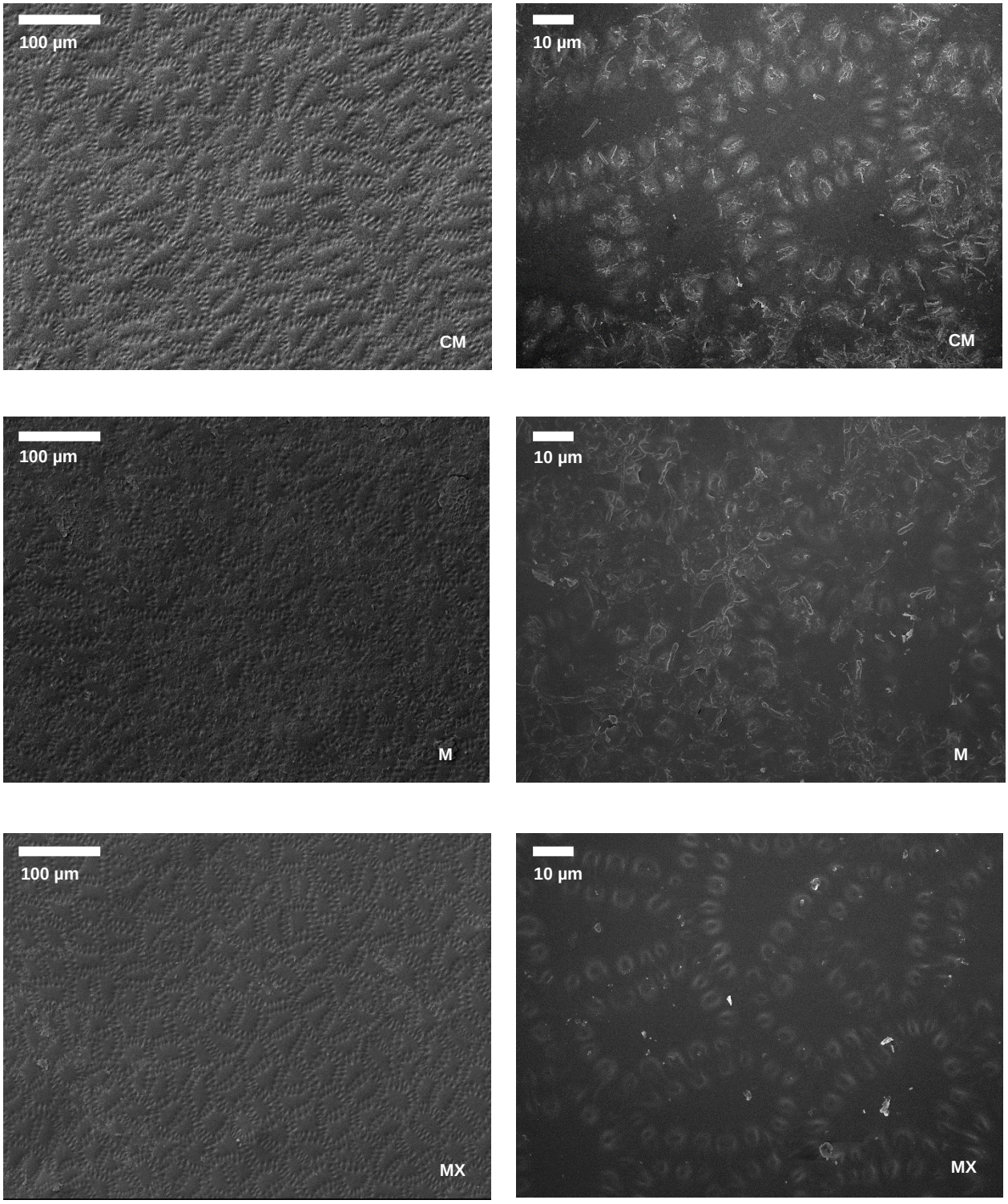

Figure 25 Scanning electron microscopy images of the upper side of isolated adaxial cuticular membranes (CM), methanol treated membranes (M) and chloroform treated membranes (MX) of *Garcinia xanthochymus*

Membranes of *Prunus laurocerasus* showed a surface morphology with imprints of the epidermal cells below the cuticle (Figure 26). These imprints were more distinct for M and MX than for CM. CM showed a high proportion of wax platelets whereas M exhibited only a small amount of wax platelets. M also showed smooth areas without wax platelets. Same was observed for MX.

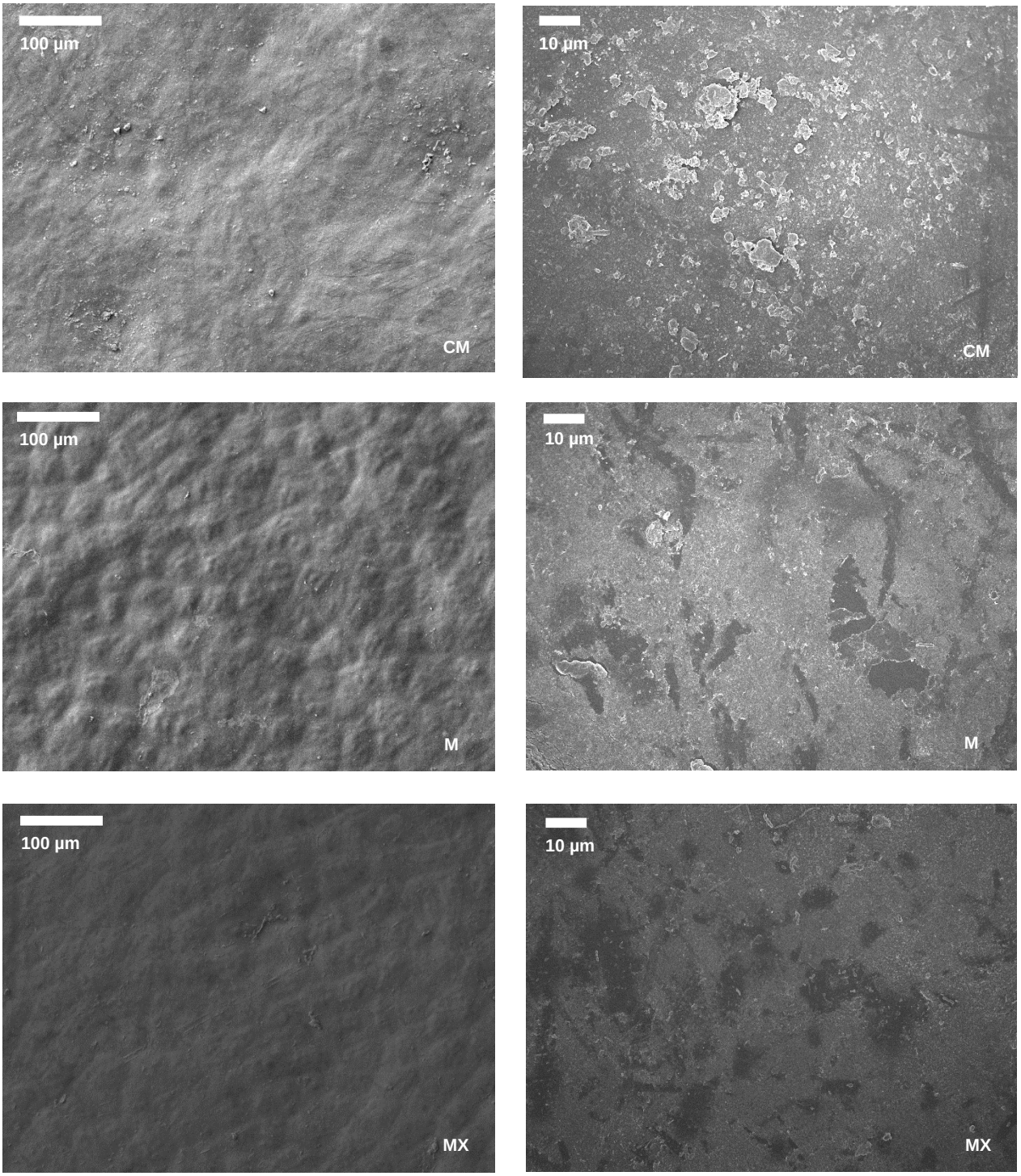

Figure 26 Scanning electron microscopy images of the upper side of isolated adaxial cuticular membranes (CM), methanol treated membranes (M) and chloroform treated membranes (MX) of *Prunus laurocerasus*

2.4 Discussion

2.4.1 Wax composition, selective extraction and surface morphology

This study was conducted with two plants (*G. xanthochymus* and *P. laurocerasus*) with different cuticular wax compositions. *G. xanthochymus* represented the species with low cyclic proportion. Total wax coverage yielded 6.15 (± 0.05) µg cm^{-2} comprising 3 % of cyclic compounds. In contrast, cuticular wax of *P. laurocerasus* comprised 88 % of cyclic compounds and was selected due to the high content of triterpenoids (Table 2, Figure 20). Since now, no data on cuticular wax composition of *G. xanthochymus* exists. Only one study by Jetter and Riederer (2016) examined the cuticular wax of *G. spicata*. Comparing the wax coverage of these two *Garcinia* species, adaxial cuticular wax of *G. spicata* was nearly threefold higher than wax of *G. xanthochymus.* In contrast, a similar trend was found regarding proportions of VLCAs and cyclics for the two species. Domination of VLCAs like *n*-alkanes and primary alcohols were reported (90 % of total wax) whereas tocopherols, sterols and triterpenoids only amounted to 10 % of total wax of *G. spicata*. This is explicable by the fact that cuticular wax of the same genus but different species can vary widely (Cameron *et al.*, 2002).

Similar total wax coverages of adaxial cuticles of *P. laurocerasus* have been reported by Zeisler and Schreiber (2016) ranging from 55.4 (± 2.0) µg cm^{-2} to 75.6 (± 4.73) µg cm^{-2}. The proportion of VLCAs (30 % of total wax) was found to be higher than 12 % as found in our study. Differences in proportions could be due to the use of different cultivars of *P. laurocerasus,* propably varying genetically. It must also be kept in mind that the two plants grew in different areas and were not harvested at the same time of the year. In this case, it is well known that cuticular wax coverage can vary quantitatively and qualitatively during the year (Hauke and Schreiber, 1998).

For both species it was possible to selectively extract cyclic compounds out of the cuticle (Figure 21, Figure 22). VLCAs remained within the cuticular membrane and were only extracted after a subsequent treatment with chloroform. Using methanol, it was possible to extract the cyclic fraction while more than 85 % of the VLCAs remained inside the membrane. Comparison of combined wax extracts of methanol and chloroform to pure chloroform extracts resulted in similar total wax amounts for each species. It was reported that the waxes are associated with the plant cuticle impregnating the cutin matrix (intracuticular waxes) and are deposited on the outer surface as a thin film (epicuticular waxes) sometimes together with epicuticular wax

crystals (Jetter *et al.*, 2000; Jetter *et al.*, 2006). Previous studies demonstrated that the epicuticular wax consisted of VLCAs, while the cyclic fraction was located mainly in the interior of the cutin matrix (Jetter *et al.*, 2000; Zeisler and Schreiber, 2016; Jetter and Riederer, 2016; Zeisler-Diehl *et al.*, 2018). Treating the intact adaxial surface of leaves of *P. laurocerasus* with methanol did not release any triterpenoids (Figure 22) proving that the cyclic compounds are located in the inner layers of the cuticle and are effectively shielded from the extractive action of methanol by a superficial layer of VLCAs. Using enzymatically isolated plant cuticles, however, overcomes this obstacle, as methanol can reach the intracuticular cyclic domains by entering the cuticle from its inner side. This side is not coated with VLCAs and therefore accessible for methanol. Supporting this concept of different solubility, a recent study showed that only small amounts of the main epicuticular wax compound 1-octacosanol could be extracted from wheat leaf surfaces using methanol (Myung *et al.*, 2013). On the contrary, chloroform could quantitatively extract 1-octacosanol after 3 min. The authors stated that polar solvents like methanol or isopropanol solubilize long-chain aliphatic primary alcohols to a very low degree, which had also been found by Hoerr *et al.* (1944). As very long-chain aliphatic alkanes are even less polar than the corresponding alcohols, they can be assumed to be less soluble in methanol. This was confirmed by experiments using shorter-chain compounds showing a higher solubility in methanol, *e.g.* for 1-decanol (> 1310 g 100 mL^{-1}) and *n*-decane (8.1 g 100 mL^{-1}) at 20°C (Hoerr *et al.*, 1944; Kiser *et al.*, 1961). Solubility data for higher alcohols and alkanes above 18 carbon atoms in methanol have not yet been published. However, it is clear that a higher hydrocarbon-chain length will drastically decrease the solubility as seen with alcohols in the range of C10 (18.8 g 100 mL^{-1}) to C18 (0.3 g 100 mL^{-1}, Hoerr *et al.*, 1944). In contrast to that, a higher solubility in methanol was reported for cyclic triterpenoids like ursolic acid (0.76 g 100 mL^{-1}), the main compound of the cyclic wax fraction of *P. laurocerasus* (Jin *et al.*, 1997).

SEM images of CM and M showed that waxes were still detectable after methanol treatment. For M of *G. xanthochymus* the surface looked partially smeared and smoother compared to CM (Figure 25). As methanol dissolved a low amount of VLCAs, a part of the remaining VLCAs might be partially redistributed on the surface of M, but without a significant effect on cuticular permeability. It can only be hypothesized that the surface of the cuticular waxes get partially dissolved and redistributed, while the inner part remains in its original state. Fully dewaxing the cuticles resulted in

membranes without any wax visible on the surface. SEM of *P. laurocerasus* showed smooth areas without wax platelets for M an MX (Figure 26). It is known that triterpenoids are mainly embedded intracuticularly whereas VLCAs are located intra- and epicuticularly (Zeisler and Schreiber, 2016; Jetter and Riederer, 2016; Zeisler-Diehl *et al.*, 2018). As discussed above, the VLCAs might shield the triterpenoids from the upper side of the cuticle against extraction using methanol. Therefore, the cyclics are assumed to be extracted from the bottom of the membrane still leaving the VLCAs within the membrane. As the triterpenoids yielded 75 % of the total wax, one might assume that removing this high amount of waxes would lead to holes or gaps within the cuticle. This assumption could not be confirmed *via* SEM, as holes should not be visible when looking at the physiologically upper side of the cuticle. As methanol also dissolved a small proportion of the VLCAs, redistribution as also found for *G. xanthocyhmus* could be possible, leading to smooth areas where triterpenoids and also some VLCAs had been removed (Figure 26).

2.4.2 Permeance and crystallinity

Dewaxing the cuticles using chloroform resulted in an increase of permeance confirming the well-established thesis that waxes build the cuticular permeation barrier to organic solutes (Riederer and Schönherr, 1985; Kerler and Schönherr, 1988b; Popp *et al.*, 2005). Permeance was lower with CM of *P. laurocerasus* than *G. xanthochymus* whereas *P. laurocerasus* showed a higher total wax coverage than *G. xanthochymus*. Several studies proposed that VLCAs rather than cyclic compounds build the permeation barrier to water (Vogg *et al.*, 2004; Jetter and Riederer, 2016), but studies on cuticular permeability to organic solutes have been lacking. The selective extraction of cyclic compounds using methanol was successful and permeance of native and extracted membranes did not differ significantly (Figure 21, Figure 22). Contrastingly, fully dewaxing the cuticles via chloroform, resulted in a statistically (Figure 24) significant enhancement except for caffeine with cuticles of *G. xanthochymus*. These results indicate that VLCAs constitute the major permeation barrier to organic solutes, while cyclic compounds have a minor impact. As the current study deals with compounds of different lipophilicity, different mechanisms of the VLCA building the cuticular barrier to hydrophilic and lipophilic solutes need to be observed. It is well known that lipophilic AIs like azoxystrobin diffuse through cuticular waxes to reach the interior of the leaf (Riederer and Schönherr, 1985; Kerler and Schönherr, 1988b). They

can permeate through lipophilic wax compounds within the cuticle (Schönherr and Baur, 1994) whereas uncharged hydrophilic AIs take a different pathway (Schreiber, 2005; Popp *et al.*, 2005). In literature, this is described as the lipophilic and hydrophilic pathway. The first is built of lipophilic wax compounds like VLCAs (Riederer and Schreiber, 1995) while the latter mainly consists of a hydrophilic domain like *i.a.*. polysaccharide strands and hydrophilic functional groups of cutin within the cuticle (Guzmán *et al.*, 2014; Fernández *et al.*, 2017). The lipophilic pathway is depicted as waxes consisting of crystalline and amorphous fractions (Riederer and Schneider, 1990; Reynhardt and Riederer, 1991; Riederer and Schreiber, 1995). The crystalline fraction comprises VLCAs forming a regular, orthorhombic lattice while the amorphous zones are built in between those highly structured crystals. They are formed by chain ends of VLCAs and functional groups, *e.g.* alcohols. Lipophilic AIs can only diffuse through amorphous parts while the crystalline fraction is inaccessible (Buchholz, 2006). Therefore, the diffusion path length can be longer than expected by the thickness of the barrier (Baur *et al.*, 1999a). The effect of wax extraction for azoxystrobin and caffeine was higher in *P. laurocerasus* than in *G. xanthochymus,* whereas crystallinity did not differ significantly. This possibly indicates that the VLCAs of the first are more effective in building a barrier than the latter, but this can only be hypothesized. Permeance of azoxystrobin and caffeine with MX (Table 3) and the effect of wax extraction (Table 4) are higher for *P. laurocerasus* than for *G. xanthochymus*, which induces a better barrier of the first to the semi-lipophilic and lipophilic compound built by the waxes. Looking at the hydrophilic theobromine, the effect of wax extraction is also higher for *P. laurocerasus* than for *G. xanthochymus* (Table 4). With a log K_{OW} of -0.78 (Table 1), theobromine is a hydrophilic compound and diffuses across the cuticle *via* the hydrophilic pathway. Unlike the lipophilic pathway which is formed by VLCAs, the hydrophilic one consists *i.a.* of polysaccharide strands that can absorb water from the surrounding air leading to a swelling of the cuticle (Arand *et al.*, 2010). With wetting of the cuticle, it is likely that the absorbed water will lead to a formation of water clusters within the cuticle (Fernández *et al.*, 2017). Thereby, a continuous connection between upper and lower side of the cuticle called ‘dynamic aqueous continuum’ is built. As the current study deals with cuticular membranes mounted between two aqueous compartments, complete water absorption is given as well as the formation of the dynamic aqueous continuum. This is a prerequisite for permeation measurements under constant conditions. Removing the

VLCAs after the extraction of the cyclic fraction resulted in a significant increase of the permeance of theobromine for both species whereas permeance with CM and M did not differ (Table 3). The VLCAs do not only limit the barrier to lipophilic compounds, but also to hydrophilic ones by possibly blocking the hydrophilic domains as was reported by Popp *et al.* (2005) and Arand *et al.* (2010). After wax removal, aqueous hydrophilic areas like polysaccharide strands within the cuticle can be directly available for hydrophilic compounds and thereby lead to an enhanced permeation. As mentioned before, the effect of wax extraction for theobromine was higher in *P. laurocerasus* than in *G. xanthochymus* (Table 4) while the permeance showed lower values (Table 3). This indicates that lipophilic wax compounds like VLCAs within the plant cuticle can block the hydrophilic pathway in *P. laurocerasus* more efficiently than in *G. xanthochymus*. The high effect of wax extraction for caffeine with membranes of *P. laurocerasus* is striking (Table 4), but can be explained by the fact that caffeine with a log K_{OW} of nearly zero (Table 1) is a semi-hydrophilic/semi-lipophilic compound which can possibly permeate across both pathways. A similar phenomenon was reported by Popp (2005), as benzoic acid showed the ability to take the lipophilic and the hydrophilic pathway according to the adjusted pH. Fully dewaxing the cuticle did not only lead to an increased permeability of caffeine, because the hydrophilic pathway is now better accessible, but also permeation across the cutin matrix without any limiting wax is possible. Contrastingly, no effect was seen using caffeine and membranes of *G. xanthochymus* (Table 3, Table 4). Surprisingly, the hydrophilic theobromine and the lipophilic azoxystrobin showed an effect of wax extraction for both species. One possible explanation could be the influence of the cutin matrix on the diffusion of a semi-hydrophilic compound in *G. xanthochymus*, but the exact mechanism remains uncertain.

If cyclic compounds do not constitute the permeation barrier to organic solutes, it has to be asked what their function is. Tsubaki *et al.* (2013) found that triterpenoids are produced by the plant for mechanical stability of the cuticle. They stated that triterpenoids like ursolic acid could act as nanofillers to strengthen the cuticle of the fruit of *Diospyros kaki* Thunb. cv. *Fuyu* (*fuyu* persimmon fruit). In 2016, it was also proposed that triterpenoids embedded in the cutin matrix of the desert plant *Rhazya stricta* limit thermal expansion of cutin (Schuster *et al.*, 2016). Therefore, even at high temperatures, triterpenoids in *Rhazya stricta* are assumed to prevent thermal damage to the aliphatic wax barrier. In addition to the influence of triterpenoids on mechanical

properties, they are also known for their anti-oxidant (Collins and Charles, 1987) and antimicrobial function (Wolska *et al.*, 2010; Szakiel *et al.*, 2012; Pensec *et al.*, 2014).
To sum up, it was possible to extract the aliphatic waxes and subsequently measure the permeation of three organic solutes. Native cuticles and cyclic-free membranes showed no significant difference between permeances whereas fully dewaxed membranes did. This verified our hypothesis that VLCAs build the major permeation barrier to organic solutes while cyclic wax compounds are of minor concern. It was assumed that hydrophilic and lipophilic organic solutes are affected by VLCAs in a different way. Permeance of hydrophilic compounds is possibly influenced by VLCAs by blocking the polysaccharide strands of the cuticular membrane whereas lipophilic AIs are affected by VLCAs due to crystalline fractions increasing the tortuosity.

3 Chapter 2: The mode of action of oil adjuvants and selected alcohol ethoxylates

3.1 Introduction

3.1.1 Objectives and research questions

As the uptake process of the AI into the plant is related to bioefficacy, adjuvants can help to improve this process. In the last decades, industrial formulations and the use of adjuvants to optimize the uptake process were heuristically and empirically driven, mainly following the principle of 'trial and error', but with little focus and reflectance on the actual modes of action of adjuvants. Modern formulation design is done using a more rational approach. Thereby, the main focus of formulation design is on understanding the basic principles of adjuvancy and the modes of action including physicochemical principles (Knowles, 1998). The AI application process can be distinguished into four main processes (Nairn *et al.*, 2016):

- spray droplet dynamics (drift, velocity, evaporation),
- leaf impingement dynamics (retention, bouncing, shattering)
- fate of the droplet on the leaf (spreading, AI distribution, droplet drying)
- the AI action (permeation/penetration, persistence).

The first three factors have been studied extensively (Cook and Duncan, 1978; Abbott *et al.*, 1990; Gauvrit and Dufour, 1990; Wirth *et al.*, 1991; Ramsey *et al.*, 2005; Koch *et al.*, 2008; Ryckaert *et al.*, 2008; W.A. Forster *et al.*, 2012; Dorr *et al.*, 2015; Forster and Kimberley, 2015; Chiu *et al.*, 2016; Asmus *et al.*, 2016b; Arand *et al.*, 2018). A study by Arand *et al.* (2018) tried to uncouple all four processes by starting with the droplet formation, retention and spreading to the behaviour of adjuvants on the leaf surface and ending with penetration enhancement experiments in *vitro* and *vivo.* The last process of penetration enhancement was also reported by various authors in the last three decades (Gauvrit and Dufour, 1990; Urvoy *et al.*, 1992; Schönherr, 1993a; Serre *et al.*, 1993; Schönherr, 1993b; Schreiber and Schönherr, 1993; Schönherr and Baur, 1996; Schönherr and Baur, 1997; Mercier *et al.*, 1997; Baur *et al.*, 1997b; Petracek *et al.*, 1998; Burghardt *et al.*, 1998; Burghardt *et al.*, 2006; Fagerström *et al.*, 2013a; Gutenberger *et al.*, 2013). All authors reported an enhanced uptake of the AI

into the plant or across the cuticle after addition of the adjuvant and higher bioefficacy. The increased penetration was explained by *i.a.* the wax adjuvant interaction, mainly focusing on alcohol ethoxylates and their ability to plasticize the wax. The plasticization process is assumed to result in a decreased crystallinity. One study by Zhang *et al.* (2016) reported crystallinity data for carnauba and beeswax in combination with polysorbates, reporting a decrease in crystallinity. A change of the crystallite-level was also reported by Webster *et al.* (2018) who studied the artificial model compound tristearin and *Ficus macrophylla* leaf wax in combination with several oil adjuvants. In addition, several other studies focused on the investigation of the phase behaviour of plant wax adding adjuvants like alcohol ethoxylates and oil adjuvants observing a decrease of the start of melting and the melting enthalpy (Coret and Chamel, 1994; Coret and Chamel, 1995; Perkins *et al.*, 2005; Fagerström *et al.*, 2014). The effects were always reported for temperatures higher than 45°C which is usually above the physiological temperature in the field during application. Not only the permeability to AIs was studied, but also the use of oil adjuvants like methyl oleate for grape drying for raisin production was reported (Bolin and Stafford, 1980; Saravacos *et al.*, 1988; Doymaz and Pala, 2002). As it is assumed that water can take partly the same pathway as lipophilic AIs (Schreiber, 2005) and permeation is limited by crystalline aliphatic domains (Staiger *et al.*, 2019), applying penetration enhancers like surfactants or oils should lead to an increased water transpiration even at room temperature. If the AI is applied to maintain crop vitality, increased transpiration is an unfavored side effect that should be avoided. Studies reported a significant increase of the transpiration after applying methylated rape seed oil (Räsch *et al.*, 2018) and polydisperse surfactants (Riederer and Schönherr, 1990). However, comprehensive studies using other adjuvants, especially the well-studied and commonly used alcohol ethoxylates have been lacking to date.

The objective of this work was to study the interaction of the plant cuticular wax with two different adjuvant types with a special focus on the mode of action of penetration enhancement not only for AIs, but also for water. As the VLCAs build the major permeation barrier to AIs (Staiger *et al.*, 2019), a pure aliphatic cuticular leaf wax of *Schefflera elegantissima* was selected to exclusively study the phase behaviour of the VLCAs by DSC and the wax crystallinity using FTIR. Thereby, the interaction of the adjuvant with the leaf wax was elucidated to exactly identify the mode of action of penetration enhancers. Pure wax and 5, 25, 50 % (*w/w*) wax adjuvant blends were

investigated using four oil adjuvants and three alcohol ethoxylates. These two adjuvant types were selected as they are commonly used in agriculture. Because of the high amount of leaves that are needed to get a sufficient amount of cuticular wax, an artificial model wax comprising the four most abundant compounds of the cuticular wax according to Seufert (2019) were also used to study the effect of adjuvants. The two wax types should be compared to check if the adjuvants affect the phase behaviour and crystallinity in similar ways to validate the artificial wax as a model wax. Thus, it would easily provide a wax available in sufficient amounts for further experiments, *e.g.* adjuvant screenings and diffusion studies. In addition, isolated cuticles and leaf envelopes of *Prunus laurocerasus* and *Garcinia xanthochymus* in combination with the adjuvants were examined to check the influence of adjuvants on the transpiration. Wetting behaviour of the three surfactants on a hydrophobic parafilm surface was also studied using the contact angle (CA).

3.2 Materials and Methods

3.2.1 Chemicals

Isolation of cuticular membranes was performed using pectinase, cellulose, citric acid monohydrate and sodium azide, as described previously in 2.2.1 (Table 1). The adjuvant methyl oleate (MeO) which is the methyl ester of oleic acid (OA), OA and the other chemical modfications methyl linolenate (MeLin) and methyl stearate (MeSt) were used for DSC, FTIR and cuticular transpiration experiments (Figure 27, Table 1).

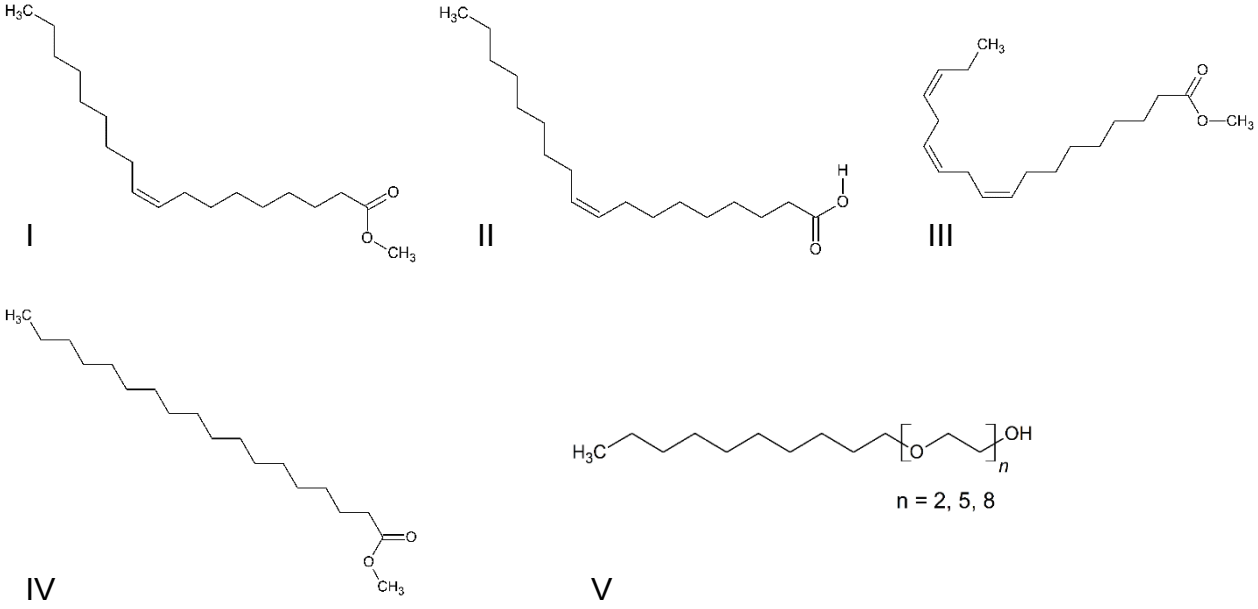

Figure 27 Chemical structure of the used oil derivatives methyl oleate (I), oleic acid (II), methyl linolenate (III), methyl stearate (IV) and C10E2, C10E5, C10E8 (V)

The different chemical modifications were used to study the effect of the methyl group, of one double bond and of multiple double bonds on the phase behaviour (Table 5). The alcohol ethoxylates C10E2, C10E5 and C10E8 were used for FTIR, transpiration studies and CA measurement (Figure 27, Table 1). DSC and study of the phase behaviour using an FTIR temperature ramp was carried out only using C10E2 and C10E8.

Table 5 Concept to identify the effect of different chemical modifications of methyl oleate on the phase behaviour using pairs for investigation

question	compound A	compound B
effect of methyl group	MeO	OA
effect of one double bond	MeO	MeSt
effect of multiple double bonds	MeO	MeLin

Table 6 Physicochemical properties of the used adjuvants

compound	$\log K_{OW}$[a]	melting point (°C)
MeO	7.45	-19.9[a]
MeLin	6.92	-35.0[b]
MeSt	8.35	39.1[a]
OA	7.64	13.0[c]
C10E2	4.22	liquid at room temperature - N.D.[d]
C10E5	2.42	14[e]
C10E8	1.59	amorphous at room temperature[f]

[a] Values taken from the EPI Suite™ v4.11 (United States Environmental Protection Agency, Washington, DC, USA)

[b] Sigma-Aldrich (2019a)

[c] Abrahamsson and Ryderstedt-Nahringbauer (1962)

[d] N.D. -not declared, optical observation at 25°C

[e] Ohta *et al.* (2000)

[f] measured using FTIR, see Appendix 28 for phase behaviour

3.2.2 Plant material and preparation of wax extracts

Prunus laurocerasus were chosen for isolation of cuticular membranes and extraction of cuticular waxes. Due to the good mechanical stability, this species was chosen, making it feasible for transport experiments. *Schefflera elegantissima* was selected because of its high proportion of VLCAs in the cuticular wax.

Leaves of *Schefflera elegantissima* (false aralia) and *Prunus laurocerasus cv.* Herbergii (laurel cherry) were harvested at the botanical garden in Würzburg, Germany.

Isolated cuticular membranes of the non-stomatous, adaxial side of the leaf were prepared according to the method of Schönherr and Riederer (1986). Enzymatic isolation was done as described previously (2.2.2). Wax extracts of isolated cuticular membranes (CM) were prepared by extracting them with 5 mL of chloroform for 30 min (referred to as cuticular wax). To obtain a high amount of wax of *S. elegantissima*, fully expanded leaves were dipped into chloroform for 30 s (referred to as leaf wax). Solvents of wax extracts were evaporated under a flow of nitrogen.

Mixtures of 5, 25 and 50 % (*w/w*) adjuvant and leaf wax of *S. elegantissima* as well as mixtures of adjuvant and an artificial model wax (Table 7) were prepared. MeO, MeLin, MeSt and OA were used as adjuvants. The model wax was prepared according to Table 7. It consisted of the four most abundant wax compounds of the cuticular wax of *S. elegantissima* (Seufert, 2019): *n*-hentriacontane (C31), *n*-nonacosane (C29), 1-dotriacontanol (C32-1-ol), 1-triacontanol (C30-1-ol). For DSC, all wax mixtures and the leaf wax were molten at 90°C before preparing the wax adjuvant mixtures. For FTIR, the wax was dissolved in chloroform and applied onto the crystal, heated to 90°C for several minutes and cooled down to 20°C for further measurements.

Table 7 Proportion in mol per mol of the model wax compounds in the different mixtures

mixture	proportion (mol/mol)
pure C30-1-ol	1
C31/C29	2.3/1
C31/C29/C30-1-ol	2.3/1/1.4
C31/C29/C32-1-ol/C30-1-ol	5.4/2.3/2.3/1

GC-analysis of the leaf and cuticular wax of *S. elegantissima* was done using the method described previously (2.2.3).

3.2.3 Differential scanning calorimetry

The thermotropic phase behaviour of different model wax compounds and model wax mixtures as well as plant cuticular wax was studied by differential scanning calorimetry (DSC 1, Mettler Toledo, Greifensee, Switzerland). Pure wax and adjuvant wax mixtures (5, 25 and 50 % (*w/w*)) were examined. Therefore, the desired amount of adjuvant and wax (model wax or leaf wax) were weighed into 40 µl standard aluminium crucibles (Mettler Toledo) and sealed hermetically. Two subsequent cycles of heating and cooling were conducted. The heating and cooling rate was 2°C min^{-1}. Dry nitrogen gas was used for purging the furnace chamber. For analysis of the phase behaviour, the second heating cycle was used, as the first heating and cooling cycle provided a homogenous wax adjuvant blend.

3.2.4 Infrared spectroscopy

The same Fourier-transform infrared spectrometer (FTIR, Bruker Tensor 27 with BIO-ATR II® unit, Bruker, Ettlingen, Germany) as mentioned previously (2.2.5) was used for spectra recording in horizontal attenuated total reflection mode (h-ATR). Wax solution and adjuvant wax mixture in chloroform (dry weight of ca. 200 µg) was deposited on the crystal. The crystal was heated up to 90°C to ensure that chloroform was fully evaporated. This procedure was done for cuticular wax solution in chloroform and solid wax samples to ensure that the wax built a film on the crystal surface. Leaf wax and model wax samples in combination with adjuvants were also examined. Therefore, the DSC samples from 3.2.3 were used. With a spatula, ca. 200 µg were taken from the aluminium crucible and placed on the h-ATR crystal. The crystal was heated up to 90°C to provide direct contact of the wax with the crystal. For FTIR measurement, the crystal was cooled down to 20°C. The infrared spectra were recorded in wavenumber range of 4000 to 670 cm^{-1} at temperatures from 20°C to 90°C. Temperature was adjusted by connecting the stainless-steel envelope to the water circuit of a thermostat (Thermo Scientific Haake DC30-K20, Karlsruhe, Germany). The BIO-ATR II® unit was purged with dry CO_2-free air (K-MT-LAB 3, Parker Hannifin, Kaarst, Germany). Initial temperature was set to 20°C and was increased up to 44°C in intervals of 4°C. From 44°C to 90°C, FTIR spectra were recorded at temperature intervals of 1°C. Resolution was set to 2 cm^{-1} with an acquisition time of 120 scans. OPUS 7 software (Bruker) was used to analyse spectra and to control the spectrometer and thermostat. Baseline adjustment was done before smoothing the spectrum.

Due to the long sampling time, temperature ramps were recorded only for one sample (n = 1). For determination of crystallinity, spectra were recorded for three to four samples ($3 < \bar{n} < 4$) and OriginPro 2019 (OriginLab, Northampton, USA) was used for Gaussian deconvolution of the two rocking bands at 720 and 730 cm-1 (for calculation see Equation 10 in 1.3.3). FTIR spectra of the pure adjuvants were recorded at 20°C.

3.2.5 Cuticular transpiration experiments and determination of water permeance

Water permeance was determined gravimetrically by measuring the water deficit over time. Therefore, the cuticular membranes of *P. laurocerasus* and *G. xanthochymus* were dried using pressurized air and attached on a chamber of stainless steel by using Teflon paste (Carl Roth, Karlsruhe, Germany). Membranes were mounted on the chamber so that the physiological outer side faced the atmosphere. Cells were sealed with adhesive tape (Beiersdorf, Hamburg, Germany). To measure the effect of oil adjuvants on the permeance, one µl of the pure oil derivative, C10E2, C10E5 was pipetted on the membrane and left to dry for at least one h. In the case of C10E8, which is amorphous at room temperature (Table 6), an aqueous solution of 50 % C10E8 (*w/w*) was prepared. Two µL of this solution were applied onto the cuticular surface and left to dry for at least one h. One mL of high purity water was filled into the cell. The cells were sealed using adhesive tape (Tesa, Beiersdorf, Hamburg, Germany). To ensure a relative humidity of nearly zero and a maximum driving force, the cells were placed in boxes over silica gel (Applichem, Darmstadt, Germany). Temperature was held at 25 ± 0.1°C using a Peltier-cooled incubator IPP110 (Memmert, Schwabach, Germany). The weight of the water-filled chambers was measured as a function of time using an analytical electronic balance (MC-1 AC210S, Sartorius, Göttingen, Germany).

Leaf envelopes were prepared by sealing the abaxial surface with self-adhesive aluminum tape (Tesa, Beiersdorf) after cutting the leaf edges. The leaf envelopes were placed into a box filled with silica gel (Applichem). Temperature was held at 25 ± 0.1°C using an incubator IPP110 (Memmert). The weight of the leaf envelopes was measured as a function of time using an electronic balance (MC-1 AC210S, Sartorius). Leaf temperatures were checked using an FTIR laser thermometer (Harbor Freight Tools, Calabasas, USA). The corresponding water vapour saturation as driving force was taken from tabulated values (Nobel, 2009).

For the leaf envelopes, paired data was generated as the leaf envelopes were first measured without the adjuvant and after the application of the pure MeO.
The isolated cuticles were also measured before and after the application of the pure MeO (paired MeO), generating paired data. Unpaired data was obtained applying one µL of MeO, MeLin, OA, C10E2, C10E5 and C10E8 directly onto the cuticular surface and measuring the cuticular water permeance.

3.2.6 Contact angle measurements

A contact angle (CA) measuring device OCA 15 plus (DataPhysics Instruments, Filderstadt, Germany) was selected. Specimen slides with parafilm (Parafilm M, Bemis Company, Neenah, Wisconsin, USA) with double-side adhesive tape (Tesa double face, Beiersdorf) were used. Parafilm was selected as a standardized, apolar surface. Ten replicates per substance were examined (n = 10). A 3 µL droplet was applied on to the parafilm. Solutions (4 µg μL^{-1}) of the surfactants C10E2, C10E5 and C10E8 were prepared in high-purity water and used for CA measurement. Water was used as control. The shadow image of the sessile droplet was taken for CA determination (drop shape analysis software, Krüss, Hamburg, Germany). A geometrical model was fitted to the shape of the droplet for calculation of the CA. After the application of the droplet, a camera with 1fps recorded the process for 60 s.

3.2.7 Statistics

Statistical analysis was done using RStudio 2016 (RStudio, Boston, MR, USA) and OriginPro 2019 (OriginLab).

Water permeance

Outliers for cuticular transpiration were removed according to the method of the interquartile range. Cuticular water permeance did not show normality according to Shapiro-Wilk test ($p < 0.1$). Lognormal transformation of the permeance did result in normality for the paired samples of isolated cuticles and envelopes using MeO with *Prunus laurocerasus* and *Garcinia xanthochymus*, but not for unpaired samples of *Prunus laurocerasus.* Variance homogeneity was not given according to Levene's test ($p < 0.01$) for unpaired samples. Significant difference between unpaired data was checked using Kruskal-Wallis ANOVA with post-hoc Dunn's test ($p < 0.05$). A paired t-test of lognormal transformed permeances was conducted to check difference between

the paired samples of no adjuvant and MeO ($p < 0.05$). Welch two-sample t-test because of non-variance homogeneity on lognormal transformed data was conducted to test difference between the CM and envelopes of one species and the same condition ‘no adjuvant’ or ‘MeO’ ($p < 0.05$). Effects of the MeO addition were calculated using the quotient of the mean permeance with MeO and permeance without adjuvant. The mean and confidence intervals of lognormal transformed permeance data were used for calculation and retransformed.

Infrared data

Normalitiy and variance homogeneity was checked for crystallinity data. Normality was given according to Shapiro-Wilk test ($p < 0.1$), as well as variance homogeneity (Levene’s test, $p < 0.01$). Differences between the data of the artificial model wax and the leaf wax was checked at one level of the adjuvant (5, 25, or 50 %) using a two-sided t-test ($p < 0.05$). Dunnett’s test ($p < 0.05$) was applied to detect significant difference between crystallinity of wax adjuvant blends and the control (pure leaf or artificial wax).

Contact angle measurements

CA data showed normality according to Shapiro-Wilk test ($p < 0.1$). Variance homogeneity was not given according to Levene’s test ($p < 0.01$), also not for lognormal transformed data. Kruskal-Wallis ANOVA with post-hoc Dunnett’s T3 all-pairs comparison test for normally distributed data with unequal variances ($p < 0.01$) was conducted to test significant difference.

3.3 Results

3.3.1 Wax composition of *S. elegantissima* leaf and cuticular wax

Median total leaf wax coverage yielded 4.3 µg cm^{-2} (25^{th}- 75^{th} quartile, 3.9 - 4.9 µg cm^{-2}) and was smaller than the value for the adaxial cuticular wax extract (6.8 µg, 6.8 - 6.9 µg cm^{-2}) (Figure 28, Table 8). Statistical parameters can be found in Appendix 5. The main compounds found in both waxes were alcohols, alkanes and acids. Aldehydes were only detected for the leaf wax, whereas cyclics were solely

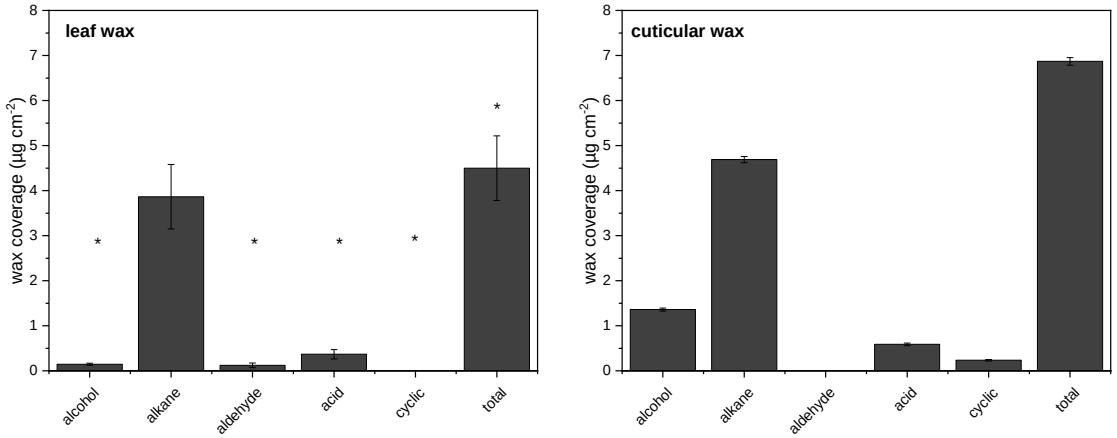

Figure 28 Wax composition of *Schefflera elegantissima* leaf wax (left, both leaf sides) and adaxial cuticular wax (right) grouped by alcohols, alkanes, aldehydes, acids, cyclic wax compounds and total wax amount. Error bars represent standard deviation. Asterisk indicates significant difference between the leaf and the cuticular wax (Mann-Whitney Rank sum test, $p < 0.05$, $n = 4$).

found in the cuticular wax. Alkanes were the most abundant aliphatic compounds found in both waxes, followed by the alcohols.

Table 8 Composition of the leaf and cuticular wax of *Schefflera elegantissima* given as median values (µg cm^{-2}; $n = 4$) and 25^{th} to 75^{th} quartile

compound classes	leaf wax	25^{th} - 75^{th} quartile	cuticular wax	25^{th} - 75^{th} quartile
fatty acids	0.4	0.3 - 0.4	0.6	
primary alcohols	0.2	0.1 - 0.2	1.4	1.3 - 1.4
aldehydes	0.1	0.1 - 0.2	N.D.[a]	N.D.[a]
n-alkanes	3.7	3.4 - 4.2	4.7	4.6 - 4.7
cyclics	N.D.[a]	N.D.[a]	0.23	0.22 - 0.24
not identified	0.3	0.3 -0.4	1.39	1.38 - 1.43
total	4.3	3.9 - 4.9	6.8	6.8 - 6.9

[a] N.D. - not detected

The amount of alkanes did not differ significantly between the leaf and the cuticular wax (Mann-Whitney Rank sum test, $p = 0.05$, $n = 4$), but the amounts of *n*-nonacosane (C29) and *n*-tritriacontane (C33) showed different proportions (Figure 29). C29 was more abundant in the cuticular wax, while the amount of C33 was higher in the leaf

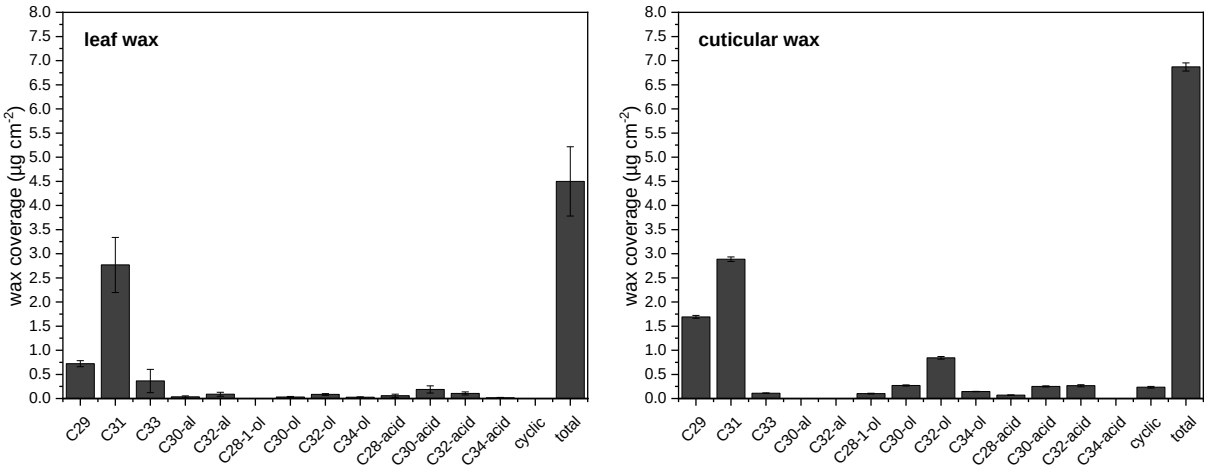

Figure 29 Wax composition of *Schefflera elegantissima* leaf wax (both sides) and adaxial cuticular wax. Error bars represent standard deviation ($n = 4$).

wax. C31 showed similar proportions in both wax samples. No cyclics were found in the leaf wax, but to a minor amount in the cuticular wax. Here, they made up 3 % of the total wax. Alcohols found in the cuticular wax yielded 20 % of the total wax and were less abundant in the leaf wax. 1-Dotriacontanol (C32-1-ol) followed by 1-triacontanol (C30-1) were the main alcohols found in the cuticular wax in proportions of 4 and 12 %.

Selecting only the four most abundant compounds within the cuticular wax, the mol ratio was calculated and yielded: 11 / 7 / 3 / 1 (C31 / C29 / C32-1-ol / C30-1-ol). For the leaf wax a mol ratio of 88 / 11 / 2.5 / 1 (C31 / C29 / C32-1-ol / C30-1-ol) was found.

3.3.2 Differential scanning calorimetry

3.3.2.1 Comparison of the model wax mixtures to S. elegantissima leaf wax

Both cycles, heating and cooling of the *S. elegantissima* leaf wax and the quaternary mixture yielded three phase transitions, the last one representing the melting/crystallization (Figure 30). The transitions were not clearly separated from each other but were overlapping. Comparing the second heating cycle to the second cooling cycle of the *S. elegantissima* leaf wax, it is obvious that phase transitions and the end of melting was driven to lower temperatures for the cooling cycle. Same was observed for C31/C29/C32-1-ol/C30-1-ol.

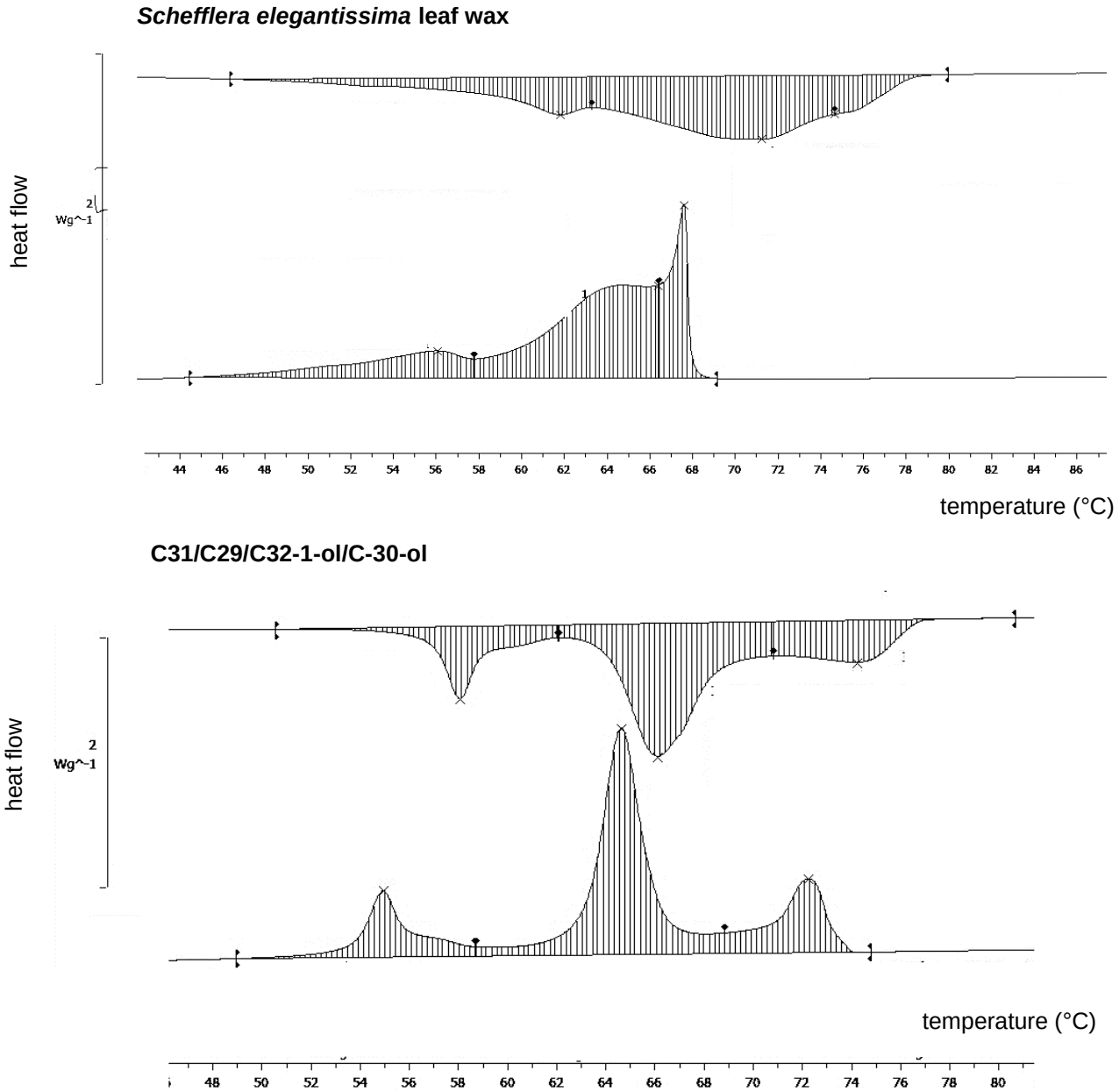

Figure 30 Thermograms of *Schefflera elegantissima* leaf wax and mixture of *n*-hentriacontane, *n*-nonacosane, 1-triacontanol, 1-dotriacontanol (C31/C29/C32-1-ol/C30-ol). First line represents second heating cycle. Second line represents cooling cycle 2

Except for onset temperature of phase transition 2, the onset and offset temperatures for the leaf wax were found to be higher than for the quaternary mixture (Table 9). The difference of the EOT of the first phase transition between leaf and model wax was 2 J g^{-1}, while the differences of the last two phase transitions were above 20 J g^{-1}. Total EOT of heating 2 differed about 50 J g^{-1}.

Table 9 DSC parameters for *Schefflera elegantissima* leaf wax and the quaternary mixture of *n*-hentriacontane, *n*-nonacosane, 1-triacontanol, 1-dotriacontanol (C31/C29/C32-1-ol/C30-ol, 5.4/2.3/2.3/1) for heating cycle 2

sample type	phase transition	enthalpy of transition (J g^{-1})	onset (°C)	peak (°C)	offset (°C)
S.elegantissima	1	-41.96	57.35	61.81	66.51
	2	-105.03	59.80	71.26	77.86
	3	-16.69	74.60	74.59	81.18
	total	-163.68	N.A.[a]	N.A.[a]	N.A.[a]
quaternary mixture	1	-43.41	56.88	58.06	59.25
	2	-126.91	63.88	66.12	69.11
	3	-46.6	62.42	74.22	76.62
	total	-216.92	N.A.[a]	N.A.[a]	N.A.[a]

[a] N.A. – not available

3.3.2.2 Addition of the oil adjuvants MeO, OA, MeLin, MeSt to the model wax and Schefflera elegantissima leaf wax

The thermograms of 5 and 50 % adjuvant wax proportion are shown in this chapter. Additional thermograms and data can be found in Appendix 6 - Appendix 27. Pure C30-1-ol showed only one phase transition (Figure 31). Addition of 5 % adjuvant to C30-1-ol resulted in a slight reduction (mostly < 1°C) of onset and offset temperature compared to the pure alcohol. While the onset temperatures of the 50 % mixture were reduced by 10°C, offset temperatures decreased by nearly 5°C. The alcohol-MeSt mix showed another phase transition at temperatures between 36°C and 39°C which was only observed for this compound. This transition was also found in pure MeSt as the only phase transition (Appendix 20).

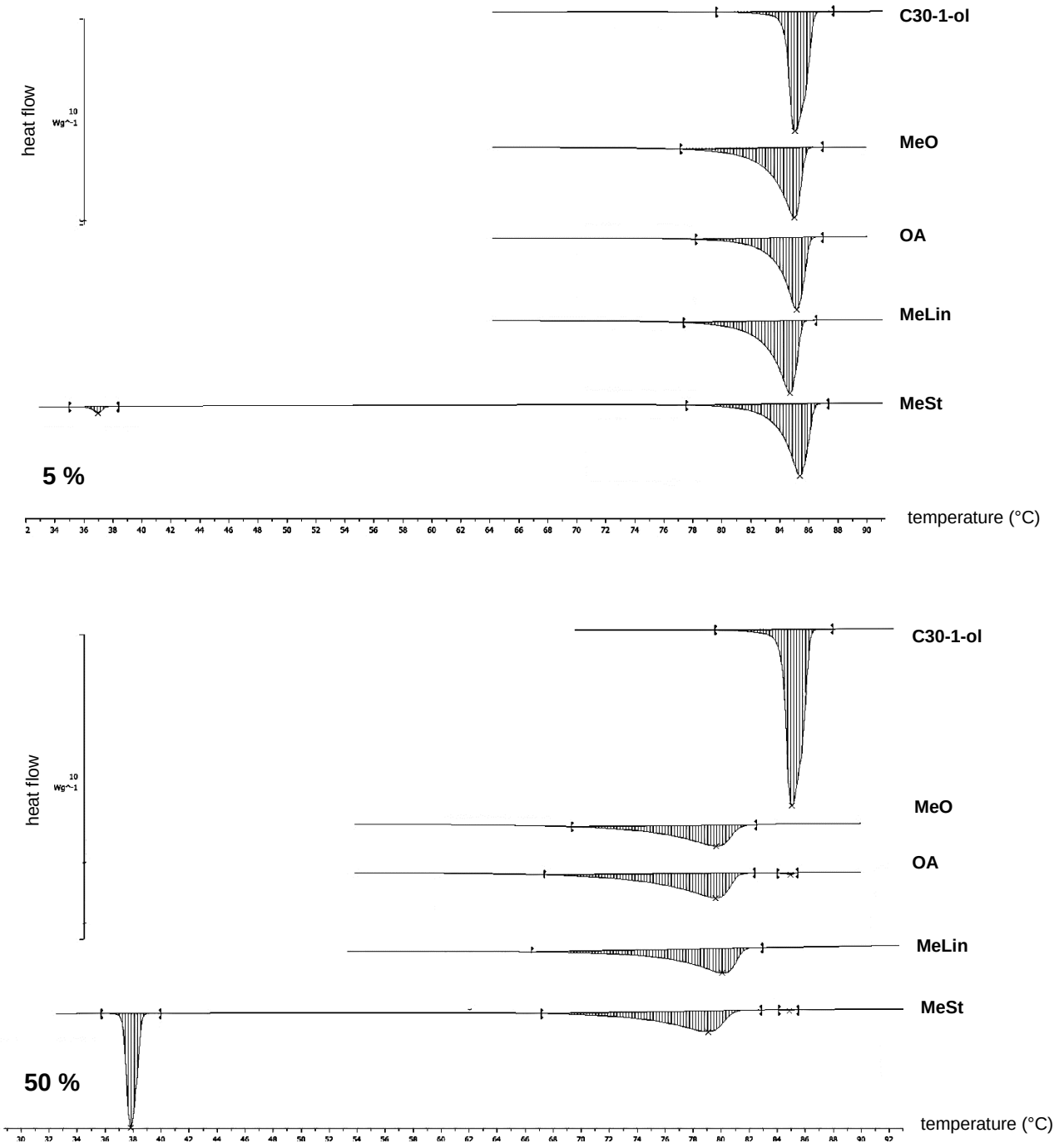

Figure 31 Thermograms of 1-triacontanol (C30-1-ol) and 5, 50 % (*w/w*) of methyl oleate (MeO), oleic acid (OA), methyl linolenate (MeLin) and methyl stearate (MeSt) for heating cycle 2

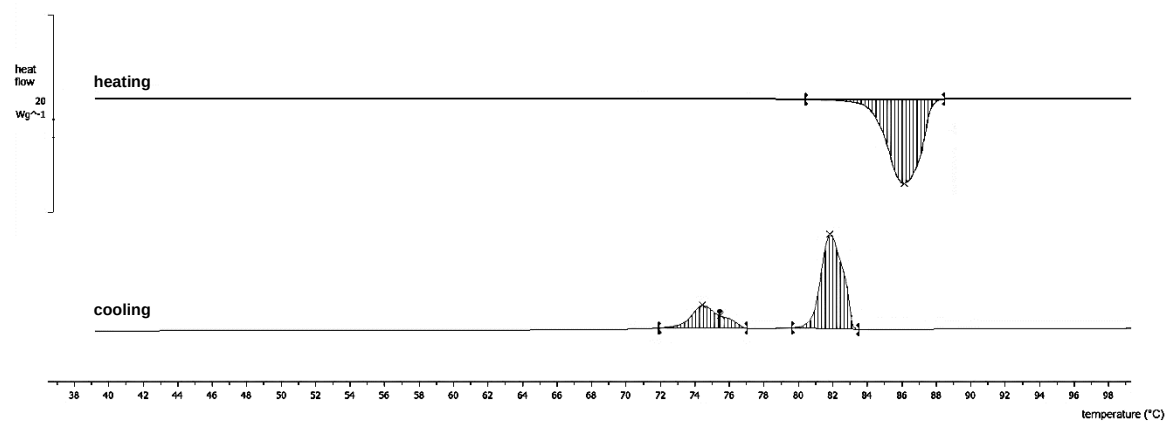

Figure 32 Thermogram of pure 1-triacontanol (C30-1-ol) at heating cycle 2 (heating) and cooling cycle 2 (cooling)

The pure C30-1-ol exhibited only one phase transition during heating, whereas the cooling revealed two transitions (Figure 32).

For the alkane mixture (C31/C29), addition of 5 % adjuvant decreased the onset and

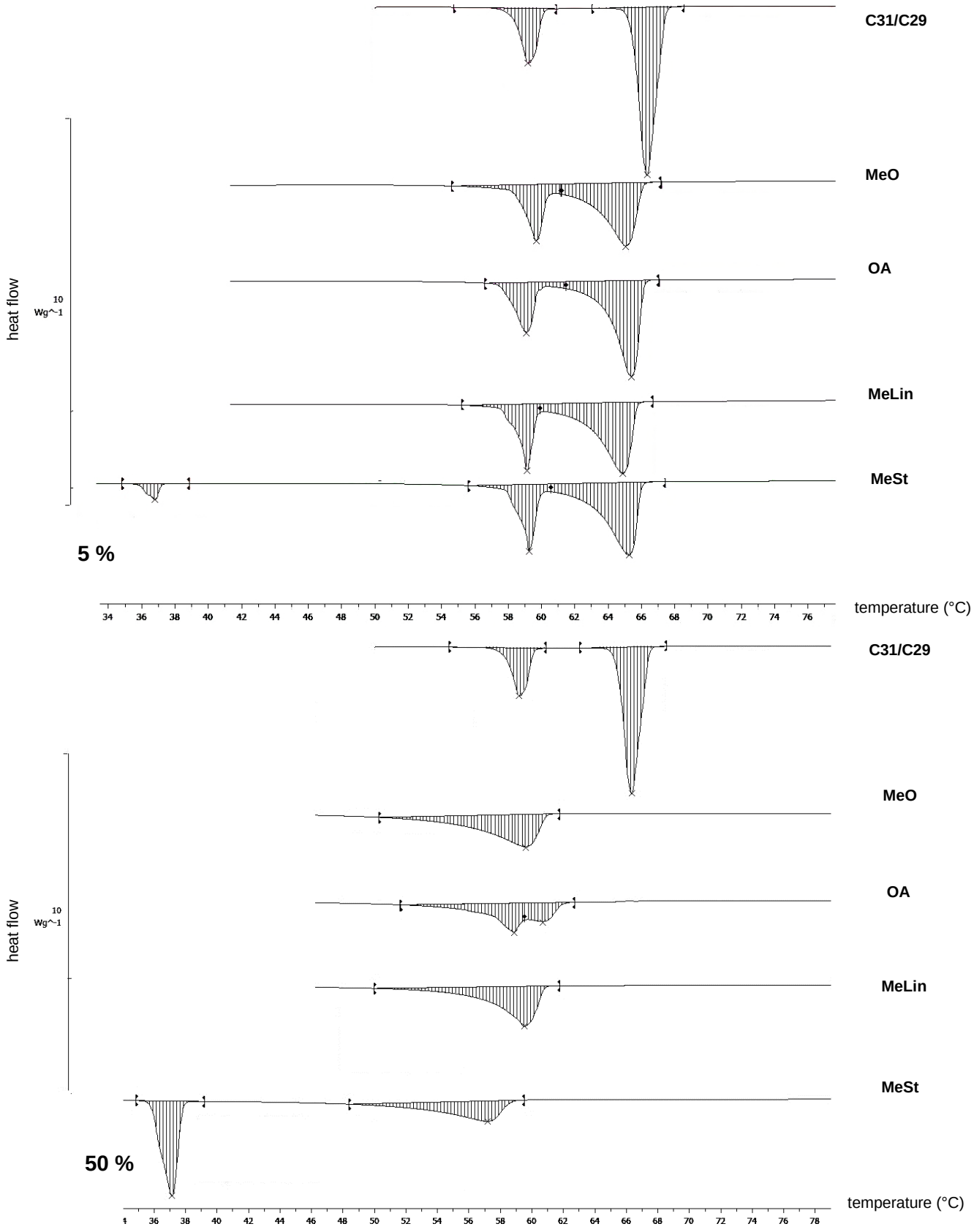

Figure 33 Thermograms of *n*-hentriacontane, *n*-nonacosane (C31/C29) and 5, 50 % (*w/w*) of methyl oleate (MeO), oleic acid (OA), methyl linolenate (MeLin) and methyl stearate (MeSt) for heating cycle 2

offset temperatures of both phase transitions by 1°C to 2°C while addition of 50 % had a higher impact (Figure 33). For the 50 % mixture, only one phase transition was observed for all adjuvants except OA. Offset temperatures decreased between 7°C to 9°C in comparison to the pure alkane mixture. Broadening of the peaks in the thermograms were observed.

The ternary mixture C31/C29/C30-1-ol showed four phase transitions (Figure 34). 5 % OA decreased the number of phase transitions to three, whereas four transitions were still observed for MeO and MeLin. At the adjuvant proportion of 50 %, only two phase transitions were found for MeO, MeLin and OA. Offset temperatures of the melting were reduced the most for MeLin. As described previously, the quaternary mixture

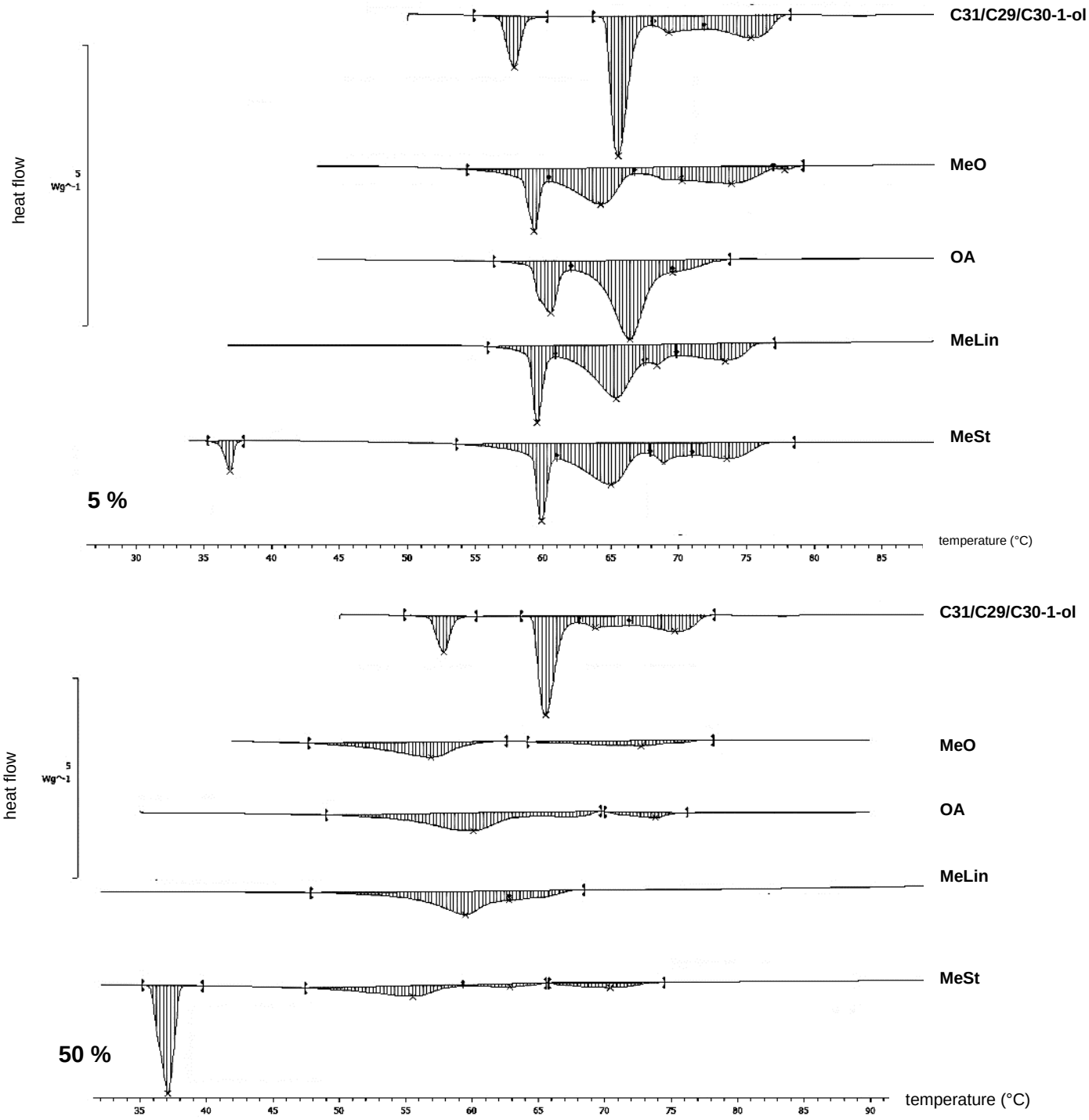

Figure 34 Thermograms of *n*-hentriacontane, *n*-nonacosane and 1-triacontanol (C31/C29/C30-1-ol) and 5, 50 % (*w/w*) of methyl oleate (MeO), oleic acid (OA), methyl linolenate (MeLin) and methyl stearate (MeSt) for heating cycle 2

showed three phase transitions (Figure 30, Figure 35). Addition of 5 % adjuvant resulted in an additional phase transition for MeO and MeLin. The OA mixture did not show this phenomenon, whereas MeSt showed four and one additional (below 40°C)

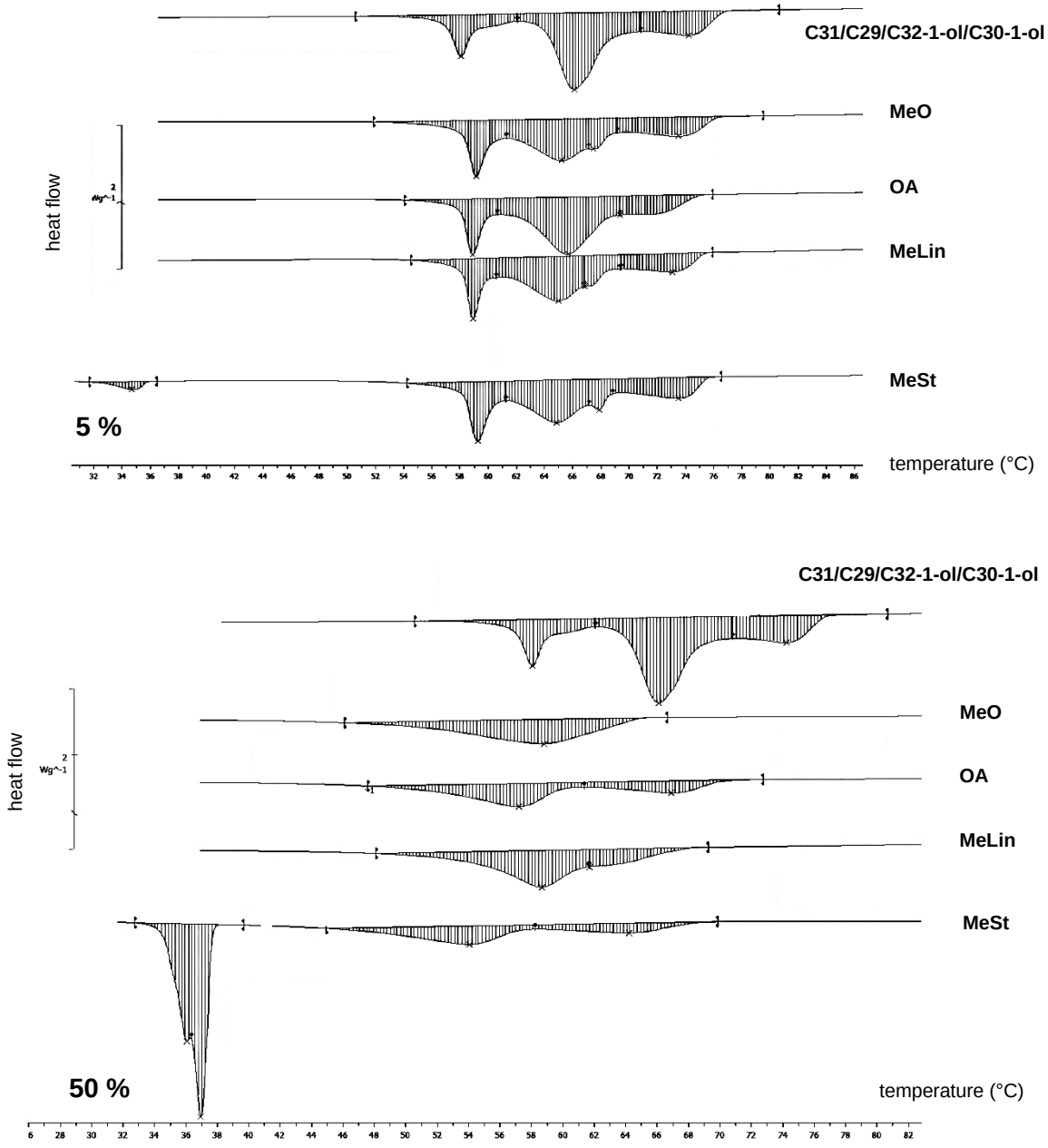

Figure 35 Thermograms of *n*-hentriacontane, *n*-nonacosane, 1-dotriacontanol and 1-triacontanol (C31/C29/C32-1-ol/C30-1-ol) and 5, 50 % (*w/w*) of methyl oleate (MeO), oleic acid (OA), methyl linolenate (MeLin) and methyl stearate (MeSt) for heating cycle 2

phase transitions. Looking at the 50 % mixture, it could be observed that MeO only showed one phase transition (melting), while addition of the other adjuvants resulted in two. The onset temperature of the first phase transition was reduced for all adjuvants (Δ 3°C - 10°C). The offset temperature of the last phase transition was lowered the most for MeO (Δ 12°C), followed by MeSt (Δ 8°C), OA and MeLin (both Δ 7°C). The

leaf wax of *S. elegantissima* also showed a reduction of melting offset temperatures for the 5 % mixture (Δ 3°C) and for the 50 % mixture (Δ 2°C - 7°C, Figure 36). In comparison to the 50 % MeO - quaternary mixture, the reduction of the melting offset was lower for the leaf wax than for the quaternary mixture.

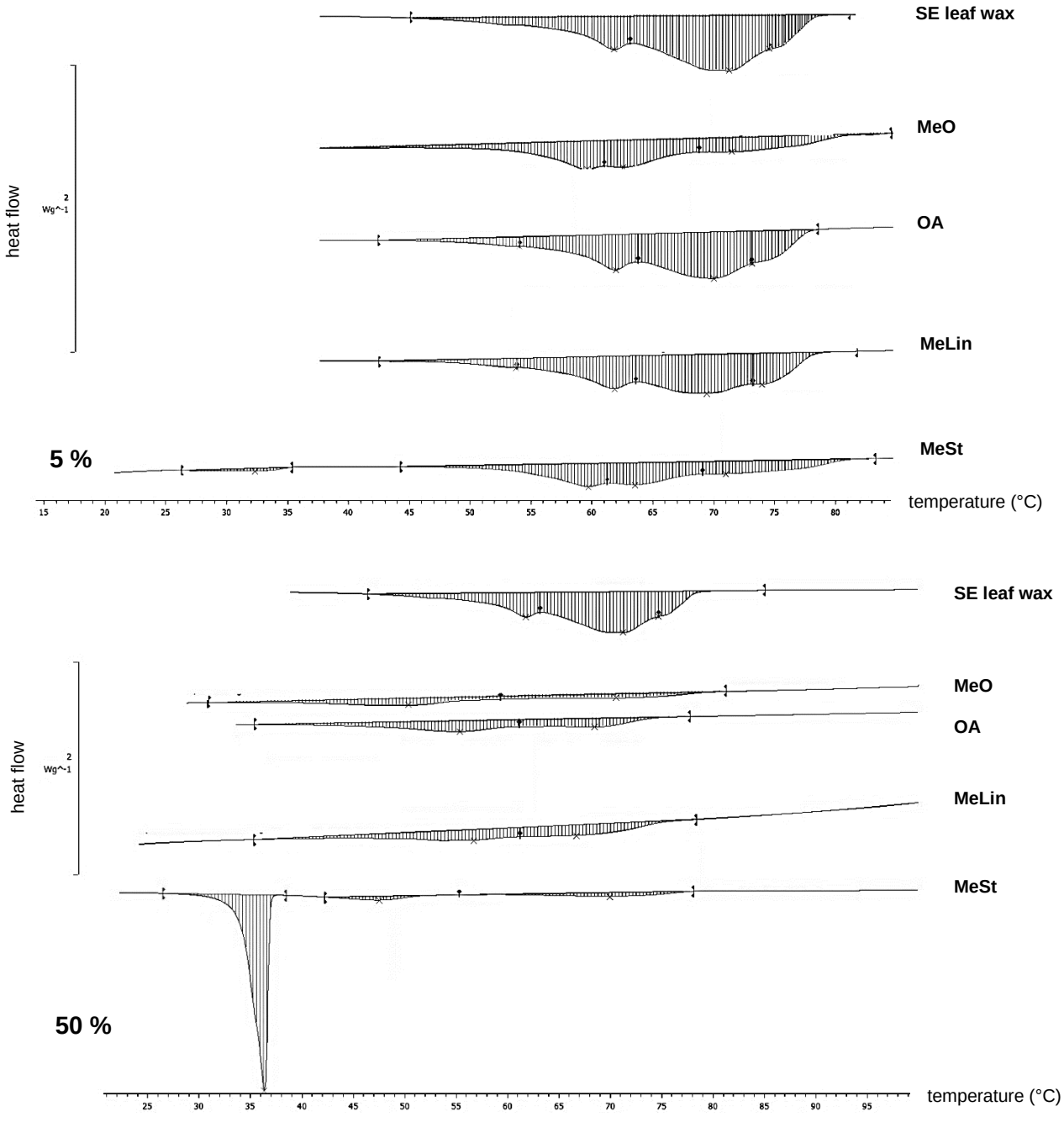

Figure 36 Thermograms of *Schefflera elegantissima* leaf wax (SE leaf wax) and 5, 50 % (*w/w*) of methyl oleate (MeO), oleic acid (OA), methyl linolenate (MeLin) and methyl stearate (MeSt) for heating cycle 2

3.3.2.3 Addition of the adjuvant C10E2, C10E8 to the model wax and Schefflera elegantissima leaf wax

The addition of the alcohol ethoxylates resulted in slight decreases of the start melting temperature from 69.1°C to 62.3°C (50 % C10E2) and 66.8°C (50 % C10E8) (Figure 37). The onset temperature of the first phase transition decreased with 50 % C10E2 from 57.4°C (pure leaf wax) to 49.5°C, whereas the use of 50 % C10E8 increased the temperature slightly to 58.0°C. Both adjuvants showed only two phase transitions when added to the leaf wax. Data of the thermograms can be found in Appendix 26.

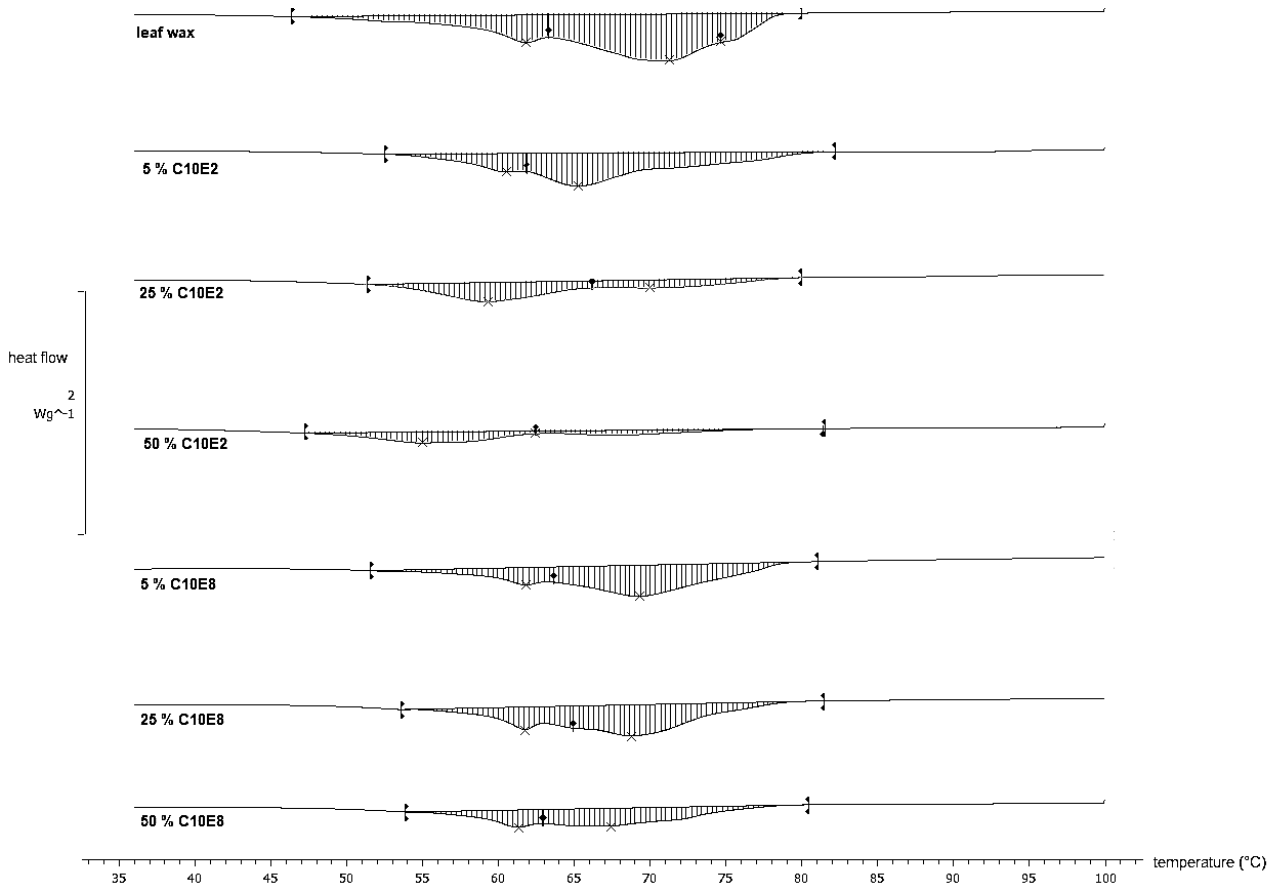

Figure 37 Thermograms of *Schefflera elegantissima* leaf wax (no adjuvant) and 5, 25, 50 % (*w/w*) of diethylene glycol monodecyl ether (C10E2) and octaethylene glycol monodecyl ether (C10E8)

3.3.2.4 Enthalpy of transition

The enthalpy of transition (EOT) describes the energy of a phase transition due to polymorphic transitions, melting or crystallization. All adjuvants decreased the absolute value of the total EOT, being the sum of the single EOTs in one thermogram, with all wax mixtures by influencing the endothermic phase transition during the heating cycle (Figure 38). MeSt showed the lowest decrease of the total EOT with no effect between 5 and 50 % adjuvant proportion with all mixtures starting from 5 % or from 25 % adjuvant proportion. The other oil adjuvants decreased the absolute values of the total EOT in a similar way amongst themselves by nearly showing a linear relation to the added amount of adjuvant. The surfactants in combination with the leaf wax also showed a decrease of the total EOT, even higher than the oil adjuvant blends. Within the leaf wax blends, the highest decrease was found for the mixture of C10E2.

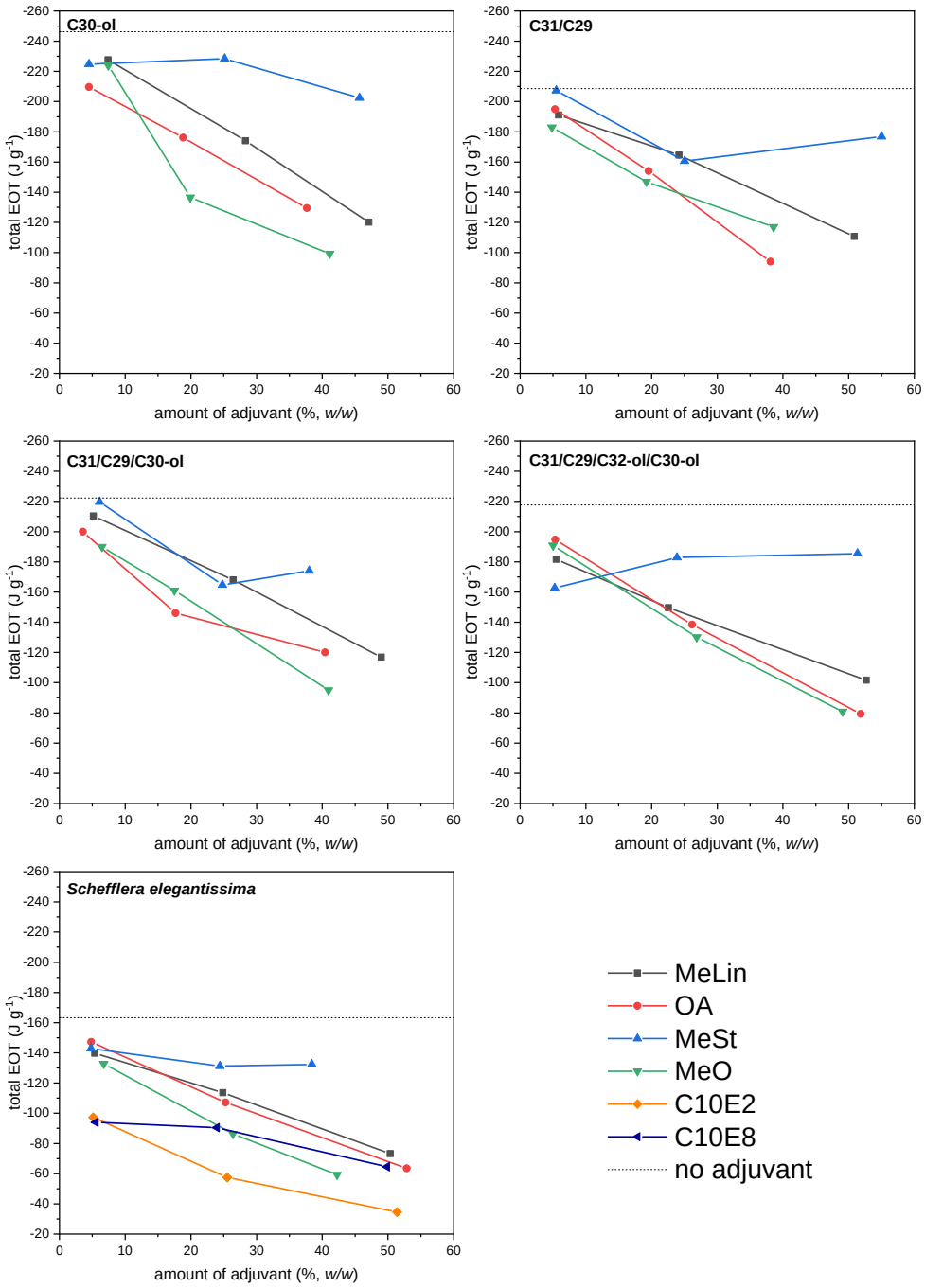

Figure 38 Total enthalpy of transition (EOT) for heating cycle 2 plotted *vs.* the amount of adjuvant (% *w/w*) for methyl linolenate (MeLin), oleic acid (OA), methyl stearate (MeSt) and methyl oleate (MeO), diethylene glycol monodecyl ether (C10E2), octaethylene glycol monodecyl ether (C10E8) in 1-triacontanol (C30-1-ol), mixture of *n*-hentriacontane and *n*-nonacosane (C31/C29), mixture of *n*-hentriacontane, *n*-nonacosane, 1-triacontanol (C31/C29/C30-1-ol), mixture of *n*-hentriacontane, *n*-nonacosane, 1-triacontanol, 1-dotriacontanol (C31/C29/C32ol/C301-ol) and *Schefflera elegantissima* leaf wax. Dotted line represents total EOT of the non-adjuvanted control.

3.3.3 Infrared spectroscopy

3.3.3.1 Phase behaviour of Schefflera elegantissima leaf wax

To study the phase behaviour of the wax samples, the wavenumber of the asymmetric stretching band, which is the maximum between 2915 and 2924 cm^{-1}, was plotted *versus* the temperature (Figure 39, Figure 40). The leaf wax and the oil adjuvants showed a curve of sigmoidal shape. The oil adjuvants decreased the melting range (5 to 95 % wavenumber change) below 65°C - 80°C. At all adjuvant levels the whole melting range shifted to lower temperatures. No difference in melting ranges or curve shapes between the different oil adjuvant wax mixtures was seen at any adjuvant level.

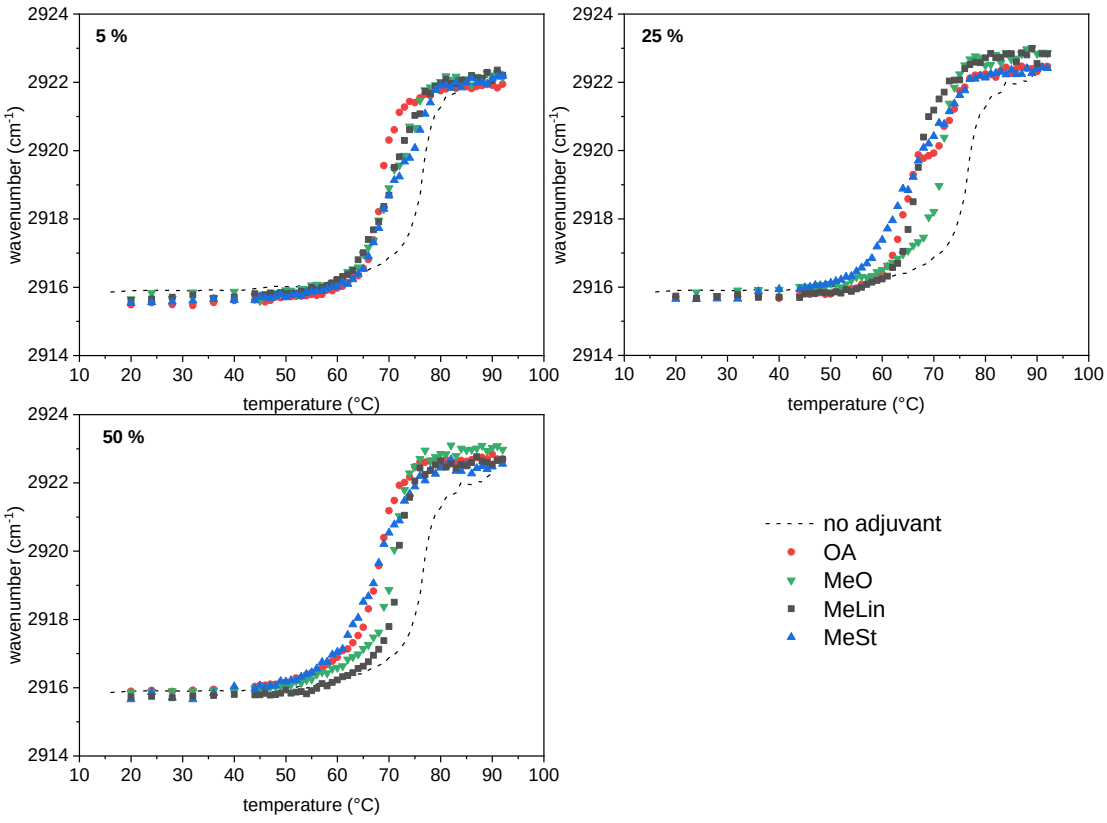

Figure 39 Phase behaviour measured by h-ATR-FTIR with pure *Schefflera elegantissima* leaf wax (no adjuvant) and in combination with 5, 25 and 50 % (*w/v*) methyl linolenate (MeLin), oleic acid (OA), methyl stearate (MeSt) and methyl oleate (MeO). The wavenumber of the asymmetric stretching band in the range of 2915 to 2924 cm^{-1} *vs.* the temperature is shown.

The addition of the alcohol ethoxylates C10E2 and C10E8 showed a similar phase behaviour like the oil adjuvants (Figure 40). The addition of each surfactant yielded in the shifts of the melting ranges at 5, 25 and 50 % to lower temperatures starting at 55°C (50 % surfactant) instead of 65°C (pure leaf wax).

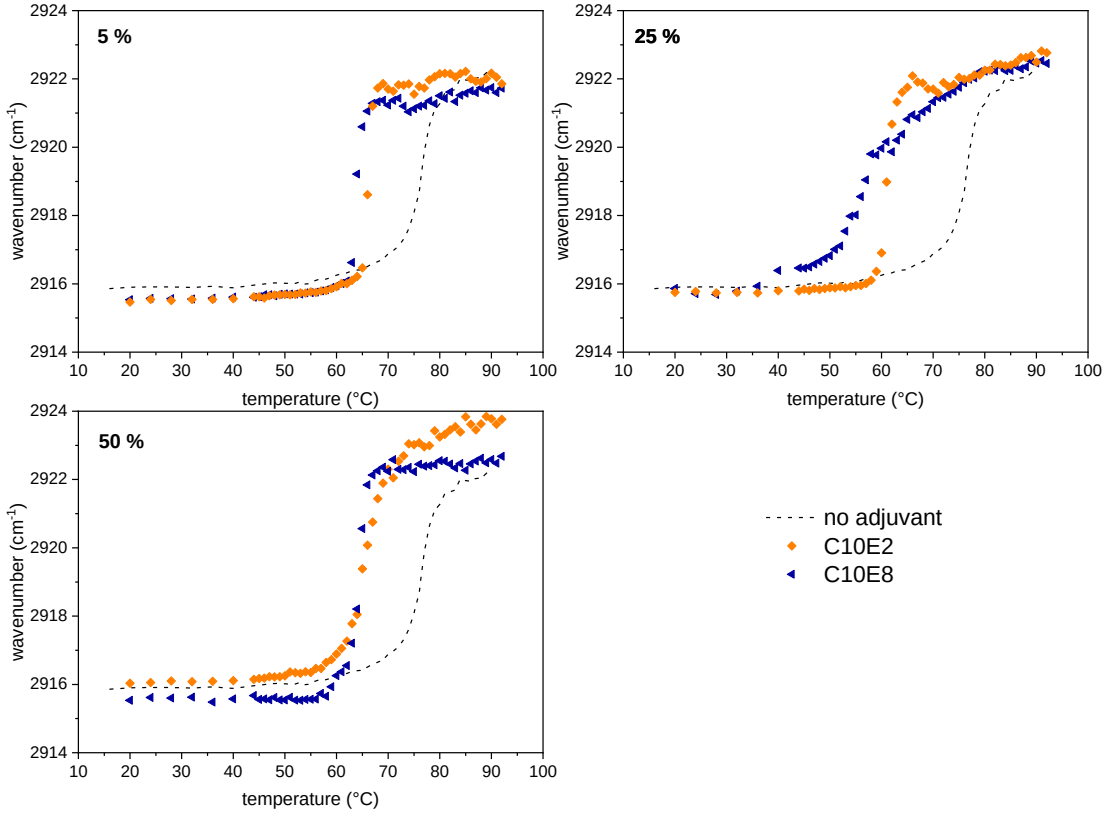

Figure 40 Phase behaviour measured by h-ATR-FTIR with pure *Schefflera elegantissima* leaf wax (no adjuvant) and in combination with 5, 25 and 50 % diethylene glycol monodecyl ether (C10E2) and octaethylene glycol monodecyl ether (C10E8). The wavenumber of the asymmetric stretching band in the range of 2915 to 2924 cm^{-1} *vs.* the temperature is shown.

3.3.3.2 Aliphatic crystallinity

Aliphatic crystallinity at 20°C was calculated according to Equation 10 and is shown in Figure 41 and Figure 42. Pure *S. elegantissima* leaf wax showed a value of 90.7 % (0.95-CI 88.4 % - 93.1 %) and crystallinity showed similar values (t-test, $p = 0.05$) to the pure artificial leaf wax (91.1 %; 84.2 % - 98.1 %). Statistical parameters are given in Appendix 29. The crystallinity of the leaf wax with one adjuvant at the same level of adjuvant proportion (5, 25, 50 %) was compared to the values of the artificial wax mixture (t-test, $p < 0.05$, $3 < \bar{n} < 4$). The comparison resulted in no significant difference, except at 25 % OA and 5 % C10E8. For 5 % C10E8, the crystallinity was slightly lower for the artificial wax (82.7 %; 79.9 %- 85.6 %) than the leaf wax 91.2 % (89.3 % - 93.1 %) while 25 % OA showed higher values for the artificial 92.0 % (86.0 % - 98.0 %) than the leaf wax 84.6 % (81.2 % - 88.1 %).

While crystallinity only decreased using the leaf wax in combination with 50 % MeO, the artificial wax mixture also showed a decrease with 50 % MeLin. The addition of the surfactants C10E2, C10E5 and C10E8 at the three adjuvant proportions did not significantly differ in comparison to the control of pure leaf or artificial wax (Figure 42; Dunnett's test, $p < 0.05$, $3 < \bar{n} < 4$). For the oil adjuvants, a significant decrease for both waxes after the addition of 50 % MeO was found (Figure 41; Dunnett's test, $p < 0.05$, $p < 0.05$, $3 < \bar{n} < 4$). At the levels of 5 and 25 % oil adjuvant wax proportion, no differences were observed.

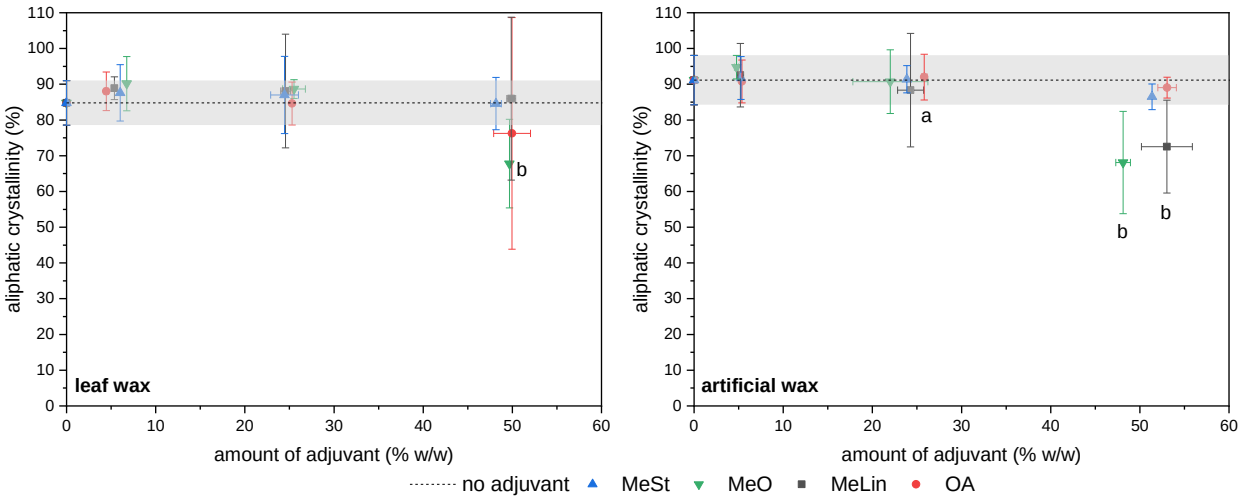

Figure 41 Aliphatic crystallinity at 20°C for the artificial model wax and the *Schefflera elegantissima* leaf wax pure (grey hatching) and with 5, 25, 50 % adjuvant (*w/w*) using methyl linolenate (MeLin), oleic acid (OA), methyl stearate (MeSt) and methyl oleate (MeO).). (a) represents significant difference between leaf and artificial wax at one level of one adjuvant (t-test, $p < 0.05$, $3 < \bar{n} < 4$); (b) represents significant difference of one wax adjuvant blend to the pure wax control (Dunnett's test, $p < 0.05$, $3 < \bar{n} < 4$). Data points represent the mean value, error bars indicate the 95%-confidence interval.

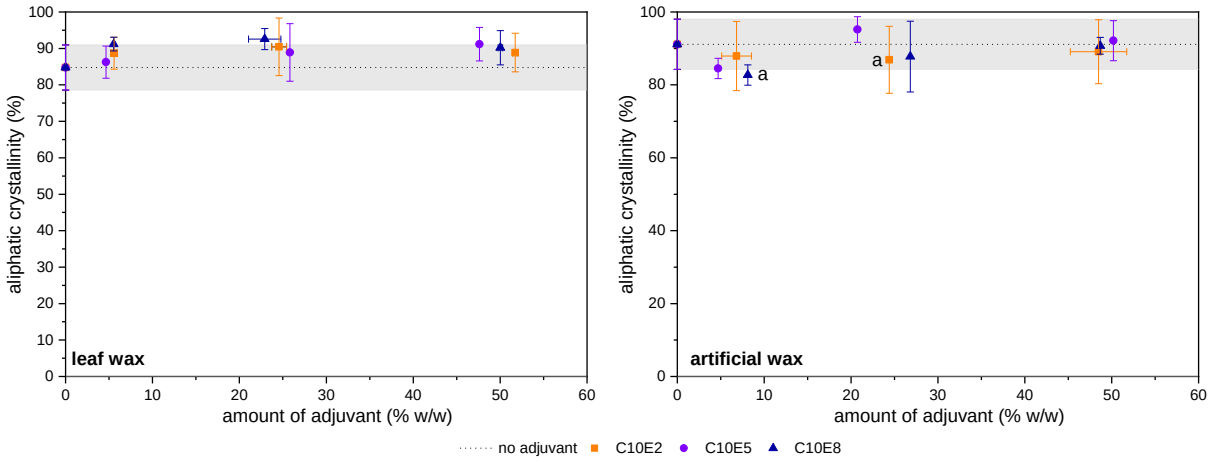

Figure 42 Aliphatic crystallinity at 20°C for the artificial model wax and the *Schefflera elegantissima* leaf wax pure (grey hatching) and with 5, 25, 50 % adjuvant (*w/w*) using diethylene glycol monodecyl ether (C10E2), pentaethylene glycol monodecyl ether (C10E5) and octaethylene glycol monodecyl ether (C10E8). Data points represent the mean value, error bars indicate the 95%-confidence interval. Grey hatching indicates 95%-confidence interval of the pure leaf and artificial wax, respectively. (a) represents significant difference between leaf and artificial wax at one level of one adjuvant (t-test, $p < 0.05$, $3 < \bar{n} < 4$). (b) represents significant difference of one wax adjuvant blend to the pure wax control (Dunnett's test, $p < 0.05$, $3 < \bar{n} < 4$). Data points represent the mean value, error bars indicate the 95%-confidence interval.

3.3.4 Cuticular water permeance

3.3.4.1 Isolated cuticular membranes and leaf envelopes using pure MeO

Mean cuticular water permeance ranged from 4.73 (25th – 75th quartile, 3.87 - 6.25) x 10^{-6} m s^{-1} with CM of *P. laurocerasus* to 34.28 (30.59 - 41.38) x 10^{-6} m s^{-1} with leaf envelopes of *G. xanthochymus* (Figure 43). Statistical parameters are given in Appendix 30. Effects of the water permeance using pure MeO, CM and envelopes showed values between 1.65 and 3.44 (Table 10).

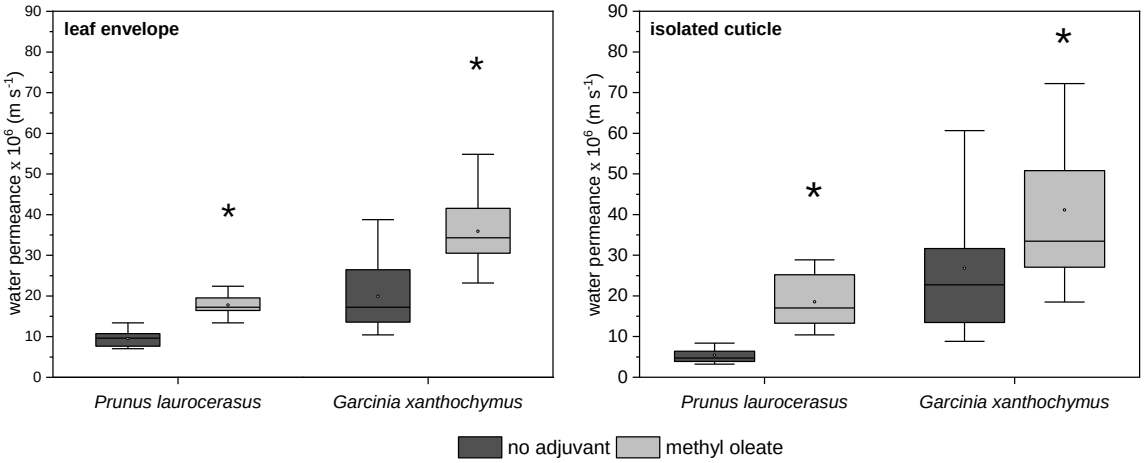

Figure 43 Cuticular water permeance using leaf envelopes and isolated cuticles with and without methyl oleate for *Prunus laurocerasus* and *Garcinia xanthochymus.* Boxes represent 25th and 75th percentile. Horizontal line represents the median. Whiskers represents 10th and 90th percentile. Asterisk above the box represents significant difference to the control without adjuvant (paired t-test, $p < 0.05$, $12 < \bar{n} < 22$).

For both species (*P. laurocerasus* and *G. xanthochymus*) and conditions (CM - envelopes), data showed a significant increase using pure MeO in comparison to the non-adjuvanted control (paired t-test, $p < 0.05$, $12 < \bar{n} < 22$). Comparison of the permeances of one species between the two different methods (CM - envelopes) at the levels ‘no adjuvant’ and ‘MeO’ yielded no significant difference except for *P. laurocerasus* without adjuvant (Welch Two-sample t-test, $p < 0.05$, $12 < \bar{n} < 22$).

Table 10 Effects of the water permeance between methyl oleate (MeO) and no-adjuvant with cuticular membranes (CM) and leaf envelopes (env) of *Prunus laurocerasus* and *Garcinia xanthochymus*[g]

species	treatment	effect	0.95 - confidence interval
Prunus laurocerasus	CM	3.44	3.00 - 3.95
	env	1.88	1.69 - 2.10
Garcinia xanthochymus	CM	1.65	1.31 - 2.07
	env	1.89	1.67 - 2.14

[g] Data is given as quotient of the mean permeance with MeO and permeance without adjuvant calculated using mean and confidence intervals of lognormal transformed permeance data and retransformation.

3.3.4.2 Isolated cuticular membranes using oil derivatives and surfactants

Investigation of the cuticular water permeance with CM of *P. laurocerasus* and the surfactants C10E2, C10E5, C10E8 resulted in median values ranging from 23.8 x 10^{-6} m s^{-1} (25^{th} – 75^{th} quartile, 20.4 - 68.6 x 10^{-6} m s^{-1}) to 97.2 x 10^{-6} m s^{-1} (34.6 - 163.5 x 10^{-6} m s^{-1}) and showed a significant difference to the non-adjuvanted control (Figure 44). Statistical parameters are given in Appendix 31.

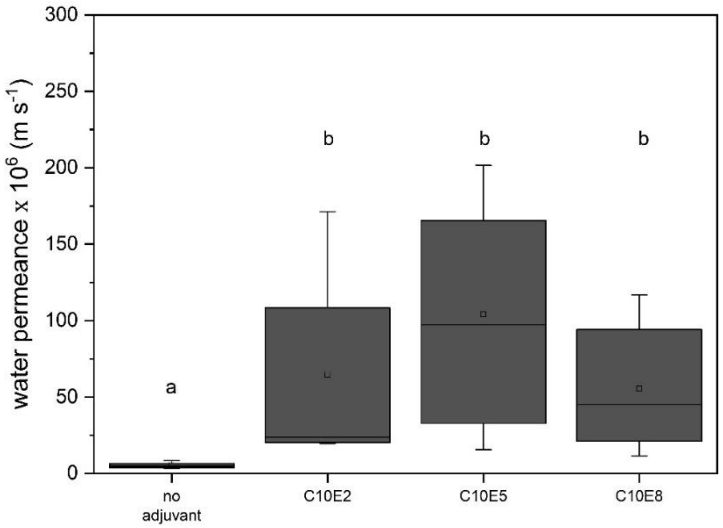

Figure 44 Cuticular water permeance using isolated cuticles for *Prunus laurocerasus.* Boxes represent 25^{th} and 75^{th} percentile. Horizontal line represents the median. Whiskers represent 10^{th} and 90^{th} percentile. Letters indicate significant difference for unpaired samples (Kruskal-Wallis ANOVA with post-hoc Dunn's test, $p < 0.05$, $6 < \bar{n} < 22$). Diethylene glycol monodecyl ether (C10E2), pentaethylene glycol monodecyl ether (C10E5), octaethylene glycol monodecyl ether (C10E8).

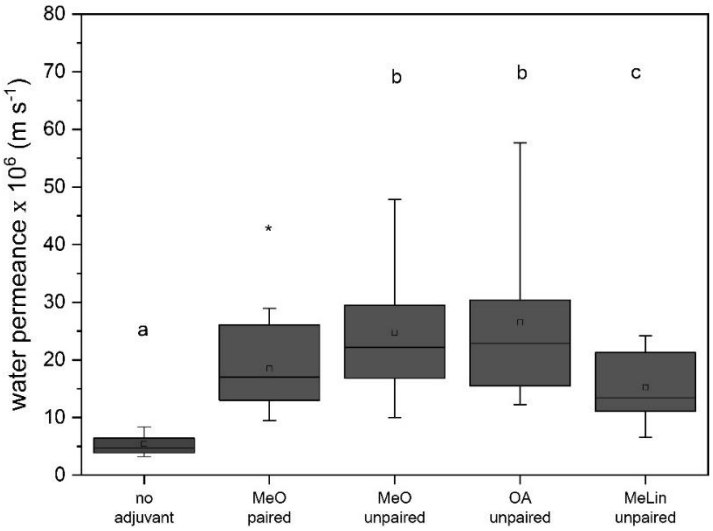

Figure 45 Cuticular water permeance using isolated cuticles for *Prunus laurocerasus.* Boxes represent 25th and 75th percentile. Horizontal line represents the median. Whiskers represent 10th and 90th percentile. Asterisk above the box represents significant difference to the control without adjuvant (no adjuvant) for paired samples (paired t-test, $p < 0.05$, $22 < \bar{n} < 27$). Letters indicate significant difference for unpaired samples (Kruskal-Wallis ANOVA with post-hoc Dunn's test, $p < 0.01$, $12 < \bar{n} < 28$). Methyl oleate unpaired (MeO unpaired), methyl oleate paired (MeO paired), oleic acid unpaired (OA unpaired), methyl linolenate unpaired (MeLin unpaired).

The use of pure MeO, OA and MeLin showed increased median values ranging from 13.42 x 10^{-6} m s^{-1} (11.19 - 20.98 x 10^{-6} m s^{-1}) to 22.85 x 10^{-6} m s^{-1} (15.68 - 30.20 x 10^{-6} m s^{-1}, Figure 45). Water permeances with the oil adjuvants were significantly higher than permeances of the control (Figure 45). Statistical parameters can be found in Appendix 31. The paired sample as well as the unpaired sample using pure MeO showed a significant increase of the permeance. Effects of the water permeance (quotient of median permeance with adjuvant and without adjuvant) to the non-adjuvanted control were generally lower for the oil adjuvants than the effects for the surfactants.

3.3.5 Contact angle measurements

The highest CA after 60 s was measured for pure water (mean 108.1° ± SD 0.7°) while the surfactant solutions showed CAs declining from C10E8 (60.9° ± 0.3°), C10E5 (49.3° ± 1.4°) to C10E2 (44.4° ± 3.0°, Figure 46). Significant differences were found between all treatments (ANOVA with post-hoc Dunnett's T3 test $p < 0.01$, $6 < \bar{n} < 12$). Statistics are given in Appendix 34. CAs for C10E2 and C10E5 were below 50 % of the CA for the water control. The CA increased with the EO number, also shown in Figure 48.

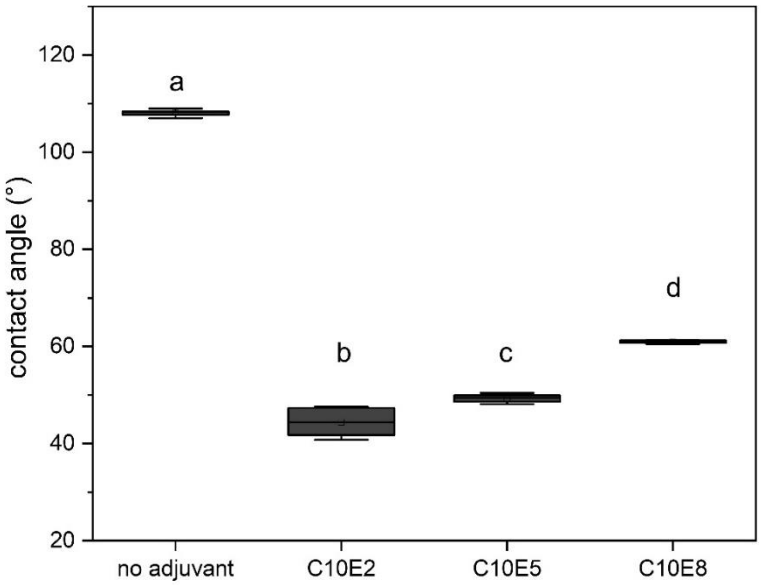

Figure 46 Contact angles of water, diethylene glycol monodecyl ether (C10E2), pentaethylene glycol monodecyl ether (C10E5) and octaethylene glycol monodecyl ether (C10E8) measured at 60 s. Box plots represent 25th and 75th percentile. Horizontal line represents median. Whiskers represent 10th and 90th percentile. Different letters above the box represent significant difference (ANOVA with post-hoc Dunnett's T3 test $p < 0.01$, $6 < \bar{n} < 12$).

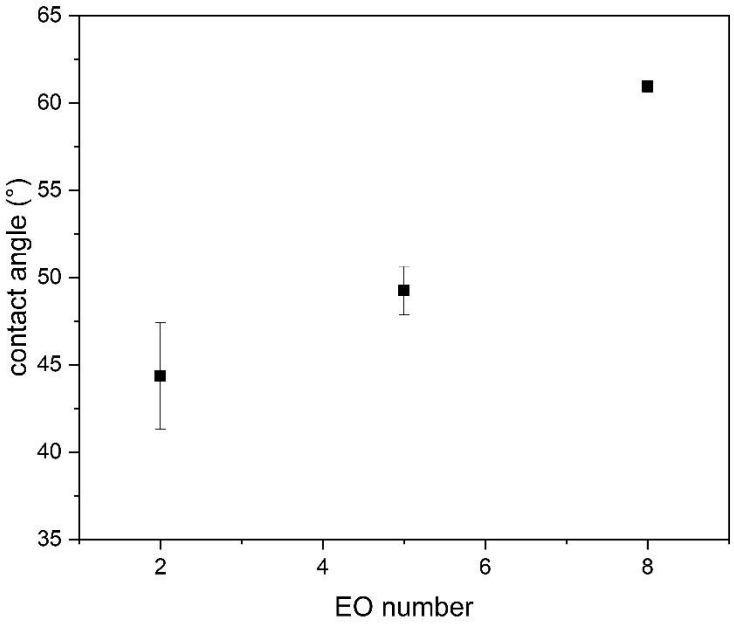

Figure 48 Contact angles at 60 s plotted *versus* the ethylene oxide monomer number (EO number). Data points represent mean values. Error bars represent standard deviation ($6 < \bar{n} < 12$).

The CA stayed constant for water over 60 s, as was also seen with C10E5 and C10E8 (Figure 47). Only C10E2 showed a slight decline of the CA of 4° over the sampling time.

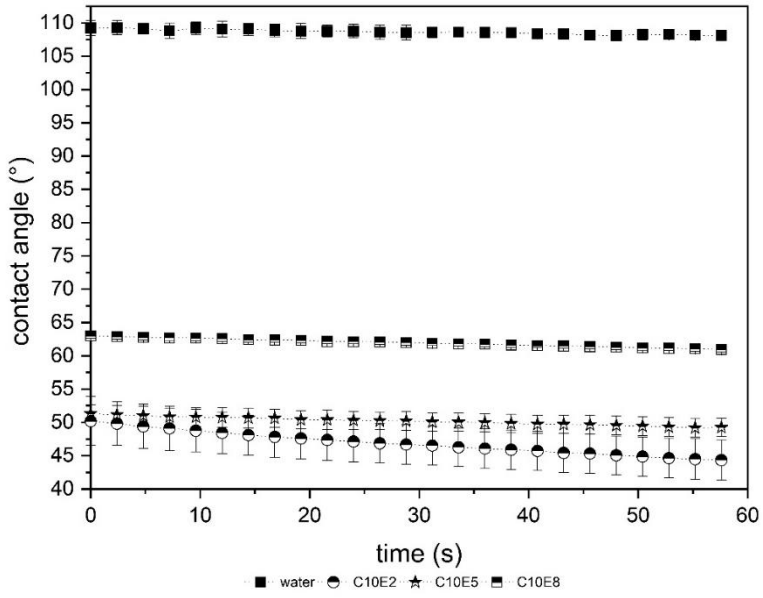

Figure 47 Contact angles of water, diethylene glycol monodecyl ether (C10E2), pentaethylene glycol monodecyl ether (C10E5) and octaethylene glycol monodecyl ether (C10E8) measured over 60 s. Dots represent the mean, whiskers indicate standard deviation ($6 < \bar{n} < 12$).

3.4 Discussion

3.4.1 *Schefflera elegantissima* wax

As dipping the whole leaves of *S. elegantissima* included both leaf sides (abaxial and adaxial), it is not surprising that the amounts and also the composition of the wax differs to some extent. A previous study by Jetter and Riederer (2016) reported a total wax coverage of 18.4 µg cm^{-2}. This value is nearly threefold higher than the present experimental data. Alkanes comprised 80 % of the total wax, followed by the alcohols (9 %), fatty acids and aldehydes (both 3 %). Although the percentages given in this publication differ from the present investigation, the alkanes and alcohols appear to be the most abundant chemical classes in both studies. It was reported that C31, C29 and C32-1-ol, C30-1-ol were the predominant aliphatic compounds (Jetter and Riederer, 2016). Similar results were also found in the present study (Figure 29).

As reported by Hauke and Schreiber (1998), cuticular wax coverage can vary quantitatively and qualitatively during the year. Growing conditions can influence the wax composition as well as the cultivar (Svenningsson, 1988; Zeisler and Schreiber, 2016). Therefore, it is not surprising that the two observations of *S. elegantissima* cuticular wax differ in terms of wax amount and composition.

Seufert (2019) was able to mimic the cuticular wax of *S. elegantissima* using the four most abundant aliphatic compounds in the proportion of 5.4/2.3/2.3/1 (C31 / C29 / C32-1-ol / C30-1-ol). This composition was investigated using XRD and DSC and was found to be well suited as an artificial model wax based on the cuticular wax of *S. elegantissima.* The same plant for the study by Seufert (2019) and the current study was used, differing only in the harvest time. The ratio of the C32-1-ol and C30-1-ol stayed the same, while the ratio of the alkanes in comparison to the alcohols increased for the batch used in the current study. As it was mentioned above, the wax coverage can quantitatively differ during the year (Hauke and Schreiber, 1998). Hence, the differences in wax composition and wax amount can easily be explained. Seufert (2019) accomplished the imitation of the cuticular wax of *S. elegantissima* providing a feasible artificial model wax for further studies in terms of phase behaviour, permeability and crystallinity. Even though the absolute amounts of the wax compounds differed between the two studies, the leaf wax was further used and physicochemical parameters in comparison to the model wax provided by Seufert (2019) were checked.

3.4.2 Comparison of the model wax to the *S. elegantissima* leaf wax

The wax phase behaviour, hence the phase transition properties during heating, is an important parameter for the basic understanding of plant waxes. Several studies dealt with the imitation of a plant cuticular wax and investigated the effect of adjuvants on the phase behaviour (Schreiber, 1995; Carreto *et al.*, 2002; Fagerström *et al.*, 2013b; Fagerström *et al.*, 2014; Webster *et al.*, 2018). The objectives were mainly to provide an artificial model wax which can be easily produced and is available in high amounts for *e.g.* screenings. Thus, harvesting of a huge amount of plant leaves would not be necessary anymore. Carreto *et al.* (2002) used a binary mixture of 1-tetradecanol and 1-octadecanol, whereas Schreiber (1995) selected tetracosanoic acid as a typical plant cuticular wax representative. Another study used two surfactants in combination with a model wax of *Clivia miniata* Regel and studied the wax fluidity and softening effects of a mixture of 1-docosanol, dotriacontane and water (Fagerström *et al.*, 2014). Previously, Webster *et al.* (2018) reported the use of tristearin as an artificial wax representative. They used DSC and XRD and examined the wax after adding several oil adjuvants. The authors represented tristearin as a model wax for a high-throughput screening of adjuvants. The oil adjuvants were premixed with the plant wax of *Ficus macrophylla* and tristearin and investigated by DSC and XRD. A concentration-dependent change of the *α*-crystallite-level of tristearin was found after adding the adjuvants which correlated between the artificial and the plant wax. As it has been reported, the *α*-crystallite-level of tristearin is the kinetically stable form (Matovic *et al.*, 2005), whereas it changes into the thermodynamically stable *β*-crystallite after addition of the adjuvants. Total crystallinity values for the wax adjuvant blends were not reported, only changes in the *α*-crystallite-level were shown. Seufert (2019) reported the use of an artificial mode wax related to the four compounds C31/29/C30-1-ol/C32-1-ol based on the adaxial cuticular leaf wax. As he provided data on feasibility of the quaternary mixture as a model wax, the objective of this study was to investigate the phase behaviour of the wax in combination with oil and surface active adjuvants.

It was reported that the binary alkane mixture showed two phase transitions, as well as the alcohol-mixture C32-1-ol/C30-1-ol (Seufert, 2019). For the alkanes and plant waxes in general, it is well established that they are packed in an orthorhombic lattice at room temperature and undergo a transition into the hexagonal-state when temperature is increased (Basson and Reynhardt, 1991; Reynhardt and Riederer, 1994). For a binary mixture of *n*-octadecane and *n*-tetradecane (C28/C24) in the molar

proportion of 3.5/1.5, the hexagonal-transition was found in the range of 47°C to 57°C being slightly below the transition of the C31/C29-alkane mixture (Figure 33). It is not surprising that the C31/C29-blend showed higher values than the C28/C24-mixture, as it is well-known that longer alkanes have higher melting-points and also higher temperatures for the hexagonal-phase transition (Briard *et al.*, 2003). Three transitions were found for the quaternary mixture (C31/C29/C32-1-ol/C30-1-ol) as well as the leaf wax (Figure 30). Onset and offset temperatures of the phase transitions of the alkanes were lower and in a smaller range than the alcohol-mixture (C32-1-ol/C30-1-ol) reported by Seufert (2019). It has been reported that *n*-octadecane and *n*-tetradecane (C28-1-ol /C24-1-ol) undergo a solid-solid transition from hexagonal to orthorhombic state (Carreto *et al.*, 2002). This transition was only visible during the recrystallization cycle as the two transitions are believed to be in a similar temperature range during heating. The two phase transitions of the alcohol-mixture (C32-1-ol/C30-1-ol) reported by Seufert (2019) are assumed to be a solid-solid phase transition (solid-hexagonal) of the alcohols followed by the melting (Tasumi *et al.*, 1964; Cholakova and Denkov, 2019). The quaternary mixture showed three transitions during the heating cycle. It was proposed that the first one is the solid-solid phase transition of the alkanes decreasing to lower temperatures in comparison to the pure alkanes (Figure 30). The second transition could be the melting of the alkanes, including the hexagonal phase transition of the alcohols. It is assumed that the last transition is the melting of the alcohols. Looking at the EOT, similar values for the first transition were found between the leaf and artificial wax (Table 9). The energy of the second transition was slightly more negative for the leaf than for the artificial wax, while the value of the last transition of the artificial wax was nearly threefold the value of the leaf wax. The onset and offset temperature for the last transition were higher for the leaf wax than the model wax, indicating a melting range at higher temperatures for the first. This is not surprising, as the leaf wax contains a higher proportion of compounds, *e.g.* triacontanoic acid having a higher melting point (94.0°C, Wishart *et al.*, 2018) than the pure compounds C31 (67.56°C, Serrato-Palacios *et al.*, 2015), C29 (63.45°C, Broadhurst, 1962), C30-1-ol (93.6°C - 93.9°C, Piper *et al.*, 1934), C32-1-ol (96.1°C - 96.3°C, Piper *et al.*, 1934). For both native waxes, this study showed good consistency of the onset, offset temperatures and the EOT of the first and second phase transition. Only slightly differences for the second transition were found between the two waxes, while the last

transition showed higher deviations for the onset, offset and the EOT. However, the peak temperature was similar.

To sum up, this study correlates well with the results reported by Seufert (2019) and showed, that the quaternary mixture is a feasible artificial model wax to mimic the cuticular leaf wax properties of *S. elegantissima*.

3.4.3 Interaction between the adjuvants and the model and leaf wax

One major aim of agrochemistry is to provide high biodelivery and efficacy of the applied pesticide formulation. Thereby, the cuticular barrier is often manipulated to enhance the AI permeation into underlying plant tissue, but the exact mode of the manipulation process has been unkown to date. Providing a model wax, which can be easily produced at low costs, the influence of formulants like adjuvants on the cuticular, waxy barrier can be investigated. Thus, the objective of this chapter was to test the validity of the model wax adjuvants blends in comparison to the aliphatic plant cuticular wax mixtures. As it was shown previously, the model wax is well suited to mimic the cuticular leaf wax properties of *S. elegantissima*. As a next step, the interaction of adjuvants with the leaf and the model wax should be tested. The pure C30-1-ol, binary alkane-mixtures, the ternary mixture (C31/29/C30-1-ol) and the quaternary mixture (C31/29/C32-1-ol/C30-1-ol) were studied without and with oil and surface active adjuvants.

The pure C30-1-ol melted in the range of 84.4°C – 86.4°C which is in good agreement with reported values (86.3°C – 86.5°C, Piper *et al.*, 1934). Even-numbered higher alcohols like *e.g.* C32-1-ol crystallize in the monoclinic *γ*-polymorph with *trans*-hydroxyl orientation (Tasumi *et al.*, 1964). Data for C30-1-ol is lacking, but it is assumed that C30-1-ol consists of a similar polymorph, as every alcohol between chain lengths of C18 to C34 exhibited the monoclinic *γ*-polymorphism. It has been reported, that primary alcohols can undergo a phase transition similar to alkanes from the monoclinic lattice to the hexagonal state (Larsson, 1986; Cholakova and Denkov, 2019). This could not be seen within this study showing only one transition from the monoclinic to the liquid state during the heating cycle (Figure 31). As a publication by Sirota and Wu (1996) showed, the transition temperatures for higher alcohols until a chain-length of 26 were in a narrow range. It might be possible, that both transitions are in an even smaller range for the C30-1-ol than the alcohols described by Sirota and Wu (1996). Hence, the transitions would overlap and only one phase transition would be

investigated. This is shown in the thermogram of the cooling cycle in Figure 32. Here, it becomes obvious that the alcohol underwent two phase transitions, the orthorhombic-hexagonal and hexagonal-liquid one. Adding the oil adjuvants, the melting onset and offset decreased with increasing adjuvant proportion, as well as the absolute value of the total EOT (Figure 38). This indicates an interaction of the adjuvants with the alcohol and possibly a mixing of the adjuvant with the compound. The hexagonal phase transition during the heating cycle was not seen for the oil adjuvant-alcohol mixture, as was observed for the pure alcohol. The cooling cycles showed the two transitions, but only for 5 % adjuvant proportion (Appendix 11 - Appendix 19). For higher adjuvant levels, the hexagonal phase transition was suppressed.

The alkane mixture (C31/29) showed two phase transitions (Figure 33) known as the solid-solid transition (orthorhombic-hexagonal) and the hexagonal-liquid transition (Basson and Reynhardt, 1991). After adding the oil adjuvants, the absolute value of the EOT, onset and offset temperature decreased for the second transition, while the parameters for the first transition stayed constant (Figure 33, Figure 38). As the second transition is associated with the melting, it is obvious that this process was driven to lower temperatures. At the highest adjuvant proportion, only one phase transition which derived from the initial thermogram of the pure binary mixture was seen for all adjuvants except OA. It can not be defined which polymorph those mixtures have before they transition from the crystalline to the liquid state. Methods like XRD are needed in future, to check the polymorphism. It has been reported that the thermodynamically stable *β*-crystallite state of tristearin is formed after addition of oil adjuvants, whereas the kinetically stable *α*-crystallite (stable at room temperature) vanishes completely at higher adjuvant proportions (Webster *et al.*, 2018). Accordingly, it can only be assumed that the single phase transition at 50 % adjuvant proportion within this study is assigned to the hexagonal-liquid transition. It might be possible, that both transitions overlap even during the cooling cycle and therefore do not split into two peaks. This hypothesis could be checked in future experiments with heating and cooling cycles using heating rates below 2°C min^{-1}. In contrast to the other adjuvants, 50 % OA alone showed two phase transitions (orthorhombic-hexagonal and hexagonal-liquid). A possible explanation could be, that the chemical structure of OA and its carboxylic functional group, are not as effective as the other methylated adjuvants in influencing the wax structure, merging both transitions into one

temperature range, or in suppressing the orthorhombic-hexagonal transition completely.

The first phase transitions of the ternary mixture (C31/C29/C30-1-ol) can be associated with the transition of the C31/C29 blend from orthorhombic to hexagonal state, whereas the second one could be assigned to the hexagonal-liquid transition of the alkanes (Figure 34). This is supported by the similar onset and offset temperatures of the first and second peak of C31/C29 and C31/C29/C30-1-ol. If it is assumed that the alcohol and the alkanes do not form a homogeneous solid-solid solution, the last two transitions could be assigned to the solid-hexagonal and the hexagonal-liquid transition of the alcohol. Addition of the adjuvants reduced the offset temperatures of the melting transition. Proportion of 5 % MeLin, MeSt and MeO showed four transitions derived from the ternary mixture with a broader peak of the second transition. In contrast, only three transitions were observed for OA, possibly merging the transitions of the alcohols to the melting of the alkanes. At 50 % adjuvant-proportion, the number of phase transitions was further decreased to two for all adjuvants except MeSt (three plus one assigned to the solid transition of pure MeSt). Onset temperatures for the first transition were driven to temperatures below the native ternary mixture, but the offset temperature increased. This indicates a broadening of the transition, especially strongly seen with OA. The onset and offset of the second transition of 50 % MeO were nearly in the same range as the onset of the second transition of C31/C28/C30-1-ol and the offset of its fourth transition. It is assumed that the transitions of the native ternary mixture are merged after adding the adjuvant, and only show the transition into the liquid state.

In contrast to the four peaks that were found for the ternary mixture, the quaternary mixture (C31/C29/C32-1-ol/C30-1-ol) showed only three transitions (Figure 35). As was discussed in 3.4.2, the first transition can be associated with the solid-solid alkane transition from orthorhombic to hexagonal state, while the second peak could be a mixture of the hexagonal-liquid transition of the alkanes and the solid-hexagonal transition of the alcohols. The last peak might be the melting of the alcohols. Adding the adjuvants decreased the melting offset temperature with the highest effect at 50 % adjuvant proportion. At 5 % four phase transitions were seen for MeO, as well as for MeLin and MeSt. This indicates that the methyl ester group could be the cause of the separation of the second peak, as OA did not show this trend and possesses a carboxylic group instead of the methyl ester. It is striking that MeO only showed one

phase transition at 50 % adjuvant proportion, whereas the other adjuvants showed two (OA, MeLin) or more (MeSt). The total EOT showed the same trends for each adjuvant when increasing the adjuvant proportion, except for MeSt (Figure 38). Due to the addition of the liquid oil adjuvant to the different wax mixtures, the absolute value of the total EOT, which characterizes the absorbed or released energy during the phase transition, is reduced, as would be assumed due to a melting point depression. A similar behaviour of the total EOT for the leaf wax was investigated, indicating that the quaternary mixture can provide a feasible model wax (Figure 38). This was also supported by the investigation of decreased melting offset temperatures with the leaf wax in a similar range like the quaternary mixture.

The leaf and the artificial wax showed different number of peaks at 5 % adjuvant proportion for the methylated adjuvants. At 50 % adjuvant proportion, a similar number of peaks was detected, except for MeO. Only one peak was found for MeO with the quaternary mix, whereas the leaf wax showed two. As the leaf wax consists of more than four compounds, it is obvious that thermograms would differ as minor compounds can influence the phase behaviour.

Thermograms of leaf wax in combination with C10E2 and C10E8 showed decreased melting offsets and absolute value of the total EOT; the highest for C10E2 followed by C10E8 (Figure 37, Figure 38). Absolute values of total EOT also declined, showing the highest reduce of all adjuvants with C10E2, indicating the most effective interaction of the adjuvant with the wax to decrease the energy that is needed for phase transitioning. In general, it could be seen that the adjuvants decreased the total EOT and the melting offsets. Thereby, C10E2 was the most effective adjuvant with the highest decrease of total EOT and melting offset at 50 % adjuvant proportion, followed in the order: MeO > OA and C10E8 > MeLin > MeSt. As several authors stated, decreased melting offsets and total EOT indicate a plasticizing effect within the waxes (Coret and Chamel, 1994; Perkins *et al.*, 2005; Fagerström *et al.*, 2014). It was proposed that this disruption could be depicted as an influence on the cuticular wax domains influencing the amorphous and/or crystalline fraction (Fagerström *et al.*, 2014; Zhang *et al.*, 2016). The current data shows that C10E2 might be able to disrupt the wax structure the most, followed by the other adjuvants in the previously stated order (MeO > OA and C10E8 > MeLin > MeSt). As far as the oil adjuvants are concerned, it is obvious that two more double bonds (MeLin) and no double bond (Mest) are not as effective as MeO (one double bond) in decreasing the total EOT and melting behaviour. Concerning the alcohol

ethoxylates, a lower EO number is more effective than a higher EO number, which was also reported by Perkins *et al.* (2005).

It could be observed that the artificial wax provides a feasible model wax, as a similar tendency of the total EOT and the melting offset were found. To date, studies which tried to mimic cuticular wax only dealt with pure compounds (Webster *et al.*, 2018), binary (Carreto *et al.*, 2002) or ternary mixtures (Fagerström *et al.*, 2013b), but a higher number of compounds have not been reported. This is the first study to provide data on quaternary wax mixtures with decent phase behaviour in comparison to the related leaf wax. Comparing the results obtained with DSC to FTIR, it is obvious that DSC is more feasible than FTIR to determine phase transition parameters like start and end of melting. Parameters for the hexagonal phase transition can not be determined using FTIR as has also been reported by Merk (1998). The FTIR showed that for the oil and the surface active adjuvants, the melting range shifted to lower temperatures also with enhanced adjuvant proportion which is consistent with the DSC. As one sample takes more than 10 hours to measure one heating and cooling cycle by FTIR in comparison to DSC which only takes 2-3 h, it is obvious that DSC is more feasible to study the phase behaviour of plant wax. Nevertheless, the important parameter of crystallinity can not be measured using DSC, therefore the following section (3.4.4) will discuss the part of crystallinity using FTIR in detail.

3.4.4 Aliphatic crystallinity and plasticization

Within this chapter, it was possible to comprehensively study the phase behaviour of the adjuvant wax blends using the methods DSC and FTIR. It was possible to detect similar results for both methods: a shift of the melting range to lower temperatures after adding the adjuvants. The next step was to have a look into the aliphatic crystallinity before and after the application of adjuvants. As it was reported by several authors, adjuvants like oil derivatives and alcohol ethoxylates should act as plasticizers influencing the wax crystallinity and thus leading to enhanced AI penetration (Coret and Chamel, 1994; Coret and Chamel, 1995; Schreiber *et al.*, 1996; Burghardt *et al.*, 1998; Perkins *et al.*, 2005; Fagerström *et al.*, 2014; Zhang *et al.*, 2016). The current results show a decrease of the crystallinity for MeO at 50 % adjuvant proportion for the leaf and the artificial quaternary wax, but not at 5 or 25 %. With 50 % MeLin and the quaternary wax, the crystallinity also decreased significantly (Figure 41). *Prima facie*, it is striking that the leaf wax did not show this decline with MeLin. At second glance, this can be explained by the fact that the leaf wax consists of more than four compounds used in the quaternary mixture leading to different interactions of the adjuvant and the wax compounds. Looking at the crystallinities measured for the surfactants, it is striking that the values remained constant even at 50 % adjuvant proportion (Figure 42). As the studies by Perkins *et al.* (2005), Coret and Chamel (1994) and Fagerström *et al.* (2014) reported, the plasticizing effect of adjuvants was derived from the decreased melting onset and the decrease of total EOT. Applying this knowledge to the current study, it is obvious that all adjuvants are supposed to act as plasticizer by interacting with the wax compounds. However, the aliphatic crystallinity values do not match this theory as plasticization would mean a decrease of the crystallinity after adding the adjuvant. For MeO, the crystallinity did not decrease at 5 and 25 % adjuvant proportion which could be caused by an embedding of the adjuvant into the crystalline phase with a simultaneous increase of the amorphous phase (Figure 49). Here, it is assumed that the alkyl chain is be embedded into the aliphatic hydrocarbon wax chains, whereas the methyl ester group is situated in the amorphous fraction build by functional groups and chain ends of VLCAs. Even at 50% adjuvant proportion, the crystallinity was not decreased to 42.4 % crystallinity (which would represent a decrease of 50 % in comparison to the pure leaf wax). This indicates that amorphization and crystallization evenly take place at 5, and 25 % adjuvant proportions. Contrastingly, at 50 % adjuvant application, amorphization dominates the

crystallization process. It has been reported that the addition of polysorbates to carnauba wax leads to an adjuvant-specific amorphization as well as a crystallization (Zhang *et al.*, 2016). For some adjuvants both processes were simultaneously proposed, whereas other adjuvants were assumed to increase the amorphous domains to a higher extent than the crystalline ones. This theory would also explain the decreased absolute value of the total EOT and the shift of the melting range, as different interactions between the new built crystallites and the original wax crystallites are possible. As far as the leaf wax in combination with MeLin, OA, MeSt and the

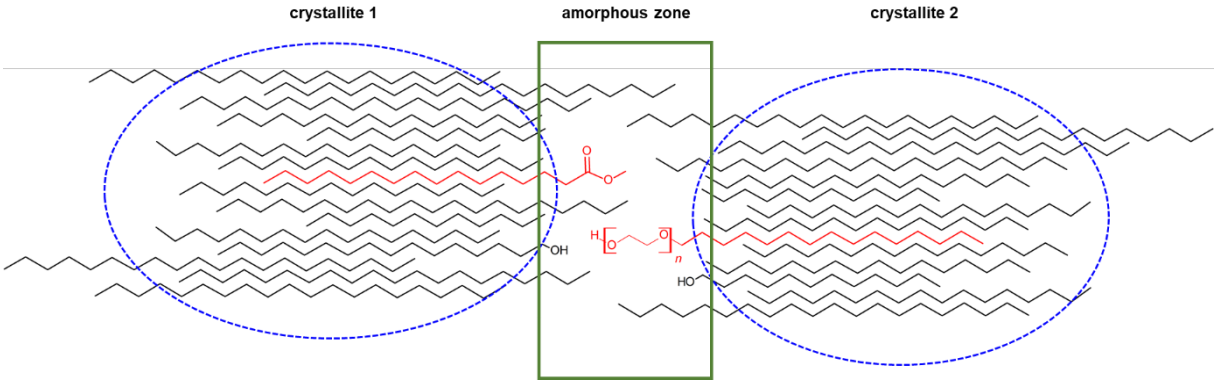

Figure 49 Schematic drawing of the model of wax plasticization with plasticizers (red) and very long-chain aliphatic compounds (black) at different crystalline domains (crystallite) and amorphous zones according to Zhang *et al.* (2016). The figure is not drawn to scale and does not represent the true structure, molecule size or chain length.

alcohol ethoxylates are concerned, similar assumptions can be made. Here, no process dominated the other and amorphization as well as crystallization equally took place at all measured adjuvant proportions. As previous studies also dealt with XRD to check polymorphism and crystallinity and methods for mechanical characterization, further investigations using those methods should be applied to check the exact interactions of the adjuvants with the wax. In addition to that, the application of the adjuvant onto the cuticle or the cuticular wax without premixing, in contrast to this study where the samples were heated up first, should be considered. This experimental setup would represent the actual field application in an even more realistic way.

3.4.5 Cuticular transpiration

As it is believed that water loss through stomata is of great relevance, cuticular water diffusion also appears to be important, especially after stomata closure (Martin and Juniper, 1970). Cuticular transpiration is a diffusion process across the cuticular membrane being limited by crystalline domains similar to lipophilic AIs (Schreiber, 2005). Water can take the lipophilic and the hydrophilic pathway because it is a small, uncharged molecule. As adjuvants like penetration enhancers, which affect the waxy barrier of the cuticle, increase the penetration of lipophilic AIs, it is assumed that water permeability is also influenced. This was shown in previous studies by Räsch *et al.* (2018) applying methylated rape seed oil on *Brassica oleracea* (kohlrabi) and by Riederer and Schönherr (1990) using polydisperse surfactants with isolated leaf cuticles of *Citrus aurantium* L. (Seville orange) and *Pyrus communis* L. (pear). Both found an increased water transpiration after applying the adjuvants. It was stated that the increased transpiration was due to plasticization of cuticular waxes. Effects for *in vivo* experiments with methylated rape seed oil were reversible one week after the application of the adjuvant. As the AI is applied to maintain crop vitality and control pest organisms, increased transpiration is an unfavored side effect. Repeated application of the AI together with the adjuvant, especially in dry scenarios, could impair the crop vitality because of increased transpiration and altering drought tolerance (Burghardt and Riederer, 2003). Comprehensive studies using other adjuvants, *e.g.* alcohol ethoxylates, especially monodisperse ones, have been lacking to date. Therefore, this study was conducted to extensively investigate the cuticular transpiration after the application of oil adjuvants and surfactants. With pure MeO, two experimental setups were used: leaf envelopes and isolated cuticular membranes. Here, it should be tested if there were differences between the two setups.

Within this study, slightly lower values with CM of *P. laurocerasus* were found (4.7×10^{-6} m s^{-1}) in comparison to the permeance determined using leaf envelopes of *P. laurocerasus* (9.6×10^{-6} m s^{-1}). Variability could be explained due to the use of cuticles harvested at a different time of the year in comparison to leaves used for leaf envelopes. However, the same variability should have occurred after the application of pure MeO, because the same samples were used. Here, the values between CM and envelopes did not differ significantly and showed a general increase of the permeance in comparison to the native samples.

The use of unpaired samples with pure MeO resulted in significantly increased permeances, as was also seen for MeLin, OA and the surfactants (Figure 44). For both adjuvant classes, it is assumed that they can act as plasticizers modifying the wax fluidity and thus enhance the permeability of the cuticle to lipophilic AIs. This was shown above, when using DSC and FTIR yielded shifted melting ranges and a modification of the wax phase behaviour after adding the adjuvants. All adjuvants showed this phenomenon. Therefore, it is not surprising that the oil and the surface active adjuvants increased the water permeance three to 21-fold, especially as it was shown that the aliphatic wax crystallinity declined or was modified after adding the adjuvants.

3.4.6 Surface activity

As alcohol ethoxylates are amphiphilic organic compounds with a hydrophilic head (ethylene oxide group) and a lipophilic aliphatic tail, they have surface active properties (Semenov *et al.*, 2015). Hence, they can reduce the surface tension and lower the contact angle of a sessile droplet applied on the leaf surface. The contact angle is a feasible and easy method to study the wetting behaviour of plant surfaces which are mainly hydrophobic due to epicuticular waxes (Koch *et al.*, 2008). Surfactants like alcohol ethoxylates are added to the formulation of AIs to reduce the surface tension and the contact angle (CA) to increase the wetting of the leaf (Hazen, 2000).

It is not surprising that alcohol ethoxylates with a higher EO number showed higher CAs (Figure 48). The higher the EO number, the more hydrophilic the molecule as was reported by (Johansson and Voets, 2004). Hence, the tendency to sorb at the hydrophobic surface, which is given here for parafilm with a CA of 108.1° for water (Koch *et al.*, 2008), is less pronounced. It is has been reported, that surfactants which decrease the contact angle in comparison to the non-adjuvanted control also show higher spreading areas (Arand *et al.*, 2018). Therefore, it can be assumed that the spreading area is increased using the surface active adjuvants.

4 Chapter 3: The interaction of caffeine and azoxystrobin with selected adjuvants

4.1 Introduction

4.1.1 Objectives and research questions

Penetration of an AI into the plant across the plant cuticle and the effect of adjuvants have been extensively studied, showing that adjuvants can increase the AI penetration process (Schönherr, 1993b, 1993a; Riederer *et al.*, 1995; Baur *et al.*, 1997b; Burghardt *et al.*, 1998; Petracek *et al.*, 1998; Baur *et al.*, 1999b; Shi *et al.*, 2005; Fagerström *et al.*, 2013a). Enhanced penetration of the AI across the cuticle is provoked due to the interaction of the AI and the adjuvant both applied onto the plant cuticle. Chapter 1 and 2 dealt with the constitution of the actual permeation barrier and the effects of adjuvants on the aliphatic wax fraction which builds the barrier. Both chapters studied either the AI or the adjuvant, but did not investigate the coupled effect. The aim of this study was to investigate the effect of oil adjuvants and alcohol ethoxylates on the penetration behaviour of the organic solutes caffeine and azoxystrobin *in vitro* using isolated cuticular membranes of *Prunus laurocerasus* as model species. The technique of simulation of foliar penetration (SOFP) was used. Additionally, penetration studies using caffeine were conducted at different relative humidities (RH) to observe humectant properties of the adjuvants. Therefore, the levels of 30, 50 and 80 % were used. The results about the interaction of adjuvants and AIs together with the results gained in chapter 1 and 2 should provide a better understanding of the mode of action of adjuvants and its influence on the permeation barrier of the plant cuticle.

4.2 Materials and Methods

4.2.1 Chemicals

Caffeine was used as a semi-hydrophilic model compound, azoxystrobin as a lipophilic fungicide. The same adjuvants as in 2.2.1 were selected. A water dispersable granule (WDG 50, Syngenta Crop protection AG, Münchwilen, Switzerland) formulation of azoxystrobin was used, due to the low solubility of azoxystrobin in water. The formulation is known to have no effect on the cuticular AI permeability.

4.2.2 Plant material and preparation of isolated cuticles

Leaves *of Prunus laurocerasus cv*. Herbergii (cherry laurel) were harvested at the botanical garden in Würzburg, Germany. Isolated cuticular membranes of the non-stomatous, adaxial side were prepared according to the method of Schönherr and Riederer (1986) as described previously (2.2.2).

4.2.3 Cuticular penetration experiments *via* SOFP and UHPLC-MS

Cuticular penetration was studied using simulation of foliar penetration (SOFP) (Schönherr and Baur, 1994). Cuticular membranes were smoothed under pressurized air. They were mounted on a chamber of stainless steel by using Teflon paste (Carl Roth, Karlsruhe, Germany) the physiological outer side facing the atmosphere. Cells were sealed using adhesive tape (Beiersdorf, Hamburg, Germany).

To measure cuticular penetration of caffeine and azoxystrobin (Table 1), respectively, 5 µL of an aqueous solution of the organic compound (2 µg μL^{-1}) were pipetted on the membrane and left to dry for at least one h.

The same process was done using an aqueous solution consisting of MeO (EW 400 diluted with high-purity water to 4 µg μL^{-1}) and the organic solute (2 µg μL^{-1}). Due to low water solubility, azoxystrobin was used as a solution of WDG 50 whereas caffeine could be diluted using the pure substance and water. Same setup was done using C10E8 together with each organic solute. Caffeine was also sampled in combination with C10E2 and C10E5.

Another setup was conducted using caffeine and the pure, liquid adjuvants MeO, OA and MeLin. A droplet of one µL pure oil adjuvant was applied on the cuticle and left to equilibrate overnight. Five µL of an aqueous solution of caffeine (2 µg μL^{-1}) was pipetted on the membrane and left to dry for one h.

After droplet drying, one mL of high-purity water was applied to the receiver cell. Afterwards, the cell was inverted, the sampling port was sealed with adhesive tape and the cell placed in a box of 30, 50 or 80 % RH. RH was adjusted with glycerol and water as described by Forney and Brandl (1992). Temperature was held at 25 ± 0.1°C using a Peltier-cooled incubator IPP110 (Memmert, Schwabach, Germany).
Azoxystrobin was measured at 50 % RH, as well as the pure oil compounds together with caffeine. Caffeine in combination with the surfactants and formulated MeO was measured at 30, 50 and 80 % RH.

As temperature and humidity can strongly affect the penetration process, this chapter dealt with SOFP under controlled temperature (25°C) and RH (30, 50, 80 %, Figure 50).

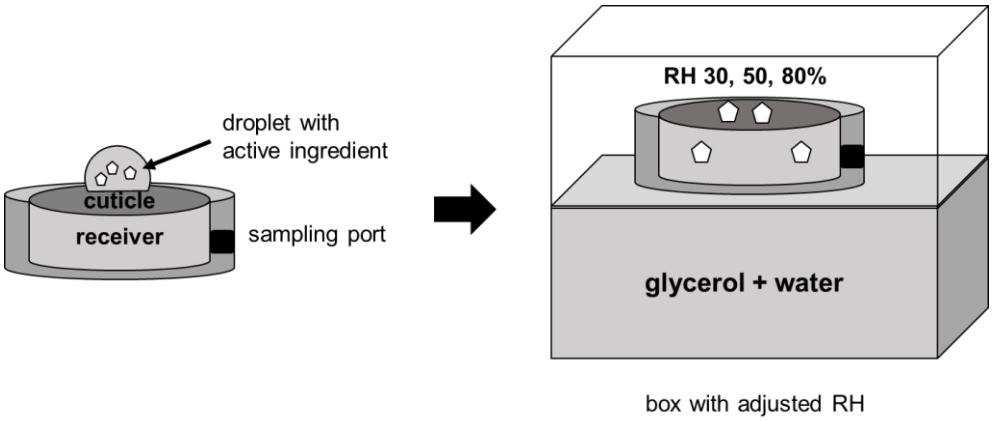

Figure 50 Schematic drawing of the simulation of foliar penetration experiment with adjusted relative humidity (RH)

SOFP experiments in combination with the experiments performed in chapter 2, might provide a better understanding of the mode of action of oil adjuvants and surfactants when applied onto the cuticle.

UHPLC-MS analysis

Ultra-high performance liquid chromatography coupled with mass spectroemtry (UHPLC-MS, ACQUITY H-Class system with QDa detector, Waters, Eschborn, Germany) was used for detection and quantification of permeated caffeine and azoxystrobin across the cuticular membrane. The previously described methods for both compounds (2.2.4) were used.

4.2.4 Statistics

Statistical analysis was done using RStudio 2016 (RStudio, Boston, MR, USA) and OriginPro 2019 (OriginLab, Northampton, USA).

Outliers were removed according to the method of the interquartile range. Flow rates did not show normality according to Shapiro-Wilk test ($p < 0.1$). Lognormal transformation of the data did not result in normality. Therefore, a Kruskal-Wallis ANOVA with post-hoc Dunn's test ($p < 0.05$) was selected to detect significant differences.

4.3 Results

The median flow rate of azoxystrobin at 50 % RH was 3.6 x 10^{-7} µg s^{-1}, whereas caffeine showed a flow rate of 2.2 x 10^{-8} µg s^{-1} at the same RH. Comparing the flow rates of azoxystrobin and caffeine, higher flow rates were found for the latter (Figure 51). For caffeine and azoxystrobin a significant increase was found for the formulated MeO and C10E8 at 50 % RH in comparison to the non-adjuvanted control. No significant difference of the flow rates was found between the two adjuvants with azoxystrobin. Statistical parameters can be found in Appendix 35 - Appendix 38. In contrast to that, caffeine showed a significant increase between the flow rates using C10E8 and MeO. Flow rates of caffeine with C10E8 showed the highest effect, followed by MeO.

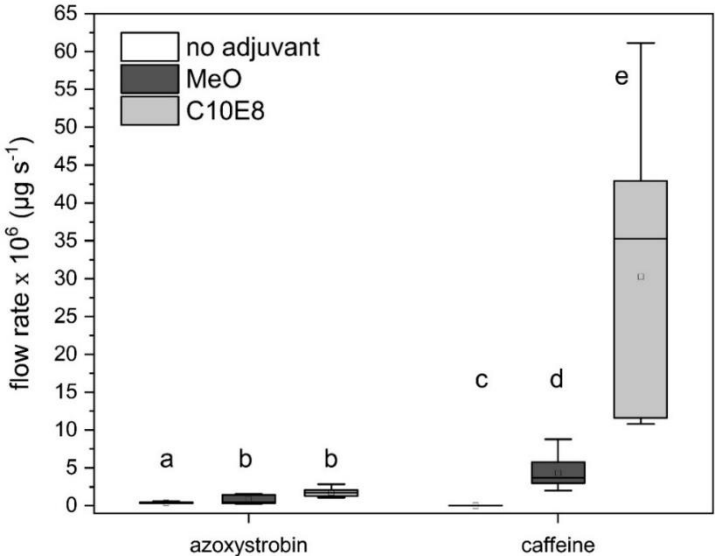

Figure 51 Box plots of flow rates of cuticular penetration of caffeine and azoxystrobin pure and in the presence of different adjuvants at 50 % relative humidity. Isolated cuticular membranes of *Prunus laurocerasus* were used. Box represents 25th and 75th percentiles and Whiskers indicate 10th and 90th percentiles. Horizontal lines within the boxes indicate the median. Different letters above the box represent significant difference using the same organic solute (Kruskal-Wallis ANOVA with post-hoc Dunn's test $p < 0.05$, $8 < \bar{n} < 12$). Formulated methyl oleate (MeO) and octaethylene glycol monodecyl ether (C10E8) were used as adjuvants applied as a 5 µL droplet onto the cuticle dissolved in an aqueous solution (4 µg $µL^{-1}$) together with caffeine (2 µg $µL^{-1}$).

The use of pure oil adjuvants resulted in a significant increase of the caffeine flow rate for all oil adjuvants at 50 % RH (Figure 52). Effects in relation to the non-adjuvanted control ranged from 223 (MeO) to 897 (MeLin). The flow rates of caffeine with OA and MeLin did not differ, whereas MeO showed significant lower values than OA and MeLin.

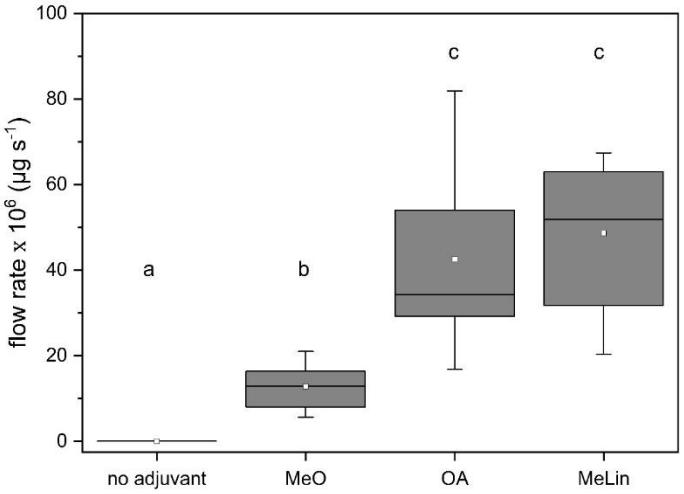

Figure 52 Box plots of flow rates of cuticular penetration of caffeine (no adjuvant) in the presence of pure methyl oleate (MeO), oleic acid (OA), methyl linolenate (MeLin) at 50 % relative humidity. Isolated cuticular membranes of *Prunus laurocerasus* were used. Box represents 25th and 75th percentiles and Whiskers indicate 10th and 90th percentiles. Horizontal lines within the boxes indicate the median. Different letters above the box represent significant difference (Kruskal-Wallis ANOVA with post-hoc Dunn's test $p < 0.05$, $12 < \bar{n} < 15$). One µL of the liquid adjuvants was applied onto the cuticle, followed by the application of a 5 µL droplet caffeine solution (4 µg µL^{-1}).

Within the group of the surfactants the highest values were found at 80 % RH for C10E2, C10E5 and C10E8. Increasing the RH did not affect the flow rate of pure caffeine (Figure 53, ANOVA with post-hoc Dunn's test, p = 0.05). Formulated MeO significantly increased the flow rate in comparison to pure caffeine but altering the RH showed no effect on the flow rate. All alcohol ethoxylates except C10E2 at 30 % RH (1.8×10^{-6} µg s^{-1}) significantly enhanced the flow rate in comparison to caffeine. Flow rates of caffeine with the alcohol ethoxylates at 80 % RH and 50 % did not significantly differ.

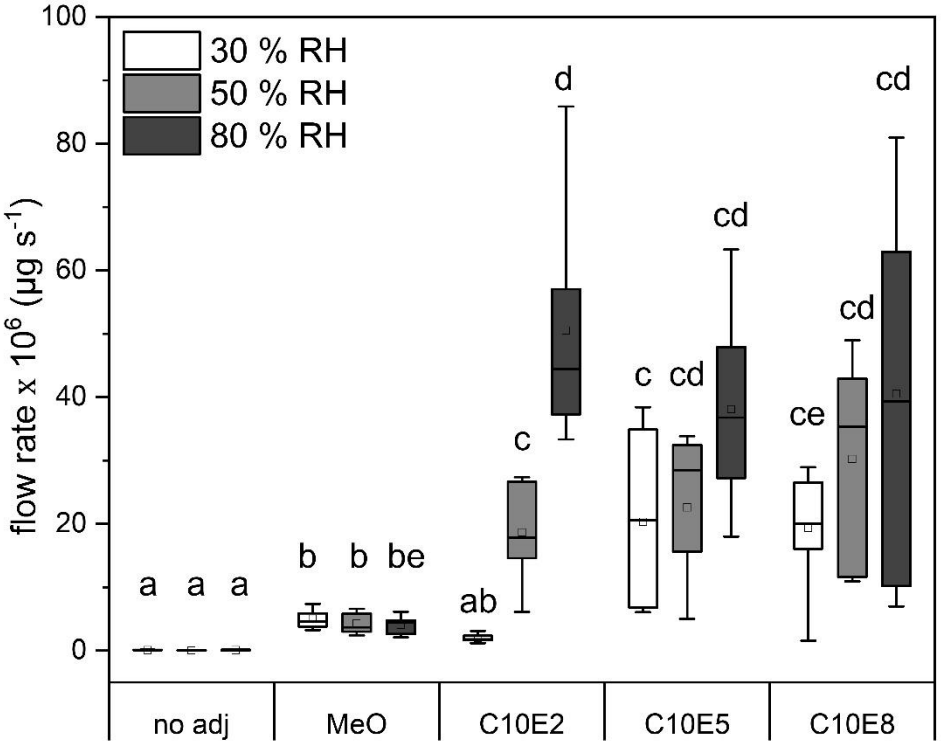

Figure 53 Box plots of flow rates of cuticular penetration of caffeine (no adj) in the presence of different adjuvants at 30, 50 and 80 % relative humidity (RH). Isolated cuticular membranes of *Prunus laurocerasus* were used. Box represents 25th and 75th percentiles and Whiskers indicate 10th and 90th percentiles. Horizontal lines within the boxes indicate the median. Different letters above the box represent significant difference (Kruskal-Wallis ANOVA with post-hoc Dunn's test $p < 0.05$, $9 < \bar{n} < 15$). Formulated methyl oleate (MeO), diethylene glycol monodecyl ether (C10E2), pentaethylene glycol monodecyl ether (C10E5), octaethylene glycol monodecyl ether (C10E8) were used as adjuvants applied as a 5 µL droplet onto the cuticle dissolved in an aqueous solution (4 µg $µL^{-1}$) together with the organic solute (2 µg $µL^{-1}$).

4.4 Discussion

Within this study the penetration effects of three oil adjuvants and three surfactants on the semi-lipophilic caffeine were examined at three different RHs (30, 50, 80 %) using the technique of simulation of foliar penetration (SOFP). In addition, the lipophilic azoxystrobin was investigated using C10E8 and MeO at 50 % RH. The aim was to observe the interaction of two organic solutes in combination with different adjuvants applied onto the plant cuticle. Humectant properties should be determined to get a better understanding of the mode of action of the applied adjuvants.

As SOFP provides non-steady state conditions, the permeance can hardly be determined as with double-chamber systems and can often only be discussed qualitatively (Baur *et al.*, 1997a). Due to evaporation and hydration effects after droplet application, the driving force can change rapidly over a short time. Therefore, the flow rates can be used to compare different adjuvants and compounds, while permeance can not be calculated. One advantage of SOFP is its more realistic experimental setup to the field application than other techniques like simultaneous bilateral desorption (BIDE) and unilateral desorption from the outer surface (UDOS) (Schönherr and Baur, 1994).

It is assumed that caffeine can take the hydrophilic and lipophilic pathway due its semi-lipophilicity. Hence, its flow rate would increase using adjuvants that can influence both pathways. It was hypothesized, that the surfactants C10E2, C10E5, C10E8 can act as plasticizers (Coret and Chamel, 1994; Coret and Chamel, 1995; Schreiber *et al.*, 1996; Schreiber *et al.*, 1997; Burghardt *et al.*, 1998; Perkins *et al.*, 2005; Burghardt *et al.*, 2006). Additionally, it was also proposed that alcohol ethoxylates possess humectant properties and can increase the AI biodelivery into the plant by retaining moisture within the applied droplet (Stock and Holloway, 1993). Thereby, it was stated that an EO number of ≥10 would lead to humectancy and therefore to a higher effect on hydrophilic compounds, while EO numbers < 6 resulted in an increased penetration of lipophilic compounds (Cook *et al.*, 1977; Stock and Holloway, 1993; Burghardt *et al.*, 1998). In addition, a previous study by Asmus *et al.* (2016b) reported that humectant activity per oxygen content increased for oleyl alcohol ethoxylates ranging between mean oxygen contents of 6 and 21 from 0 % RH to 80 % RH and above. Therefore, it is assumed that humectancy generally increases with increasing oxygen content even at lower EO numbers than 10. Nevertheless, due to the lipophilic aliphatic tail of the surfactants used in this study, it is presumed that the waxy barrier of the plant cuticle

is somehow modified, probably affecting the cuticular wax structure (Coret and Chamel, 1994; Coret and Chamel, 1995; Schreiber *et al.*, 1996; Schreiber *et al.*, 1997; Burghardt *et al.*, 1998; Perkins *et al.*, 2005; Burghardt *et al.*, 2006). As humectant activity can occur at mean oxygen contents of 6 and higher, it is striking that the flow rates did not differ significantly between the different RH levels, except with C10E2 (Figure 53). This supposes that flow rates using C10E2 are dependent on the RH, while surfactants with higher EO numbers reach their optimum RH conditions at low RH levels like 30 %. *Prima facie*, this is does not coincide with the preliminary assumptions of humectant properties. At second glance, this discrepancy can be easily explained by the fact that humectants are supposed to be effective not only at high RHs, but should also increase penetration at low RHs (Cook *et al.*, 1977; Cook and Duncan, 1978; Ramsey *et al.*, 2005). Hence, it is assumed that the use of C10E5 and C10E8 increases the flow rate at optimum RHs starting at 30 % or possibly even lower than C10E2 which activity can be influenced by RHs between 30 to 80 %. Alcohol ethoxylates with a lower EO number are sorbed into the wax to a higher extent than alcohol ethoxylates with a higher EO amount (Riederer *et al.*, 1995; Burghardt *et al.*, 1998). Therefore, a higher amount of surfactant should be sorbed in the wax regarding C10E2 in comparison to C10E5 or C10E8 possibly leading to an effect on the wax chemistry and thus permeability (Burghardt *et al.*, 1998). At lower RH levels, less moisture is retained by C10E2 in comparison to C10E5 or C10E8, which are assumed to have a higher water retaining capacity due to the longer EO chain (Asmus *et al.*, 2016b), leading to a crystalline form of caffeine on the cuticular surface after the application. Thus, the SOFP flow rate at 30% RH is lower for C10E2 than the rates with C10E5 or C10E8 at the same RH level (Figure 53). Increased RH leads to a dissolution of caffeine, but the concentration is assumed to be higher in the case of C10E2 as less water is retained by the adjuvant with the lowest EO number in comparison to the adjuvants with higher EO numbers as was seen for oleyl alcohol ethoxylates (Asmus *et al.*, 2016a). If more water is retained, the concentration of the AI, thus the driving force, within the droplet decreases leading to a lower flow rate. As the surfactants can still act as accelerators by modifying the wax structure, the SOFP rates stay the same as far as C10E5 and C10E8 are concerned. In the case of C10E2, which is not showing same humectant potency like the two other surfactants, water is retained within the droplet, but modification of the wax structure is still possible leading to a significant increase of the caffeine permeation.

As it has been reported by Burghardt *et al.* (2006) using the desorption method with aluminium discs and lipophilic AIs, the logtransformed effects of alcohol ethoxylates plotted versus the EO number revealed a negative, linear correlation for bitertanol and benzoic acid. These effects are calculated by dividing the parameter (diffusion coefficient, permeance, flow rate etc.) measured with the adjuvant by the value of the non-adjuvanted control. Burghardt *et al.* (2006) reported a positive linear dependency between the effects and the maximum concentration of the surfactant within the wax, as was found by several other studies (Riederer *et al.*, 1995; Burghardt *et al.*, 1998). The authors stated that the alcohol ethoxylates possess an intrinsic activity and provoke a non-specific plasticizing effect which is only dependent on the EO number. The higher the EO number, the lower the amount of sorbed alcohol ethoxylate in the wax. Those studies dealt with steady-state experiments and wax or cuticles mounted between two aqueous compartments, but correlations with SOFP flow rates have been lacking to date. The attempt to correlate the measured values of this study to the EO number, did not yield viable results as the same statistical increase was detected for C10E2, C10E5 and C10E8 in comparison to pure caffeine at 50 and 80 % RH (Kruskal-Wallis-ANOVA with post-hoc Dunn's test, $p < 0.05$; Figure 53). Therefore, no correlation between the effect and the EO number can be derived. The study by Burghardt *et al.* (1998) dealt with aluminum discs loaded with wax and AI placed into an aqueous adjuvant solution, this provided steady-state conditions. For the current SOFP setup, steady-state was not given and possible humectant and plasticization effects can not be uncoupled.

As the permeation of AIs across the plant cuticle can be divided into two pathways, it is assumed that caffeine can take both pathways due to its semi-lipophilicity. As it was reported, permeation of hydrophilic AIs was strongly increased with surfactants of higher EO contents (Riederer and Schönherr, 1990; Coret and Chamel, 1993). Therefore, the surfactants C10E5 and C10E8 should lead to a higher effect with caffeine, which can permeate across both pathways, than azoxystrobin, which only permeates across the lipophilic one. This hypothesis can only be valid if it is assumed that the surfactants possess wax modification and humectant properties and that both effects are additive. As the lipophilic and hydrophilic pathway can possibly be manipulated, caffeine penetration with the adjuvants should be higher than the flow rate of the lipophilic azoxystrobin as shown in Figure 51. As MeO and the other oil adjuvants are supposed to act as plasticizer alone (Santier and Chamel, 1996), the

flow rates of the lipophilic azoxystrobin, as well as the semi-lipopohilic caffeine should be enhanced which was found for both compounds (Figure 51 - Figure 53). It is obvious that the lipophilic azoxystrobin penetrates the cuticle of *P. laurocerasus* faster than caffeine. The flow rates with the adjuvants MeO and C10E8 were higher with caffeine than with azoxystrobin, showing that both adjuvants have a greater accelerating effect on caffeine while azoxystrobin is less affected.

Using the three oil adjuvants with caffeine, flow rates increased for pure MeO (Figure 52). Even higher effects were seen for OA and MeLin which flow rates were not significantly different to each other. The effects were also higher in comparison to the formulated MeO (Appendix 37). Recalculating the actual amount of adjuvant applied onto the isolated cuticle, it is obvious that the values are higher for the purely applied adjuvants than the formulated MeO used as an aqueous dispersion (Table 11). Therefore it is obvious that higher amounts of adjuvants sorbed to the cuticle would lead to higher accelerating effects, as was previously reported for alcohol ethoxylates (Riederer *et al.*, 1995; Burghardt *et al.*, 1998). Attempts to correlate the effect to the actual applied mass of all oil adjuvants did not yield a linear relation. This is not striking, as the single oil adjuvant could possess a different behaviour of wax plasticization itself due to its chemical properties (double bonds, methyl ester or carboxylic group). Statistically, there was no difference between the increased flow rates of caffeine with OA and MeLin. These values were higher than with MeO. It can only be assumed that oleic acid somehow affects either the lipophilic wax structure or the hydrophilic domains due to its carboxyl group, whereas methyl linolenate would have a higher impact on the lipophilic pathway due to the two more double bonds. It is proposed that the adjuvant diffuses into crystalline parts and i) increases the amorphous or ii) reduces the crystalline parts (Fagerström *et al.*, 2014). It is believed that the aliphatic hydrocarbon wax fraction builds crystalline phases whereas the chain ends and functional groups build the amorphous parts (Riederer and Schneider, 1990; Reynhardt and Riederer, 1991). If molecules with double bonds diffuse into the wax, it is assumed that they build more amorphous parts or somehow disrupt the crystalline domains due to the fact that their molecular structure is not as linear as saturated hydrocarbons. In fact, this is a common model to explain the role of polyunsaturated fatty acids in membranes of fish cells due to adaptations to cold temperatures (Bell *et al.*, 1986). Within this study it can only be said, that higher amounts of applied adjuvant lead to higher effects with caffeine. Further studies with a wide range of actual applied

amounts of adjuvant are needed to test the assumption of concentration-dependent efficacy.

Table 11 Actual amount and effects of the oil adjuvants applied onto the isolated cuticle of *P. laurocerasus.* Formulated methyl oleate (form MeO), pure methyl oleate (MeO), methyl linolenate (MeLin), oleaic acid (OA).

compound	density (g cm^{-3})[a]	actual applied amount (µg)	effect to non-adjuvanted control[b]
form MeO	0.8739	20	165
MeO	0.8739	874	223
MeLin	0.8739	895	592
OA	0.8950	894	897

[a] Values are taken from David R. Lide (2005).

[b] Data is given as the factor of the median flow rate with adjuvant divided by the value of the non-adjuvanted control at 50 % RH.

It was stated above, that the surfactants as well as the oil adjuvants possess the ability to modify the cuticular wax structure, depicted as plasticization process (Coret and Chamel, 1994; Coret and Chamel, 1995; Schreiber *et al.*, 1996; Santier and Chamel, 1996; Schreiber *et al.*, 1997; Burghardt *et al.*, 1998; Perkins *et al.*, 2005; Burghardt *et al.*, 2006). This plasticization is assumed to take place within the crystalline wax fraction by increasing the amorphous or decreasing the crystalline domains (Fagerström *et al.*, 2013a; Fagerström *et al.*, 2014). These crystalline domains are supposed to limit the diffusion of organic solutes, being inaccessible for lipophilic compounds (Buchholz, 2006). This hypothesis will be holistically discussed in the summarizing discussion (5) combining the results from chapter 1 to 3.

5 Summarizing discussion and outlook

Precise and efficient biodelivery of AIs is the key objective of agrochemical formulation. Therefore, adjuvants can be added as formulation aids to modify the cuticular barrier and increase the AI permeation. The exact mechanism of this modification process of the barrier is still not fully understood, thus this thesis had two main objectives:

i) elucidate the permeation barrier of the plant cuticle to AIs in terms of the different wax fractions and
ii) holistically investigate the modification of this barrier using selected oil and surface active adjuvants, an aliphatic leaf wax and an artificial model wax to get a better understanding of the mode of action of the adjuvants.

Using the three organic solutes theobromine, caffeine and azoxystrobin demonstrated that the aliphatic wax fraction forms the cuticular permeation barrier to organic solutes, whereas triterpenoids are of less importance. As all three compounds with a log K_{ow} ranging from -0.78 to 2.5 showed this trend, it was concluded that the aliphatic wax compounds can block the aqueous domains which form the hydrophilic pathway and limit the permeation of hydrophilic compounds as was previously reported by Popp *et al.* (2005) and Arand *et al.* (2010). The permeation of lipophilic AIs is limited by the aliphatic wax domains due to crystalline flakes which are inaccessible for AIs (Buchholz, 2006). As cyclic compounds do not constitute the permeation barrier to AIs, they need to possess other functions. Tsubaki *et al.* (2013) found that triterpenoids are produced by the plant for mechanical stability of the cuticle. Cyclic compounds like ursolic acid could act as nanofillers to strengthen the cuticle of the fruit of *Diospyros kaki* Thunb. cv. *Fuyu* (*fuyu* persimmon fruit). It was also reported that triterpenoids situated in the cutin matrix of the desert plant *Rhazya stricta* restrict thermal expansion of cutin and prevent thermal damage to the aliphatic wax barrier (Schuster *et al.*, 2016). Not only mechanical properties but also anti-oxidant (Collins and Charles, 1987) and antimicrobial functions (Wolska *et al.*, 2010; Szakiel *et al.*, 2012; Pensec *et al.*, 2014) were described concerning triterpenoids. This study showed that the VLCAs contribute the permeation barrier to AIs, but detailed knowledge about the layering of the aliphatic and cyclic fractions within the cuticle could not be provided. Therefore, future

experiments like AFM-IR/Raman could be used to examine the exact arrangement of the different fractions.

Due to the new gained knowledge about the cuticular permeation barrier, crucial information about the functionality of the different wax fractions was provided, which is important to help understanding the modification process of the barrier when adjuvants are used. Therefore, an aliphatic leaf wax (*Schefflera elegantissima*) was chosen to study the modification of the cuticular barrier and the mode of action of oil and surface active adjuvants. For a better overview, Table 12 shows a summary of the main data for all adjuvants with *Schefflera elegantissima* leaf wax and the isolated cuticles of *Prunus laurocerasus*.

Table 12 Summarized data for the pure *Schefflera elegantissima* leaf wax/isolated cuticles of *Prunus laurocerasus* (no adjuvant) in combination with the oil and surface active adjuvants[a]

description	melting offset (°C)[a]	total EOT (J g^{-1})[a]	crystallinity (%)[b]	transpiration effect[c]	wax extraction effect for permeance[c]		SOFP effect at 50 % RH[c]	
					caffeine	azoxy-strobin	caffeine	azoxy-strobin
no adjuvant	81.2	-163.7	84.8	1 (a)	194	37	1 (a)	1 (g)
C10E2	66.8	-34.6	88.9	5 (b)	N.D	N.D	797 (c)	N.D
C10E5	N.D	N.D	91.2	21 (b)	N.D	N.D	1277 (cd)	N.D
C10E8	75.7	-64.6	90.2	10 (b)	N.D	N.D	1582 (cd)	4.8 (h)
MeO	76.3	-59.3	67.8	5 (c)	N.D	N.D	223 (e)	1.3 (h)
OA	74.1	-63.5	76.2	5 (c)	N.D	N.D	592 (f)	N.D
MeLin	78.4	-73.3	86.0	3 (d)	N.D	N.D	897 (f)	N.D
MeSt	78.8	-132.4	84.6	N.D	N.D	N.D	N.A	N.D

[a] The adjuvants pure methyl oleate (MeO), oleic acid (OA), methyl linolenate (MeLin), methyl stearate (MeSt), diethylene glycol monodecyl ether (C10E2), pentaethylene glycol monodecyl ether (C10E5) and octaethylene glycol monodecyl ether (C10E8) were used.

[b] Melting offset, enthalpy of transition (EOT) and crystallinity were measured using the chloroform extracted *Schefflera elegantissima* leaf wax. Data is given for 50 % adjuvant proportion.

[c] Transpiration and SOFP effects were determined using isolated cuticles of *Prunus laurocerasus*. Effects for transpiration and caffeine are given for unpaired samples after the application of pure liquid oil adjuvants (one µL) and pure liquid C10E2, C10E5 (one µL) and C10E8 applied as 2 µL of an aqueous solution of 50 % (*w/v*). For azoxystrobin, MeO was applied as formulation (5 µL droplet of 4 µg/µL of an aqueous dispersion). Letters in brackets indicate statistical difference between each group of comparison. For water and caffeine, the values for no adjuvant, C10E2, C10E5, C10E8 were compared using Kruskal-Wallis ANOVA with post-hoc Dunn's test ($p < 0.05$) as well as the values for no adjuvant, MeO (pure), OA (pure) and MeLin (pure). For azoxystrobin, the values for no adjuvant, MeO (formulated) and C10E8 were compared using a Kruskal-Wallis ANOVA with post-hoc Dunn's test ($p < 0.05$). N.D – not determined

Oil derivatives, *e.g.* MeO and alcohol ethoxylates, accelerate the penetration of AIs by influencing the physical properties of the wax, and thus the permeation process of the AI (Nalewaja *et al.*, 1986; Mcwhorter and Barrentine, 1988; Manthey and Nalewaja, J. D., Szelezniak, E. F., 1989; Wanamarta *et al.*, 1989; Schott *et al.*, 1991; Mcwhorter *et al.*, 1993; Schreiber *et al.*, 1996; Burghardt *et al.*, 1998; Webster *et al.*, 2018). The influence of these adjuvants on the physical properties of the wax and the AI permeability is depicted as a plasticization process of the cuticular wax by i) increasing the amorphous domains and/or ii) decreasing the crystalline fraction (Buchholz, 2006;

Fagerström *et al.*, 2014; Zhang *et al.*, 2016). These processes could be found in the current study for MeO, MeLin, OA, C10E2, C10E5 and C10E8. According to literature, the alcohol ethoxylates C10E2, C10E5, C10E8 and MeO are known, *i.a.* as plasticizers, increasing the diffusion of the lipophilic AIs (Riederer *et al.*, 1995; Santier and Chamel, 1996; Burghardt *et al.*, 1998). Plasticization with alcohol ethoxylates was derived from shifted melting offsets and decreased absolute values of the total EOT using DSC (Coret and Chamel, 1994; Perkins *et al.*, 2005). This effect could also be seen in the current work with the adjuvants. DSC data for C10E5 is lacking, but it can be assumed that it would behave in a similar way like the other surfactants. In a study by Burghardt *et al.* (1998) it was reported that the effects of the alcohol ethoxylates are positively correlated to the maximum sorbed amount to the wax, which in turn is dependent on the EO number being higher for lower EO numbers. Hence, SOFP flow rates should be higher for lower EO numbers, which could not be observed in this study. Flow rates for caffeine, which is a semi-hydrophilic compound due to its log K_{OW} of -0.07, were not significantly different at 50 % RH between all adjuvants (Table 12). Following its log K_{OW}, caffeine is assumed to diffuse across the cuticle *via* the lipophilic and hydrophilic pathway as was also shown for benzoic acid at different pH values according to the state of dissociation (Popp, 2005). Within this work, effects of wax extraction using isolated membranes of *P. laurocerasus* showed higher values for caffeine than theobromine or azoxystrobin. It is depicted that the VLCAs block the hydrophilic domains within the cuticle and therefore limit not only the permeation of lipophilic solutes, but also the diffusion of hydrophilic compounds. Hence, removing the wax leads to a better accessibility of the hydrophilic domains. This was shown with caffeine and its higher effect of wax extraction in comparison to theobromine or azoxystrobin with cuticles of *P. laurocerasus*. Therefore, and due to its semi-hydrophilicity, it can be explained why caffeine acts differently than the lipophilic bitertanol (Burghardt *et al.*, 1998) when surfactants with an increased EO number are applied. The study by Burghardt *et al.* (1998) described the effect of the adjuvants as plasticization process, which is depicted as wax adjuvant interaction and influence on the wax crystallinity (Fagerström *et al.*, 2014; Zhang *et al.*, 2016). For oil adjuvants a previous study by Webster *et al.* (2018) reported that alkyl esters like MeO are effective in disrupting the wax structure of tristearin used as cuticular model wax. The authors found that mixing the oil adjuvants with tristearin lead to the *β*-crystallite state which is only formed by the pure wax at increased temperatures, but is not stable at ambient

temperatures. This is a direct proof, that oil adjuvants like MeO can modify the crystalline structure of a wax, which was also found in the current study. As previously mentioned, decreased melting ranges in combination with decreased total EOT indicated plasticization of the wax after adding adjuvants (Coret and Chamel, 1994; Perkins *et al.*, 2005). Direct evidence for decreased or altered crystallinity was not reported and only assumed. Hence, the current data would imply plasticization of cuticular wax after adding the adjuvants. Contrastingly, crystallinity only showed declined values at 50 % MeO proportion but was not altered for smaller proportions and the other adjuvants. *Prima facie*, this does not coincide with the hypothesis in literature of decreased crystallinity after adding the adjuvants to the wax. At second glance, this can be explained by assuming that the adjuvants equally undergo amorphization and crystallization, still having an influence on the wax structure as shown by Zhang *et al.* (2016). The aliphatic tail of the surfactant (the C10-hydrocarbon chain) can be embedded in the aliphatic crystalline wax, whereas the hydrophilic ethylene oxide head is assumed to be situated in the amorphous part of the wax (Figure 54). This disruption of the wax structure is one important mode of action of alcohol ethoxylates which is assumed to increase AI penetration reported in various studies using different alcohol ethoxylates (Schönherr, 1993b, 1993a; Riederer *et al.*, 1995; Baur *et al.*, 1997b; Burghardt *et al.*, 1998; Petracek *et al.*, 1998; Baur *et al.*, 1999b; Shi *et al.*, 2005; Fagerström *et al.*, 2013a). As far as the oil adjuvants are concerned, a similar behaviour is depicted as their aliphatic C18-hydrocarbon chain can be situated in the crystalline wax leading to crystallization (Figure 54). Simultaneously, the part of the more hydrophilic methyl ester or carboxylic acid group can be embedded in the amorphous zone. Both processes evenly take place at lower adjuvant levels (5, 25 %) whereas amorphization dominates at the highest level for MeO. For the other oil adjuvants, amorphization and crystallization equally occur at 5, 25 and 50 % adjuvant proportion. This observation also coincides with the findings by

Webster *et al.* (2018) that MeO is more effective than other oil adjuvants in disrupting the wax structure, *e.g.* lecithin or mineral oil. It is striking that amorphization and

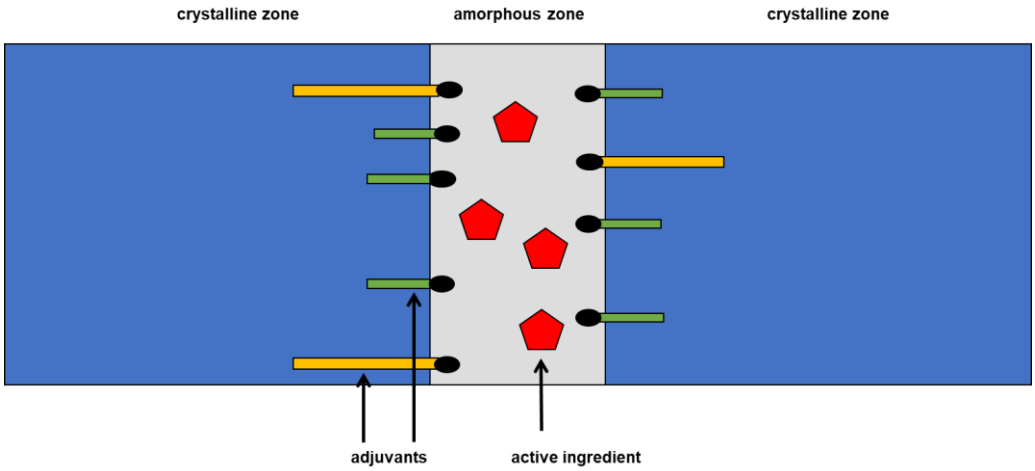

Figure 54 Schematic drawing of the model of wax plasticization with adjuvants (yellow and green) and the distribution of the active ingredient (red) according to Zhang *et al.* (2016). The figure is not drawn to scale and does not represent the true structure or molecule size.

crystallization evenly take place using OA and MeLin in contrast to the predominant process of amorphization with MeO at 50 % adjuvant proportion. However, the different behaviour of OA and MeLin in comparison to MeO could be caused by the difference in molecular structure. OA possesses a carboxylic group instead of the methyl ester group, while MeLin has two more double-bonds than MeO. It is obvious that OA and MeLin are not as effective as MeO in reducing the crystallinity, the total EOT and the melting offset (Table 12). The study by Zhang *et al.* (2016) used other techniques to study physical and rheological properties of wax surfactant blends like XRD and tensile tests to check polymorphism, crystallinity, crystallite size and rheological properities. Those techniques would also be valid methodologies to gain more knowledge about the plasticization of the wax adjuvant blends used within this study. It was shown that DSC and FTIR provided data in good agreement with the data for the leaf wax, also after adding the adjuvants. Thus, the model wax is feasible for future experiments where a greater amount of wax is needed, *e.g.* screenings or diffusion experiments. It would be of considerable interest to also apply XRD and tensile tests to study parameters for crystallinity and rheology in the future.

Looking at DSC thermograms of the quaternary model wax during heating, it was proposed that the alcohols and the alkanes form separate phases. The exact layering of the alcohols and alkanes within the model wax could be elucidated using AFM-IR/Raman to visualize possible phase separation in detail. If it is clear if and how the alcohols build separate phases from the alkanes, the influence of adjuvants on this

phase could be elucidated. Thus, an even more detailed picture about the wax adjuvant interaction could be drawn.

In the field, adjuvants are usually applied as a formulation onto the leaf surface and need to diffuse across the wax layer to modify its structure. The current work dealt with premixed adjuvant wax blends, so the diffusion process of the adjuvant into the wax was excluded. Nevertheless, this process is important to predict AI penetration enhancement. Webster *et al.* (2018) reported similar trends for premixed samples and external adjuvant application on a model wax using DSC and XRD. This possibly indicates that the adjuvants used in the current study would show a similar effect when applied on the waxy surface as described in the study by Webster *et al.* (2018). Only for MeSt this assumption can not be made because of its solid state at ambient temperature. MeSt would not be capable of permeating into the cuticular wax layer to influence the wax structure and alter the penetration process.

Cuticular transpiration significantly increased using the adjuvants, supporting the model of the barrier modification as it is assumed that water partly diffuses across the lipophilic pathway and therefore is limited by crystalline wax (Schönherr, 2006). Hence, it is not striking that the water permeance enhanced using the adjuvants as a consequence of wax disruption. Direct evidence for increased SOFP effects with a semi-lipophilic and a lipophilic compound was given after the adjuvant application, strongly supporting the hypothesis that the interaction of the adjuvants with the wax results in increased AI penetration. Increased flow rates for C10E2, C10E5 and C10E8 with caffeine and for C10E8 with azoxystrobin were also observed. As the methodology of SOFP was used, enhanced flow rates could be provoked by plasticization and humectant properties of the adjuvants. The flow rates of caffeine after the addition of the surfactants increased but dependency on RH was not found for C10E5 and C10E8. In contrast, the flow rates using C10E2 increased significantly with the RH. It is assumed that C10E5 and C10E8 can sorb more moisture after the application and drying of the droplet, leading to high effects even at low humidity. In contrast, it is presumed that due to the low EO number of C10E2, the increase of the RH leads to an increased amount of sorbed moisture. Hence, the sorbed moisture possibly results in a more gel-like/amorphous state of the organic solute which can positively affect the AI penetration (Cook *et al.*, 1977; Stock and Holloway, 1993; Asmus, 2016). Increased RH results in a dissolution of caffeine, but the concentration is assumed to be higher with C10E2 as the moisture retaining capacity is less pronounced for lower EO

numbers previously reported for oleyl alcohol ethoxylates (Asmus *et al.*, 2016a). If more water is retained, the driving force of the AI within the droplet decreases and leads to a lower flow rate. The surfactants can still act as accelerators by modifying the wax structure, keeping the SOFP flow rates constant in terms of C10E5 and C10E8. In case of C10E2, moisture is sorbed but plasticization of the wax is still possible. As a result, increased SOFP flow rates for caffeine with C10E2 dependent on RH could be detected. The influence on the physical state of the AI when applied onto the cuticular surface is not the only factor leading to increased AI penetration. The wetting of the leaf surface can also be an important process affecting the AI uptake. The current work found possible wetting properties for the surfactants due to decreased CAs in comparison to pure water on parafilm. Hence, it has to be kept in mind that the uptake process of the AI is always influenced by the adjuvants due to coupled modes of action. This is not only true for the surfactants but also for the oil adjuvants. They can keep the AI in a more gel-like state improving AI availability as a result of their physicochemical properties (Hess and Falk, 1990). Coupled modes of action of the adjuvants can also be a possible explanation concerning the following described discrepancy of transpiration and SOFP effects. Cuticular water permeance was similarly enhanced with MeO and OA and higher in comparison to transpiration using MeLin. This trend was not seen with SOFP flow rates as OA and MeLin showed higher effects with caffeine than MeO.

The current work showed for the first time that the aliphatic rather than the cyclic fraction builds the permeation barrier to lipophilic and hydrophilic organic compounds. Further investigation of the barrier modification using surfactants and oil adjuvants revealed a wax disruption effect for all adjuvants. It was also shown that the uptake process of the AI is influenced by several modes of action which are coupled mechanisms. Hence, this work provides crucial knowledge about how adjuvants modify the cuticular barrier and enhance AI penetration and therefore important information about adjuvants with respect to AI formulation. As precise biodelivery derives from optimized formulation, the findings of the current work can help to improve the process of selecting the right adjuvant for formulation according to its mode of action and penetration enhancing properties.

6 References

Abbott HA, van Dyk LP, Grobbelaar N. 1990. Spreading of spray mixtures on leaf surfaces: I. relative effectiveness of various physico-chemical predictors. *Pesticide Science* **28,** 419–429.

Abrahamsson S, Ryderstedt-Nahringbauer I. 1962. The crystal structure of the low-melting form of oleic acid. *Acta Crystallographica* **15,** 1261–1268.

Aggarwal P. 2001. Phase transition of apple cuticles: A DSC study. *Thermochimica Acta* **367-368,** 9–13.

American Society for Testing and Materials. 1999. *Annual Book of ASTM Standards, Vol. 11.05. Designation E 1519-95*. Standard Terminology Relating to Agricultural Tank Mix Adjuvants pp. 905–906.

Arand K, Asmus E, Popp C, Schneider D, Riederer M. 2018. The Mode of Action of Adjuvants-Relevance of Physicochemical Properties for Effects on the Foliar Application, Cuticular Permeability, and Greenhouse Performance of Pinoxaden. *Journal of Agricultural and Food Chemistry* **66,** 5770–5777.

Arand K, Stock D, Burghardt M, Riederer M. 2010. pH-dependent permeation of amino acids through isolated ivy cuticles is affected by cuticular water sorption and hydration shell size of the solute. *J. Exp. Bot.* **61,** 3865–3873.

Asmus E. 2016. Mode of Action of Adjuvants for Foliar Application: Wirkmechanismen von Adjuvantien für die Blattflächenapplikation, Doctoral thesis University of Würzburg.

Asmus E, Arand K, Popp C, Friedman A, Riederer M. 2016a. Water sorption potential of non-ionic adjuvants and its impact on cuticular penetration. *Proceedings ISAA 2016,* 177–182.

Asmus E, Popp C, Friedmann AA, Arand K, Riederer M. 2016b. Water Sorption Isotherms of Surfactants: A Tool To Evaluate Humectancy. *Journal of Agricultural and Food Chemistry* **64,** 5310–5316.

Basson I, Reynhardt EC. 1991. Identification of defect chain motions in the low temperature orthorhombic phase of binary mixtures of n -alkanes by means of nuclear magnetic resonance spin-lattice relaxation time measurements. *The Journal of Chemical Physics* **95,** 1215–1222.

Bauer H, Schönherr J. 1992. Determination of mobilities of organic compounds in plant cuticles and correlation with molar volumes. *Pesticide Science* **35,** 1–11.

Baur P. 1999. Surfactant Effects on Cuticular Penetration of Neutral Polar Compounds: Dependence on Humidity and Temperature. *Journal of Agricultural and Food Chemistry* **47,** 753–761.

Baur P, Buchholz A, Schönherr J. 1997a. Diffusion in plant cuticles as affected by temperature and size of organic solutes: Similarity and diversity among species. *Plant, Cell and Environment* **20,** 982–994.

Baur P, Grayson BT, Schönherr J. 1997b. Polydisperse ethoxylated fatty alcohol surfactants as accelerators of cuticular penetration. 1. Effects of ethoxy chain length and the size of the penetrants. *Pesticide Science* **51,** 131–152.

Baur P, Marzouk H, Schönherr J, Bauer H. 1996a. Mobilities of organic compounds in plant cuticles as affected by structure and molar volumes of chemicals and plant species. *Planta* **199**.

Baur P, Marzouk H, Schönherr J, Grayson BT. 1997c. Partition Coefficients of Active Ingredients between Plant Cuticle and Adjuvants As Related to Rates of Foliar Uptake. *Journal of Agricultural and Food Chemistry* **45,** 3659–3665.

Baur P, Marzouk, K, H., Schönherr J. 1999a. Estimation of path lengths for diffusion of organic compounds through leaf cuticles. *Plant, Cell and Environment* **22,** 291–299.

Baur P, Schönherr J, Grayson BT. 1999b. Polydisperse ethoxylated fatty alcohol surfactants as accelerators of cuticular penetration. 2: Separation of effects on driving force and mobility and reversibility of surfactant action. *Pesticide Science* **55,** 831–842.

Baur P, Terence Grayson B, Schönherr J. 1996b. Concentration-Dependent Mobility of Chlorfenvinphos in Isolated Plant Cuticles. *Pesticide Science* **47,** 171–180.

Bell MV, Henderson RJ, Sargent, JR. 1986. The role of polyunsaturated fatty acids in fish. *Comparative Biochemistry and Physiology Part B: Comparative Biochemistry* **83,** 711–719.

Benitez JJ, Matas AJ, Heredia A. 2004. Molecular characterization of the plant biopolyester cutin by AFM and spectroscopic techniques. *Journal of structural biology* **147,** 179–184.

Blakeman JP. 1993. Pathogens in the foliar environment. *Plant Pathology* **42,** 479–493.

Bolin HR, Stafford AE. 1980. Fatty acid esters and carbonates in grape drying. *Journal of Food Science* **45,** 754–755.

Brabham C, Norsworthy JK, Sandoski CA, Varanasi VK, Schwartz-Lazaro LM. 2019. Spray deposition, adjuvants, and physiochemical properties affect benzobicyclon efficacy. *Weed Technology* **33,** 258–262.

Briard A-J, Bouroukba M, Petitjean D, Hubert N, Dirand M. 2003. Experimental Enthalpy Increments from the Solid Phases to the Liquid Phase of Homologous n - Alkane Series (C 18 to C 38 and C 41 C 44 C 46 C 50 C 54 and C 60). *Journal of Chemical & Engineering Data* **48,** 497–513.

Broadhurst MG. 1962. An analysis of the solid phase behavior of the normal paraffins. *Journal of research of the National Bureau of Standards, Sect. A* **66,** 241–249.

Buchholz A. 2006. Characterization of the diffusion of non-electrolytes across plant cuticles: properties of the lipophilic pathway. *Journal of Experimental Botany* **57,** 2501–2513.

Burghardt M, Friedmann A, Schreiber L, Riederer M. 2006. Modelling the effects of alcohol ethoxylates on diffusion of pesticides in the cuticular wax of *Chenopodium album* leaves. *Pest management science* **62,** 137–147.

Burghardt M, Riederer M. 2003. Ecophysiological relevance of cuticular transpiration of deciduous and evergreen plants in relation to stomatal closure and leaf water potential. *Journal of Experimental Botany* **54,** 1941–1949.

Burghardt M, Schreiber L, Riederer M. 1998. Enhancement of the Diffusion of Active Ingredients in Barley Leaf Cuticular Wax by Monodisperse Alcohol Ethoxylates. *Journal of Agricultural and Food Chemistry* **46,** 1593–1602.

Cameron KD, Teece MA, Bevilacqua E, Smart LB. 2002. Diversity of cuticular wax among Salix species and Populus species hybrids. *Phytochemistry* **60,** 715–725.

Carreto L, Almeida AR, Fernandes AC, Vaz WLC. 2002. Thermotropic Mesomorphism of a Model System for the Plant Epicuticular Wax Layer. *Biophysical Journal* **82,** 530–540.

Casado CG, Heredia A. 1999. Structure and dynamics of reconstituted cuticular waxes of grape berry cuticle (*Vitis vinifera* L.). *Journal of Experimental Botany* **50,** 175–182.

Chamel AR, Marecha Y. 1992. Characterisation of isolated plant cuticles using Fourier transform infrared (FTIR) spectroscopy. *Comptes rendus de l'Académie des sciences,* 347–354.

Chapman D, Goni FM. 1986. Physical properties: optical and spectral characteristics. In: Gunstone FD, ed. *The lipid handbook*. London: Chapman and Hall, 487–560.

Chiavaro E. 2014. *Differential Scanning Calorimetry: Applications in Fat and Oil Technology*: CRC Press.

Chiu Y-C, Jenks MA, Richards-Babb M, Ratcliff BB, Juvik JA, Ku K-M. 2016. Demonstrating the Effect of Surfactant on Water Retention of Waxy Leaf Surfaces. *Journal of Chemical Education* **94,** 230–234.

Cholakova D, Denkov N. 2019. Rotator phases in alkane systems: In bulk, surface layers and micro/nano-confinements. *Advances in colloid and interface science* **269,** 7–42.

Collins MA, Charles HP. 1987. Antimicrobial activity of Carnosol and Ursolic acid: Two anti-oxidant constituents of Rosmarinus officinalis L. *Food Microbiology* **4,** 311–315.

Cook GT, Babiker AGT, Duncan HJ. 1977. Penetration of bean leaves by aminotriazole as influenced by adjuvants and humidity. *Pesticide Science* **8,** 137–146.

Cook GT, Duncan HJ. 1978. Uptake of aminotriazole from humectant-surfactant combinations and the influence of humidity. *Pesticide Science* **9,** 535–544.

Coret J, Chamel A. 1994. Effect of some ethoxylated alkylphenols and ethoxylated alcohols on the transfer of [14C] chlorotoluron across isolated plant cuticles. *Weed Research* **34,** 445–451.

Coret J, Chamel AR. 1995. Extended summaries 8th International Congress of Pesticide Chemistry (IUPAC). *Pesticide Science* **43,** 355–376.

Coret JM, Chamel AR. 1993. Influence of some nonionic surfactants on water sorption by isolated tomato fruit cuticles in relation to cuticular penetration of glyphosate. *Pesticide Science* **38,** 27–32.

Cussler EL. 2009. *Diffusion: Mass transfer in fluid systems,* 3. ed. Cambridge: Cambridge Univ. Press.

David R. Lide. 2005. *CRC Handbook of Chemistryand Physics: Internet Version 2005*. BocaRaton, FL.

Domínguez E, Heredia A. 1999. Water hydration in cutinized cell walls: a physico-chemical analysis. *Biochimica et Biophysica Acta (BBA) - General Subjects* **1426,** 168–176.

Dorr GJ, Wang S, Mayo LC *et al.* 2015. Impaction of spray droplets on leaves: influence of formulation and leaf character on shatter, bounce and adhesion. *Experiments in Fluids* **56**.

Doymaz İ, Pala M. 2002. The effects of dipping pretreatments on air-drying rates of the seedless grapes. *Journal of Food Engineering* **52,** 413–417.

Eckl K, Gruler H. 1980. Phase transitions in plant cuticles. *Planta* **150,** 102–113.

Edwards D. 1993. Cells and tissues in the vegetative sporophytes of early land plants. *New Phytologist* **125,** 225–247.

Eigenbrode SD, Jetter R. 2002. Attachment to plant surface waxes by an insect predator. *Integrative and comparative biology* **42,** 1091–1099.

Fagerström A, Kocherbitov V, Ruzgas T, Westbye P, Bergstrom K, Engblom J. 2013a. Effects of surfactants and thermodynamic activity of model active ingredient on transport over plant leaf cuticle. *Colloids and surfaces. B, Biointerfaces* **103,** 572–579.

Fagerström A, Kocherbitov V, Westbye P, Bergstrom K, Arnebrant T, Engblom J. 2014. Surfactant softening of plant leaf cuticle model wax--a Differential Scanning Calorimetry (DSC) and Quartz Crystal Microbalance with Dissipation (QCM-D) study. *Journal of Colloid and Interface Science* **426,** 22–30.

Fagerström A, Kocherbitov V, Westbye P, Bergström K, Mamontova V, Engblom J. 2013b. Characterization of a plant leaf cuticle model wax, phase behaviour of model wax–water systems. *Thermochimica Acta* **571,** 42–52.

Fernández V, Bahamonde HA, Javier Peguero-Pina J *et al.* 2017. Physico-chemical properties of plant cuticles and their functional and ecological significance. *Journal of Experimental Botany* **68,** 5293–5306.

Forney CF, Brandl DG. 1992. Control of Humidity in Small Controlled-environment Chambers using Glycerol: Water Solutions: Control of Humidity in Small Controlled-environment Chambers using Glycerol-Water Solutions. *HortTechnology,* 52–54.

Forster AW, Mercer GN, Schou WC. 2012. Development of mathematical models for the uptake of agrichemicals through plant leaves; influence of adjuvants on plant and product interactions. *New Zealand Plant Protection,* 85–92.

Forster WA, Kimberley MO. 2015. The contribution of spray formulation component variables to foliar uptake of agrichemicals. *Pest management science* **71,** 1324–1334.

Franke W. 1967. Mechanisms of Foliar Penetration of Solutions. *Annual Review of Plant Physiology* **18,** 281–300.

Fredholm BB. 2010. *Methylxanthines*: Springer Berlin Heidelberg.

Gaskin RE, Holloway PJ. 1992. Some physicochemical factors influencing foliar uptake enhancement of glyphosatemono(isopropylammonium) by polyoxyethylene surfactants. *Pesticide Science* **34,** 195–206.

Gauvrit C, Cabanne F. 1993. Oils for weed control: Uses and mode of action. *Pesticide Science* **37,** 147–153.

Gauvrit C, Dufour JL. 1990. Effects of adjuvants on herbicidal action. I. Effects of a mixture of adjuvants on diclofop-methyl retention and penetration in wheat and ryegrass. *Agronomie* **10,** 759–765.

Grant C, Twigg P, Bell G, Lu JR. 2008. AFM relative stiffness measurement of the plasticising effect of a non-ionic surfactant on plant leaf wax. *Journal of Colloid and Interface Science* **321,** 360–364.

Griffin WC. 1954. Calculation of HLB Values of Non-ionic Surfactants. *Journal of the Society of Cosmetic Chemists,* 249–256.

Günzler H, Gremlich H-U. 2012. *IR-Spektroskopie: Eine Einführung,* 4th edn. Weinheim: Wiley-VCH.

Gutenberger A, Zeisler VV, Berghaus R, Auweter H, Schreiber L. 2013. Effects of poly- and monodisperse surfactants on 14C-epoxiconazole diffusion in isolated cuticles of Prunus laurocerasus. *Pest management science* **69,** 512–519.

Guzmán P, Fernández V, García ML, Khayet M, Fernández A, Gil L. 2014. Localization of polysaccharides in isolated and intact cuticles of eucalypt, poplar

and pear leaves by enzyme-gold labelling. *Plant Physiology and Biochemistry* **76,** 1–6.

Hansch C, Leo A, Hoekman D. 1995. Exploring QSAR. Hydrophobic, electronic, and steric constants. ACS Professional Reference Book. *ACS, Washington*.

Hastie GP, Roberts KJ. 1994. Investigation of inter- and intra-molecular packing in the solid state for crystals of normal alkanes and homologous mixtures using FT-IR spectroscopy. *Journal of Materials Science* **29,** 1915–1919.

Hauke V, Schreiber L. 1998. Ontogenetic and seasonal development of wax composition and cuticular transpiration of ivy (Hedera helix L.) sun and shade leaves. *Planta* **207,** 67–75.

Hazen JL. 2000. Adjuvants—Terminology, Classification, and Chemistry 1. *Weed Technology* **14,** 773–784.

Heredia-Guerrero JA, Benitez JJ, Dominguez E *et al.* 2014. Infrared and Raman spectroscopic features of plant cuticles: a review. *Frontiers in plant science* **5,** 305.

Heredia-Guerrero JA, Benítez, José, J., Domínguez E *et al.* 2016. Infrared spectroscopy as a tool to study plant cuticles. *SPECTROSCOPY EUROPE* **28,** 10–13.

Heredia-Guerrero JA, Lara R de, **Dominguez E, Heredia A, Benavente J, Benitez JJ.** 2012. Chemical-physical characterization of isolated plant cuticles subjected to low-dose gamma-irradiation. *Chemistry and physics of lipids* **165,** 803–808.

Hess FD, Falk RH. 1990. Herbicide Deposition on Leaf Surfaces. *Weed Science* **38,** 280–288.

Hess FD, Foy CL. 2000. Interaction of Surfactants with Plant Cuticles. *Weed Technology* **14,** 807–813.

Hoerr CW, Harwood HJ, Ralston AW. 1944. Solubilites Of High Molecular Weight Normal Aliphatic Primary Alcohols. *The Journal of Organic Chemistry* **09,** 267–280.

Höhne G, Hemminger WF, Flammersheim HJ. 2013. *Differential Scanning Calorimetry*: Springer Berlin Heidelberg.

Holloway PJ, Rees RT, Stock D. 1994. *Interactions Between Adjuvants, Agrochemicals and Target Organisms*. Berlin, Heidelberg: Springer Berlin Heidelberg.

Jeffree CE. 1986. The cuticle, epicuticular waxes and trichomes of plants, with reference to their structure, functions and evolution. *Insects on the plant surface,* 23–64.

Jeffree CE. 1996. Structure and ontogeny of plant cuticles. In: Kerstiens G, ed. *Plant cuticles: An integrated functional approach*. Oxford: BIOS Scientif. Publ, 33–82.

Jetter R, Kunst L, Samuels AL. 2006. Composition of Plant Cuticular Waxes. In: Riederer M, Müller C, eds. *Biology of the Plant Cuticle*. Oxford, UK: Blackwell Publishing Ltd, 145–181.

Jetter R, Riederer M. 2016. Localization of the Transpiration Barrier in the Epi- and Intracuticular Waxes of Eight Plant Species: Water Transport Resistances Are Associated with Fatty Acyl Rather Than Alicyclic Components. *Plant Physiology* **170,** 921–934.

Jetter R, Schäffer S, Riederer M. 2000. Leaf cuticular waxes are arranged in chemically and mechanically distinct layers: Evidence from Prunus laurocerasus L. *Plant, Cell and Environment* **23,** 619–628.

Jin IJ, Ko YI, Kim YM, Han SK. 1997. Solubilization of oleanolic acid and ursolic acid by cosolvency. *Archives of pharmacal research* **20,** 269–274.

Johansson I, Voets I. 2004. About Characterization of surfactaants outside the HLB-System: Proceedings of the 6th World SurfactantsCongress, CESIO 2004, Berlin.

Kerler F, Riederer M, Schönherr J. 1984. Non-electrolyte permeability of plant cuticles: A critical evaluation of experimental methods. *Physiologia plantarum* **62,** 599–602.

Kerler F, Schönherr J. 1988a. Accumulation of lipophilic chemicals in plant cuticles: Prediction from octanol/water partition coefficients. *Archives of Environmental Contamination and Toxicology* **17,** 1–6.

Kerler F, Schönherr J. 1988b. Permeation of lipophilic chemicals across plant cuticles: Prediction from partition coefficients and molar volumes. *Archives of Environmental Contamination and Toxicology* **17,** 7–12.

Kirkwood RC. 1993. Use and mode of action of adjuvants for herbicides: A review of some current work. *Pesticide Science* **38,** 93–102.

Kirsch T, Kaffarnik F, Riederer M, Schreiber L. 1997. Cuticular permeability of the three tree species Prunus laurocerasus L., Ginkgo biloba L. and Juglans regia L:

Comparative investigation of the transport properties of intact leaves, isolated cuticles and reconstituted cuticular waxes. *Journal of Experimental Botany* **48,** 1035–1045.

Kiser RW, Johnson GD, Shetlar MD. 1961. Solubilities of Various Hydrocarbons in Methanol. *Journal of Chemical & Engineering Data* **6,** 338–341.

Knowles DA. 1998. *Chemistry and Technology of Agrochemical Formulations*. Dordrecht: Springer Netherlands.

Koch K, Bhushan B, Barthlott W. 2008. Diversity of structure, morphology and wetting of plant surfaces. *Soft Matter* **4,** 1943.

Kudsk P, Olesen T, Thonke KE. 1990. The influence of temperature, humidity and simulated rain on the performance of thiameturon-methyl. *Weed Research* **30,** 261–269.

Larsson K. 1986. Physical Properties — Structural and Physical Characteristics. In: Gunstone FD, ed. *The lipid handbook*. London: Chapman and Hall, 321–384.

Lavieille D, Ter Halle A, Bussiere P-O, Richard C. 2009. Effect of a spreading adjuvant on mesotrione photolysis on wax films. *Journal of agricultural and food chemistry* **57,** 9624–9628.

Laville E. 1963. Contribution à l'étude de la pénétration et de la localisation des huiles dans la feuille de bananier. *Fruits* **18,** 339–344.

Luque P, Heredia A. 1997. The glassy state in isolated cuticles: differential scanning calorimetry of tomato fruit cuticular membranes. *Plant Physiology and Biochemistry,* 251–256.

Luque P, Ramirez FJ, Heredia A, Bukovac MJ. 1994. Fourier Transform IR Studies on the Interaction of Selected Chemicals with Isolated Cuticles. In: Percy KE, Cape JN, Jagels R, Simpson CJ, eds. *Air Pollutants and the Leaf Cuticle*, Vol. 36. Berlin, Heidelberg: Springer Berlin Heidelberg, 217–223.

Manthey FA, Nalewaja, J. D., Szelezniak, E. F. 1989. Esterified seed oils with herbicides. In: Grant CA, Hinshalwood AM, Simundsson E, eds. *Adjuvants and Agrochemicals*. Florida: CRC Press, 139–148.

Manthey FA, Szelezniak EF, Nalewaja JD. 1996. Relationship Between Spray Droplet Spread and Herbicide Phytotoxicity. In: Hopkinson MJ, ed. *Pesticide*

formulations and application systems: 16th volume, Vol. 1312. West Conshohocken, Pa.: ASTM, 182-182-10.

Martin JT, Juniper BE. 1970. *The Cuticles of Plants*. London: Edward Arnold (Publishers) Ltd,

Mastovska K. 2019. *AZOXYSTROBIN*. http://www.fao.org/fileadmin/templates/agphome/documents/Pests_Pesticides/JMPR/Evaluation08/Azoxystrobin.pdf. 04 Apr. 2019.

Matas AJ, Cobb ED, Bartsch JA, Paolillo DJ, Niklas KJ. 2004. Biomechanics and anatomy of *Lycopersicon esculentum* fruit peels and enzyme-treated samples. *American journal of botany* **91,** 352–360.

Matovic M, van Miltenburg JC, Los J, Gandolfo FG, Flöter E. 2005. Thermal Properties of Tristearin by Adiabatic and Differential Scanning Calorimetry. *Journal of Chemical & Engineering Data* **50,** 1624–1630.

Mcwhorter CG, Barrentine WL. 1988. Spread of Paraffinic Oil on Leaf Surfaces of Johnsongrass (*Sorghum halepense*). *Weed Science* **36,** 111–117.

Mcwhorter CG, Ouzts C, Hanks JE. 1993. Spread of Water and Oil Droplets on Johnsongrass (*Sorghum halepense*) Leaves. *Weed Science* **41,** 460–467.

Mercier L, Serre I, Cabanne F, Gauvrit C. 1997. Behaviour of alkyl oleates following foliar application in relation to their influence on the penetration of phenmedipham and quizalofop-P-ethyl. *Weed Research* **37,** 267–276.

Merk S. 1998. FTIR-spektroskopische Untersuchungen zum Phasenverhalten und zur Kristallinität pflanzlicher kutikularer Wachse. Doctoral Thesis University of Würzburg.

Merk S, Blume A, Riederer M. 1997. Phase behaviour and crystallinity of plant cuticular waxes studied by Fourier transform infrared spectroscopy. *Planta* **204,** 44–53.

Miller P, Westra P. 1998. Herbicide surfactants and adjuvants. *Crop series. Production; no. 0.559*.

Myung K, Parobek AP, Godbey JA, Bowling AJ, Pence HE. 2013. Interaction of organic solvents with the epicuticular wax layer of wheat leaves. *Journal of Agricultural and Food Chemistry* **61,** 8737–8742.

Nairn JJ, Forster WA, van Leeuwen RM. 2016. Effect of solution and leaf surface polarity on droplet spread area and contact angle. *Pest management science* **72,** 551–557.

Nalewaja JD, Devilliers B, Matysiak R. 1996. Surfactant and salt affect glyphosate retention and absorption. *Weed Research* **36,** 241–247.

Nalewaja JD, Skrzypczak GA, Gillespie GR. 1986. Absorption and Translocation of Herbicides with Lipid Compounds. *Weed Science* **34,** 564–568.

Nič M, Jirát J, Košata B, Jenkins A, McNaught A. 2009. *IUPAC Compendium of Chemical Terminology*. Research Triagle Park, NC: IUPAC.

Niederl S, Kirsch T, Riederer M, Schreiber L. 1998. Co-Permeability of 3 H-Labeled Water and 14 C-Labeled Organic Acids across Isolated Plant Cuticles. *Plant Physiology* **116,** 117–123.

Nobel PS. 2009. *Physicochemical and environmental plant physiology*. San Diego: Academic Press Inc.

Ohta A, Murakami R, Takiue T, Ikeda N, Aratono M. 2000. Calorimetric Study of Micellar Solutions of Pentaethylene Glycol Monooctyl and Monodecyl Ethers. *The Journal of Physical Chemistry B* **104,** 8592–8597.

Oosterhuis DM, Walker S. 1987. Stomatal resistance measurement as an indicator of water deficit stress in wheat and soybeans. *South African Journal of Plant and Soil* **4,** 113–120.

Orgell WH. 1955. The Isolation of Plant Cuticle with Pectic Enzymes: Analysis of the barrier properties of plant cuticles. *PLANT PHYSIOLOGY* **30,** 78–80.

Pambou E, Hu X, Li Z *et al.* 2018. Structural Features of Reconstituted Cuticular Wax Films upon Interaction with Nonionic Surfactant C12E6. *Langmuir the ACS journal of surfaces and colloids* **34,** 3395–3404.

Paranjape K, Gowariker V, Krishnamurthy VN, Gowariker S. 2014. *The Pesticide Encyclopedia*: CABI.

Pensec F, Pączkowski C, Grabarczyk M *et al.* 2014. Changes in the triterpenoid content of cuticular waxes during fruit ripening of eight grape (*Vitis vinifera*) cultivars grown in the Upper Rhine Valley. *Journal of Agricultural and Food Chemistry* **62,** 7998–8007.

Perkins MC, Roberts CJ, Briggs D *et al.* 2005. Macro and microthermal analysis of plant wax/surfactant interactions: Plasticizing effects of two alcohol ethoxylated surfactants on an isolated cuticular wax and leaf model. *Applied Surface Science* **243,** 158–165.

Petracek PD, Fader RG, Knoche M, Bukovac MJ. 1998. Surfactant-Enhanced Penetration of Benzyladenine through Isolated Tomato Fruit Cuticular Membranes. *Journal of Agricultural and Food Chemistry* **46,** 2346–2352.

Piper SH, Chibnall AC, Williams EF. 1934. Melting-points and long crystal spacings of the higher primary alcohols and n-fatty acids. *The Biochemical journal* **28,** 2175–2188.

Popp C. 2005. Cuticular transport of hydrophilic molecules with special focus on primary metabolites and active ingredients. Doctoral Thesis University of Würzburg.

Popp C, Burghardt M, Friedmann A, Riederer M. 2005. Characterization of hydrophilic and lipophilic pathways of Hedera helix L. cuticular membranes: permeation of water and uncharged organic compounds. *Journal of Experimental Botany* **56,** 2797–2806.

Price CE. 1982. A review of the factors influencing the penetration of pesticides through plant leaves. *The Plant Cuticle,* 237–252.

Ramirez FJ, Luque P, Heredia A, Bukovac MJ. 1992. Fourier transform IR study of enzymatically isolated tomato fruit cuticular membrane. *Biopolymers* **32,** 1425–1429.

Ramsey RJL, Stephenson GR, Hall JC. 2005. A review of the effects of humidity, humectants, and surfactant composition on the absorption and efficacy of highly water-soluble herbicides. *Pesticide Biochemistry and Physiology* **82,** 162–175.

Ramsey RJL, Stephenson GR, Hall JC. 2006. Effect of humectants on the uptake and efficacy of glufosinate in wild oat (*Avena fatua*) plants and isolated cuticles under dry conditions. *Weed Science* **54,** 205–211.

Räsch A, Hunsche M, Mail M, Burkhardt J, Noga G, Pariyar S. 2018. Agricultural adjuvants may impair leaf transpiration and photosynthetic activity. *Plant physiology and biochemistry PPB* **132,** 229–237.

Remus-Emsermann MNP, Oliveira S de, **Schreiber L, Leveau JHJ.** 2011. Quantification of lateral heterogeneity in carbohydrate permeability of isolated plant leaf cuticles. *Frontiers in microbiology* **2,** 197.

Reynhardt EC. 1985. NMR investigation of Fischer-Tropsch waxes. II. Hard wax. *Journal of Physics D: Applied Physics* **18,** 1185–1197.

Reynhardt EC. 1986. Temperature dependence of the cell parameters of Fischer-Tropsch waxes: hard wax and oxidised hard wax. *Journal of Physics D: Applied Physics* **19,** 1925–1938.

Reynhardt EC. 1997. The role of hydrogen bonding in the cuticular wax of Hordeum vulgare L. *European Biophysics Journal* **26,** 195–201.

Reynhardt EC, Riederer M. 1991. Structure and molecular dynamics of the cuticular wax from leaves of Citrus aurantium L. *Journal of Physics D: Applied Physics* **24,** 478–486.

Reynhardt EC, Riederer M. 1994. Structures and molecular dynamics of plant waxes: II. Cuticular waxes from leaves of Fagus sylvatica L. and Hordeum vulgate L. *European Biophysics Journal* **23**.

Riederer M, Burghardt M, Mayer S, Obermeier H, Schönherr J. 1995. Sorption of Monodisperse Alcohol Ethoxylates and Their Effects on the Mobility of 2,4-D in Isolated Plant Cuticles. *Journal of Agricultural and Food Chemistry* **43,** 1067–1075.

Riederer M, Schneider G. 1990. The effect of the environment on the permeability and composition of Citrus leaf cuticles: II. Composition of soluble cuticular lipids and correlation with transport properties. *Planta* **180,** 154–165.

Riederer M, Schönherr J. 1984. Accumulation and transport of (2,4-dichlorophenoxy)acetic acid in plant cuticles: I. Sorption in the cuticular membrane and its components. *Ecotoxicology and Environmental Safety* **8,** 236–247.

Riederer M, Schönherr J. 1985. Accumulation and transport of (2,4-dichlorophenoxy) acetic acid in plant cuticles. *Ecotoxicology and Environmental Safety* **9,** 196–208.

Riederer M, Schönherr J. 1990. Effects of surfactants on water permeability of isolated plant cuticles and on the composition of their cuticular waxes. *Pesticide Science* **29,** 85–94.

Riederer M, Schreiber L. 1995. Waxes: the transport barriers of plant cuticles. In: Hamilton RJ, ed. *Waxes: Chemistry, molecular biology and functions*, Vol. 6. Dundee: The Oily Press, 131–156.

Riederer M, Schreiber L. 2001. Protecting against water loss: Analysis of the barrier properties of plant cuticles. *Journal of Experimental Botany* **52,** 2023–2032.

Robertson MM, Parham PH, Bukovac MJ. 1971. Penetration of diphenylacetic acid through enzymically-isolated tomato fruit cuticle as influenced by substitution on the carboxyl group. *Journal of Agricultural and Food Chemistry* **19,** 754–757.

Rohrbaugh PW. 1941. Physiological Effects of Petroleum Oil Sprays on Citrus. *Journal of Economic Entomology* **34,** 812–815.

Ruiter H de, **Uffing AJM, Meinen E.** 1996. Influence of Surfactants and Ammonium Sulfate on Glyphosate Phytotoxicity to Quackgrass. *Weed Technology* **10,** 803–808.

Ruiter H de, **Uffing AJM, Meinen E, Prins A.** 1990. Influence of Surfactants and Plant Species on Leaf Retention of Spray Solutions. *Weed Science* **38,** 567–572.

Ryckaert B, Spanoghe P, Heremans B, Haesaert G, Steurbaut W. 2008. Possibilities to use tank-mix adjuvants for better fungicide spreading on triticale ears. *Journal of agricultural and food chemistry* **56,** 8041–8044.

Santier S, Chamel A. 1996. Penetration of triolein and methyl oleate through isolated plant cuticles and their effect on penetration of [14C]quizalofop-ethyl and [14C]fenoxaprop-ethyl. *Weed Research* **36,** 167–174.

Saravacos GD, Marousis SN, Raouzeos GS. 1988. Effect of ethyl oleate on the rate of air-drying of foods. *Journal of Food Engineering* **7,** 263–270.

Schönherr J. 1976. Water permeability of isolated cuticular membranes: The effect of cuticular waxes on diffusion of water. *Planta* **131,** 159–164.

Schönherr J. 1993a. Effects of alcohols, glycols and monodisperse ethoxylated alcohols on mobility of 2,4-D in isolated plant cuticles. *Pesticide Science* **39,** 213–223.

Schönherr J. 1993b. Effects of monodisperse alcohol ethoxylates on mobility of 2,4-D in isolated plant cuticles. *Pesticide Science* **38,** 155–164.

Schönherr J. 2006. Characterization of aqueous pores in plant cuticles and permeation of ionic solutes. *Journal of Experimental Botany* **57,** 2471–2491.

Schönherr J, Baur P. 1994. Modelling penetration of plant cuticles by crop protection agents and effects of adjuvants on their rates of penetration. *Pesticide Science* **42,** 185–208.

Schönherr J, Baur P. 1996. Effects of temperature, surfactants and other adjuvants on rates of uptake of organics. In: Kerstiens G, ed. *Plant cuticles: An integrated functional approach*. Oxford: BIOS Scientif. Publ, 135–155.

Schönherr J, Baur P. 1997. Effects of tetraethyleneglycol monooctylether (C_8E_4) on mobilities of selected pesticides in Citrus leaf cuticles. *Journal of Plant Diseases and Protection,* 246–253.

Schönherr J, Riederer M. 1986. Plant cuticles sorb lipophilic compounds during enzymatic isolation. *Plant, Cell and Environment* **9,** 459–466.

Schönherr J, Schreiber L. 2004. Size selectivity of aqueous pores in astomatous cuticular membranes isolated from *Populus canescens* (Aiton) Sm. leaves. *Planta* **219,** 405–411.

Schott JJ, Dufour JL, Gauvrit C. 1991. Effects of adjuvants on herbicidal action. III. Effects of petroleum and rapeseed oils on diclofop-methyl action on ryegrass. *Agronomie* **11,** 27–34.

Schreiber L. 1995. A mechanistic approach towards surfactant/wax interactions: Effects of octaethyleneglycolmonododecylether on sorption and diffusion of organic chemicals in reconstituted cuticular wax of barley leaves. *Pesticide Science* **45,** 1–11.

Schreiber L. 2001. Effect of temperature on cuticular transpiration of isolated cuticular membranes and leaf discs. *Journal of Experimental Botany* **52,** 1893–1900.

Schreiber L. 2002. Co-permeability of 3H-labelled water and 14C-labelled organic acids across isolated Prunus laurocerasus cuticles: Effect of temperature on cuticular paths of diffusion. *Plant, Cell and Environment* **25,** 1087–1094.

Schreiber L. 2005. Polar paths of diffusion across plant cuticles: new evidence for an old hypothesis. *Annals of botany* **95,** 1069–1073.

Schreiber L, Bach S, Kirsch T, Knoll D, Schalz K, Riederer M. 1995. A simple photometric device analysing cuticular transport physiology: Surfactant effect on permeability of isolated cuticular membranes of Prunus laurocerasus L. *Journal of Experimental Botany* **46,** 1915–1921.

Schreiber L, Riederer M. 1996. Ecophysiology of cuticular transpiration: Comparative investigation of cuticular water permeability of plant species from different habitats. *Oecologia* **107,** 426–432.

Schreiber L, Riederer M, Schorn K. 1996. Mobilities of Organic Compounds in Reconstituted Cuticular Wax of Barley Leaves: Effects of Monodisperse Alcohol Ethoxylates on Diffusion of Pentachlorophenol and Tetracosanoic Acid. *Pesticide Science* **48,** 117–124.

Schreiber L, Schönherr J. 1993. Mobilities of organic compounds in reconstituted cuticular wax of barley leaves: Determination of diffusion coefficients. *Pesticide Science* **38,** 353–361.

Schreiber L, Schönherr J. 2009. *Water and Solute Permeability of Plant Cuticles: Measurement and Data Analysis*. Berlin, Heidelberg: Springer Berlin Heidelberg.

Schreiber L, Schorn K, Heimburg T. 1997. 2 H NMR study of cuticular wax isolated from Hordeum vulgare L. leaves: Identification of amorphous and crystalline wax phases. *European Biophysics Journal* **26,** 371–380.

Schuster A-C. 2016. Chemical and functional analyses of the plant cuticle as leaf transpiration barrier: Chemie-Funktionsanalysen der pflanzlichen Kutikula als Transpirationsbarriere, Doctoral thesis University of Würzburg.

Schuster A-C, Burghardt M, Alfarhan A *et al.* 2016. Effectiveness of cuticular transpiration barriers in a desert plant at controlling water loss at high temperatures. *AoB PLANTS* **8**.

Schuster A-C, Burghardt M, Riederer M. 2017. The ecophysiology of leaf cuticular transpiration: Are cuticular water permeabilities adapted to ecological conditions? *Journal of Experimental Botany*.

Semenov S, Starov V, Rubio RG. 2015. Chapter 21 - Droplets with Surfactants. In: Brutin D, ed. *Droplet wetting and evaporation: From pure to complex fluids*. Amsterdam, Boston, Heidelberg: Elsevier/AP Academic Press, 315–337.

Serrato-Palacios LL, Toro-Vazquez JF, Dibildox-Alvarado E *et al.* 2015. Phase Behavior and Structure of Systems Based on Mixtures of n-Hentriacontane and Melissic Acid. *Journal of the American Oil Chemists' Society* **92,** 533–540.

Serre I, Cabanne F, Gauvrit C. 1993. Seedoil derivatives as adjuvants: influence of methyl to octadecyl oleates on the penetration of herbicides through various plant cuticles. *Med. Fac. Landbouww. Rijksuniv. Gent*.

Seufert P. 2019. Chemical and physical structure of the barrier against water transpiration of leaves: Contribution of different wax compounds: Chemischer und

physikalischer Aufbau der Wassertranspirationsbarriere von Blättern: Beitrag verschiedener Wachskomponenten, Doctoral thesis University of Würzburg.

Shi T, Simanova E, Schönherr J, Schreiber L. 2005. Effects of accelerators on mobility of 14C-2,4-dichlorophenoxy butyric acid in plant cuticles depends on type and concentration of accelerator. *Journal of agricultural and food chemistry* **53,** 2207–2212.

Sigma-Aldrich. 2019a. *Specification sheet*. https://www.sigmaaldrich.com/Graphics/COfAInfo/SigmaSAPQM/SPEC/L2/L2626/L2626-BULK_____SIGMA____.pdf. 23 Aug. 2019.

Sigma-Aldrich. 2019b. *Caffeine Safety Data Sheet*. 04 Apr. 2019.

Sirota EB, Wu XZ. 1996. The rotator phases of neat and hydrated 1-alcohols. *The Journal of Chemical Physics* **105,** 7763–7773.

Slavík B, Jarvis MS. 1974. *Methods of studying plant water relations*. Berlin: Springer.

Smirnova A, Leide J, Riederer M. 2013. Deficiency in a very-long-chain fatty acid β-ketoacyl-coenzyme a synthase of tomato impairs microgametogenesis and causes floral organ fusion. *PLANT PHYSIOLOGY* **161,** 196–209.

Staiger S, Seufert P, Arand K, Burghardt M, Popp C, Riederer M. 2019. The permeation barrier of plant cuticles: uptake of active ingredients is limited by very long-chain aliphatic rather than cyclic wax compounds. *Pest Management Science*.

Stammitti L, Garrec JP, Derridj S. 1995. Permeability of isolated cuticles of Prunus laurocerasus to soluble carbohydrate. *Plant Physiology and Biochemistry* **1995**.

Stenersen J. 2004. *Chemical Pesticides Mode of Action and Toxicology*: CRC Press.

Stevens PJG, Bukovac MJ. 1987a. Studies on octylphenoxy surfactants. Part 1: Effects of oxyethylene content on properties of potential relevance to foliar absorption. *Pesticide Science* **20,** 19–35.

Stevens PJG, Bukovac MJ. 1987b. Studies on octylphenoxy surfactants. Part 2: Effects on foliar uptake and translocation. *Pesticide Science* **20,** 37–52.

Stock D, Holloway PJ. 1993. Possible mechanisms for surfactant-induced foliar uptake of agrochemicals. *Pesticide Science* **38,** 165–177.

Stock D, Holloway PJ, Grayson BT, Whitehouse P. 1993. Development of a predictive uptake model to rationalise selection of polyoxyethylene surfactant adjuvants for foliage-applied agrochemicals. *Pesticide Science* **37,** 233–245.

Stoytcheva M. 2011. *Pesticides in the modern world: Trends in pesticides analysis,* Ed. 2014. Rijeka, Croatia: InTech.

Svenningsson M. 1988. Epi- and intracuticular lipids and cuticular transpiration rates of primary leaves of eight barley (*Hordeum vulgare*) cultivars. *Physiologia plantarum* **73,** 512–517.

Szakiel A, Pączkowski C, Pensec F, Bertsch C. 2012. Fruit cuticular waxes as a source of biologically active triterpenoids. *Phytochemistry reviews* **11,** 263–284.

Tasumi M, Shimanouchi T, Watanabe A, Goto R. 1964. Infrared spectra of normal higher alcohols—I. *Spectrochimica Acta* **20,** 629–666.

Tsubaki S, Sugimura K, Teramoto Y, Yonemori K, Azuma J-I. 2013. Cuticular membrane of Fuyu persimmon fruit is strengthened by triterpenoid nano-fillers. *PloS one* **8,** e75275.

Turner JA. 2018. *The pesticide manual: A world compendium,* Eighteenth edition. Alton: BCPC.

Urvoy C, Gauvrit C. 1991. Seed oils as adjuvants: penetration of glycerol trioleate, methanol oleate and diclofop-methyl in maize leaves. *Proceedings of the Brighton Crop Protection Conference* **1991**.

Urvoy C, Pollasek M, Gauvrit C. 1992. Seed oils as additives: Penetration of triolein, methyloleate and diclofop-methyl in maize leaves. *Weed Research* **32,** 375–383.

USDA ARS. 2019. *Taxonomy - GRIN-Global Web v 1.10.4.0: National Plant Germplasm System*. https://npgsweb.ars-grin.gov/gringlobal/taxonomydetail.aspx?id=30027. 02 Apr. 2019.

van Os NM. 1997. *Nonionic Surfactants: Organic Chemistry,* 1st ed. New York: CRC Press.

Villena JF, Domínguez E, Heredia A. 2000. Monitoring Biopolymers Present in Plant Cuticles by FT-IR Spectroscopy. *Journal of Plant Physiology* **156,** 419–422.

Vogg G, Fischer S, Leide J *et al.* 2004. Tomato fruit cuticular waxes and their effects on transpiration barrier properties: functional characterization of a mutant deficient in a very-long-chain fatty acid beta-ketoacyl-CoA synthase. *Journal of Experimental Botany* **55,** 1401–1410.

W.A. Forster, G.N. Mercer, W.C. Schou. 2012. Spray droplet impaction models and their use within AGDISP software to predict retention. *New Zealand Plant Protection* **65**.

Wanamarta G, Penner D, Kells JJ. 1989. Identification of Efficacious Adjuvants for Sethoxydim and Bentazon. *Weed Technology* **3,** 60–66.

Webster GR, Bisset NB, Cahill DM *et al.* 2018. Tristearin as a Model Cuticle for High-Throughput Screening of Agricultural Adjuvant Systems. *ACS Omega* **3,** 16672–16680.

Wenzel RN. 1936. Resistance of solid surfaces to wetting by water. *Industrial & Engineering Chemistry* **28,** 988–994.

Wiedemann P, Neinhuis C. 1998. Biomechanics of Isolated Plant Cuticles. *Botanica Acta* **111,** 28–34.

Wirth W, Storp S, Jacobsen W. 1991. Mechanisms controlling leaf retention of agricultural spray solutions. *Pesticide Science* **33,** 411–420.

Wishart DS, Feunang YD, Marcu A *et al.* 2018. HMDB 4.0: the human metabolome database for 2018. *Nucleic acids research* **46,** D608-D617.

Wolska K, Grudniak A, Fiecek B, Kraczkiewicz-Dowjat A, Kurek A. 2010. Antibacterial activity of oleanolic and ursolic acids and their derivatives. *Open Life Sciences* **5,** 202.

Xu L, Zhu H, Ozkan HE, Bagley WE, Krause CR. 2011. Droplet evaporation and spread on waxy and hairy leaves associated with type and concentration of adjuvants. *Pest management science* **67,** 842–851.

Yeats TH, Rose JKC. 2013. The formation and function of plant cuticles. *Plant Physiology* **163,** 5–20.

Zeisler V, Schreiber L. 2016. Epicuticular wax on cherry laurel (*Prunus laurocerasus*) leaves does not constitute the cuticular transpiration barrier. *Planta* **243,** 65–81.

Zeisler-Diehl V, Müller Y, Schreiber L. 2018. Epicuticular wax on leaf cuticles does not establish the transpiration barrier, which is essentially formed by intracuticular wax. *Journal of Plant Physiology* **227,** 66–74.

Zerbi G, Gallino G, Del Fanti N, Baini L. 1989. Structural depth profiling in polyethylene films by multiple internal reflection infra-red spectroscopy. *Polymer* **30,** 2324–2327.

Zhang C, Zhao X, Lei J, Ma Y, Du F. 2017. The wetting behavior of aqueous surfactant solutions on wheat (*Triticum aestivum*) leaf surfaces. *Soft Matter* **13,** 503–513.

Zhang J, Jaeck O, Menegat A, Zhang Z, Gerhards R, Ni H. 2013. The mechanism of methylated seed oil on enhancing biological efficacy of topramezone on weeds. *PloS one* **8,** e74280.

Zhang Y, Adams MJ, Zhang Z, Vidoni O, Leuenberger BH, Achkar J. 2016. Plasticisation of carnauba wax with generally recognised as safe (GRAS) additives. *Polymer* **86,** 208–219.

7 Appendix

7.1 Chapter 1

Appendix 1 Data on permeance to theobromine with isolated cuticular membranes (CM), methanol treated membranes (M) and fully dewaxed cuticles (MX) of *Prunus laurocerasus* and *Garcinia xanthochymus*

species	mem-brane	n	number of removed outliers	median x 10^{11} (m s^{-1})	25th -75th quartile x 10^{11} (m s^{-1})	comparison post-hoc Dunn's test	p-value post-hoc Dunn's test with Benjamini-Hochberg adjustment
Prunus laurocerasus	CM	19	3	0.8	0.3 - 2.3	CM - M	0.537
	M	16	3	0.6	0.4 - 1.0	CM - MX	6.48E-05
	MX	10	1	15.4	12.2 - 18.8	M - MX	2.2E-05
Garcinia xanthochymus	CM	22	2	13.9	1.1 - 32.0	CM - M	0.7307
	M	15	1	7.9	1.6 - 25.3	CM - MX	0.0076
	MX	11	0	153.0	21.6 - 258.3	M - MX	0.011

Appendix 2 Data on permeance to caffeine with isolated cuticular membranes (CM), methanol treated membranes (M) and fully dewaxed cuticles (MX) of *Prunus laurocerasus* and *Garcinia xanthochymus*

species	mem-brane	n	number of removed outliers	median x 10^{11} (m s^{-1})	25th -75th quartile x 10^{11} (m s^{-1})	comparison post-hoc Dunn's test	p-value post-hoc Dunn's test with Benjamini-Hochberg adjustment
Prunus laurocerasus	CM	17	4	0.2	0.1 - 1.2	CM - M	0.142
	M	9	2	0.7	0.5 - 1.7	CM - MX	9.9E-06
	MX	9	0	45.6	44.8 - 64.6	M - MX	0.008
Garcinia xanthochymus	CM	11	1	11.9	1.1 - 25.8	CM - M	0.352
	M	18	2	4.3	1.6 - 29.8	CM - MX	0.227
	MX	20	3	5.8	21.6 - 16.5	M - MX	0.514

Appendix 3 Data on permeance to azoxystrobin with isolated cuticular membranes (CM), methanol treated membranes (M) and fully dewaxed cuticles (MX) of *Prunus laurocerasus* and *Garcinia xanthochymus*

species	mem-brane	n	number of removed outliers	median x 10^{11} (m s^{-1})	25% -75% quartile x 10^{11} (m s^{-1})	comparison post-hoc Dunn's test	p-value post-hoc Dunn's test with Benjamini-Hochberg adjustment
Prunus laurocerasus	CM	30	4	3.4	0.7 - 9.6	CM - M	0.021
	M	18	2	8.4	6.5 - 21.6	CM - MX	5.99E-07
	MX	9	1	123.6	87.8 - 162.0	M - MX	0.002
Garcinia xanthochymus	CM	9	1	14.9	10.5 - 34.5	CM - M	0.977
	M	9	2	15.4	9.6 - 18.4	CM - MX	0.024
	MX	10	2	52.3	38.3 - 131.6	M - MX	0.013

Appendix 4 Data on crystallinity at 20°C of extracted adaxial cuticular wax of *Prunus laurocerasus* and *Garcinia xanthochymus*

wax	n	mean aliphatic crystallinity (%)	SD (%)	p-value for two-sided t.test
Prunus laurocerasus	4	81.7	2.2	0.222890023
Garcinia xanthochymus	3	84.7	3.5	

7.2 Chapter 2

Appendix 5 Data on wax comparison of *Schefflera elegantissima* leaf and cuticular wax grouped by functionality, very long-chain aliphatic compounds (VLCA), cyclics, not identified (N.I) and total wax amount

group	p-value for Mann-Whitney Rank sum test
alcohol	0.029
alkane	0.343
acid	0.029
cyclic	0.021
aldehyde	0.021
VLCA	0.029
cyclic	0.021
NI	0.029
total	0.029

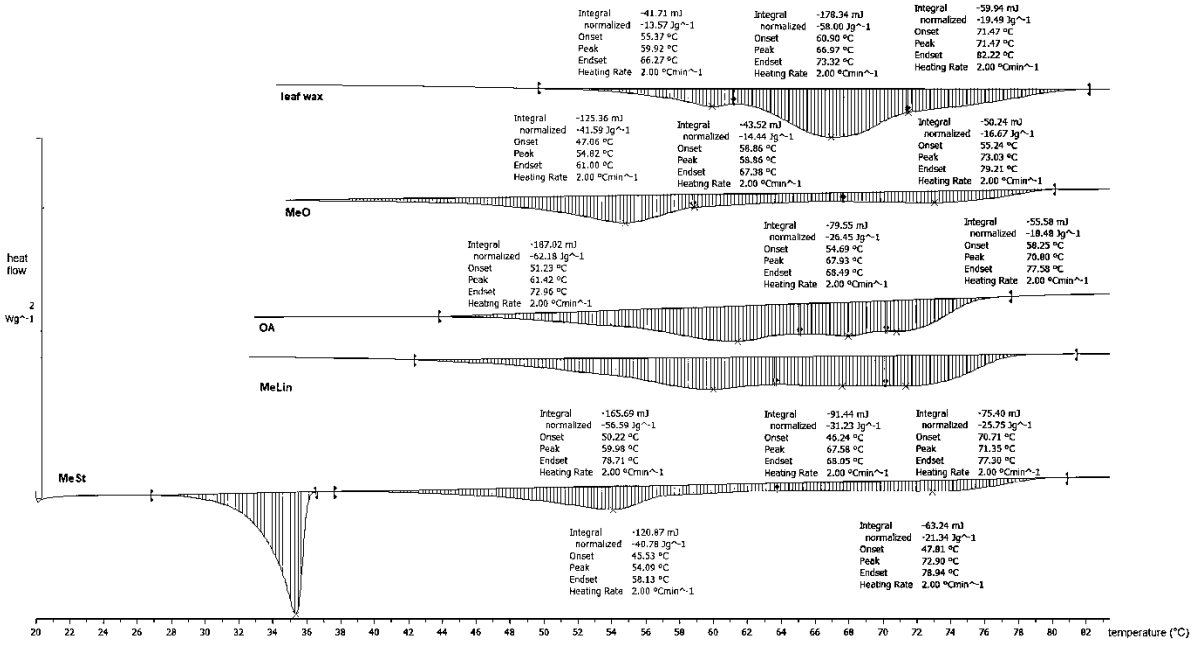

Appendix 6 Thermograms of *Schefflera elegantissima* leaf wax (SE leaf wax) and 25 % (*w/w*) of methyl oleate (MeO), oleic acid (OA), methyl linolenate (MeLin) and methyl stearate (MeSt) for heating cycle 2

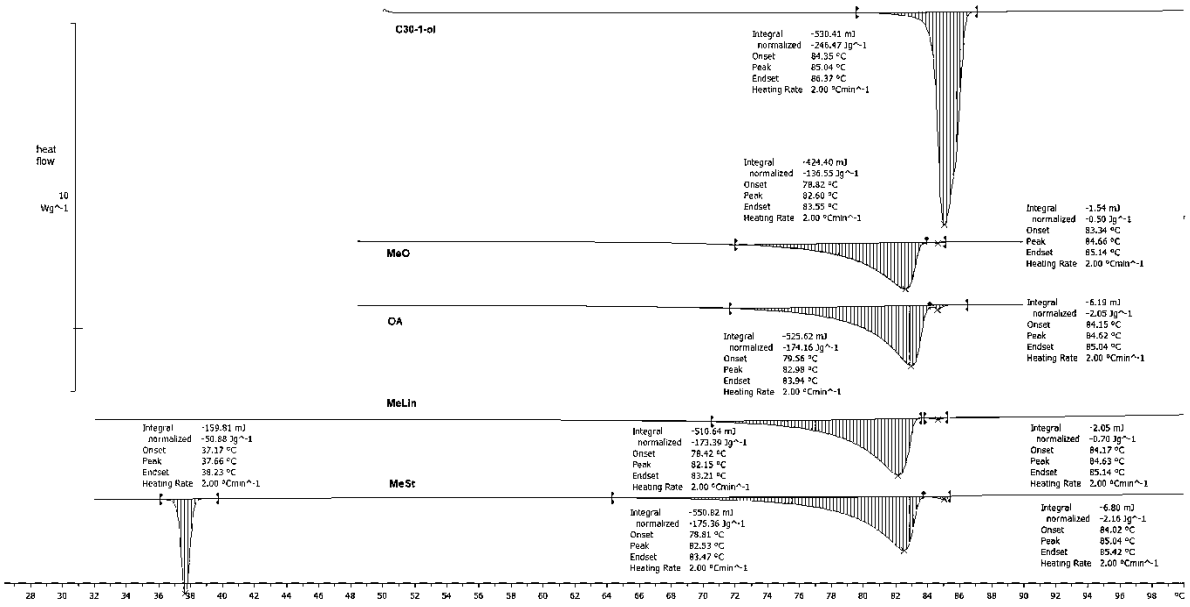

Appendix 7 Thermograms of C30-1-ol and 25 % (*w/w*) of methyl oleate (MeO), oleic acid (OA), methyl linolenate (MeLin) and methyl stearate (MeSt) for heating cycle 2

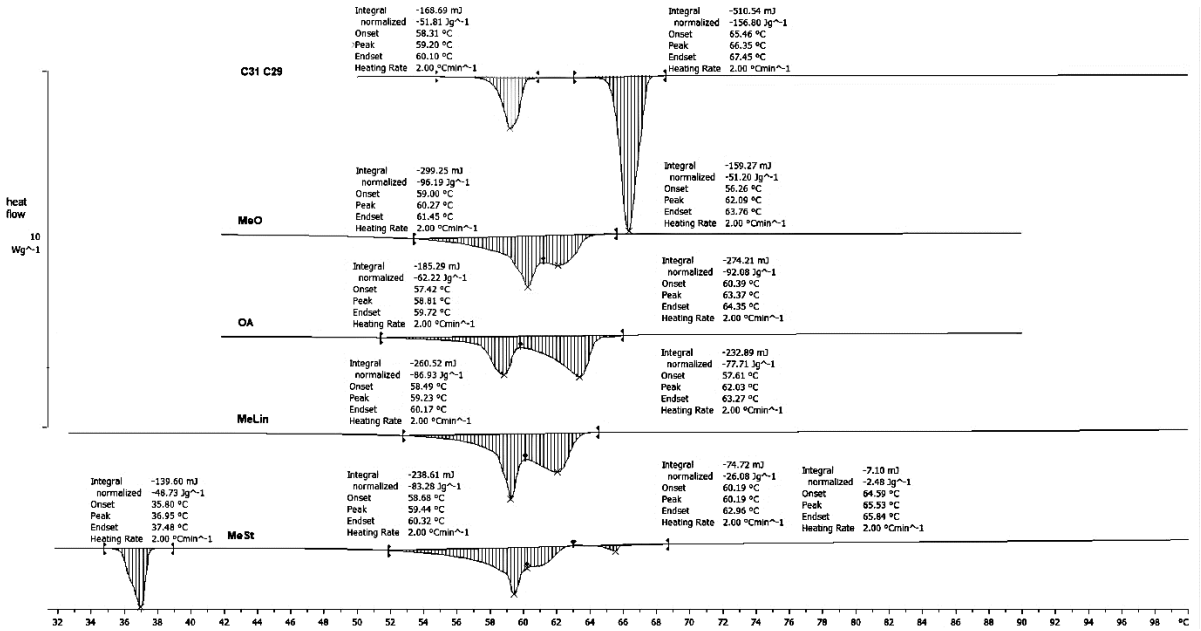

Appendix 8 Thermograms of C31/C29 and 25 % (*w/w*) of methyl oleate (MeO), oleic acid (OA), methyl linolenate (MeLin) and methyl stearate (MeSt) for heating cycle 2

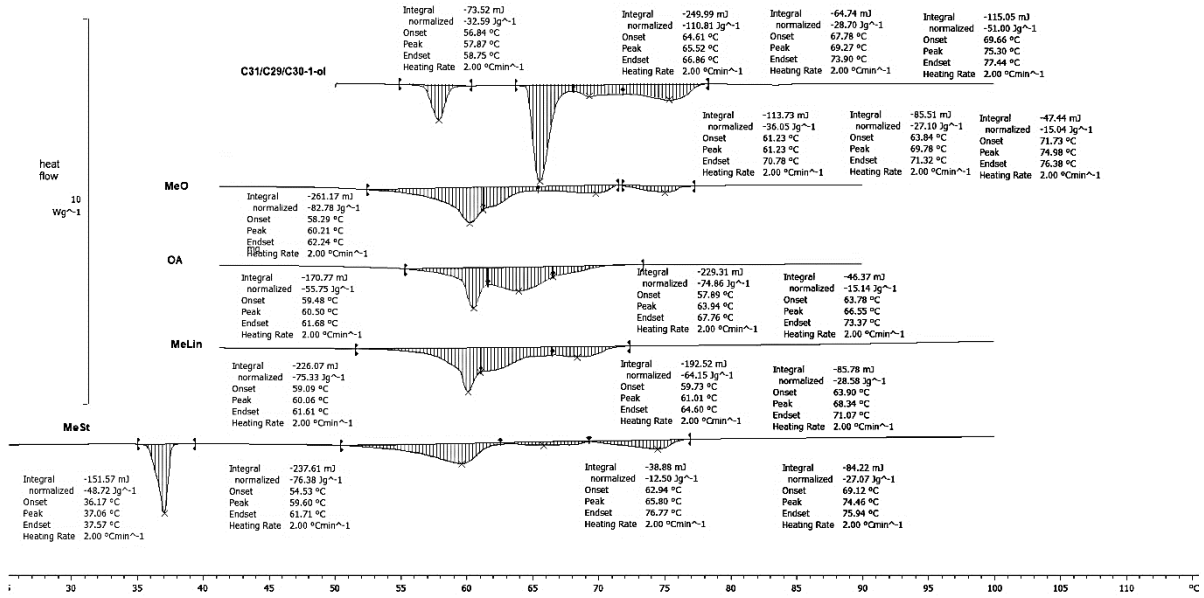

Appendix 9 Thermograms of C31/C29/C30-1-ol and 25 % (*w/w*) of methyl oleate (MeO), oleic acid (OA), methyl linolenate (MeLin) and methyl stearate (MeSt) for heating cycle 2

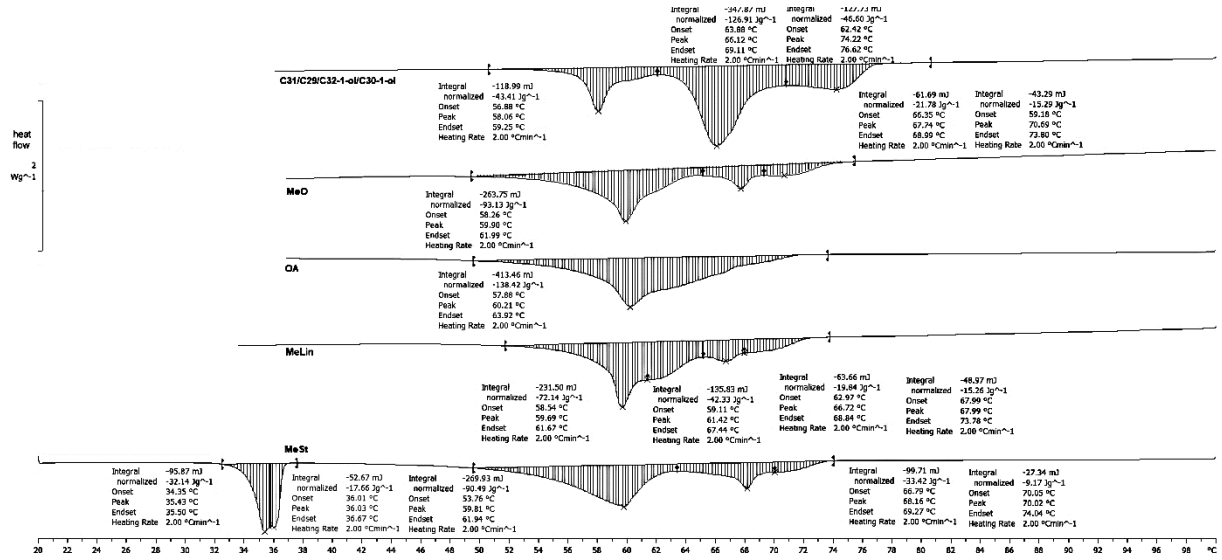

Appendix 10 Thermograms of C31/C29/C30-1-ol/C32-1-ol and 25 % (*w/w*) of methyl oleate (MeO), oleic acid (OA), methyl linolenate (MeLin) and methyl stearate (MeSt) for heating cycle 2

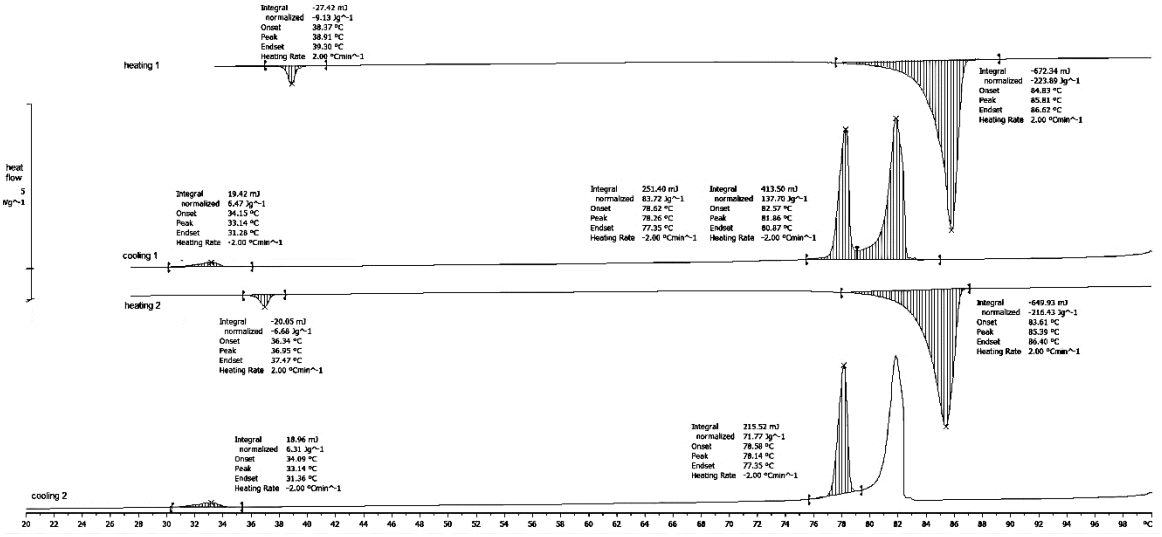

Appendix 11 Thermogram of 1-triacontanol (C30-1-ol) with 5 % methyl stearate for all heating and cooling cycles.

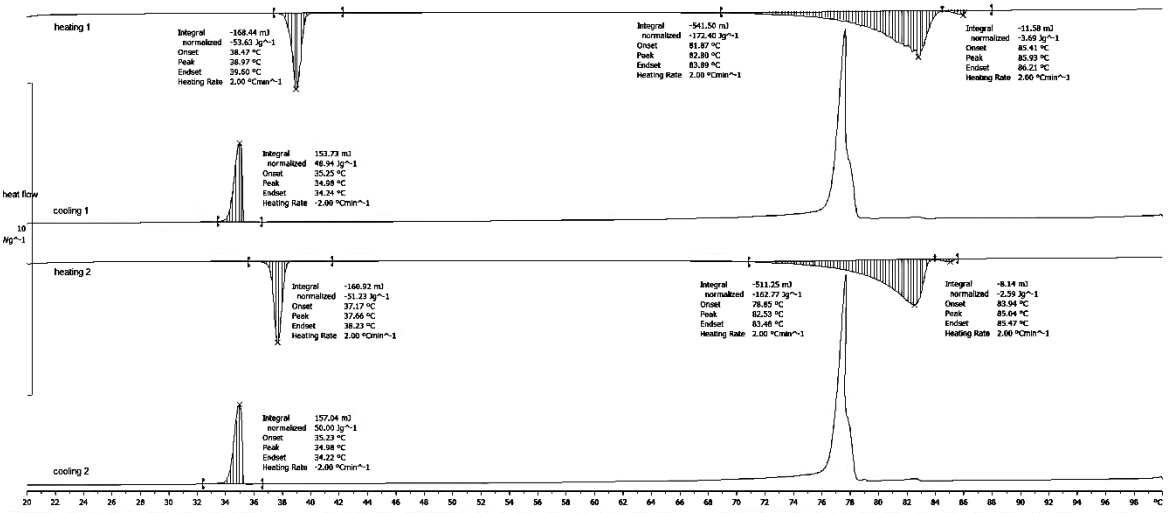

Appendix 12 Thermogram of 1-triacontanol (C30-1-ol) with 25 % methyl stearate for all heating and cooling cycles

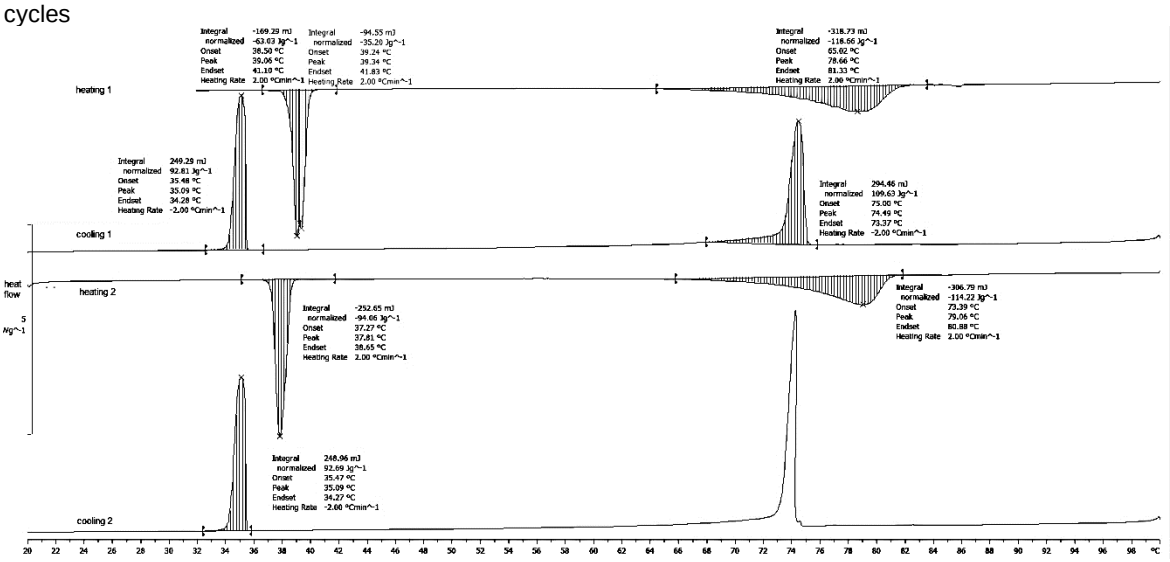

Appendix 13 Thermogram of 1-triacontanol (C30-1-ol) with 50 % methyl stearate for all heating and cooling cycles

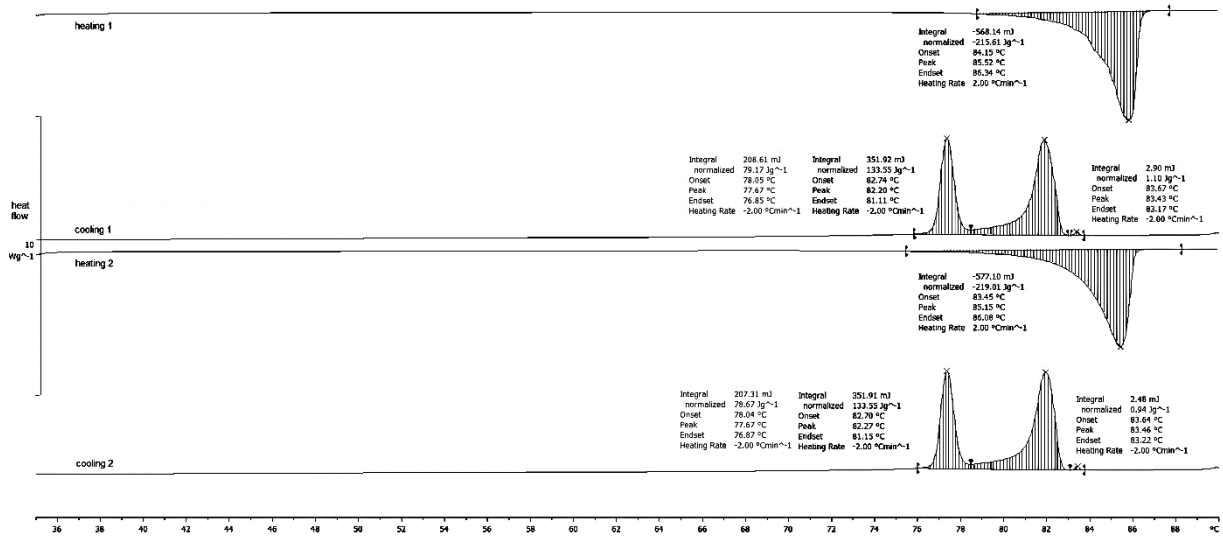

Appendix 14 Thermogram of 1-triacontanol (C30-1-ol) with 5 % oleic acid for all heating and cooling cycles

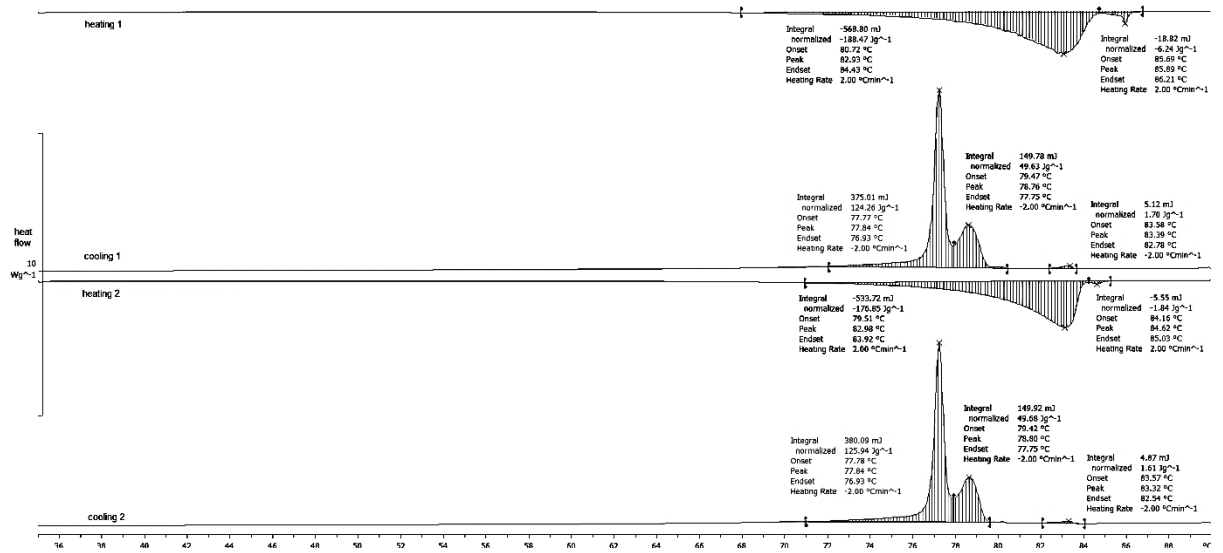

Appendix 15 Thermogram of 1-triacontanol (C30-1-ol) with 25 % oleic acid for all heating and cooling cycles

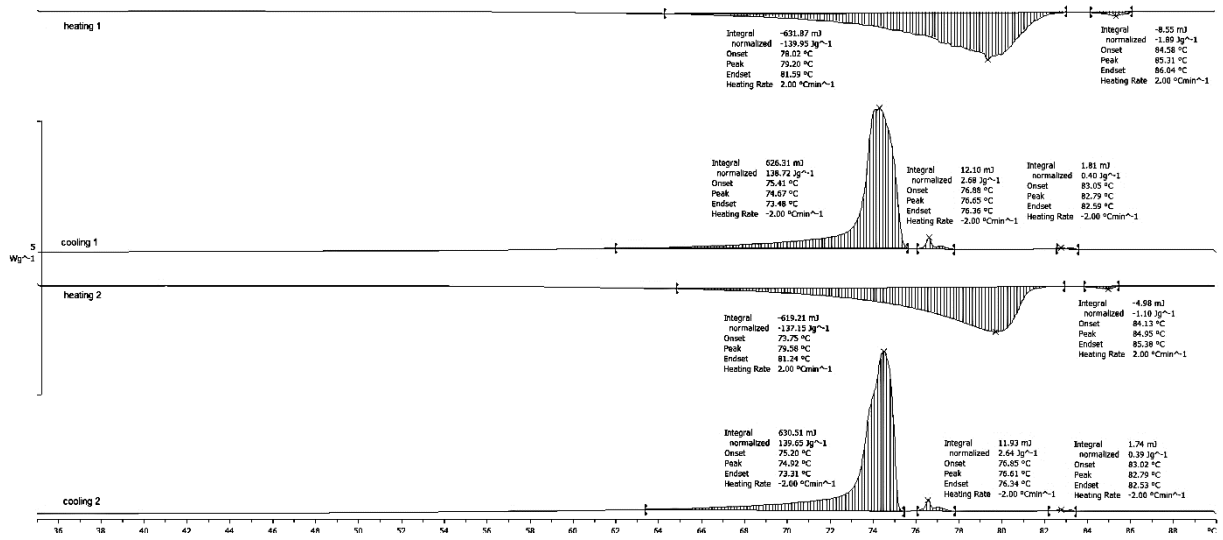

Appendix 16 Thermogram of 1-triacontanol (C30-1-ol) with 50 % oleic acid for all heating and cooling cycles

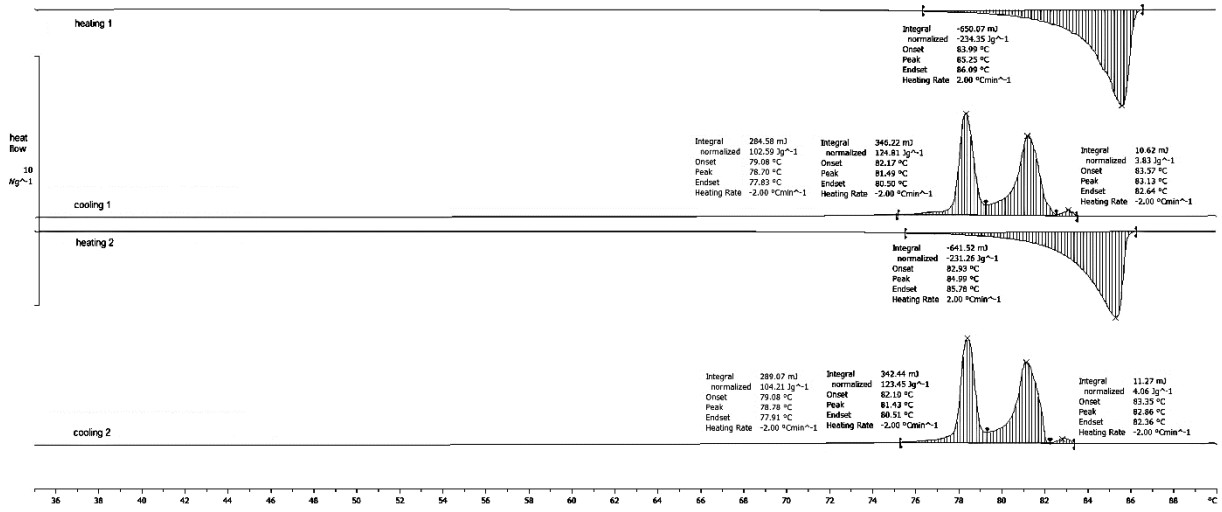

Appendix 17 Thermogram of 1-triacontanol (C30-1-ol) with 5 % methyl oleate for all heating and cooling cycles

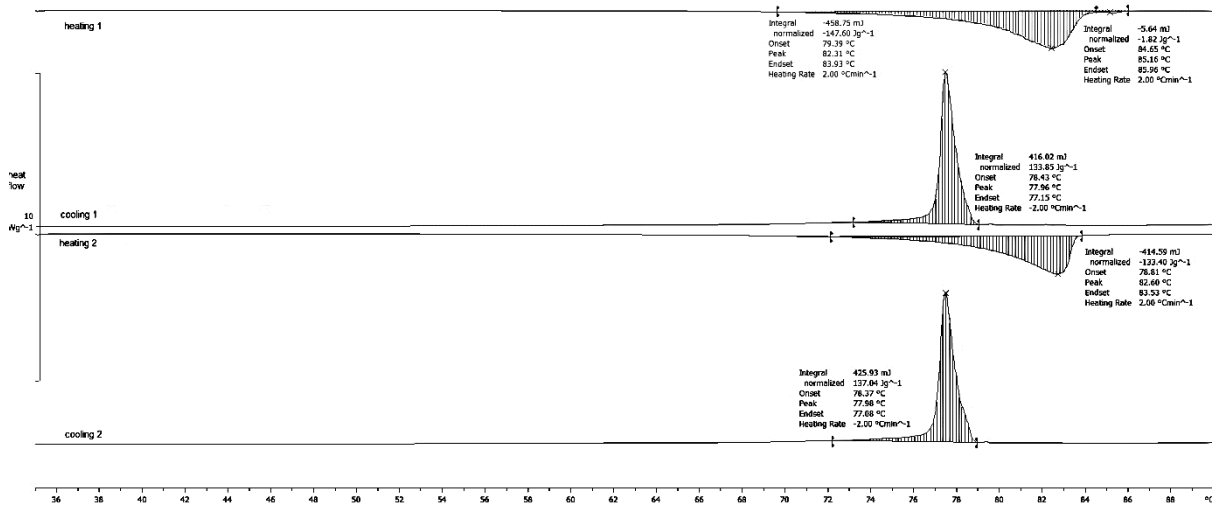

Appendix 18 Thermogram of 1-triacontanol (C30-1-ol) with 25 % methyl oleate for all heating and cooling cycles

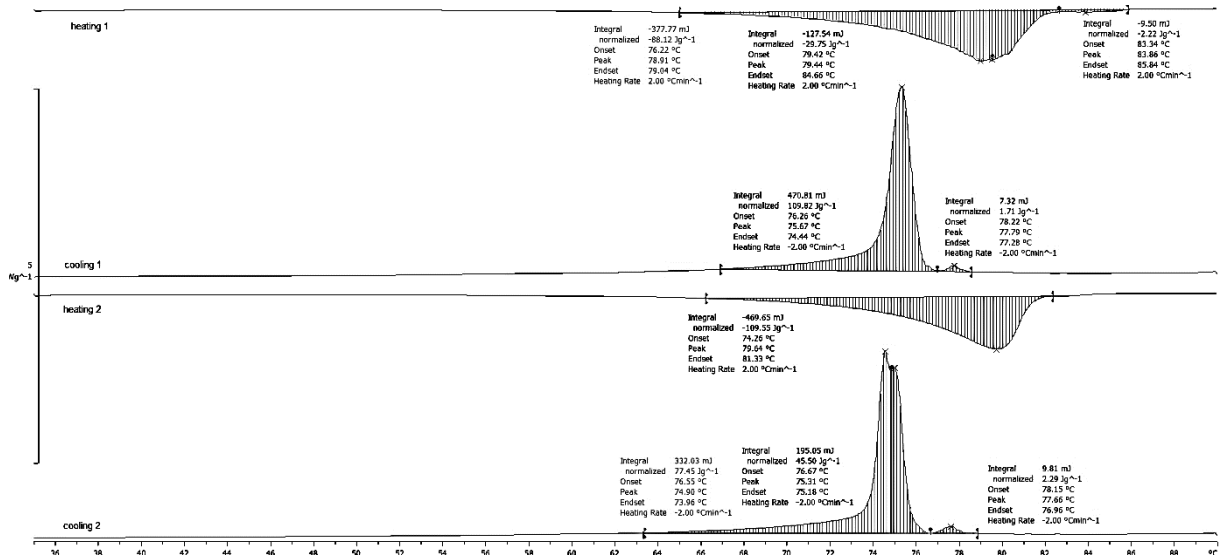

Appendix 19 Thermogram of 1-triacontanol (C30-1-ol) with 50 % methyl oleate for all heating and cooling cycles

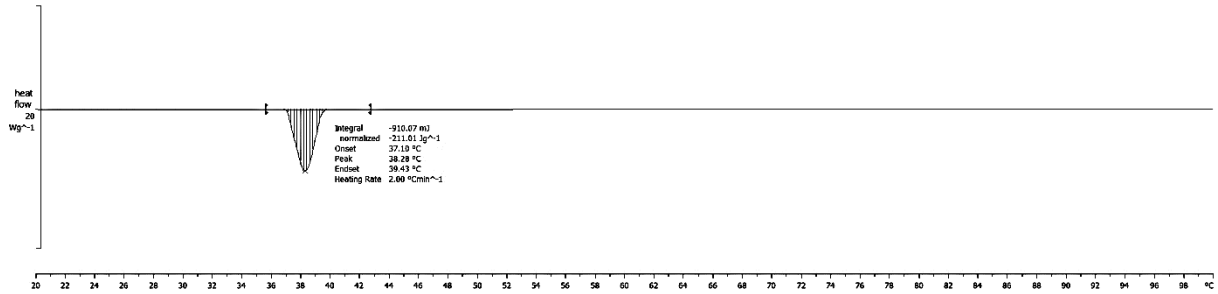

Appendix 20 Thermograms of pure methyl stearate for heating cycle 2

Appendix 21 Enthalpy of transition (EOT), onset temperature, peak temperature and offset temperature measured by DSC of the different phase transitions of the C30-1-ol adjuvant blend with methyl linolenate (MeLin), oleic acid (OA), methyl oleate (MeO), methyl stearate (MeSt).

amount of adjuvant (%)	Phase transition											
	EOT (J g-1)			onset (°C)			Peak (°C)			offset (°C)		
0	-246.36			84.35			85.04			86.37		
	MeLin1	MeLin2		MeLin1	MeLin2		MeLin1	MeLin2		MeLin1	MeLin2	
7.3955	-227.73			82.82			84.69			85.57		
28.31919	-173.39	-0.7		78.42	84.17		82.15	84.63		83.21	85.14	
47.08041	-120.09			75.33			80.08			81.59		
	OA1	OA2		OA1	OA2		OA1	OA2		OA1	OA2	
4.51613	-209.68			83.55			85.15			86.1		
18.82041	-174.16	-2.05		79.56	84.15		82.98	84.62		83.94	85.04	
37.65227	-128.57	-0.97		73.91	84.19		79.61	84.95		81.25	85.37	
	MeO1	MeO2		MeO1	MeO2		MeO1	MeO2		MeO1	MeO2	
7.4261	-223.96			83.03			84.99			85.81		
19.91634	-136.55	-0.5		78.82	83.34		82.6	84.66		83.55	85.14	
41.12433	-99.23			74.48			79.64			81.34		
	EOT (J g-1)			onset (°C)			Peak (°C)			offset (°C)		
	MeSt1	MeSt2	MeSt3	MeSt1	MeSt2	MeSt3	MeSt1	MeSt2	MeSt3	MeSt1	MeSt2	MeSt3
4.4955	-6.92	-217.88		36.33	83.61		36.95	85.39		37.47	86.4	
25.15123	-50.88	-175.36	-2.16	37.17	78.81	84.02	37.66	82.53	85.04	38.23	83.47	85.42
45.68131	-93.95	-108.1	-0.41	37.27	73.5	84.32	37.81	79.06	84.85	38.65	80.87	85.38

Appendix 22 Enthalpy of transition (EOT), onset temperature, peak temperature and offset temperature measured by DSC of the different phase transitions of the C31/29 adjuvant blend with methyl linolenate (MeLin), oleic acid (OA), methyl oleate (MeO), methyl stearate (MeSt).

amount of adjuvant (%)	Phase transition															
	EOT (J g-1)				onset (°C)				Peak (°C)				offset (°C)			
0	-51.81	-156,80			58.31	65.46			59.20	66.35			60.1	67.45		
amount of adjuvant (%)	**MeLin1**	**MeLin2**	**MeLin3**	**MeLin4**	**MeLin1**	**MeLin2**	**MeLin3**	**MeLin4**	**MeLin1**	**MeLin2**	**MeLin3**	**MeLin4**	**MeLin1**	**MeLin2**	**MeLin3**	**MeLin4**
5.18234	-56.42	-134.68			58.48	62.43			59.13	64.88			59.78	65.73		
26.45785	-86.93	-77.71			58.49	57.61			59.23	62.03			60.17	63.27		
49.00826	-110.72				57.74				59.52				60.78			
	OA1	**OA2**	**OA3**	**OA4**	**OA1**	**OA2**	**OA3**	**OA4**	**OA1**	**OA2**	**OA3**	**OA4**	**OA1**	**OA2**	**OA3**	**OA4**
5.32081	-57.6	-137.53			57.82	63.69			58.81	63.37			59.82	66.17		
19.54332	-62.22	-92.08			57.42	60.39			58.86	60.69			59.72	64.35		
38.10079	-62.61	-31			56.93	54.81							60.05	61.94		
	MeO1	**MeO2**	**MeO3**	**MeO4**	**MeO1**	**MeO2**	**MeO3**	**MeO4**	**MeO1**	**MeO2**	**MeO3**	**MeO4**	**MeO1**	**MeO2**	**MeO3**	**MeO4**
4.83221	-63.46	-119.19			58.6	62.66				59.13	64.88		60.43	66.08		
19.22212	-96.19	-51.2			59	56.26				59.23	62.03		61.45	63.76		
38.56492	-116.99				55.21					59.52			60.92			
	MeSt1	**MeSt2**	**MeSt3**	**MeSt4**	**MeSt1**	**MeSt2**	**MeSt3**	**MeSt4**	**MeSt1**	**MeSt2**	**MeSt3**	**MeSt4**	**MeSt1**	**MeSt2**	**MeSt3**	**MeSt4**
5.50162	35.81	58.54	62.72		36.8	59.24	65.26		36.8	59.24	65.26		37.2	59.97	66.03	
25.02618	35.8	58.68	60.19	64.59	36.95	59.44	60.19	65.53	36.95	59.44	60.19	65.53	37.48	60.32	62.96	65.84
55.0065	35.84	52.19			37.14	57.18			37.14	57.18			37.82	58.59		

Appendix 23 Enthalpy of transition (EOT), onset temperature, peak temperature and offset temperature measured by DSC of the different phase transitions of the C31/29/C30-1-ol adjuvant blend with methyl linolenate (MeLin), oleic acid (OA), methyl oleate (MeO), methyl stearate (MeSt).

amount of adjuvant (%)	Phase transition																			
	EOT (J g-1)				onset (°C)				Peak (°C)				offset (°C)							
0	-32.59	-110.81	-27.94	-51.00	56.84	64.61	67.78	69.66	57.87	65.52	69.29	75.30	58.75	66.86	73.9	77.44				
	MeLin1	MeLin2	MeLin3	MeLin4	MeLin1	MeLin2	MeLin3	MeLin4	MeLin1	MeLin2	MeLin3	MeLin4	MeLin1	MeLin2	MeLin3	MeLin4				
5.18234	-44.1	-106.01	-19.73	-40.52	58.95	61.81	64.31	66.21	59.54	65.38	68.43	73.44	60.38	67.79	70.13	75.64				
26.45785	-75.33	-64.15	-28.58		59.09	59.73	63.9		60.06	61.01	68.34		61.61	64.6	71.07					
49.00826	-95.92	-21			55.1	62.77			59.5	62.77			62.56	68.44						
	OA1	OA2	OA3	OA4	OA1	OA2	OA3	OA4	OA1	OA2	OA3	OA4	OA1	OA2	OA3	OA4				
3.55221	-49.48	-137.41	-13.24		59.1	63.86	69.58		60.56	66.41	69.55		61.51	68.43	73.83	3.55221				
17.69507	-55.75	-74.86	-15.14		59.48	57.89	63.78		60.5	63.94	66.55		61.68	67.76	73.37	17.69507				
40.45184	-107.43		-12.73		53.96		70.01		60.07		73.81		63.5		75.08	40.45184				
	EOT (J g-1)					onset (°C)					Peak (°C)						offset (°C)				
0	-32.59	-110.81	-27.94	-51.00			56.84	64.61	67.78	69.66								58.75	66.86	73.9	77.44
	MeSt1	MeSt2	MeSt3	MeSt4	MeSt5	MeSt1	MeSt2	MeSt3	MeSt4	MeSt5	MeSt1	MeSt2	MeSt3	MeSt4	MeSt5	MeSt1	MeSt2	MeSt3	MeSt4	MeSt5
6.10425	-12.28	-53.65	-94.22	-34.67	-24.77	36.16	59.2	60.16	65.39	67.31	36.95	59.87	64.99	73.56	68.89	37.36	60.72	67.25	76.26	71.02
24.81517	-48.72	-76.38	-12.5	-27.07		36.17	54.53	62.94	69.12		37.06	59.6	65.8	74.46		37.57	61.71	76.77	75.94	
38.01956	-100.53	-45.35	-9.51	-18.71		35.82	48.96	59.07	65.83		37.11	55.54	62.83	70.43		37.98	58.39	65.46	73.45	
	MeO1	MeO2	MeO3	MeO4	MeO5	MeO1	MeO2	MeO3	MeO4	MeO5	MeO1	MeO2	MeO3	MeO4	MeO5	MeO1	MeO2	MeO3	MeO4	MeO5
6.45651	-43.49	-76.92	-48.34	-18.47	-2.56	58.39	59.73	61.75	67.17	75.8	59.34	64.24	73.84	70.24	77.79	60.07	66.44	77.22	76.31	78.84
17.49604	-82.78	-36.05	-27.1	-15.04		58.29	61.23	63.84	71.73		60.21	61.23	69.78	74.98		62.24	70.78	71.32	76.38	
40.94694	-66.96		-28.12			50.76		64.23			56.91		72.74			59.76		75.88		

Appendix 24 Enthalpy of transition (EOT), onset temperature, peak temperature and offset temperature measured by DSC of the different phase transitions of the C31/29/C30-1-ol/C32-1-ol adjuvant blend with methyl linolenate (MeLin), oleic acid (OA), methyl oleate (MeO).

amount of adjuvant (%)	Phase transition															
	EOT (J g-1)				onset (°C)				Peak (°C)				offset (°C)			
0	-43.41	-126.91	-46.6		56.88	63.88	62.42		58.06	66.12	74.22		59.25	69.11	76.62	
	MeLin1	MeLin2	MeLin3	MeLin4	MeLin1	MeLin2	MeLin3	MeLin4	MeLin1	MeLin2	MeLin3	MeLin4	MeLin1	MeLin2	MeLin3	MeLin4
5.51	-39.98	-83.22	-22.53	-35.88	58.12	59.83	64.06	62.56	58.94	64.99	66.82	73.06	60.01	69.06	74.16	75.31
22.59271	-72.14	-42.33	-19.84	-15.26	58.54	59.11	62.97	67.99	59.69	61.42	66.72	67.99	61.67	67.44	68.84	73.78
52.67797	-77.8	-23.86			53.76	61.68			58.69	61.68			62.64	69.24		
	OA1	OA2	OA3	OA4	OA1	OA2	OA3	OA4	OA1	OA2	OA3	OA4	OA1	OA2	OA3	OA4
5.35952	-39.22	-121.68	-33.76		58.01	61.57	58.03		58.9	65.67	69.37		60.1	69.59	74.85	
26.18011	-138.42				57.88				60.21				63.92		63.92	
51.8531	-53.38	-25.95			50.88	60.89			57.22	66.87			60.34	70.11	70.11	
	EOT (J g-1)					onset (°C)					Peak (°C)					offset (°C)				
	MeO1	MeO2	MeO3	MeO4	MeO5	MeO1	MeO2	MeO3	MeO4	MeO5	MeO1	MeO2	MeO3	MeO4	MeO5	MeO1	MeO2	MeO3	MeO4	MeO5
5.01767	-50.06	-76.84	-20.02	-43.99		58.16	60.03	67.41	63.31		59.14	65.19	67.44	73.49		60.52	70.05	69.41	76.21	
26.87147	-93.13	-21.78	-15.29			58.26	66.35	59.18			59.9	67.74	70.69			61.99	68.99	73.8		
49.07735	-80.84					49.86					58.81					64.83				

Appendix 25 Enthalpy of transition (EOT), onset temperature, peak temperature and offset temperature measured by DSC of the different phase transitions of the C31/29/C30-1-ol/C32-1-ol adjuvant blend with methyl stearate (MeSt).

amount of adjuvant (%)	Phase transition																							
	EOT (J g-1)						onset (°C)						Peak (°C)						offset (°C)					
0			-43.41	-126.91	-46.6				56.88	63.88	62.42				58.06	66.12	74.22				59.25	69.11	76.62	
	MeSt1	MeSt1b	MeSt2	MeSt3	MeSt4	MeSt5	MeSt1	MeSt1b	MeSt2	MeSt3	MeSt4	MeSt5	MeSt1	MeSt1b	MeSt2	MeSt3	MeSt4	MeSt5	MeSt1	MeSt1b	MeSt2	MeSt3	MeSt4	MeSt5
5.2597	-6.63		-49.97	-78.06	17.19	-45.1	32.67		58.21	60.15	65.07	64.33	34.69		59.26	64.85	67.86	73.51	35.73		60.73	69.16	69.04	75.52
23.86859	-32.14	-17.66	-90.49		-33.42	-9.17	34.35	36.01	53.76		66.79	70.05	35.43	36.03	59.81		68.16	70.02	35.5	36.67	61.94		69.27	74.04
51.37006	-51.6	-63.3	-45.92	-24.66			34.81	35.82	47.26	55.74			36.06	36.94	54.03	64.21			36.08	37.68	57.74	68.02		

Appendix 26 Enthalpy of transition (EOT), onset temperature, peak temperature and offset temperature measured by DSC of the different phase transitions of the leaf wax adjuvant blend with diethylene glycol monodecyl ether (C10E2), octaethylene glycol monodecyl ether (C10E8), methyl linolenate (MeLin), oleic acid (OA), methyl oleate (MeO).

amount of adjuvant (%)	Phase transition															
	EOT (J g-1)				onset (°C)				Peak (°C)				offset (°C)			
0		-41.96	-105.03	-16.69		57.35	59.8	74.6		61.81	71.26	74.59		66.51	77.86	81.18
	C10E21	C10E22	C10E23	C10E24	C10E21	C10E22	C10E23	C10E24	C10E21	C10E22	C10E23	C10E24	C10E21	C10E22	C10E23	C10E24
5.14608		-20.05	-77.25			56.37	59.71			60.51	65.27			77.64	72.64	
25.54622		-39.58	-17.93			53.32	60.6			59.31	69.96			67.72	78.52	
51.37353		-34.55	-0.004			49.46	62.39			54.98	62.38			62.71	66.78	
	C10E81	C10E82	C10E83	C10E84	C10E81	C10E82	C10E83	C10E84	C10E81	C10E82	C10E83	C10E84	C10E81	C10E82	C10E83	C10E84
5.53691		-21.55	-72.43			58.29	60.74			61.82	69.28			66.90	78.66	
23.98453		-28.94	-61.52			58.86	60.95			61.74	68.77			64.78	75.58	
49.87843		-21.55	-43.03			58.29	66.79			61.82	67.38			66.90	75.71	
	MeLin1	MeLin2	MeLin3	MeLin4	MeLin1	MeLin2	MeLin3	MeLin4	MeLin1	MeLin2	MeLin3	MeLin4	MeLin1	MeLin2	MeLin3	MeLin4
5.37245	-8.66	-41.18	-68.24	-21.71	42.48	55.91	57.81	73.63	53.79	61.85	69.41	73.95	76.43	67.62	79.96	78.13
24.86339		-56.59	-31.23	-25.75		50.22	46.24	70.71		59.98	67.58	71.35		78.71	68.05	77.3
50.34347		-39.89	-33.38			45.51	64.65			56.74	66.68			58.42	78.40	
	OA1	OA2	OA3	OA4	OA1	OA2	OA3	OA4	OA1	OA2	OA3	OA4	OA1	OA2	OA3	OA4
4.83651	-9.29	-42.54	-75.27	-20.19	47.3	56.96	58.56	73.18	54.02	61.95	70.01	73.18	76.82	66.88	78.07	78.62
25.2992		-62.18	-26.45	-18.48		51.23	54.69	58.25		61.42	67.93	70.80		72.96	68.49	77.58
52.86094		-38.88	-24.62			44.95	54.97			55.36	68.46			65.21	74.1	
	MeO1	MeO2	MeO3	MeO4	MeO1	MeO2	MeO3	MeO4	MeO1	MeO2	MeO3	MeO4	MeO1	MeO2	MeO3	MeO4
6.74362	-52.92	-91.95			53.51	63.57			64.00	70.97			74.75	77.47		
26.41335	-43.97	-42.36			58.99	68.28			61.37	69.27			62.54	77.72		
42.26475	-22.11	-37.17			48.12	49.4			56.62	70.25			73.31	76.34		

Appendix 27 Enthalpy of transition (EOT), onset temperature, peak temperature and offset temperature measured by DSC of the different phase transitions of the leaf wax adjuvant blend with methyl stearate (MeSt).

amount of adjuvant (%)	Phase transition																							
	EOT (J g-1)						onset (°C)						Peak (°C)						offset (°C)					
0			-41.96	-105.03	-16.69			57.35	59.8	74.6				61.81	71.26	74.59				66.51	77.86	81.18		
	MeSt1	MeSt1b	MeSt2	MeSt3	MeSt4	MeSt5	MeSt1	MeSt1b	MeSt2	MeSt3	MeSt4	MeSt5	MeSt1	MeSt1b	MeSt2	MeSt3	MeSt4	MeSt5	MeSt1	MeSt1b	MeSt2	MeSt3	MeSt4	MeSt5
6.0054		-50.45	-64.21	-28.21				55.67	56.61	73.76				62	69.33	74.2				67.22	71.57	78.17		
26.24831	-33.56	-44.43	-53.18				31.01	46.83	45.91				35.05	59.49	72.79				36.3	71.6	77.24			
48.85225	-70.65	-61.7					33.34	61.93					36.16	69.67					36.81	78.84				

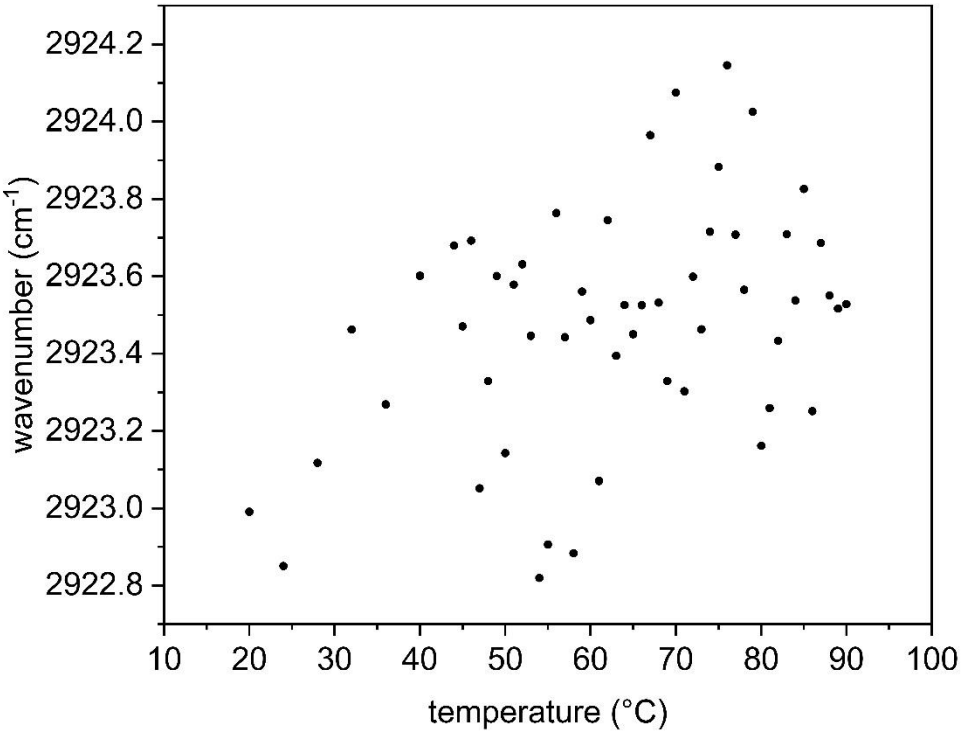

Appendix 28 Wavenumber of the maximum of the asymmetric stretching signal for pure octaethylene glycol monodecyl ether plotted *versus* the temperature

Appendix 29 Data on crystallinity at 20°C of *Schefflera elegantissima* leaf wax (SE) and artificial model wax (QM) pure (non) and with the adjuvants methyl oleate (MeO), oleic acid (OA), methyl linolenate (MeLin), methyl stearate (MeSt) (non), diethylene glycol monodecyl ether (C10E2), pentaethylene glycol monodecyl ether (C10E5) and octaethylene glycol monodecyl ether (C10E8)

wax	adjuvant	proportion of adjuvant	n	mean aliphatic crystallinity (%)	0.95 - confidence intervals (%)	standard deviation (%)	p-value for Dunnett's test against control	p-value for two-sided t-test between SE and QM
QM	non	0	4	91.1	84.2-98.1	2.490838	not tested	0.07646
QM	MeO	5	3	94.8	91.5-98.0	1.300472	0.872	0.341
		25	3	90.7	81.8-99.7	3.593003	1.000	0.07402
		50	3	68.1	53.8-82.4	5.772981	< 0.0001	0.9458
QM	OA	5	3	90.8	84.4-97.2	2.579302	1.000	0.2376
		25	3	92.0	86.0-98.0	2.420094	1.000	0.01007
		50	3	89.0	86.1-92.0	1.170518	0.999	0.1651
QM	MeLin	5	3	92.5	83.6-101.0	3.605887	1.000	0.1752
		25	3	88.3	72.4-104.0	6.424852	0.982	0.9581
		50	3	72.5	59.5-85.5	5.237857	< 0.0001	0.09245
QM	MeSt	5	3	91.8	85.8-97.7	2.407836	1.000	0.1457
		25	3	91.4	87.6-95.2	1.524052	1.000	0.173
		50	3	86.5	82.9-90.0	1.429572	0.589	0.5292
QM	C10E2	5	3	87.9	78.4-97.5	3.849811	0.941	0.86
		25	3	86.9	77.7-96.1	3.712061	0.705	0.3604
		50	3	89.1	80.3-98.0	3.563954	1.000	0.9259
QM	C10E5	5	3	84.5	81.7-87.4	1.148616	0.152	0.2205
		25	3	95.2	91.7-98.7	1.4222	0.761	0.03491
		50	3	92.1	86.6-97.6	2.2188	1.000	0.5998
QM	C10E8	5	3	82.7	79.9-85.6	1.142124	0.028	0.0004394
		25	3	87.8	78.1-97.5	3.907534	0.920	0.1114
		50	3	90.7	88.4-93.1	0.937001	1.000	0.6693
SE	non	0	4	84.8	78.6-91.0	2.490838	not tested	0.07646
SE	MeO	5	3	90.2	82.6-97.7	3.05218	0.823	0.341
		25	4	88.6	86.0-91.3	1.647983	0.970	0.07402
		50	3	67.8	55.4-80.2	5.000972	0.001	0.9458
SE	OA	5	3	88.0	82.6-93.5	2.204623	0.997	0.2376
		25	3	84.6	81.2-88.1	1.385474	1.000	0.0101
		50	3	76.2	43.8-109.0	13.03789	0.258	0.1651
SE	MeLin	5	3	88.9	85.7-92.1	1.300774	0.971	0.1752
		25	4	88.1	79.2-97.0	5.563918	0.993	0.9581
		50	3	86.0	63.2-109.0	9.164072	1.000	0.09245
SE	MeSt	5	3	87.6	79.7-95.5	3.194336	1.000	0.1457
		25	3	87.0	76.2-97.8	4.338062	1.000	0.173
		50	4	84.6	77.3-91.9	4.608022	1.000	0.5292
SE	C10E2	5	3	88.7	74.0-103.0	5.913699	0.982	0.860
		25	3	90.4	78.8-102.0	4.675843	0.774	0.3604
		50	3	88.9	83.6-94.1	2.109908	0.973	0.9259
SE	C10E5	5	3	86.3	81.9-90.6	1.738469	1.000	0.2205
		25	3	88.9	81.0-96.8	3.175375	0.970	0.03491
		50	3	91.2	86.6-95.8	1.835768	0.626	0.5998

SE	C10E8	5	3	91.2	89.3-93.1	0.772003	0.625	0.0004
		25	3	92.6	89.7-95.4	1.138302	0.372	0.1114
		50	3	90.2	85.5-94.8	1.872102	0.821	0.6693

Appendix 30 Data on water permeance of isolated cuticular membranes (CM) and leaf envelopes (env) of *Prunus laurocerasus* and *Garcinia xanthochymus* with no adjuvant and pure methyl oleate (MeO)

plant species	adjuvant	treat-ment	n	number of removed outliers	p-value of paired t-test to non-adjuvanted control	p-value of Welch t-test between CM and env	median permeance x 10^6 (m s^{-1})	25% -75% quartile x 10^6 (m s^{-1})
Prunus laurocerasus	no no	CM env	22 12	3 1	not tested	< 0.001	4.73 9.6	3.87 - 6.25 7.77 - 10.69
Prunus laurocerasus	MeO MeO	CM env	22 12	3 1	< 0.001 < 0.001	0.897	17.01 17.22	13.15 - 25.65 16.53 - 18.45
Garcinia xanthochymus	no no	CM env	17 12	3 1	not tested	0.334	22.75 17.20	13.44 - 31.63 13.67 - 26.27
Garcinia xanthochymus	MeO MeO	CM env	17 12	3 1	< 0.001 < 0.001	0.733	33.46 34.28	27.04 - 50.82 30.59 - 41.38

Appendix 31 Data on water permeance of isolated cuticular membranes (CM) of *Prunus laurocerasus* with no adjuvant and pure methyl oleate unpaired (MeO unpaired), methyl linolenate unpaired (MeLin unpaired), oleic acid unpaired (OA unpaired), diethylene glycol monodecyl ether unpaired (C10E2 unpaired), pentaethylene glycol monodecyl ether unpaired (C10E5 unpaired) and octaethylene glycol monodecyl ether unpaired (C10E8 unpaired)

adjuvant	n	number of removed outliers	median permeance x 10^6 (m s^{-1})	25% -75% quartile x 10^6 (m s^{-1})	effect to non-adjuvant condition
MeO unpaired	28	1	22.20	17.04 - 29.06	5
MeLin unpaired	27	1	13.42	11.19 - 20.98	3
OA unpaired	28	2	22.85	15.68 - 30.20	5
C10E2 unpaired	11	1	23.80	20.43 - 68.62	5
C10E5 unpaired	12	1	97.24	34.62 - 163.49	21
C10E8 unpaired	6	0	45.02	21.57 - 87.28	10

Appendix 32 Multiple comparisons (post-hoc Dunn's test after Kruskal-Wallis ANOVA) of the water permeance with isolate cuticular membranes (CM) of *Prunus laurocerasus* using no adjuvant (no_CM) and the pure unpaired adjuvants methyl oleate (MeO_CM), methyl linolenate (MeLin_CM), oleic acid (OA_CM), diethylene glycol monodecyl ether (C10E2_CM), pentaethylene glycol monodecyl ether (C10E5_CM) and octaethylene glycol monodecyl ether (C10E8_CM).

comparisons	adjusted p-value according to Benjamini-Hochberg
C10E2_CM - C10E5_CM	0.197747798
C10E2_CM - C10E8_CM	0.496795407
C10E5_CM - C10E8_CM	0.236527376
C10E2_CM - no_CM	1.29819E-05
C10E5_CM - no_CM	5.28824E-08
C10E8_CM - no_CM	0.000384588
MeLin_CM - MeO_CM	0.004174
MeLin_CM - no_CM	3.41E-05
MeO_CM - no_CM	3.71E-11
MeLin_CM - OA_CM	0.002367
MeO_CM - OA_CM	0.425173
no_CM - OA_CM	1.13E-11

Appendix 33 Data for contact angle measurements with parafilm and water (non), diethylene glycol monodecyl ether (C10E2), pentaethylene glycol monodecyl ether (C10E5) and octaethylene glycol monodecyl ether (C10E8)

adjuvant	n	p-value of Kruskal-Wallis ANOVA	mean contact angle (°)	standard deviation (°)	median contact angle (°)	25th -75th quartile (°)	effect to non-adjuvant condition
non	6	< 0.01	108.1	0.7	108.3	107.9 – 108.4	1.0
C10E2	12	< 0.01	44.4	3.0	44.4	41.8 – 47.2	0.4
C10E5	12	< 0.01	49.3	1.4	49.4	48.9 – 49.8	0.5
C10E8	12	< 0.01	60.9	0.3	61.0	60.7 – 61.2	0.6

Appendix 34 P-values for Dunnett's T3 post-hoc test for contact angle measurements of water (non), diethylene glycol monodecyl ether (C10E2), pentaethylene glycol monodecyl ether (C10E5) and octaethylene glycol monodecyl ether (C10E8)

	C10E2	C10E5	C10E8
C10E5	1.98E-03	not tested	not tested
C10E8	7.61E-13	< 10E-16	not tested
non	< 10E-16	< 10E-16	< 10E-16

7.3 Chapter 3

Appendix 35 Flow rates for caffeine and azoxystrobin with formulated methyl oleate (MeO form) and octaethylene glycol monodecyl ether (C10E8)

treatment	RH (%)	n	number of removed outliers	Dunn's test comparison	Dunn's test adjusted p-value	post-hoc-test p-adjustment	median flow rate x 10^6 (µg s^{-1})	25^{th} -75^{th} quartile x 10^6 (µg s^{-1})	effect to non-adjuvant condition
caffeine	50	12	2	caffeine - MeO form	0.002	Benjamini-Höchberg	0.022	0.020 - 0.027	1
caffeine + MeO form	50	14	1	MeO form – C10E8	0.002	Benjamini-Höchberg	3.68	3.02 - 5.57	165
caffeine + C10E8	50	11	0	caffeine - C10E8	< 0.001	Benjamini-Höchberg	35.3	12.0 – 42.9	1582
azoxystrobin	50	8	1	azoxystrobin - MeO form	0.123	Benjamini-Höchberg	0.36	0.34 - 0.41	1
azoxystrobin + MeO form	50	8	2	azoxystrobin MeO form – C10E8	0.013	Benjamini-Höchberg	0.48	0.36 - 1.40	1.3
azoxystrobin + C10E8	50	10	1	azoxystrobin - C10E8	< 0.001	Benjamini-Höchberg	1.74	1.28 – 2.11	4.8

Appendix 36 Multiple comparisons (post-hoc Dunn's test after Kruskal-Wallis ANOVA) for caffeine (non) with one µL of pure methyl oleate (MeO), methyl linolenate (MeLin) and oleic acid (OA)

comparison	adjusted p-value according to Benjamini-Hochberg
MeLin - MeO	0.008190255
MeLin - non	1.40895E-06
MeO - non	0.015364424
MeLin - OA	0.557420621
MeO - OA	0.001157584
non - OA	7.13087E-08

Appendix 37 Flow rates for caffeine with formulated methyl oleate (MeO form), pure methyl oleate (MeO), oleic acid (OA), methyl linolenate (MeLin), methyl stearate (MeSt), diethylene glycol monodecyl ether (C10E2), pentaethylene glycol monodecyl ether (C10E5) and octaethylene glycol monodecyl ether (C10E8)

treatment	RH (%)	n	number of removed outliers	median flow rate x 10^6 (µg s^{-1})	25^{th} -75^{th} quartile x 10^6 (µg s^{-1})	effect to non-adjuvant condition
caffeine	30 50 80	14 12 11	0 2 1	0.06 0.022 0.12	0.04 - 0.11 0.020 - 0.027 0.034 – 0.13	1 1 1
caffeine + MeO form	30 50 80	14 14 10	0 1 1	4.62 3.68 4.39	3.90 - 5.79 3.02 - 5.57 2.69 - 4.78	80 165 38
caffeine + MeO	50	15	0	12.9	8.77 – 15.0	223
caffeine + OA	50	14	1	34.2	29.2 – 54.0	592
caffeine + MeLin	50	14	0	51.8	34.4 – 61.4	897
caffeine + C10E2	30 50 80	12 13 9	1 0 0	1.78 17.8 44.5	1.68 - 2.26 14.6 – 26.6 37.2 – 57.0	31 797 388
caffeine + C10E5	30 50 80	15 13 13	0 0 0	20.5 28.5 36.8	7.51 – 29.3 15.6 - 32.5 27.3 – 48.0	355 1277 321
caffeine + C10E8	30 50 80	9 11 10	1 0 0	20.0 35.3 39.3	16.1 – 26.5 12.0 – 42.9 15.9 – 58.4	346 1582 343

Appendix 38 Multiple comparisons (post-hoc Dunn's test after Kruskal-Wallis ANOVA) of the flow rates for caffeine with formulated methyl oleate (MeO), diethylene glycol monodecyl ether (C10E2), pentaethylene glycol monodecyl ether (C10E5) and octaethylene glycol monodecyl ether (C10E8) at the different relative humidity levels 30, 50, 80 %

comparison	adjusted p-value according to Benjamini-Hochberg
C10E2 30 - C10E2 50	5.5E-04
C10E2 30 - C10E2 80	2.9E-07
C10E2 50 - C10E2 80	1.9E-02
C10E2 30 - C10E5 30	3.5E-04
C10E2 50 - C10E5 30	4.9E-01
C10E2 80 - C10E5 30	1.7E-02
C10E2 30 - C10E5 50	2.0E-04
C10E2 50 - C10E5 50	3.9E-01
C10E2 80 - C10E5 50	3.4E-02
C10E5 30 - C10E5 50	4.0E-01
C10E2 30 - C10E5 80	9.6E-07
C10E2 50 - C10E5 80	6.3E-02
C10E2 80 - C10E5 80	2.5E-01
C10E5 30 - C10E5 80	5.9E-02
C10E5 50 - C10E5 80	1.1E-01
C10E2 30 - C10E8 30	1.8E-03
C10E2 50 - C10E8 30	4.8E-01
C10E2 80 - C10E8 30	2.5E-02
C10E5 30 - C10E8 30	4.7E-01
C10E5 50 - C10E8 30	3.8E-01
C10E5 80 - C10E8 30	7.6E-02
C10E2 30 - C10E8 50	2.3E-05
C10E2 50 - C10E8 50	1.7E-01
C10E2 80 - C10E8 50	1.3E-01
C10E5 30 - C10E8 50	1.7E-01
C10E5 50 - C10E8 50	2.4E-01
C10E5 80 - C10E8 50	3.1E-01
C10E8 30 - C10E8 50	1.8E-01
C10E2 30 - C10E8 80	1.2E-05
C10E2 50 - C10E8 80	1.1E-01
C10E2 80 - C10E8 80	2.0E-01
C10E5 30 - C10E8 80	1.1E-01
C10E5 50 - C10E8 80	1.7E-01
C10E5 80 - C10E8 80	4.1E-01
C10E8 30 - C10E8 80	1.2E-01
C10E8 50 - C10E8 80	4.0E-01
C10E2 30 - MeO 30	8.3E-02
C10E2 50 - MeO 30	2.4E-02
C10E2 80 - MeO 30	5.1E-05
C10E5 30 - MeO 30	1.9E-02

C10E5 50 - MeO 30	1.2E-02
C10E5 80 - MeO 30	2.0E-04
C10E8 30 - MeO 30	4.2E-02
C10E8 50 - MeO 30	2.0E-03
C10E8 80 - MeO 30	1.1E-03
C10E2 30 - MeO 50	1.4E-01
C10E2 50 - MeO 50	1.1E-02
C10E2 80 - MeO 50	1.6E-05
C10E5 30 - MeO 50	8.4E-03
C10E5 50 - MeO 50	5.1E-03
C10E5 80 - MeO 50	6.1E-05
C10E8 30 - MeO 50	2.2E-02
C10E8 50 - MeO 50	7.8E-04
C10E8 80 - MeO 50	4.1E-04
MeO 30 - MeO 50	3.8E-01
C10E2 30 - MeO 80	1.8E-01
C10E2 50 - MeO 80	1.5E-02
C10E2 80 - MeO 80	3.9E-05
C10E5 30 - MeO 80	1.2E-02
C10E5 50 - MeO 80	7.4E-03
C10E5 80 - MeO 80	1.6E-04
C10E8 30 - MeO 80	2.6E-02
C10E8 50 - MeO 80	1.4E-03
C10E8 80 - MeO 80	7.4E-04
MeO 30 - MeO 80	3.6E-01
MeO 50 - MeO 80	4.7E-01
C10E2 30 - no adjuvant 30	1.1E-01
C10E2 50 - no adjuvant 30	1.5E-06
C10E2 80 - no adjuvant 30	1.4E-10
C10E5 30 - no adjuvant 30	5.8E-07
C10E5 50 - no adjuvant 30	3.7E-07
C10E5 80 - no adjuvant 30	2.4E-10
C10E8 30 - no adjuvant 30	1.6E-05
C10E8 50 - no adjuvant 30	2.6E-08
C10E8 80 - no adjuvant 30	1.3E-08
MeO 30 - no adjuvant 30	3.1E-03
MeO 50 - no adjuvant 30	7.5E-03
MeO 80 - no adjuvant 30	1.6E-02
C10E2 30 - no adjuvant 50	3.5E-02
C10E2 50 - no adjuvant 50	1.5E-07
C10E2 80 - no adjuvant 50	1.2E-11
C10E5 30 - no adjuvant 50	5.5E-08
C10E5 50 - no adjuvant 50	3.6E-08
C10E5 80 - no adjuvant 50	1.8E-11
C10E8 30 - no adjuvant 50	2.2E-06

C10E8 50 - no adjuvant 50	2.4E-09
C10E8 80 - no adjuvant 50	1.2E-09
MeO 30 - no adjuvant 50	5.4E-04
MeO 50 - no adjuvant 50	1.5E-03
MeO 80 - no adjuvant 50	4.1E-03
no adjuvant 30 - no adjuvant 50	2.6E-01
C10E2 30 - no adjuvant 80	1.3E-01
C10E2 50 - no adjuvant 80	6.5E-06
C10E2 80 - no adjuvant 80	1.2E-09
C10E5 30 - no adjuvant 80	3.2E-06
C10E5 50 - no adjuvant 80	1.9E-06
C10E5 80 - no adjuvant 80	2.9E-09
C10E8 30 - no adjuvant 80	4.4E-05
C10E8 50 - no adjuvant 80	1.6E-07
C10E8 80 - no adjuvant 80	7.9E-08
MeO 30 - no adjuvant 80	5.6E-03
MeO 50 - no adjuvant 80	1.2E-02
MeO 80 - no adjuvant 80	2.3E-02
no adjuvant 30 - no adjuvant 80	4.9E-01
no adjuvant 50 - no adjuvant 80	2.6E-01

Acknowledgements

Publication list

First-author ship

Staiger S, Seufert P, Arand K, Burghardt M, Popp C, Riederer M. (2019). The permeation barrier of plant cuticles: uptake of active ingredients is limited by very long-chain aliphatic rather than cyclic wax compounds, *Pest Management Science* (doi: 10.1002/ps.5589).

Co-author ship

Bueno A, Alfarhan A, Arand K, Burghardt M, Deininger AD, Hedrich H, Leide J, Seufert P, **Staiger S**, Riederer M. (2019). Temperature effects on the cuticular transpiration barrier of two desert plants with water-spender and water-saver life strategies, *Journal of Experimental Botany* (doi.org/10.1093/jxb/erz018).

Curriculum vitae

Affidavit

I hereby confirm that my thesis entitled ‘Chemical and physical nature of the barrier against active ingredient penetration into leaves: effects of adjuvants on the cuticular diffusion barrier‘ is the result of my own work. I did not receive any help or support from commercial consultants. All sources and / or materials applied are listed and specified in the thesis. Furthermore, I confirm that this thesis has not yet been submitted as part of another examination process neither in identical nor in similar form.

Würzburg,
Place, Date Signature

Eidesstattliche Erklärung

Hiermit erkläre ich an Eides statt, die Dissertation „Chemische und physikalische Beschaffenheit der Barriere gegenüber Wirkstoffen: Adjuvantieneffekte auf die kutikuläre Diffusionsbarriere“ eigenständig, d.h. insbesondere selbständig und ohne Hilfe eines kommerziellen Promotionsberaters, angefertigt und keine anderen als die von mir angegebenen Quellen und Hilfsmittel verwendet zu haben. Ich erkläre außerdem, dass die Dissertation weder in gleicher noch in ähnlicher Form bereits in einem anderen Prüfungsverfahren vorgelegen hat.

Würzburg,
Ort, Datum Unterschrift